Advanced IGCC/Hydrogen Gas Turbine Development

Final Technical Report

Reporting Period
Beginning October 1, 2005
Ending April 30, 2015

Principal Authors:

William York, Michael Hughes, Jonathan Berry, Tamara Russell, Y.C. Lau, Shan Liu, Michael D. Arnett, Arthur Peck, Nilesh Tralshawala, Joseph Weber, Marc Benjamin, Michelle Iduate, Jacob Kittleson, Andres Garcia-Crespo, John Delvaux, Fernando Casanova, Ben Lacy, Brian Brzek, Chris Wolfe, Pepe Palafox, Ben Ding, Bruce Badding, Dwayne McDuffie, Christine Zemsky

July 30, 2015

DE-FC26-05NT42643

Submitted By:

GE Power and Water
1 River Road
Schenectady, NY 12345

Submitted To:

US Department of Energy
National Energy Technology Laboratory
Morgantown, WV 26507-0880

DISCLAIMER

This report was prepared as an account of work sponsored by an agency of the United States Government. Neither the United States Government nor any agency thereof, nor any of their employees, makes any warranty, express or implied, or assumes any legal liability or responsibility for the accuracy, completeness, or usefulness of any information, apparatus, product, or process disclosed, or represents that its use would not infringe privately owned rights. Reference herein to any specific commercial product, process, or service by trade name, trademark, manufacturer, or otherwise does not necessarily constitute or imply its endorsement, recommendation, or favoring by the United States Government or any agency thereof. The views and opinions of authors expressed herein do not necessarily state or reflect those of the United States Government or any agency thereof.

ABSTRACT

The objective of this program was to develop the technologies required for a fuel flexible (coal derived hydrogen or syngas) gas turbine for IGCC that met DOE turbine performance goals. The overall DOE Advanced Power System goal was to conduct the research and development (R&D) necessary to produce coal-based IGCC power systems with high efficiency, near-zero emissions, and competitive capital cost. To meet this goal, the DOE Fossil Energy Turbine Program had as an interim objective of 2 to 3 percentage points improvement in combined cycle (CC) efficiency. The final goal is 3 to 5 percentage points improvement in CC efficiency above the state of the art for CC turbines in IGCC applications at the time the program started. The efficiency goals were for NOx emissions of less than 2 ppm NOx (@15 % O2). As a result of the technologies developed under this program, the DOE goals were exceeded with a projected 8 point efficiency improvement. In addition, a new combustion technology was conceived of and developed to overcome the challenges of burning hydrogen and achieving the DOE's NOx goal.

This report also covers the developments under the ARRA-funded portion of the program that include gas turbine technology advancements for improvement in the efficiency, emissions, and cost performance of gas turbines for industrial applications with carbon capture and sequestration. Example applications could be cement plants, chemical plants, refineries, steel and aluminum plants, manufacturing facilities, etc. The DOE's goal for more than 5 percentage point improvement in efficiency was met with cycle analyses performed for representative IGCC Steel Mill and IGCC Refinery applications.

Technologies were developed in this program under the following areas: combustion, larger latter stage buckets, CMC and EBC, advanced materials and coatings, advanced configurations to reduce cooling, sealing and rotor purge flows, turbine aerodynamics, advanced sensors, advancements in first stage hot gas path components, and systems analyses to determine benefits of all previously mentioned technologies to a gas turbine system in an IGCC configuration.

This project built on existing gas turbine technology and product developments, and developed and validated the necessary turbine related technologies and sub-systems needed to meet the DOE turbine program goals. The scope of the program did not cover the design and validation of a full-scale prototype machine with the technology advances from this program incorporated.

In summary, the DOE goals were met with this program. While the commercial landscape has not resulted in a demand for IGCC gas turbines many of the technologies that were developed over the course of the program are benefiting the US by being applied to new higher efficiency natural gas fueled gas turbines.

TABLE OF CONTENTS

FIGURES

TABLES

LIST OF ACRONYMS AND ABBREVIATIONS

AC	Autoclave
ACC	Active Clearance Control
AGR	Acid Gas Removal
AP	Aging Parameter
APM	Advanced Premixer
ARRA	American Recovery and Reinvestment Act
ASU	Air Separation Unit
BFG	Blast Furnace Gas
BO	Burnout
BOT	Blow off Time
C-free	Carbon-free
CC	Combined Cycle
CCS	Carbon Capture and Storage
CDA	Combustion Dynamics Analysis
CFD	Computational Fluid Dynamics
CH4	Methane
CHL	Chordal Hinge Leakage
CHP	Combined Heat and Power
CMC	Ceramic Matrix Composite
CO	Carbon Monoxide emissions
CO2	Carbon Dioxide emissions
CT	Computed Tomography
DDRF	Direct Deposited Radio Frequency
DLN	Dry Low NOx
DLN2.6+	5-around-1 swozzle based DLN system
DMLM	Direct Metal Laser Melted
DOE	Department of Energy
dP/P	Combustor Pressure Drop
DVC	Dense Vertically Cracked
EBC	Environmental Barrier Coating
EGV	Exit Guide Vane
EI	Emissions Index
Element #1	Stage 1 Bucket
Element #2	Stage 1 Nozzle
EQ	Equiaxed Grain Structure
FBG	Fiber Bragg Grating
FCT	Furnace Cycle Test
FEA	Finite Element Analysis
FPI	Fluorescent Penetrant Inspection
FRS	Filtered Rayleigh Scattering
FSFL	Full Speed-Full Load
GRC	GE Global Research Center
GT	Gas Turbine
GTCC	Gas Turbine Combined Cycle
GTTL	Gas Turbine Technology Laboratory
HAA	High Annulus Area

HAF	Heat Affected Zone
HCF	High Cycle Fatigue
Hg	Mercury
HGP	Hot Gas Path
HTC	Heat Transfer Coefficient
ID	Inner Diameter
IDE	Integrated Design Environment
IGCC	Integrated Gasification Combined Cycle
ILT	Inter-Laminar Tension
IR	Infrared
JETS	Jet Engine Thermal Simulation
LBO	Lean blow out
LCF	Low cycle Fatigue
LES	Large Eddy Simulation
LF	Liquid Fuel
LM/LMP	Larson Miller Parameter
LSB	Latter Stage Bucket
MCIR	Multi-Color Infrared
MI	Melt Infiltration
MT	Multi-tube
MWI	Modified Wobbe Index
M&D	Monitoring & Diagnostics
N2	Nitrogen
NDT	Non-Destructive Testing
NETL	National Energy Technology Laboratory
NOx	Oxide of Nitrogen Emissions
OD	Outer Diameter
PHM	Prognostics & Health Monitoring
PIVT	Particle Imaging Velocimetry and Thermometry
PLM	Part Life Management
PM	Particulate Matter
PSP	Pre-sintered Preforms
PWST	Passive Wireless Sensors Technology
R&D	Research and Development
RACDOV	Rapid Airfoil Concept Design Optimization and Validation
RCA	Root Cause Analysis
Re	Reynold’s Number
RRSR	Rotating Rim Seal Rig
RSC	Radiant Syngas Cooler
S1B	Turbine Stage 1 Bucket
S1N	Turbine Stage 1 Nozzle (Stationary Vane)
SAW	Surface Acoustic Wave
SEM	Scanning Electron Microscopy
SG	Strain Gauge
SGS	Sour Gas Shift
SGS	Sub-Grid Scale
SiC	Silicon Carbide
SN	Serial Number
SNR	Single Nozzle Rig
SOTA	State of the Art

ST	Steam Turbine
STL	Steam Turbine Laboratory
SX	Single crystal
T3.90	Combustor Exit Temperature
TBC	Thermal Barrier Coating
TC	Thermocouple
TDLAS	Tunable Diode Laser Absorption Spectroscopy
TGO	Thermally-Grown Oxides
TP	Combustor Transition Piece
UHC	Unburned Hydrocarbons
WALE	Wall-Adapting Local Eddy-viscosity
WB	Wheelbox
WS	Wheel Space
XRD	X-Ray Diffraction
YSZ	Yttria-Stabilized Zirconia

EXECUTIVE SUMMARY

The objective of this program was to develop the technologies required for a fuel flexible (coal derived hydrogen or syngas) gas turbine for IGCC that met DOE turbine performance goals. The overall DOE Advanced Power System goal was to conduct the research and development (R&D) necessary to produce coal-based IGCC power systems with high efficiency, near-zero emissions, and competitive capital cost. To meet this goal, the DOE Fossil Energy Turbine Program had as an interim objective of 2 to 3 percentage points improvement in combined cycle (CC) efficiency and a final goal of 3 to 5 percentage points improvement in CC efficiency above the state of the art for CC turbines in IGCC applications at the time the program started. The efficiency goals were for NOx emissions of less than 2 ppm NOx (@15 % O2). As a result of the technologies developed under this program, the DOE goals were exceeded with a projected 8 point efficiency improvement. In addition, a new combustion technology was conceived of and developed to overcome the challenges of burning hydrogen and achieving the DOE's NOx goal.

The ARRA-funded portion of the project was focused on gas turbine technology advances that are aimed at offsetting CCS penalties and improving emissions performance in preparation for CCS in industrial applications. GE Power & Water has extensive experience in supplying gas turbines for use in industrial applications such as refineries, petrochemical, iron and steel mills. Systems based on advanced gas turbines offer efficient energy conversion solutions that meet the challenge of fuel diversity, while maintaining superior environmental performance. The DOE's goal for more than five percentage point improvement in efficiency was met with cycle analyses performed for representative IGCC Steel Mill and IGCC Refinery applications.

This project built upon existing gas turbine technology and product developments, and developed and validated the necessary turbine related technologies and sub-systems needed to meet the DOE turbine program goals. The scope of the program did not cover the design and validation of a full-scale prototype machines with the technology advances from this program incorporated.

Key elements of the whole project are summarized below:

Combustion: Simply stated, the combustion goal for the program was "reliable, ultra-low NOx combustion of high hydrogen fuels for advanced gas turbine cycles".

The outcome of Task 2.1 of the program was a dry low NOx combustion system capable of operating reliably on syngas, carbon-free syngas, and a wide range of additional fuels. The system cost was brought in line with current natural gas combustion system to support plant capital cost targets. The high-hydrogen combustion system was fully demonstrated to consistently achieve single-digit (ppm) NOx emissions while operating at aggressive H2 gas turbine cycle conditions to meet program goals for IGCC-CCS plant efficiency and output.

Task 2.6 achieved its stated objectives for this area: to develop designs for an Advanced Combustor Architecture and Advanced Combustor Integration that enable firing temperature increases thereby improving efficiency while still delivering low NOx emissions, handling hydrogen and fuel flexibility, extend turndown, and maintaining existing inspection intervals and current reliability levels. $NOx/T_{3.90}$ capability was improved, turndown capability was extended,

and the system maintained the capability to run greater than 50% hydrogen in the fuel, and the tolerance to fuel MWI changes were three to five times the baseline system.

Materials: The materials task was intended to develop alloys that are specifically tailored to withstand elevated temperatures in the hot gas path in the high moisture, and potentially highly corrosive environments of hydrogen fueled industrial applications with CCS. This will enable industrial gas turbine applications with CCS improved efficiency through higher firing temperature while preserving traditional hot gas path component durability.

The HGP coating program completed under ARRA 2.7 was very successful. It gave insights into the oxidation behavior of new coatings and alloys. It also resulted in a low k TBC that improves the efficiency of the gas turbine system through enabling higher operating temperature and allowing increased service intervals. It is being incorporated into the design for several new GE gas turbines.

Under ARRA 2.7, a highly oxidation and corrosion resistant superalloy, Rene' N2M, was successfully developed, which enables stage 1 static hardware to reliably operate beyond the temperature limited by Rene' 108 alloy. Verifications of the scale-up of the alloy by making, complex nozzle castings and necessary downstream fabrication processes laid a solid foundation to deploy this material in upcoming products. In addition, without Re and with reduced Hf, the alloy is cost effective.

Sensors: The sensors task focused on the technology of utilizing and integrating a variety of advanced sensor technologies into gas turbine control and operation. This would enable the gas turbine to operate with reduced margin due to real-time knowledge of actual parameters that are affecting component conditions and operation. The most significant sensing gaps exist in the turbine hot gas path, where existing sensor technology cannot survive in the harsh environment.

Three distinct sensor technologies were selected and tested in laboratory and rig conditions for further evaluation under this program, namely, (1) Multi-color infrared (MCIR) Pyrometry, (2) Tunable Diode Laser Absorption Spectroscopy (TDLAS) and (3) Passive Wireless Sensors Technology (PWST).

Next Generation Stage 1 Architecture: This task developed technology that enables turbine cooling flow reductions and henceforth improved efficiency.

Subtask 2.9 investigated architectures of the next generation of a stage 1 hot gas path turbine components. During this subtask, it was demonstrated that these architectures met program cooling flow reduction targets with no impact to part life, while having a positive cost/benefit ratio.

Cooling/Sealing/Purge Flow Reductions: Under this task extensive research and technology development was conducted to improve cooling, sealing, and purge flow features for hot gas path parts. This reduced required flows and enabled higher temperature operation to improve efficiency and turbine throughput while enabling low NOx operation.

Multiple technologies developed in this area are now being introduced into GE's new and existing gas turbines.

CMC: The CMC task was focused on key elements of CMC development for use in gas turbine hot gas path components. The CMC material characteristics have the potential to enable uncooled components in selected turbine stages, thereby increasing efficiency.
Numerous observations and conclusions were drawn from the work completed over the duration of this program. Many of those conclusions related to the fabrication of increasingly complex CMC components for gas turbine applications. During the fabrication of the Phase 1 full-scale components, it was noticed that several processing changes needed to be made and developed in order to produce acceptable component yields for these larger parts. Phase 2 offered its own difficulties of producing acceptable parts that would be required for mass production.

Long term CMC testing in fielded gas turbine engines was performed with the 7FA stage 1 shrouds amassing over 21,740 hours of operation provided an extensive set of EBC and CMC exposure data.

In summary, the DOE goals were met with this program. While the commercial landscape has not resulted in a demand for IGCC gas turbines, many of the technologies that were developed over the course of the program are benefiting the US by being applied to new higher efficiency natural gas fueled gas turbines. At the time of the writing of this report 17 of the technologies developed under this program and scheduled for utilization in GE's advanced gas turbine products.

COMBUSTION

The initial focus of the combustion task was development and validation of a gas turbine combustion system able to reliably operate with syngas and carbon-free syngas fuels for Integrated Gasification Combined Cycle (IGCC) and IGCC with Carbon Capture and Sequestration (CCS). The requirements of the system were:

1) Support aggressive program target of 2 ppm NOx @ 15% O2 at the IGCC-CCS plant level.
2) Allow reliable operation on syngas and C-free syngas (very high hydrogen fuel) at firing temperatures required to meet gas turbine efficiency goals set forth on the program.
3) Maintain combustor pressure drop at level to meet system performance targets.
4) Keep combustion system capital cost at or near existing natural gas Dry Low NOx (DLN) systems to support aggressive Cost of Electricity target.

The high reactivity of the carbon-free syngas compared to natural gas, and even unshifted syngas, presented a great challenge in combustion system design. High flame speeds for hydrogen-in-air combustion compared to hydrocarbons-in-air results in an elevated risk of flashback (flame front traveling back into the premixer) and flame holding (the tendency of a flame inside the premixer to stay inside the premixer when the original ignition source is no longer present). Both can result in rapid component damage if they occur. Figure 1 shows the relative reactivity and Wobbe number of the syngas fuels of interest compared to natural gas. The modified Wobbe index (MWI) is a measure of energy content per unit volume, and is defined by:

$$MWI = \frac{LHV}{\sqrt{SG_{gas} \cdot T_{gas}}}$$

Blowoff time (BOT) in a perfectly-stirred reactor is taken to be a characteristic chemical time, and its inverse a relative measure of reactivity when comparing fuels and conditions. BOT is calculated using Cantera code. Carbon-free syngas that can be over 90% H2 by volume, depending on the capture rate, is more reactive than natural gas by orders of magnitude. Adding N2, which is readily available from the plant's air separation unit (ASU), to the carbon-free syngas fuel stream does little to reduce the reactivity, but has a large impact on Wobbe index and can facilitate fuel/air mixing.

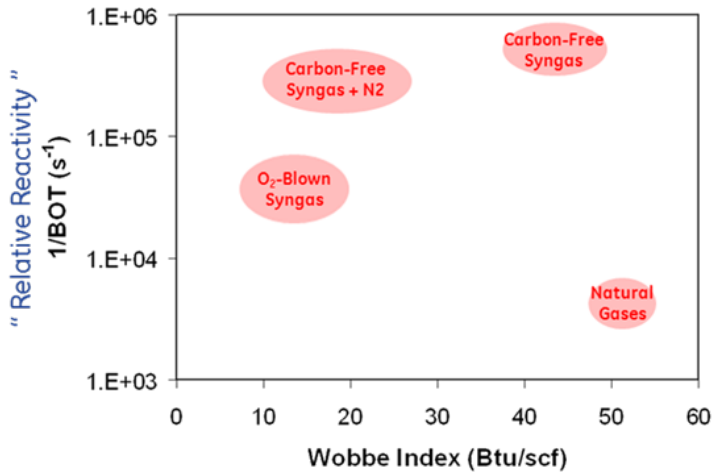

Figure 1: Ranges of relative reactivity and Modified Wobbe Index for fuels of interest in program.

As the project progressed, later goals were to identify a set of gas turbine technology advancements that would improve the efficiency, emissions, and cost performance of gas turbines for industrial applications. In addition to the traditional demands of higher efficiency from gas turbines, industrial applications typically demand high levels of operational flexibility to be able to meet the varying demands of the plant, and high levels of availability to ensure uninterrupted plant operation. Tasks 2.6.1 and 2.6.2 developed a technology suite capable of meeting these requirements. Increased efficiency is achieved by improving integration between the combustor and the turbine section. Fuel flexibility was achieved by appropriate premixer design and development beyond that being performed in Task 2.1. Operational flexibility was achieved through development of advanced combustor architecture.

Phase 1 Summary

In Phase 1 of this program (Task 1.2: 2005-2007), the combustion system requirements were defined, the fundamental physics were studies, entitlement NOx emissions were quantified, and the performance of existing gas turbine combustion systems on syngas and high-hydrogen fuels were determined. During Phase 1, the challenges of combusting high-hydrogen fuel in a gas turbine were demonstrated. Despite the aforementioned challenges with high-hydrogen fuels, a key outcome of Phase 1 was the selection of a lean premixed combustion approach instead of a diffusion combustion approach to meet the aggressive program NOx goal.

In Phase 1, over 30 sub-scale fuel-air premixer concepts were built using additive manufacturing and tested in a single nozzle rig with adiabatic (thick ceramic) liner at GE's Global Research Center in Niskayuna, NY. A model and photograph of this rig are shown in Figure 2. Early concepts tested were small-scale swirl premixers similar to natural gas versions in use in GE's heavy-duty gas turbines. Even with modifications, these premixers exhibited flashback and flame holding inside the fuel nozzle with hydrogen fuel at target conditions. Novel concepts were tested in a search for a more reliable premixer for highly-reactive fuels in support of a concept downselect early in Phase 2.

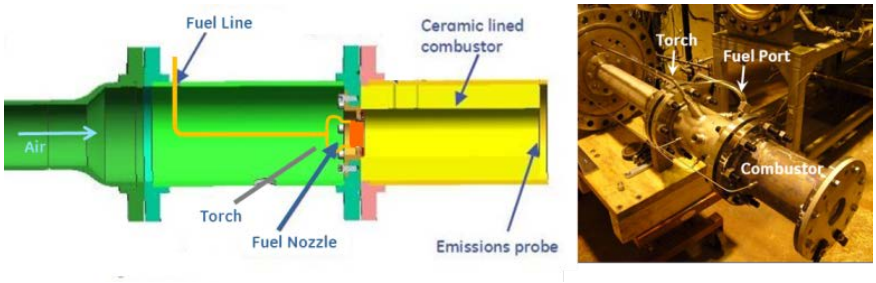

Figure 2: Model cross-section and photograph of small-scale single nozzle rig with ceramic-lined combustor used in Phase 1 concept testing for emissions, flashback, and flame holding.

Concept Downselect and Single-Element Optimization

At the beginning of Phase 2 of the project, a formal downselect of fuel nozzle/premixer technology was conducted with performance data gathered in Phase 1 single nozzle testing. The outcome was the selection of the multi-tube (MT) premixer, which uses jet-in-crossflow mixing at a very small scale to reliably mix hydrogen fuel and air in small tubes. The MT premixer concept was refined at the sub-scale level. Computational fluid dynamics (CFD) and prototype testing were used to study the impact of relevant geometric parameters on NOx emissions, flashback, and flame holding. The result was the “micromixer” concept. Figure 3 shows a model and photograph of the first small-scale micromixer prototype.

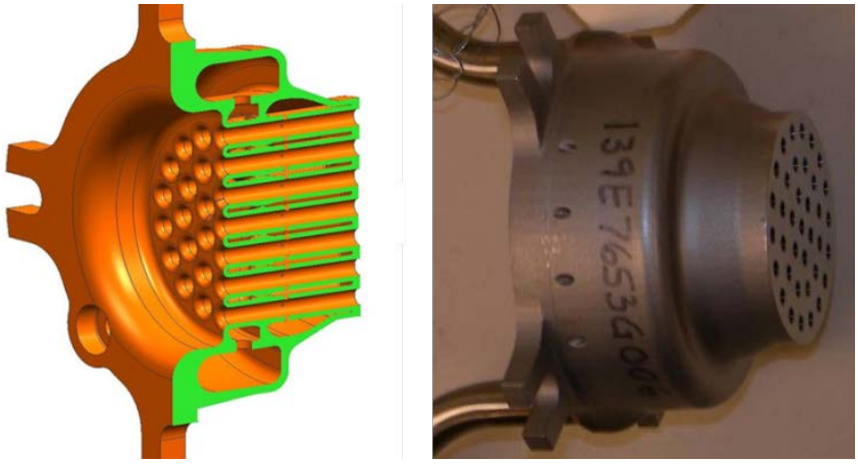

Figure 3: Model cross-section and photograph of small micromixer for high-hydrogen fuel.

The superior flashback resistance of the micromixer compared to traditional swirl-premixers (used for natural gas operation) is illustrated in Figure 4. For a basic swirl premixer (Figure 5), even with elevated premixer air-side pressure drop, flashback occurred in single nozzle testing at a bulk flame temperature of about 2500°F (1371°C). Improvements to this premixer for H2 fuel allowed for a reduction in the pressure drop, but no improvement in temperature at which flashback occurred. The prototype micromixer had a similar pressure drop to the best swirl premixer but did not exhibit flashback to flame temperatures of nearly 3000°F (1649°C).

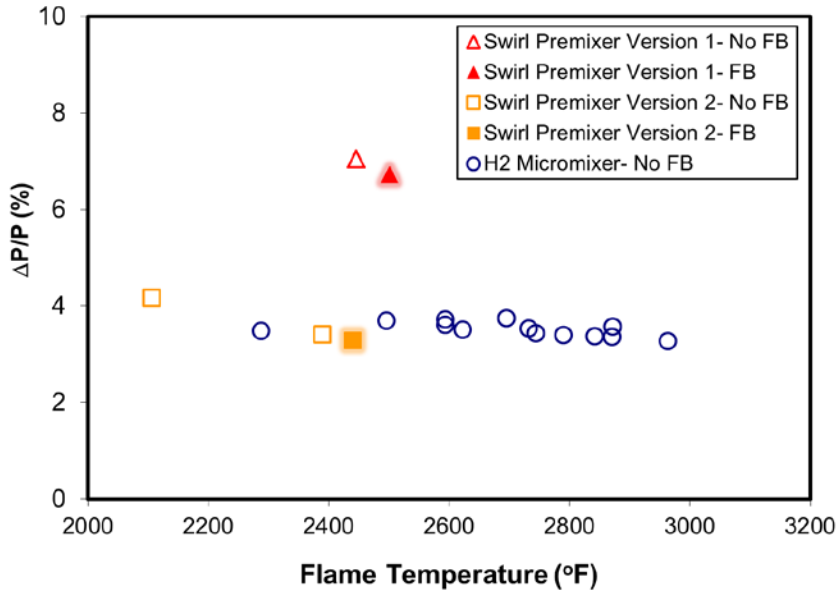

Figure 4: Flashback (FB) points (solid symbols) and normal operating points (open symbols) for two swirl premixer concepts and the micromixer prototype as a function of premixer pressure drop.

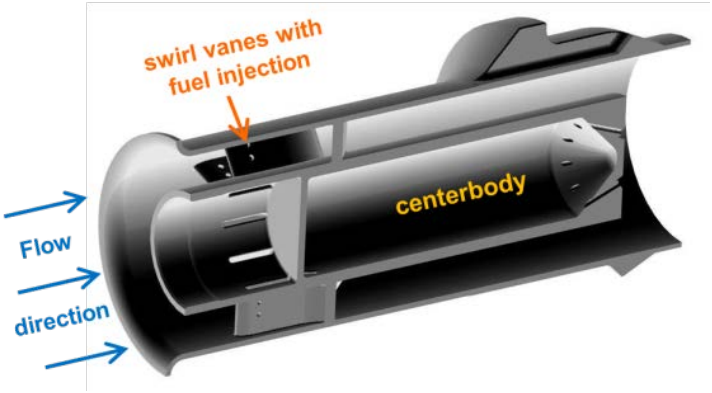

Figure 5: Cross-section view of small-scale swirl premixer tested with hydrogen fuel and compared to the performance of the micromixer in the previous figure.

After the excellent performance of the small-scale prototype micromixer was demonstrated, the focus shifted to full-scale fuel nozzle development in a configuration that could eventually be tested in a multi-nozzle (full-can) arrangement. Early full-scale micromixer nozzles were round like DLN swirl premixers. A photograph of one of these early full-scale micromixer nozzles is shown in Figure 6. A larger-scale single nozzle rig was employed to evaluate the performance of the scaled-up fuel nozzle. A key feature of this rig was an optical access window, through which a video camera monitored flame structure and could rapidly confirm flame holding during forced ignition testing to avoid nozzle damage. Figure 7 shows a photograph of the rig with the optical access window highlighted. The facility had the ability to blend fuel streams containing H2, CO, CO2, N2, and natural gas. Similar to the small-scale rig, multiple thermocouples on the nozzle and combustor face were used to detect whether a flame stabilized in the micromixer during flame holding and flashback experiments.

Figure 6: Early full-scale micromixer fuel nozzle used for single nozzle rig flame operability testing.

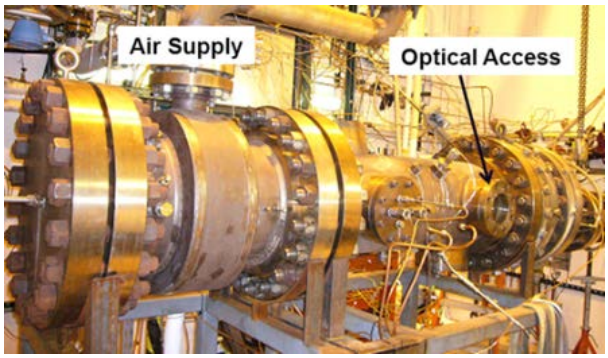

Figure 7: Large-scale single nozzle rig with optical combustor access.

Figure 8 shows measured NOx emissions for both the small-scale and full-scale prototype micromixer nozzles in single nozzle rig testing, compared to the perfectly-premixed entitlement data for the same H2-N2 fuel obtained in Phase 1. The small-scale nozzle had slightly higher emissions than the entitlement, as expected since the fuel and air are not perfectly premixed. The larger variation in geometry with more tubes of the full-scale nozzle and a rig with more cooling and leakage flows were the likely causes of higher NOx emissions for full-scale over the small-scale nozzle. Still, the scaled-up micromixer delivered single-digit (ppm) NOx emissions while retaining very good hydrogen operability.

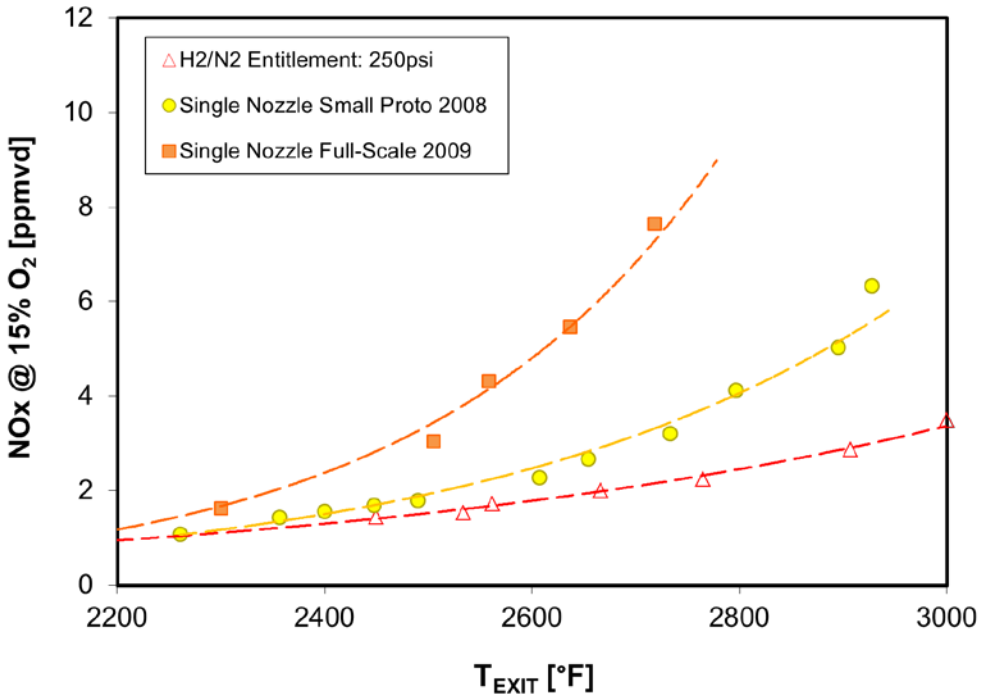

Figure 8: NOx emissions for the small-scale prototype micromixer and full-scale micromixer tested in single nozzle rigs compared to the perfectly-premixed (entitlement) emissions for H2-N2 fuel measured in Phase 1.

The full-scale micromixer was also screened for flame holding. The “torch test”, in which a H2 torch upstream of the premixer is used to put a temporary flame in the premixer and then extinguished, is much more aggressive than screening for flashback in steady-state operation. It’s possible that a premixer that operates flashback-free at a certain condition may not “pass” a flame holding test. But a premixer that passes a torch test should operate robustly at those conditions and fuel composition. Like flashback, flame holding is strongly influenced by fuel composition, equivalence ratio, pressure, temperature, and flow field. However, while flashback is strongly influenced by the flow field near the nozzle exit, flame holding is typically more sensitive to the premixer internal fluid dynamics, specifically in the fuel injection region. Figure 9 shows images taken with the camera looking into the single nozzle rig during flame holding testing. The left image is with the upstream torch on, the center image is a “no hold” condition

after the torch is extinguished, and the right image is a “hold” condition after the torch is extinguished.

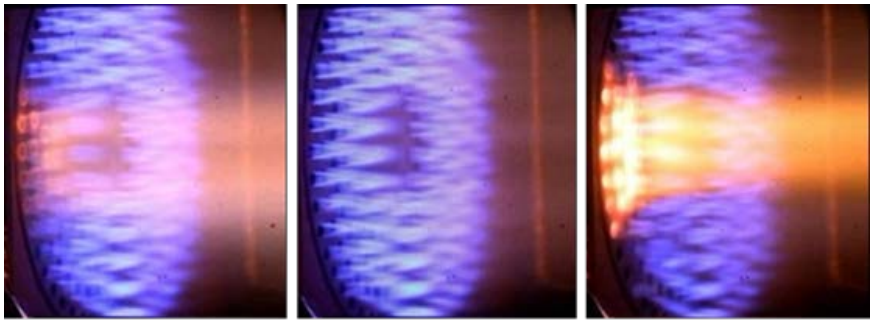

Figure 9: Images of micromixer flame holding testing in the large single nozzle rig with H2-N2 fuel containing 2-4% CH4 by volume.

Flame holding with high-hydrogen fuel was found to vary greatly with other constituents in the fuel. As the blowoff time calculations would suggest, a very small percentage of methane in the hydrogen fuel significantly reduces the tendency for flame holding to occur. Flame holding propensity also increases with equivalence ratio (flame temperature) and pressure. Figure 10 shows hold and no-hold points during torch testing of a full-scale micromixer at two different pressures over a range of flame temperatures and methane (CH4) percentage in the hydrogen-nitrogen fuel. For this particular fuel nozzle, roughly 3% to 5% CH4 is required to pass flame holding reliably at the two pressures tested. Some fuel nozzles were observed to pass flame holding tests with as low as 1% methane blended into in the hydrogen fuel. Based on these results, it is suggested that 5 to 10% natural gas is blended into the C-free syngas when practical to provide robust margin to flame holding conditions.

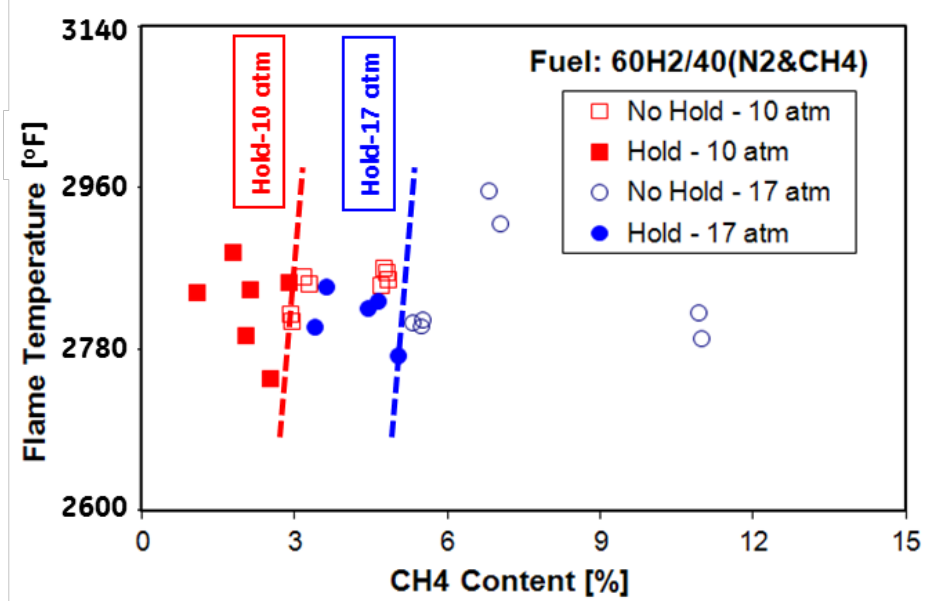

Figure 10: Micromixer flame holding test points in larger single nozzle rig with small amounts of methane in a base fuel of 60% H2 – 40% N2. More methane is required to "pass" torch test at P=17 atm vs. 10 atm.

First Full-Can High-Hydrogen Demonstration

During the first complete year of Phase 2 of the program, a major engineering effort was devoted to developing a multi-nozzle combustion system for the scaled-up high-hydrogen micromixer nozzles that was tested extensively in the single nozzle rig. This effort included the development of new components, including an endcover, cap assembly, and internal fuel delivery tubing. The system used a combustor liner and transition piece from an existing DLN combustion system, allowing it to fit in an existing test stand in GE's Gas Turbine Technology Lab (GTTL) in Greenville, SC. Computational fluid dynamics (CFD) was used to model airflow and guide the aerodynamic of the system.

The test combustion system consisted of single-nozzle and multi-nozzle operation on natural gas, pure hydrogen, and hydrogen-nitrogen fuels. Local flame temperatures were pushed in excess of F-class conditions and held there for several hours at a time to validate the thermal design. Facility fuel control issues and test stand contaminants both combined to prevent reaching a "full load" condition with all nozzles nearly uniformly fueled. Instead, operation was reached with one nozzle at an elevated flame temperature (just above the target), and the other nozzles at reduced fuel flow. Thus, the bulk combustor exit temperature was lower than the program goal. Figure 11 shows a video frame of hydrogen-nitrogen flames in this high-hydrogen combustor. The nozzle with the most luminous flame was running slightly lean, and is just above the target flame temperature condition for all nozzles to run uniformly. Faintly visible behind the primary flame is a weaker, very lean flame from a second element. Flames from the other elements are not visible in the picture, although all nozzles were being fueled. The concept demonstration was successful in that it proved that the key enabling element, the high-hydrogen micromixer, could reliably operate at target flame temperatures with C-free syngas. The testing

also spurred improvement to the lab facility to allow sustained, trouble-free testing with high-hydrogen fuels.

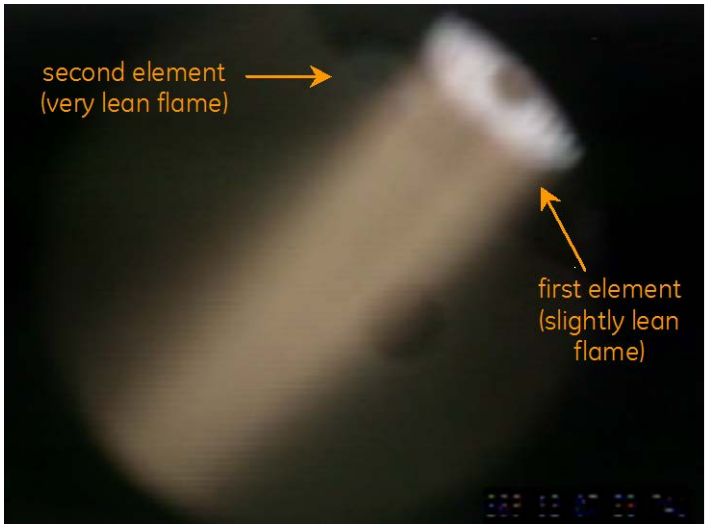

Figure 11: Flames with hydrogen-nitrogen fuel in an early multi-nozzle micromixer combustor. A prominent flame from one element is clearly visible, while a very weak flame from a second element is also faintly visible. Other fuel nozzles are not seen in this view.

RLN1 Combustion System

The next development of the "RLN1", a clean sheet combustion system based originally on the same size micromixer fuel nozzle as the earlier demonstrator. This system was designed to fit into an existing smaller test stand, and was sized to have an energy conversion rate of 15-18 megawatts when running at base load.

Testing of the RLN1 occurred with operation on various fuel blends consisting of natural gas, hydrogen, nitrogen, and/or carbon monoxide. The combustion system featured a new in-stand camera that looked through the transition piece to provide a good view of the head end. Three thermocouples were embedded in the metal of each fuel nozzle to detect flashback and flame holding if it occurred. PCB probes were used to measure dynamic pressure fluctuations on the liner and the fuel lines.

A milestone was reached when the RLN1 combustion system was able to reach the "2012 Hydrogen Gas Turbine" cycle conditions (inlet pressure and temperature and exit temperature as defined in the systems task of this project to meet requirements) on hydrogen-nitrogen fuel with and without small amounts of methane doping. A video capture from the TP camera showing operation at the 2012 conditions with even fueling to the nozzles in shown in Figure 12 for two different fuels with low modified Wobbe index. The image on the left with higher hydrogen level represents a target C-free syngas with a small amount of blended natural gas. The flame structure is clearly different than the flame on the right with much lower hydrogen and high methane. The system was also tested with different levels on nitrogen in the fuel to determine its effects on NOx and operability.

In addition, the RLN1 combustion system was operated on several blends of “traditional” syngas, or fuels typical from an oxygen-blown gasification process without carbon capture. The system exhibited acceptable operability on two fuel blends comprised of hydrogen, carbon monoxide, and nitrogen. NOx emissions were higher than with carbon-free syngas, as seen in Figure 13.

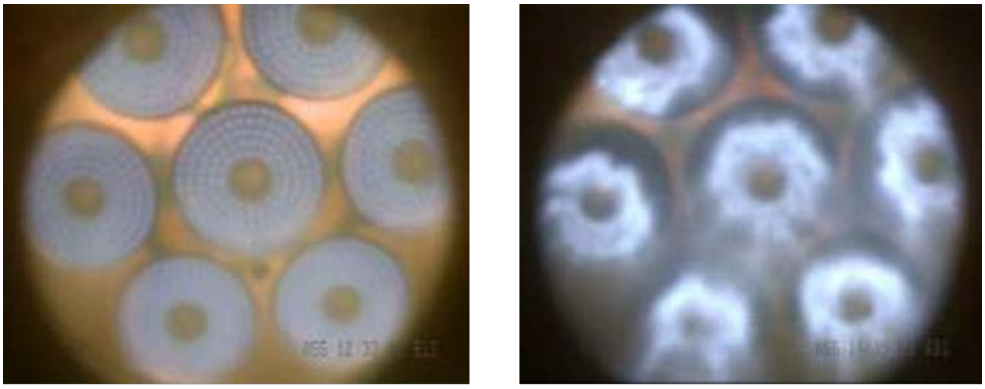

Figure 12: Flames with hydrogen-nitrogen fuel in the multi-nozzle micromixer combustor. A prominent flame from one element is clearly visible, while a very weak flame from a second element is also faintly visible. Other fuel nozzles are not seen in this view.

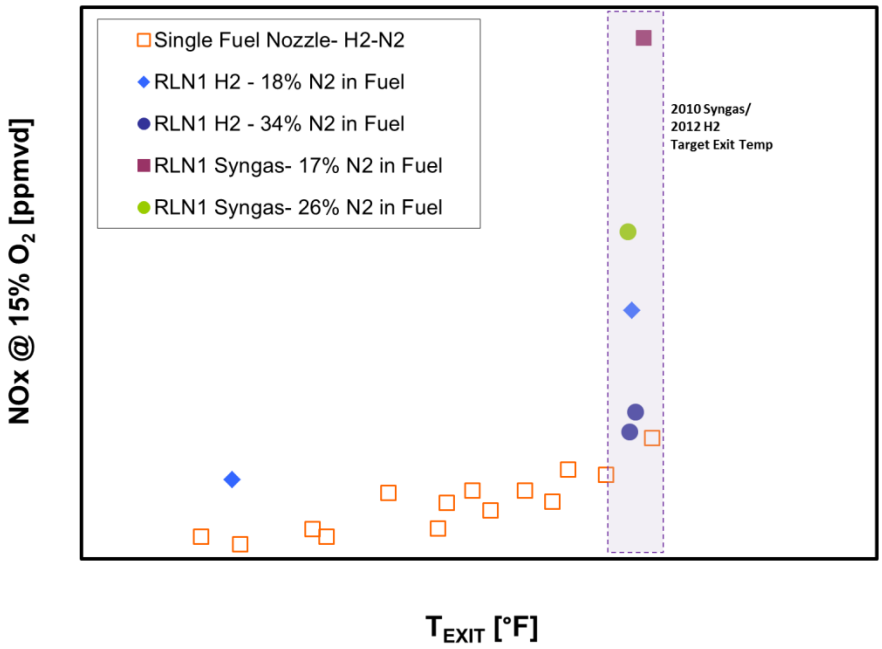

Figure 13: Measured NOx emissions for the early RLN1 combustion system on C-free (H2) fuel and traditional syngas (containing CO) with several amounts of N2 in the fuels. Full-scale single nozzle data with H2-N2 fuel is provided for comparison.

The RLN1 combustion system exhibited reasonably low “combustion dynamics” when operated at full load conditions on high-hydrogen fuels. Combustion dynamics are thermoacoustic instabilities that manifest as fairly high-frequency pressure fluctuations, and they can reduce component life. These pressure oscillations are measured at multiple places inside the combustor with fast-response pressure transducers, such as a PCB probes, and signal processing equipment. For the RLN1, combustion dynamics at full load were relatively insensitive to fuel splits between the nozzles or slight variation of fuel composition. These observations were encouraging. However, during low-temperature operations, especially when some fuel nozzles were operated very lean, high-frequency dynamics of significance were observed for short durations. Figure 14 shows a time history of the peak amplitude of a narrow range of high-frequency tones during operation at a reduced exit temperature (below the cycle condition) on high-hydrogen fuel.

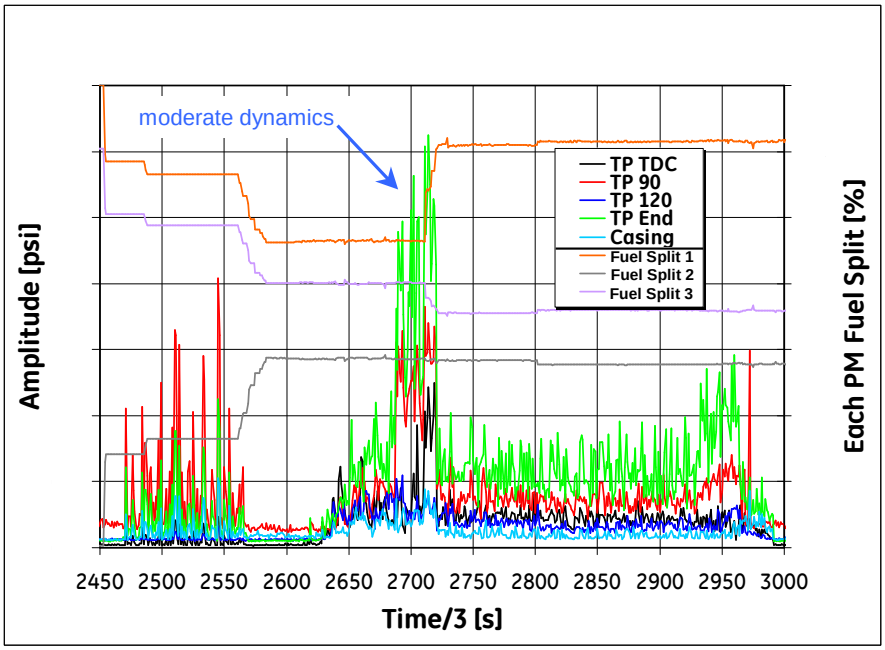

Figure 14: Fuel splits and peak amplitudes of a narrow range of high-frequency dynamics over a time period during operation of the RLN1 combustion system at reduced temperature (part load) conditions with high-hydrogen fuel.

RLN1 System Optimization

The RLN1 combustion system was optimized for NOx emissions, operability, mechanical robustness, and manufacturability. To achieve lower NOx emissions and combustor pressure drop, the outer round micromixer nozzles were switched to “full-coverage” sector fuel nozzles. This effectively eliminated the cap assembly, which had effusion cooling in the original RLN1. The full coverage micromixer therefore had reduced cooling flow and more air could be used for premixing. Because of this, the NOx emissions for the full-coverage RLN1 were the lowest seen to that point in the program. Figure 15 shows measured NOx from this configuration with ~20% of the inlet air replaced by pure nitrogen. This simulated the use of all remaining N2 from a plant’s ASU blended to the inlet air. The air side N2 reduced NOx and also was observed to reduce amplitudes of high-frequency dynamics.

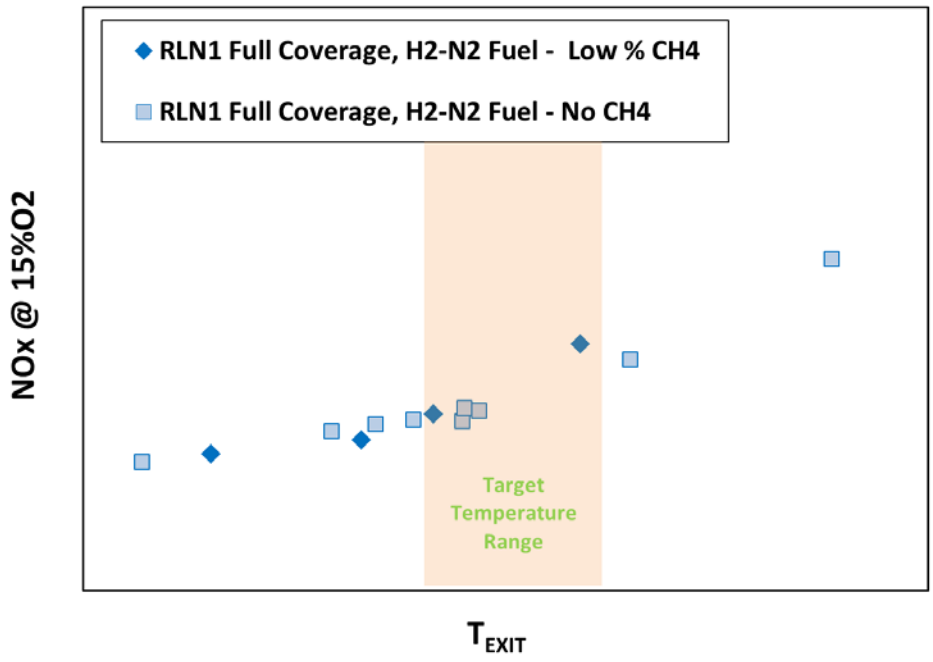

Figure 15: NOx emissions from the RLN1 full-coverage nozzles with ~20% of the inlet air replaced by pure nitrogen.

Several geometric features of the micromixer fuel nozzles were modified in an attempt to reduce high-frequency combustion dynamics in a few frequency bands. Figure 16 shows measured combustion dynamics amplitudes at two frequencies for the modified fuel nozzles compared to the original full-coverage RLN1 configuration. In both ranges, the modifications were successful in reducing dynamics amplitude.

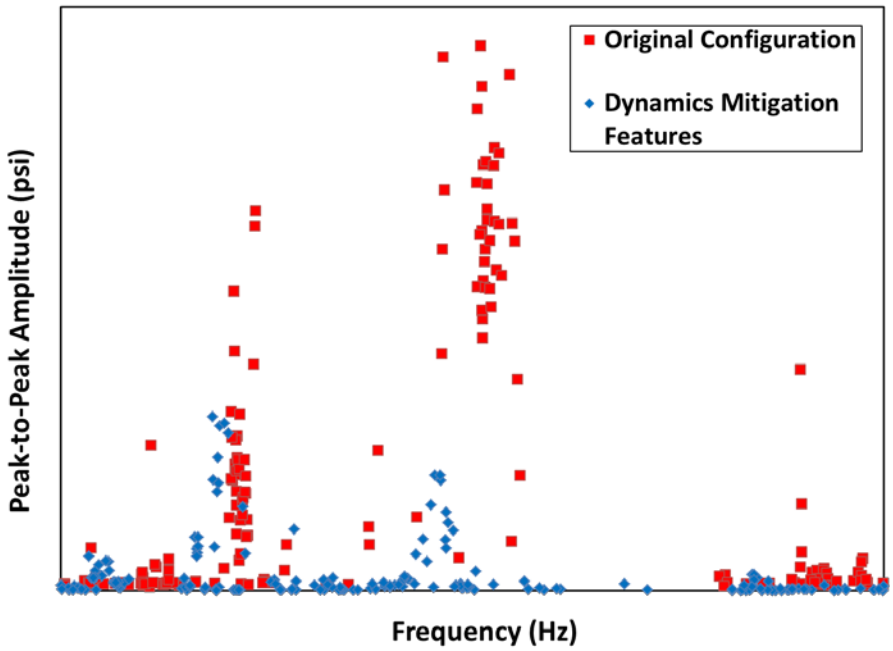

Figure 16: Dynamic pressure fluctuations measured in combustion liner at various points during operation of the RLN1 full-coverage nozzles on high-hydrogen fuel. The configuration with two key modifications reduced the amplitudes of the dynamics in most frequency bands.

RLN7 Combustion System

One significant benefit of the micromixer design is its scalability to a larger nozzle footprint without changing the basic premixing geometry within the nozzle. To demonstrate the ability to scale-up the hydrogen combustor design, the “RLN7” combustion system was developed and tested. Nominally, RLN7 had a 23 MW energy conversion rate at full load conditions. The system was based on the full-coverage micromixer fuel nozzles in the basic configuration as the RLN1. Because it had a larger head end diameter than RLN1, air flow was increased significantly, and this allowed a small residence time reduction to provide a NOx emissions benefit.

The RLN7 was tested several times with C-free syngas with very small percentages of natural gas in the fuel. NOx emissions were marginally higher than the smaller RLN1.

The RLN7 combustion system was also used for a rig test that provided accelerated thermal cycles on the high-hydrogen fuel nozzles. This was done in an attempt to expose any potential low-cycle fatigue issues with the components. The desire was to subject the fuel nozzles to the transient thermal boundary conditions they would see during a startup and shutdown cycle in a matter of minutes. In this way, the fuel nozzles would see numerous thermal cycles in one day of rig testing. Also, the fuel ramp-up and drop-off periods were much shorter than expected in the actual engine, and therefore these cycles were harsher than anticipated in the field.

Finite element analyses predicted that a steady state temperature field would be achieved about one minute after a switch. To be safe, the cycle was set at 90 seconds between fuel switches, and thermocouples embedded in the fuel nozzle surfaces indicated that this duration was acceptable to allow steady state to be reached.

A total of 90 full thermal cycles were executed during the rig test. No signs of damage were observed in the test data. Figure 17 shows the local adiabatic flame temperature transients (based on Fuel/Air) experienced during the testing. The temperature indicated by a thermocouple embedded in the surface of one of the cycled fuel nozzles is plotted in Figure 18 as a function of time. The repeatability of transient thermal boundary condition is evident. After the test, the nozzles were removed and inspected thoroughly, with no failures evident.

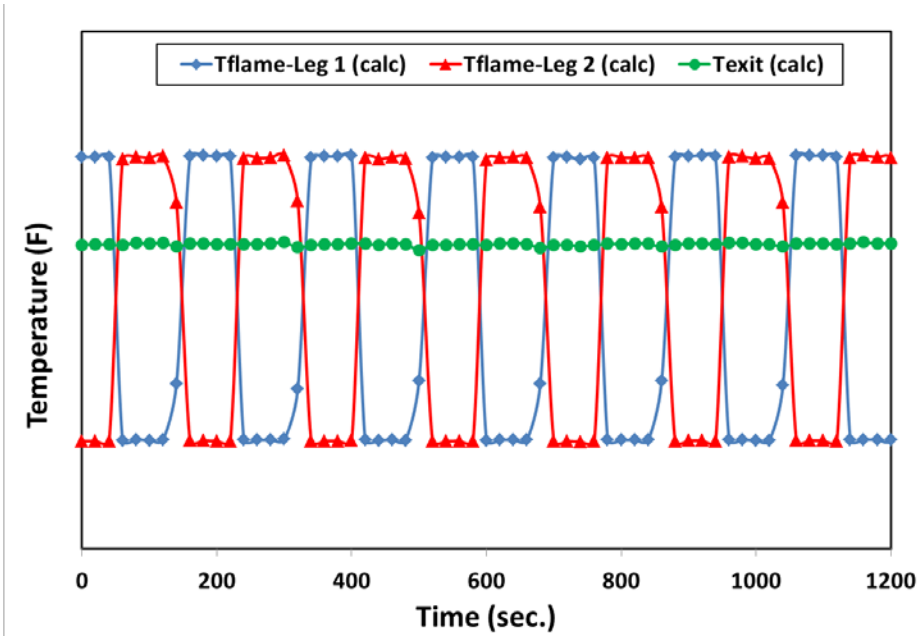

Figure 17: Local flame temperatures for cycled nozzles and combustor exit temperature over a portion of the RLN7 thermal cycle test.

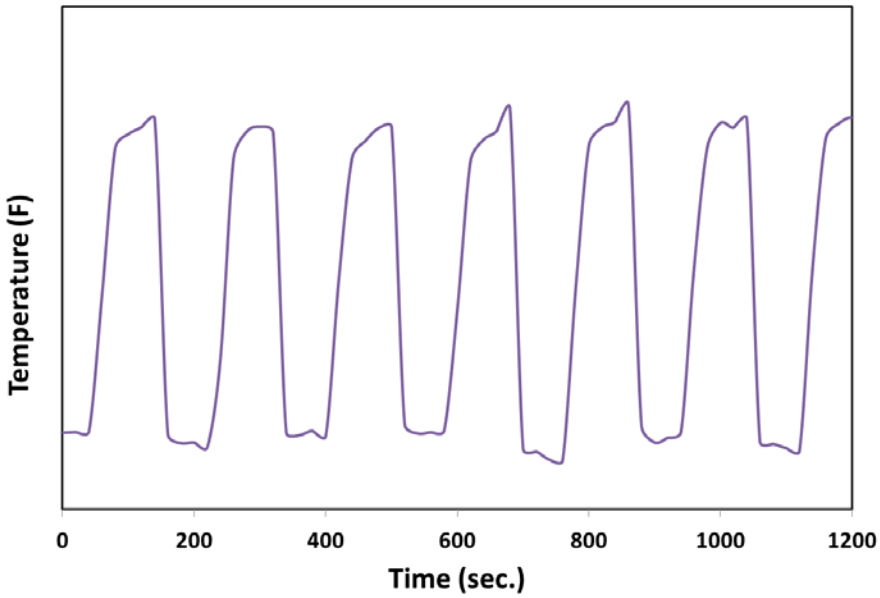

Figure 18: Temperature measured by a thermocouple on the surface of one fuel nozzle during the RLN7 thermal cycle test.

Final Fuel Nozzles and H2 Combustion Demonstration

A downselect was conducted for the prime path for manufactureable micromixer fuel nozzles based on considerations of durability, manufacturing quality, design flexibility, cost, emissions performance, and operability. Once the manufacturing method was selected, the design team implemented over a dozen improvements to the nozzles targeted at emissions, operability, and durability. These improvements were based on recent numerical analysis (computational fluid dynamics and finite element analyses for temperatures and part life prediction) and extensive testing (fired testing, thermal cycle test, shaker table testing) with these types of high-H2 nozzles.

In order to be able to do a single-test comparison of the performance of the final fuel nozzles and earlier versions, a test was performed where half of the outer fuel nozzles in the combustor were of the final style, and the other half were baseline nozzles manufactured earlier in the program. Testing was conducted on blends of natural gas, hydrogen, and nitrogen at over a range of combustor exit temperatures.

Figure 19 shows NOx emissions from the test as a function of exit temperature. The mixed set achieved the best full-load emissions measured in the program. The relative emissions performance of the final nozzles compared to baseline is shown in Figure 20 with NOx as a function of total (outer nozzle) fuel fraction sent to the final nozzles. When this fuel fraction is above 0.5, the new nozzles are running at a locally higher equivalence ratio (and flame temperature) than the baseline nozzles. Since the minimum NOx point is shifted toward the side favoring the final nozzles, these new nozzles have better emissions performance.

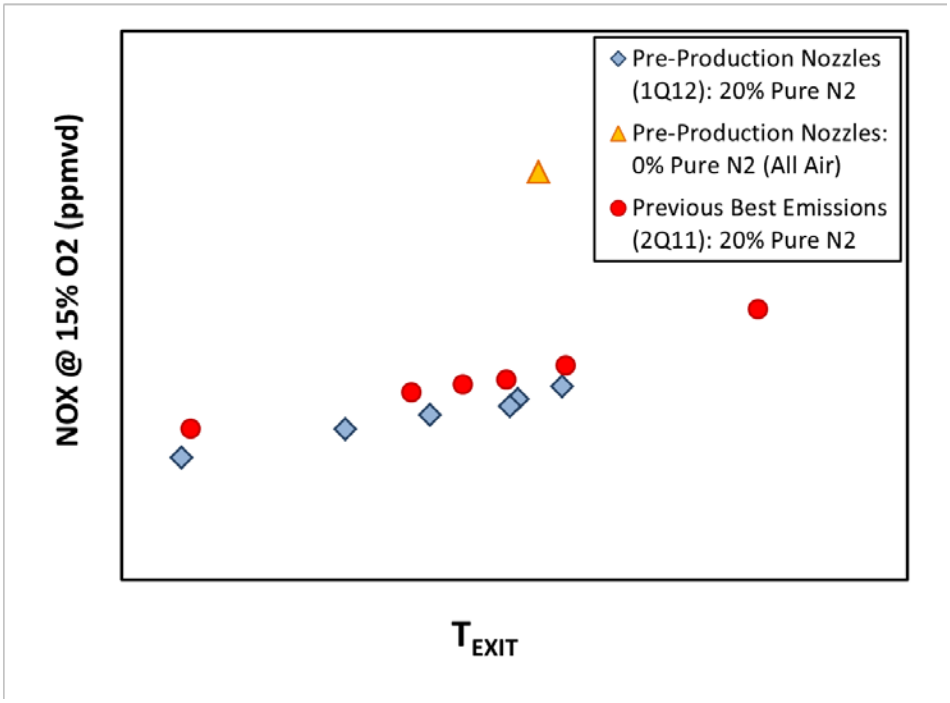

Figure 19: Corrected NOx emissions as function of temperature for final nozzle test and previous best case.

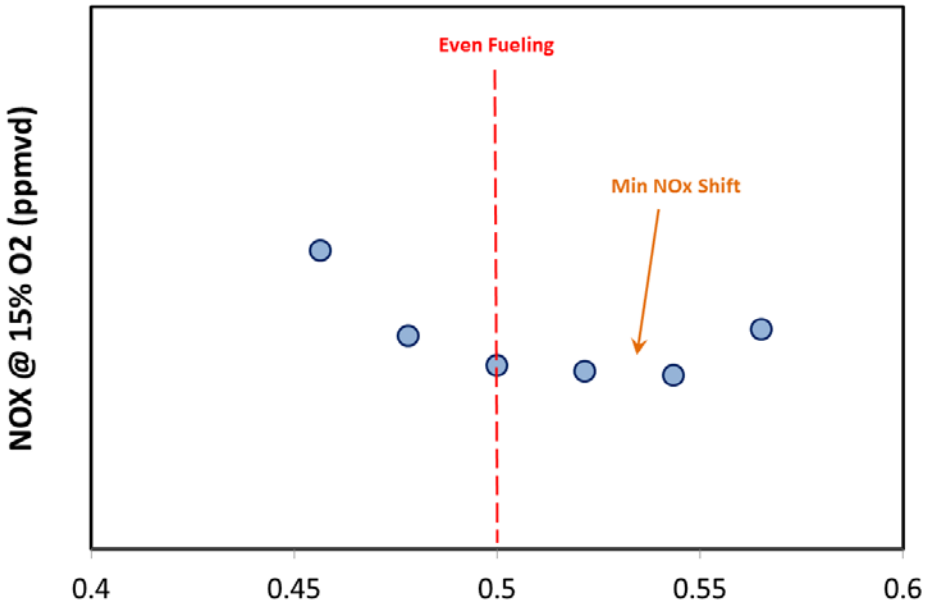

Figure 20: NOx emissions variation with fuel split to final and baseline fuel nozzles.

The effect of pure nitrogen at the combustor inlet on NOx emissions is shown in Figure 21. With a constant combustor exit temperature and a fixed H2-N2 fuel composition, increasing amounts of inlet air were replaced with pure nitrogen. NOx emissions corrected to 15% O2 falls nearly linearly from 0% to 21% pure N2. Part of the NOx reduction is a kinetic effect, while a fraction is simply attributed to the correction to 15% O2 as the air is diluted.

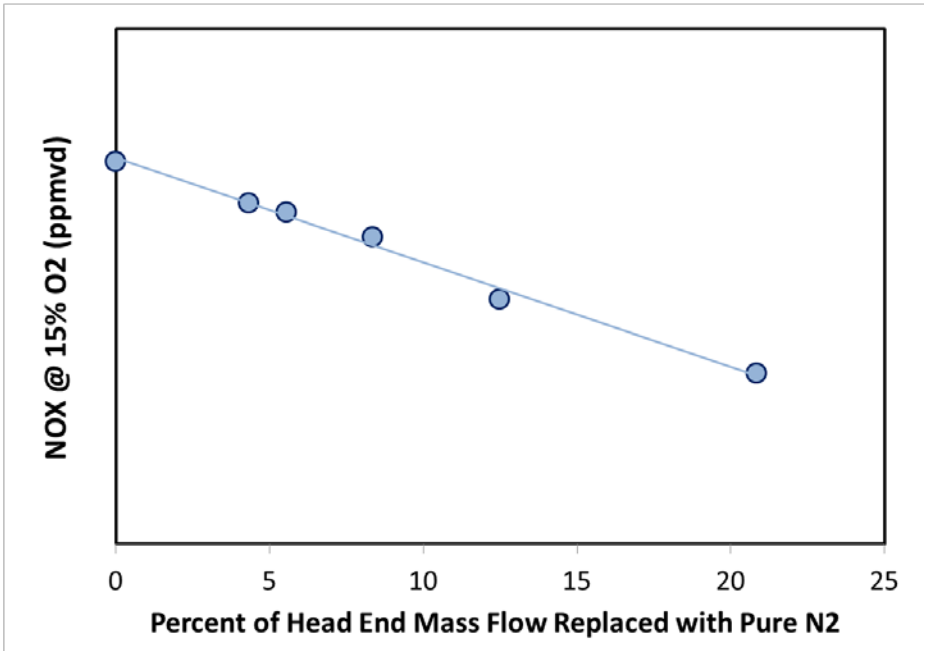

Figure 21: Effect of vitiated air (replacing air at the combustor inlet with pure N2) on NOx emissions for final nozzles with the H2-N2 fuel.

The final nozzles had no issues with flashback or thermal distress when operating on hydrogen fuel. Three thermocouples were installed in each of the new fuel nozzles. Indicated metal temperatures in the nozzles were monitored and recorded during the test. Data from the last hour of the test is plotted in Figure 22 for thermocouples in the three outer final nozzles. Despite pushing the local flame temperatures beyond their target with H2-N2 fuel, the temperatures remained consistent and well below critical levels. Overall, the final fuel nozzle test was very successful, with lowest the emissions recorded.

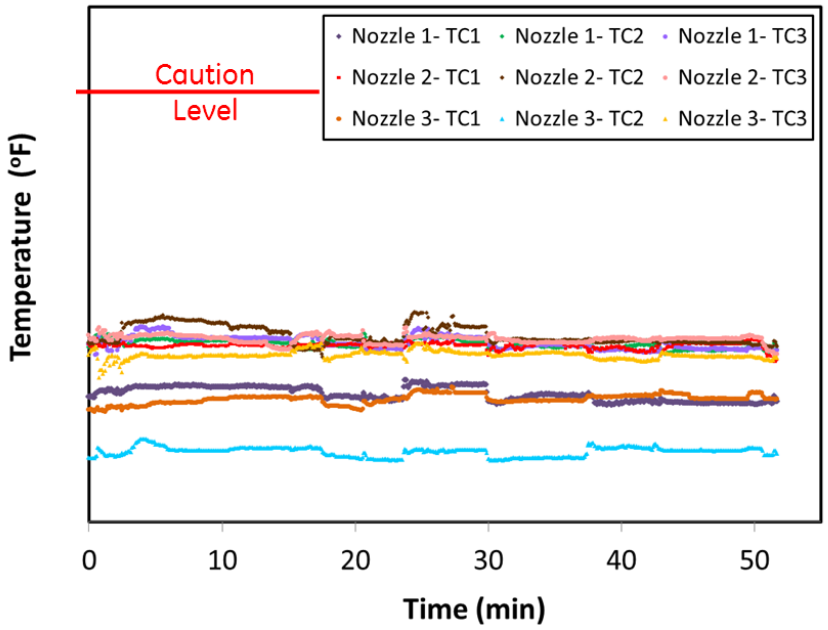

Figure 22: Temperatures measured by thermocouples embedded near the hot surface of the final fuel nozzles during an hour of testing with H2-N2 fuel.

Revised Final H2 Combustion Demonstration

A rig test of the RLN1 combustion system was conducted with variant final fuel nozzles. The test had three main purposes: 1) serve as a final validation of the emissions performance of the hydrogen combustion system, 2) determine if some relatively small modifications to fuel nozzle geometric parameters could deliver an improvement in operability, and (3) demonstrate a thermal imaging system for head end diagnostics. All fuel nozzles were of the "final" style. Half of the fuel nozzles had a "revised final" geometry. The remaining fuel nozzles were the original final hydrogen fuel nozzle that had been installed for two prior rig tests.

The combustion system was operated to full load with fuel blends of hydrogen, nitrogen, and natural gas. For part of the time at full load, the combustor was operated reliably with hydrogen as the only reactant in the fuel. This marked the third time the same set of original final fuel nozzles were operated on fuel that was 100% hydrogen (reactants) at advanced cycle conditions. The combustor exit temperature was operated up to conditions consistent with the "2015 H2 Turbine" cycle.

The revised final nozzles had a slight adverse effect on base load NOx emissions compared to the earlier final nozzle test, as seen in Figure 23. The previous test had the lowest emissions measured of any test on hydrogen fuel, and this test with half of the nozzles modified had marginally higher NOx emissions. With multiple tests achieving very low emissions levels it is clear that the fuel nozzle technology developed over the course of the program years is well-suited for this application and project goals.

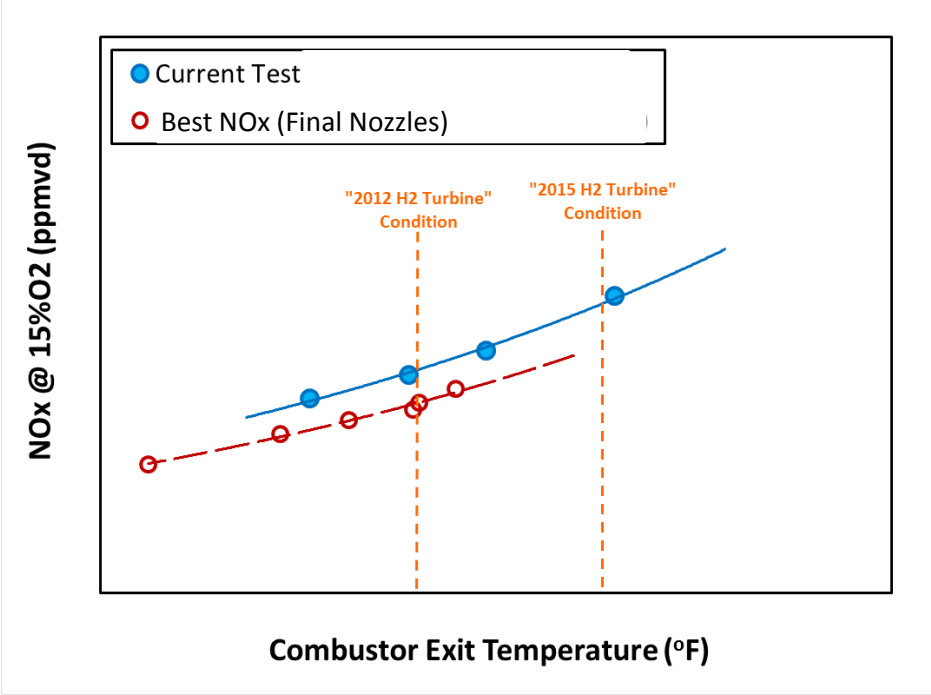

Figure 23: NOx emissions with high-hydrogen fuel over a range of combustor exit temperatures for the current configuration including revised final fuel nozzles and the original final configuration.

Advanced Combustor Architecture

The Advanced Combustion Architecture built upon the hydrogen combustion advancements that occurred in an earlier task in the program, Task 2.1. It further enabled firing temperature increases to improve efficiency while still delivering low NOx emissions, fuel flexibility, extended turndown, with nominal inspection intervals and current reliability levels. Three technology elements of such architecture were developed under this subtask.

Though initial tests showed promise, it took some time for the Architecture's emissions and pressure drop (dP/P) to reach parity with the baseline premixer. Through the work performed under the ARRA program the architecture was able to exceed the $NOx/T_{3.90}$ capability of the baseline premixer, while retaining the ability to burn greater than 50% hydrogen. In addition, it demonstrated more than three times the fuel Modified Wobbe Index (MWI) variation capability of the baseline premixer. The mechanical design went through much iteration.

Preliminary Technology Demonstration hardware was designed. In full can testing this hardware showed the performance benefits expected from conceptual design testing.

Advanced Combustor Integration

Advanced Combustor Integration went beyond the traditional bounds of the combustor. This part of the project focused on enabling greater integration between the combustion and turbine systems with the goal of increasing firing temperature and cycle efficiency.

Analytical combustor and turbine design tools were used to design multiple concepts. Conceptual designs were created and manufactured using additive processes. A multi-can cascade cold flow rig was built and used to evaluate the performance of the different concepts. Post-test data reduction was completed. Data was used to tune design models for future use. Based on the data and the modeling, the top integration concept was chosen.

Baseline Architecture

This project sought to deliver increased performance relative to the baseline architecture which is currently applied to F-Class Gas Turbines. The baseline architecture includes a combustion system based on the DLN2.6+ head end. In the baseline system the stage 1 nozzle, S1N, is a separate metal component that is cooled using compressed air that bypasses the combustion system. Seals are used to prevent air from leaking between the combustor and the S1N.

The baseline combustor architecture consists of a single flame zone fed with premixed fuel and air from six fuel nozzles arranged in a 5-around-1 configuration. Each nozzle utilizes a cast swirl vane structure to introduce fuel from internal passages into the compressed air-stream. The two streams are swirled and mixed prior to dumping into the combustion zone. It is necessary to provide significant combustor volume and residence time to allow any CO to fully oxidize to CO_2 before the end of the combustor. This traditional approach has delivered significant efficiency gains and emissions reduction over its time. Operability and emissions performance at higher operating temperatures and with more highly reactive fuels are limiting its expanded use. More advanced combustion architectures are needed to achieve the operating requirements in a high efficiency, fuel flexible, low cost, and reliable combustion system environment.

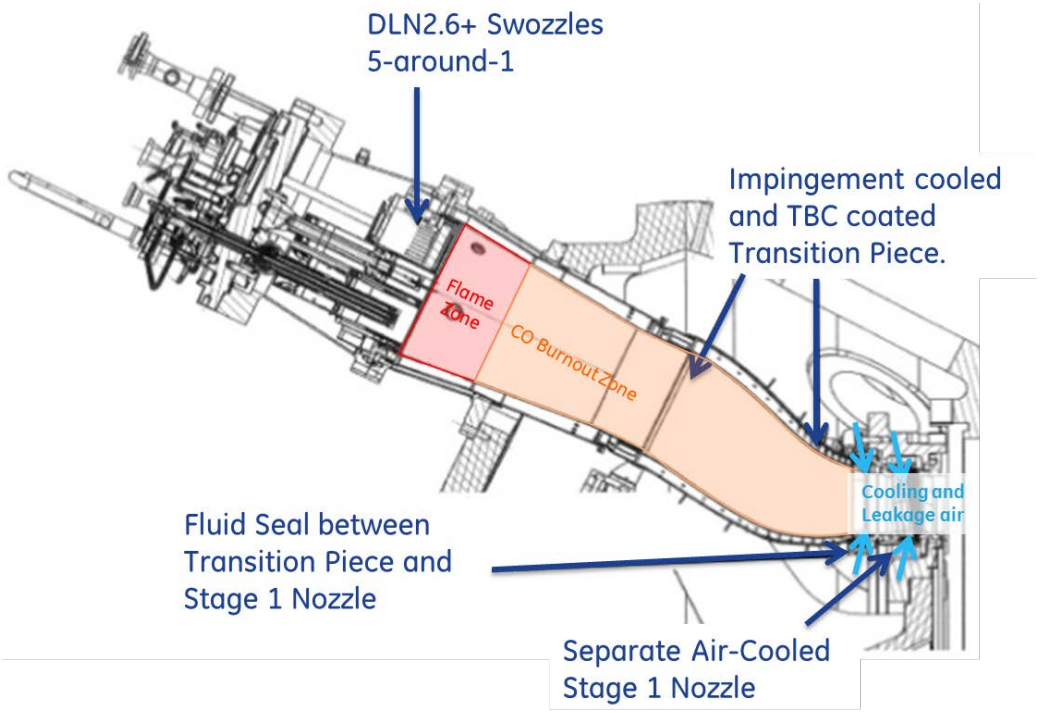

Figure 24: Baseline DLN2.6+ Combustor with Separate Air-Cooled Turbine Nozzle

Technology Elements of an Advanced Combustor Architecture
There are three technology elements developed for the Advanced Combustor Architecture under Subtask 2.6.1. Existing DLN 2.6+ hardware was leveraged to maximize hardware re-use and retrofit ability. Each technology element was first developed and tested separately. At key points the elements were brought together to test the overall system.

On the one hand, the hydrogen premixer's chief responsibility is to safely burn hydrogen. It has minimal need for residence time since hydrogen is highly reactive and there is no carbon in the fuel, and therefore no CO or UHC emissions at part load. The DLN2.6+ system on the other hand is driven by cost, durability, and turndown. Fuel flexibility and $NOx/T_{3.90}$ capability are important drivers for the baseline DLN2.6+ system; however they are coupled to the other parameters and cannot be independently optimized. The ARRA combustor fills a spot in the middle where there is a premium placed on $NOx/T_{3.90}$, but there can be little compromise on other parameters such as fuel flexibility and operational flexibility. The Advanced Architecture for the ARRA combustor uses the hydrogen premixer from Task 2.1 to deliver tolerance to reactive fuels, and pushes that component to higher $NOx /T_{3.90}$ performance.

Advanced Combustion Integration Concept
Subtask 2.6.2 was used to develop a method of integrating the combustor and turbine more closely with the goal of reducing cooling flows and increasing GT efficiency. Figure 25 is a sketch showing how the combustor transition pieces are adapted to do the turning and acceleration that would normally be done by the Stage 1 Nozzle.

Turbine design tools including 1D calculations and conjugate CFD were used to design the parts and predict possible performance gains. The main tool used for testing was a multi-can cascade cold flow rig.

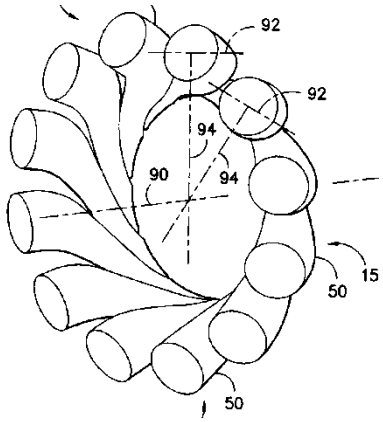

Figure 25: Transition Nozzle EP2660519A1

CFD Analysis
Component performance and durability evaluations were performed utilizing both non-reacting and reacting CFD. Test results were used to validate CFD and finite element analysis (FEA) models and establish baseline performance during concept design and evaluations phases.

Analytical methods and similar component field experience are used to predict mechanical performance and provide an expected durability.

CFD for the Advanced Premixer

There are engineering challenges specific to APM, such as fuel air mixing, and tube-to-tube fuel variation. The APM is new head end architecture in itself, and as such there are normal challenges that all head end architectures have to deal with such as achieving the target air distribution, efficient turning and conditioning of the flow, etc.

Single tube models were used to predict mixing quality and inlet dP/P. Various dimensions, fuel hole parameters, and other features were explored.

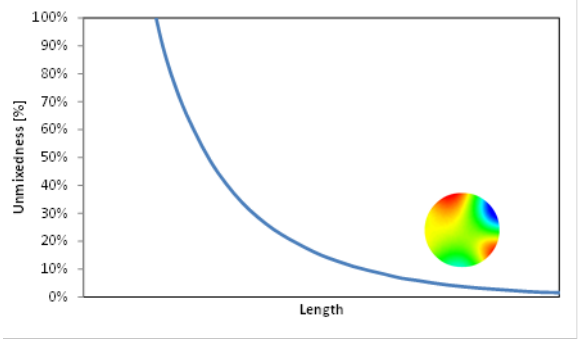

Figure 26: Tube Mixing Simulations

Fuel plenum models were used to predict fuel distribution between tubes, and to establish boundary conditions for FEA.

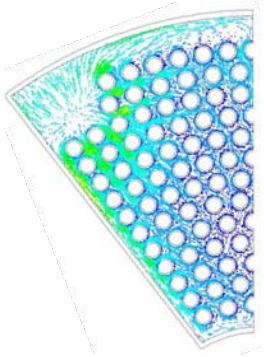

Figure 27: Fuel Plenum CFD

Upstream Air-side models to predict air uniformity and dP/P

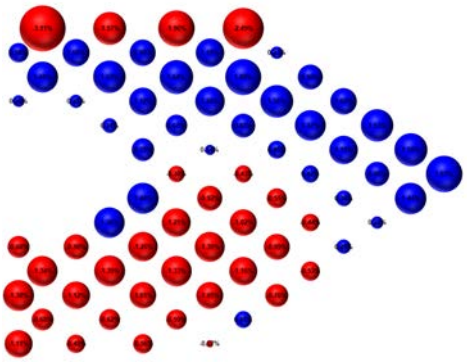

Figure 28: Upstream and Turning CFD

Reacting models of the combustion liner were used to evaluate the NOx performance of the system. The results were also used as boundary conditions for aft face thermal and FEA models.

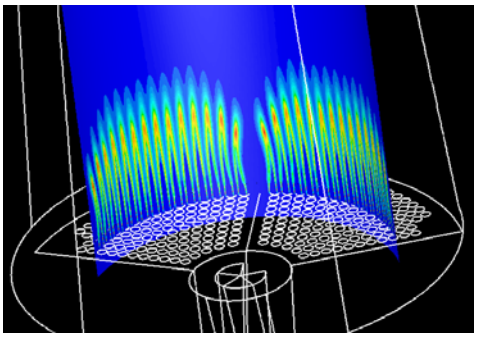

Figure 29: Liner Reacting Model

Conjugate models of the aft face were created in order to estimate the heat load and cooling effectiveness of either air or fuel cooling for the aft face.

Both RANS and LES models were performed to benchmark the CFD vs. measured data.

Advanced Combustor Integration

GE Proprietary turbine design tools were used to design combustor integration concepts for test. Key areas of interest were efficient turning and acceleration of the flow, as well as heat transfer from the hot gas to the walls of the component.

Finite Element Analysis

Finite element analysis was used to design and optimize technology elements. Studies included modal analysis of the basic structure and assembly, and individual sub-systems such as the mounting of premixing tubes. Component and system geometries as well as detailed weld and brazed joints were modeled and evaluated to predict durability.

Advanced Premixer

The Advanced Premixer (APM) technology benefited from multiple FEA studies focused on all aspects of the design from the basic mounting structure for reducing mean and alternating stresses, to detailed sub-models of individual braze joints as shown in Figure 30a and Figure 30b. Modal analyses were completed to tune the structure to avoid key rotor harmonics. Some of the basic sub-systems analyzed were the mounting, fuel plenum, air plenum, tube mounting, combustion face, fuel supply and fuel distribution plenum, and inlet flow conditioner. These studies were validated with experimental data from fired combustion tests or other mechanical methods in order to validate component and sub-component life predictions.

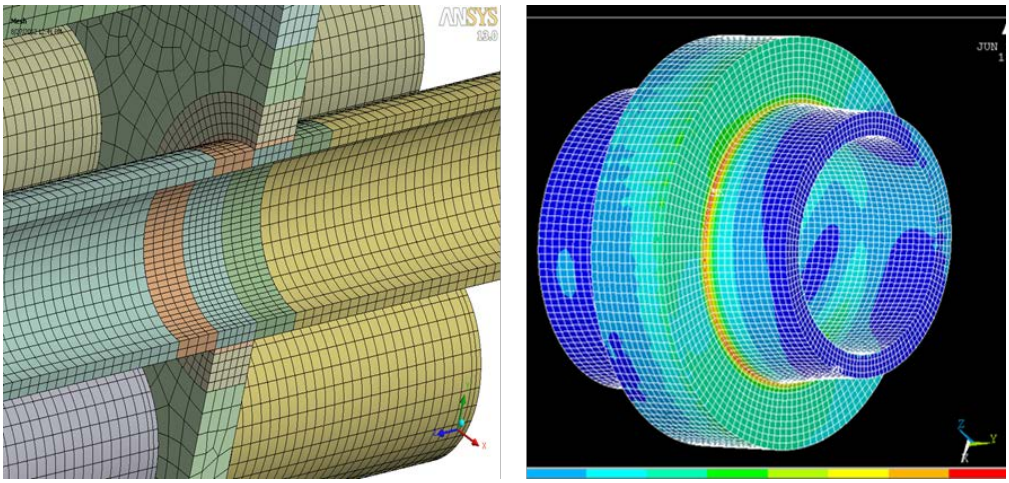

Figure 30: a) Mesh of individual tube b) Typical tube joint strain results.

Combustion Dynamics Analysis (CDA)

1D and 3D CDA tools were used to assess geometries for combustion dynamics. Use of 3D tools with rapid meshing allowed the team to do parameter sweeps analytically and understand trends faster. Figure 31 shows and example output from the 3D tool.

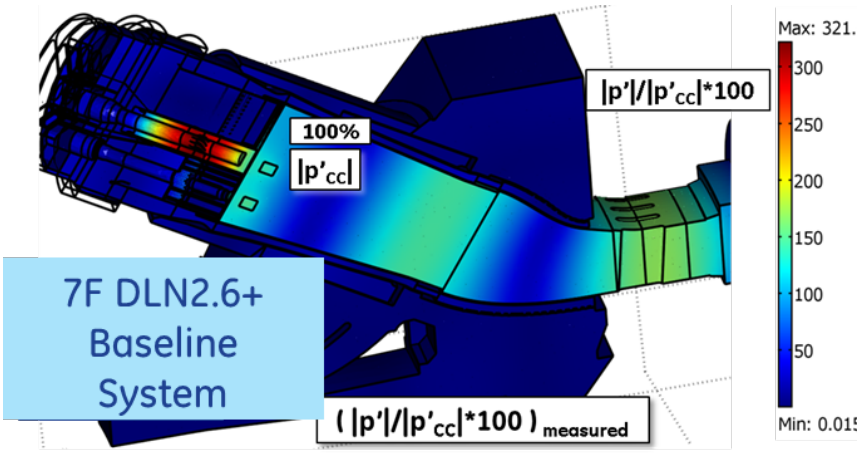

Figure 31: 3D CDA Example

Throughout the course of the program changes to the design were incorporated in order to keep the air and fuel sides in balance. Figure 32 shows as an example the dynamics outputs from two lab tests on the same hardware. Between tests a modification was performed that completely removed one of the key dynamics tones. The modification was suggested by the CDA model.

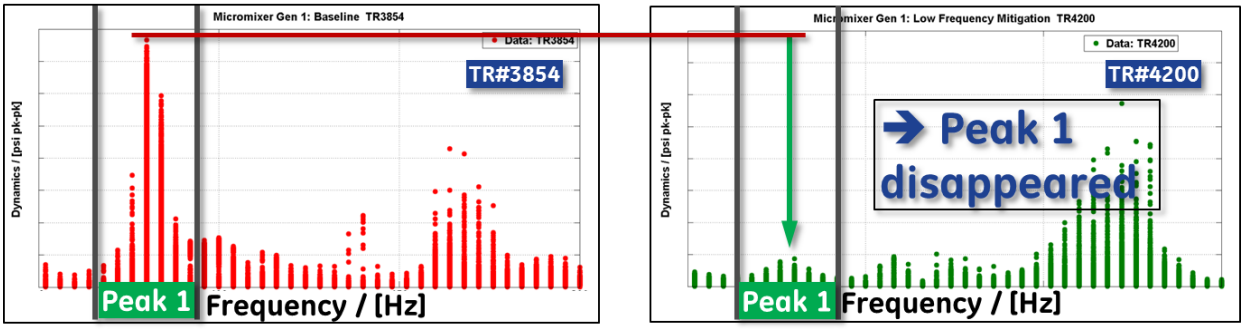

Figure 32: Lab Dynamics Showing Peak1 Removal

Kinetics Models

1D kinetics calculations were used extensively to guide the design and analysis of the CFD and laboratory data. Ultimately a framework of calculations was created to understand the impact of variations in both design and manufacturing.

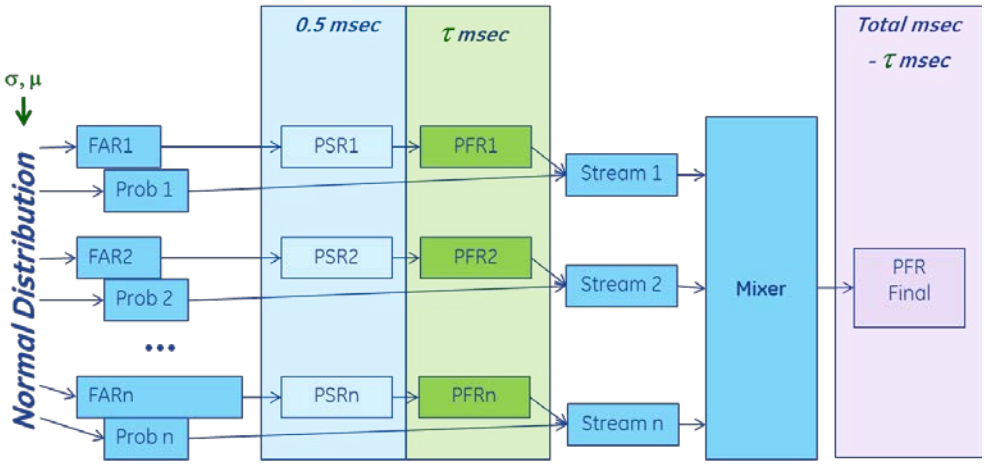

Figure 33: Chemical Reactor Network Model

Heat Transfer & Flow Network Models

1D heat transfer and flow models were particularly useful for the design of the hot face of the nozzles. 1D models were used to design each iteration. Calculations were mostly implemented in spreadsheets. Standard correlations were used, and when possible temperatures and heat transfer coefficients (HTCs) from CFD were applied as boundary conditions.

GTTL Single Can Fired Testing

The Gas Turbine Technology Laboratory, GTTL, in Greenville SC has the capability to run a single can combustor to full scale conditions for almost any machine. The types of tests completed varied widely throughout the development program. The majority of tests started out at full load conditions in order to establish $NOx/T_{3.90}$ performance. For selected configurations additional test time was devoted to assessing the system's ability to deal with varying fuel MWI by running a range of fuel compositions and temperatures. Some tests focused on part load conditions to establish Turndown/CO capability. Other tests established flashback/flame holding capability by running highly reactive fuels. Still others featured thermal paint to evaluate cooling effectiveness. Most tests featured natural gas, or natural gas doped to change reactivity or MWI. For selected tests liquid fuels were also tested.

Regardless of the type of test, there are some pieces of information that are gathered with every test. Combustor dP/P is measured in multiple locations. Exit profile can be inferred from thermocouples (TCs). Component metal temperatures are recorded, and air split information can be calculated based on static and total pressure information. Overall operating boundary conditions are always recorded (air and fuel flow rates, pressures, and temperatures).

In a relatively short test plan the performance of the new architecture was established in all aspects, on multiple fuels. The hardware constantly matured which caused changes in performance, but overall parameters were constantly improved.

Ignition Testing in Zeeland MI

Ignition performance was established through extensive atmospheric testing. An ignition test fixture was built and tested at Woodward's Zeeland Michigan facility.

Figure 34: Zeeland LF Ignition Testing

Global Research Center Single Nozzle Rig

Single nozzle tests were performed at GE's Global Research Center in order to understand the fundamental behaviors and impacts of various geometric parameters. This testing did show that additional capability can be coaxed out of the APM by changing some geometric parameters. For this project the potential for additional performance was overshadowed by the need to advance the APM architecture. The recommended geometric parameters will be implemented in a later incarnation of the APM.

GTTL Mechanical Laboratory

The GTTL Mechanical Lab houses a number of test fixtures. The shaker table was instrumental to this effort. The team ran shaker table testing to get natural frequencies for individual nozzles and for assembled systems. Parts and full assemblies were shaken to failure to establish durability and compare to analytical predictions.

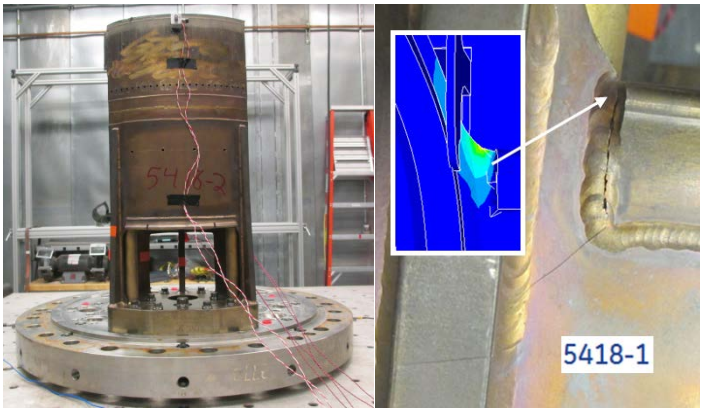

Figure 35: (a) Premixer on shaker table (b) Crack observed

Manufacturing Methods

Both traditional and advanced manufacturing methods were used to fabricate prototypes. Through the conceptual, preliminary, and detailed design phases the APM configurations were predominately fabricated using multiple brazed interfaces. Cut-ups, leak tests, and other forms of inspection were developed to ensure that quality parts could be produced for eventual production.

As each technology evolved more additive manufacturing processes were utilized in the fabrication of test components.

There are several formal milestones that completed as part of subtasks 2.6.1 and 2.6.2. Table 1 summarized those formal milestones.

Table 1 – Project Formal Milestones

Quarterly	Planned Completion Date	Verification Method
Conduct laboratory screening tests on individual advanced combustor architecture technologies in preparation for a down selection.	3/31/2011 (Complete)	Quarterly progress report documentation of lab test results and manufacturing trials
Select premixer design and advanced combustor architecture for engine test.	3/31/2012 (Complete)	Quarterly progress report documentation of rationale for decision
Identify leading advanced combustion integration concepts based on rig testing.	6/30/2012 (Complete)	Quarterly progress report documentation of test results
Complete comparison testing and selection of best manufacturing technique for near-term production of advanced combustors	12/31/2013 (Complete)	Quarterly progress report documentation of test results

Advanced Premixer Conceptual Design and Testing

The conceptual design phase was intended to transition the APM from hydrogen centric to F-class centric while retaining a high degree of tolerance to reactive fuels. Eight sets of hardware were designed during the two years of conceptual design phase. Table 2 summarizes the hardware designations, the focus of that hardware, and their successes and shortcomings.

Table 2 – Advanced Premixer Configurations

Iter	Focus	Accomplishments	Challenges	Tests
Gen 1	dP/P, NOx	Lower dP/P than round APM nozzles	NOx, flame stability, hot aft face	7
Gen 1 DF	Early Liquid Fuel Test Vehicle	Liquid fuel dynamics good LF Emissions ≅ baseline premixer	Dynamics, fuel leaks from plenum	4
Long Round	NOx	Excellent NOx Reasonable dynamics	dP/P (expected)	3
1.5.1	NOx		NOx (leaks & Control of variation)	1
1.5.2	Flame Holding, Larger Tubes	NOx and dynamics improved significantly over Gen 1	Only run as a NOx test, never for flame holding as intended	1
1.5.3	Flame Stability Rainbow Test	Low temperature stability enhanced in rainbow testing	Incremental dP/P increase	1
1.5.4	NOx, dynamics, LBO	NOx and dynamics improved significantly over Gen 1	Aft face still hot	8
1.5.7	Build on 1.5.4 gains	NOx further improved vs. 1.5.4 Dynamics better than 1.5.4	Internals are complex	2
1.5.5	Manufacturing	Easier to manufacture but with 1.5.7 performance Aft face temperatures improved		2
1.5.6	DMLM Plenum		Never tested	Stopped

Generation 1 or “Gen 1” hardware existed prior to the start of ARRA, but was frequently used as a vehicle to evaluate dynamics mitigations, sealing upgrades, etc. in order to test and learn faster. A dual fuel version of the Gen 1 was created in order to allow the current liquid fuel cartridge to pass through the APM in order to perform liquid fuel screening tests.

In the end the 1.5.7 and 1.5.5 premixers had NOx/$T_{3.90}$ and operability that was significantly better than the baseline premixer. Yet they still retained the ability to burn greater than 50% hydrogen from the original hydrogen premixer. The sections below communicate the accomplishments achieved during the test program. Due to limited test time and considerable test expense every configuration could not be tested for every parameter. As a result performance numbers quoted could be from any of the 1.5.4, 1.5.7, or 1.5.5 hardware.

Figure 36: Combustor Camera Image

Reducing NOx Due to Fuel-Air Mixing and Distribution

Design concepts were developed to decrease unmixedness at the exit of the architecture while keeping pressure loss low. Shown below in Figure 37 are results predicted from CFD for unmixedness as a function of premixer length for different fuel injection hole size. With increasing fuel hole size, pressure ratio to inject fuel decreases. It was noted that beyond a certain L/D ratio, hole size does not have much influence on the mixing.

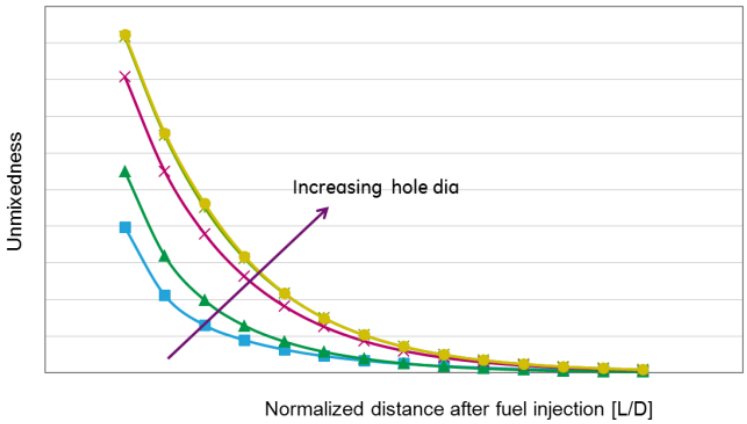

Figure 37: Unmixedness vs. Tube Length

The quality of fuel-air mixing is known to have an impact on the amount of NOx produced by a premixer. Generally it is desirable to be as close to perfectly premixed as possible, unless limited by another boundary such as LBO or combustion dynamics. Mixing calculations were performed for a number of tube and fuel holes geometries. The fuel-air profile from the mixing model was mapped to a reacting model to understand the impact of fuel-air mixing on NOx emissions. Figure 38 shows the NOx penalty vs. unmixedness for a number of mixing simulations. Based on this information an upper limit was set for unmixedness.

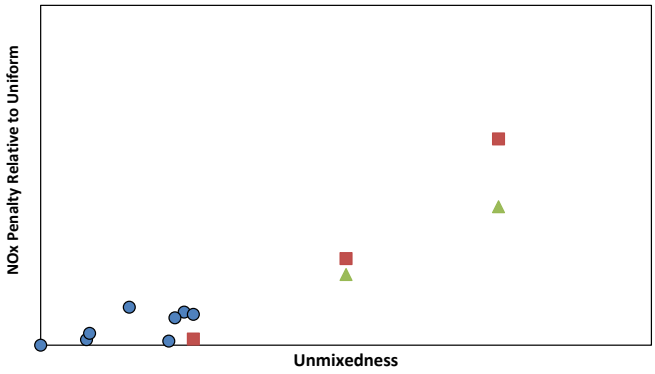

Figure 38: Impact of Mixing Quality on NOx

Another factor that determines NOx performance is the distribution of fuel and air in a multi-tube bundle. Additional CFD studies were used to quantify this effect. Once the effect of variation was understood, appropriate limits were set for design and manufacturing use. Fuel hole and tube air-side area variations contribute, as do variations due to the design of the fuel plenum and air-side inlet flow conditioner. By bringing all of these sources of variation under control, added NOx penalty can be avoided.

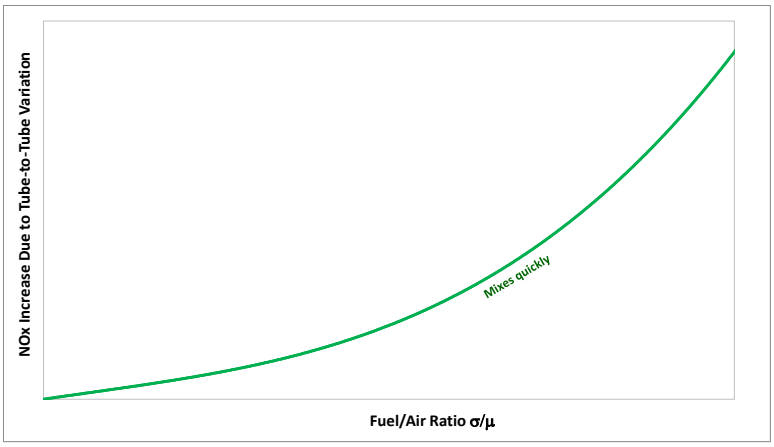

Figure 39: Impact of Tube-to-tube Variation on NOx

Throughout the Conceptual and Preliminary design phases the NOx capability of the APM improved significantly. Figure 40 compares the NOx/$T_{3.90}$ capability for the ARRA APM to the baseline premixer. The baseline premixer performance is shown at equivalent residence time and conditions. The APM hardware was tested over a range of conditions; however data is represented as the maximum temperature capability at a fixed NOx target for the same corrected conditions. The final 1.5.7 APM showed a large increase in capability vs. the baseline premixer. The 1.5.5 was very similar in capability but with less internal complexity.

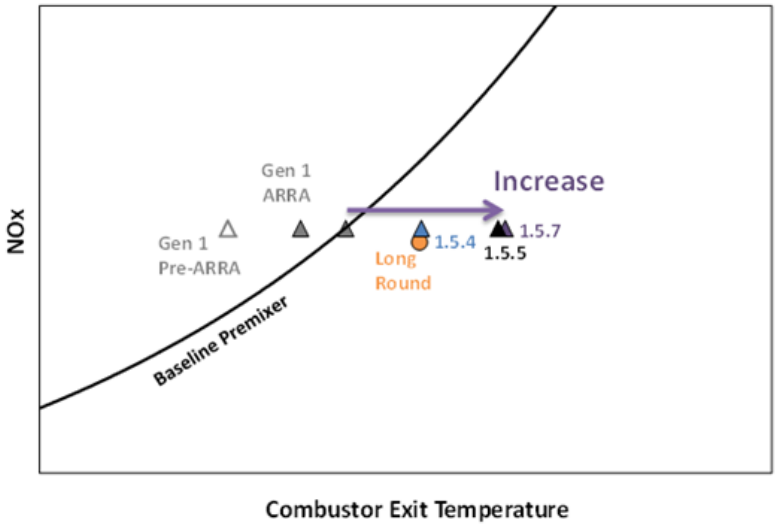

Figure 40: NOx/$T_{3.90}$ Gains for Conceptual APM Hardware

Manufacturing Studies

Initial plenums were constructed using traditional methods available at the time. Based on the trials a manufacturing process was chosen for large scale production. Figure 41 shows some examples from destructive testing.

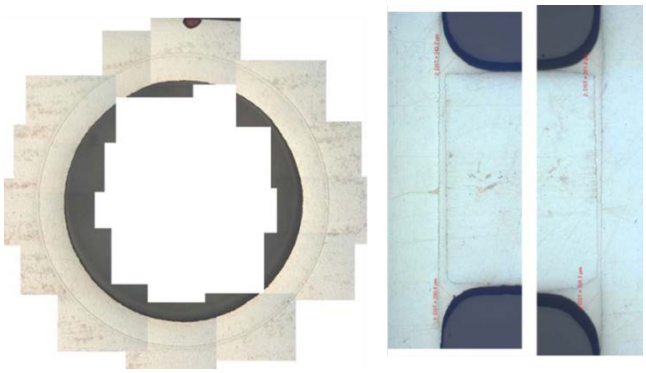

Figure 41: Braze Quality

Additional studies were completed to understand the repeatability and accuracy associated with making fuel holes in the tubes. Multiple methods were explored.

Operational Flexibility

Evaluations included both flame holding/flashback testing as well as an evaluation of the combustion dynamics as the fuel composition was changed. The baseline fuel is hot and predominantly methane. The fuel was doped with propane to increase the fuel MWI to look for elevated combustion dynamics. To go in the other direction the fuel was doped with nitrogen to decrease the MWI. Figure 42 shows a comparison of the Architecture to the baseline premixer. The baseline premixer has two peaks that are minimized at nominal fuel MWI. There is a range of MWI where the combustion dynamics are below acceptable levels between those two peaks. Outside of that range combustion dynamics are too high for continuous operation. The Architecture is able to run over a much wider range of fuel MWI with no increase in combustion dynamics. Additional MWI range can typically be gained by changing fuel splits. This plot, however, was constructed using data points where the fuel splits and exit temperature were held constant.

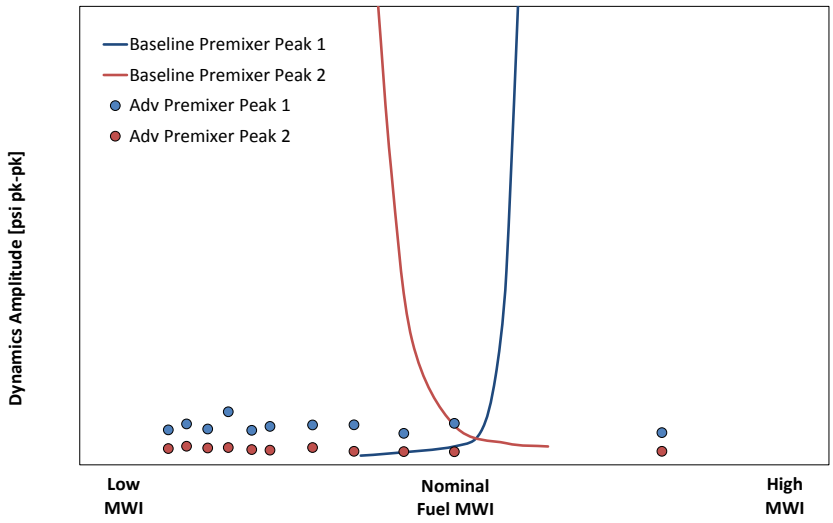

Figure 42: MWI Capability

Multiple configurations were tested for tolerance to fuel reactivity. Velocity and hydrogen content in the fuel were varied until flame holding or flashback occurred. Figure 43 shows a full-can test in process. The image was captured while the flame was downstream of the tubes with greater than 50% hydrogen in the fuel. The allowable hydrogen limit of 50% does represent a significant decrease from the hydrogen premixer which can operate at nearly 100% hydrogen, but is still several times more hydrogen than the baseline premixer can tolerate.

Figure 43: Full-Can Reactivity Test Image

Another aspect of operational flexibility is CO/Turndown. CO is at a low single digit ppm level at moderate and high temperatures. Below a certain threshold temperature the CO will increase

rapidly from single digits to thousands. The CO threshold was experimentally determined for the APM.

Combustion Dynamics
Combustion dynamics were designed out of the system by changing hardware parameters. Figure 44 shows a frequency-amplitude spectrum from an entire day of testing. This includes ignition, transients, full load operation, part-load operation, MWI sweeps, etc. This test was very quiet. The red line indicates allowable amplitudes below which mechanical damage is unlikely.

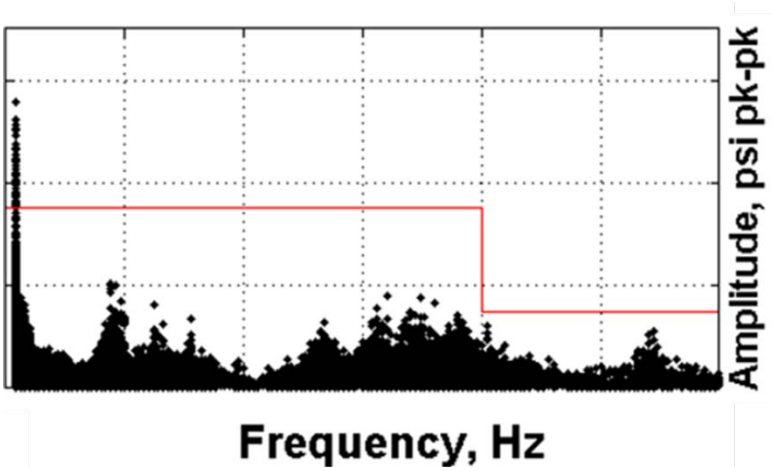

Figure 44: Frequency Amplitude Spectrum from Lab Testing

Liquid Fuel Performance
Liquid fuel performance was screened using available APM hardware. Initial tests used the Gen 1 dual fuel premixers; however as additional hardware became available liquid fuel testing generally used whatever advanced premixer was the best natural gas performer and was available at the time.

Test data provided confidence that with modification to the initial configuration, the APM is capable of starting and ramping up to full speed no load condition with good combustion efficiency on backup fuel.

Ignition Performance
Liquid and Gas ignition testing was conducted using a single APM sector nozzle in an atmospheric test stand. Igniter location was varied both axially and radially to identify optimum location for both gas and liquid ignition.

Figure 45 shows fuel air ratio versus premixer exit velocity at the optimized igniter location for gas fuel testing. The red diamond symbol indicates no ignition whereas the green indicates successful ignition. The blue dashed vertical lines indicate the velocity at the exit of the pre-mixer at conditions corresponding to 12% and 25% engine speed. The testing provides confidence that the APM is capable of providing robust ignition for the engine at the desired engine speed.

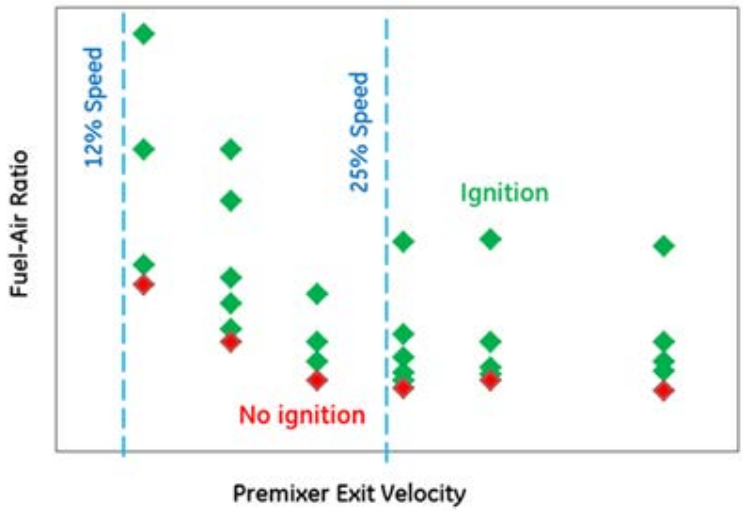

Figure 45: Gas Fuel Ignition Data

In Figure 46 comparison of fuel to air ratio at ignition are shown for different liquid fuel injector designs tested with an APM. These injector designs encompassed two different flow number and two different cone angles. As can be observed from the figure, the liquid injection systems (blue circles, red diamond, blue open squares) when integrated with the APM ignite at lower equivalence ratios than when tested with the baseline premixer (black asterisks). The liquid nozzle denoted with “FN-1, CA-1”, performed best with the APM.

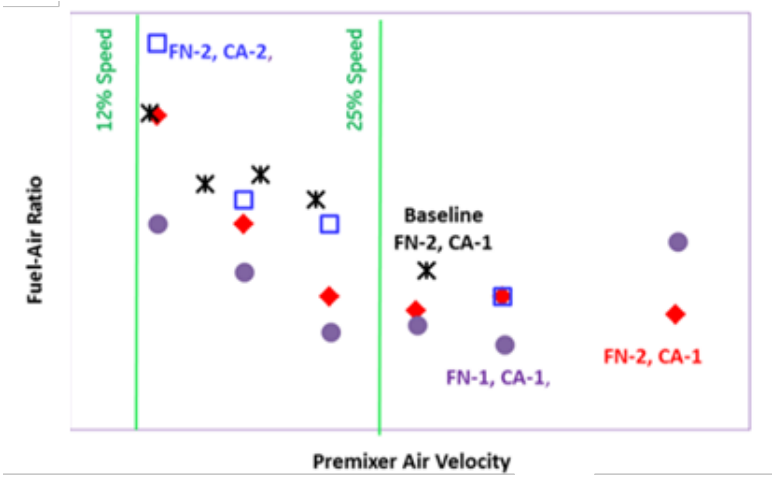

Figure 46: Liquid Fuel Ignition Data

Subscale Testing at GRC

Test cell 7 at the GE Global Research Center was used to test APM geometries at sub-scale. Key dimensions were altered in order to determine their impact on NOx, CO, and LBO. Initial testing used a rig capable of running 1 lb. /sec through the premixer. In 2013 the rig was scaled up to 5 lb. /sec.

Figure 47 shows NOx versus exit temperature for several key embodiments of “A” and “B” series premixers that ran in the 1 lb. /sec rig. Results from “A” & “B” series are also compared to the results obtained for the Small Scale “SS” configurations. Embodiments SS1 & SS2 were smaller in geometric scale than the embodiments tested in the A & B series. These different embodiments were designed with different geometric parameters. All these embodiments were tested with perfectly premixed mixture of fuel and air to decouple geometric parameter effects on NOx from premixing. Figure 47 shows that as relevant Reynolds Number ratio was increased, NOx decreases for the same flame temperature. The data suggest that by choosing geometric parameters to increase relevant ratio of Re number will lead to decrease in NOx emissions at the same exit temperature provided same premixing can be achieved.

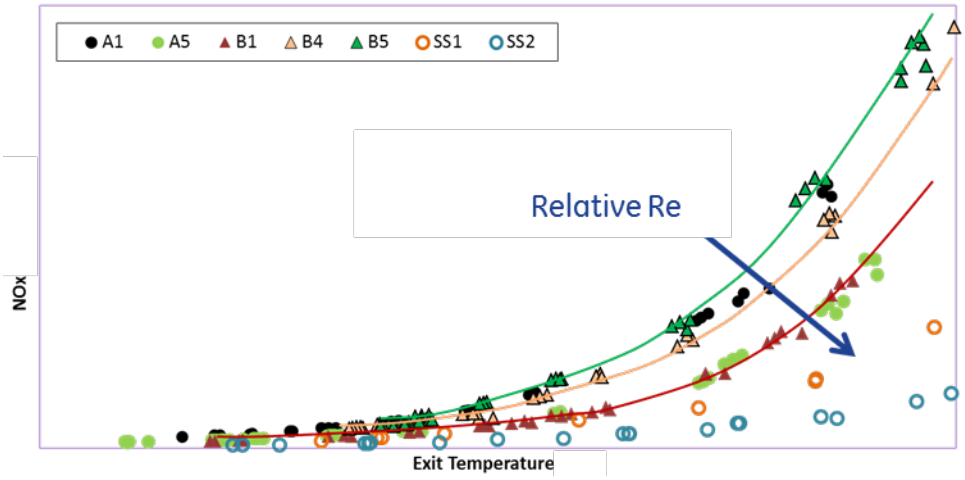

Figure 47: NOx Emissions from GRC Subscale Testing

Important design parameters were also identified for CO reduction. Figure 48 shows CO emissions vs. combustor exit temperature for the “A” series of configurations. A1, A2, and A5 provided significantly lower CO emissions compared to A3 and A4. A4 is closest to the baseline APM. CO emissions show a sensitivity to key design parameters.

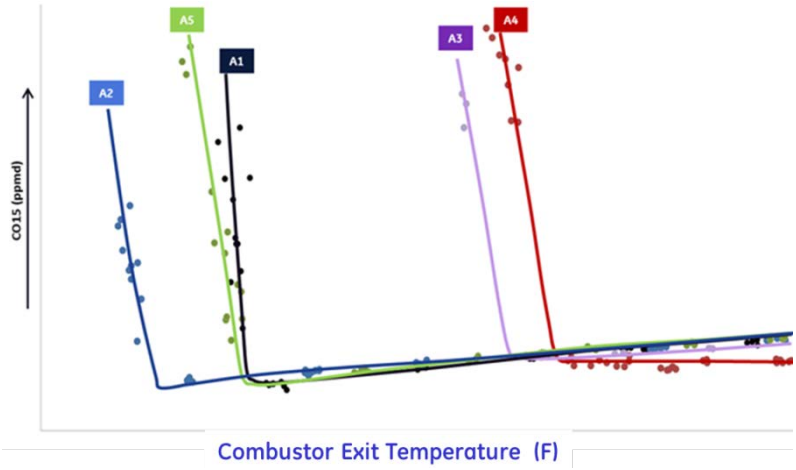

Figure 48: CO Emissions from GRC Subscale Testing

When GE uprated the rig to 5 lb. /sec it was renamed it the “Staged Injection Rig”. The rig is capable of running an Advanced Premixer with Staged Injector together at full scale conditions. Other updates to the rig include enhancements to the traverse system; several components upgraded for mechanical durability and sealing, and additional passive dynamics mitigations. The dynamics mitigations have allowed the rig to run over the full range of conditions and pre-mixer dimensions without the dynamics that limited earlier experiments.

In total, eleven configurations were tested covering a range of premixer dimensions. Emissions and LBO derivatives have been established for key dimensions. These derivatives indicate that the key dimensions of the current production-ready APM configuration can be further optimized for additional performance. The Next Gen APM is closer to the optimal configuration, but can still benefit from the experimental derivatives.

Durability

High Cycle Fatigue, HCF, testing was performed at different stages of development. The APM was evaluated at three different stages of development: a first prototype design, 2nd iteration prototype, and then as a complete head-end assembly.

Durability analysis and testing were conducted throughout development to establish robustness and life of the design. Conjugate CFD and FEA were completed for the first prototype design to establish design capability and to identify design features that are at risk of high stresses. To establish infant mortality rate for the first design, shaker table tests were conducted for the APM. These tests were started initially with 1g force at a dwell time of 10 minutes. The force was then incrementally increased by 1g until the test facility capability was reached. The design survived 8g force level at a dwell time of 10 minutes. Initially tests were not conducted beyond a dwell time of 10 minutes for each g force. This dwell time was initially deemed sufficient for establishing an acceptable infant mortality rate. Test severity increased until the first prototype cleared 2 Million cycles for a specified loading prior to crack initiation at double the target load. Crack propagation was arrested after an additional 1 million cycle.

The 2nd iteration prototype demonstrated performance well beyond acceptable limits for a single nozzle component. The APM head-end assembly was tested to simulate infinite life at each

defined load increment. Prototype hardware demonstrated 2 times the required capability defined for the full engine demonstration.

Low Cycle Fatigue: Preliminary analysis and testing showed the hot face and fuel plenum as the key joint areas of the advance pre-mixer at risk of premature low cycle fatigue failure. New cooling schemes and compliant joint designs were developed to address these risks. Some of these improvements were implemented into the 1.5.5 design. The fuel plenum thermal and structural analysis was used to identify and improve the design until the brazed configuration reached acceptable limits.

Direct Metal Laser Melted (DMLM) was an alternate manufacturing approach that opened both durability and design opportunities not achievable with conventional manufacturing.
Analysis and testing an early APM with thermal paint revealed locations of high temperature and potential thermal distress, driving design changes implemented into 1.5.4 through 1.5.7 prototypes. Testing showed reduced hot face temperatures.

DMLM Fuel Plenum
During the Conceptual design phase for the APM there were challenges encountered in creating the plenums using conventional manufacturing techniques. Even though the effort was ultimately successful, a project was initiated to develop an alternate production process using DMLM. Changing to a DMLM process required certain geometry changes to facilitate the build process, remove powder, post-process the green parts, etc.

Material properties were gathered for the DMLM process from test samples built on DMLM machines. These samples are of the same material and were built with the same machine parameters used for initial part build.

Flow testing of an alternative prototype configuration for the advanced pre-mixer concept was completed. Structural analyses of this concept showed the concept was viable for production. Various settings were explored through the additive manufacturing builds and low cycle fatigue (LCF) testing of these samples was completed.

More than 10 DMLM fuel nozzle core parts were built using DMLM, in-house and at suppliers, to determine best-practices related to design features for build success, excess powder removal, post-processing, and inspection.

Results of additive manufacturing advanced combustor structural analysis, demonstration builds, inspections, and flow testing showed that additive manufacturing techniques are a viable manufacturing method for this combustion technology.

Production Ready APM
From a cost and durability standpoint the APM was not yet ready for high volume production. The intent of this project was to further mature the mechanical design of the APM developed under ARRA to the point where it had an acceptable cost and manufacturability position.

The hardware for this part of the program evolved to address several themes:
- Structural Mounting Move to a DMLM fuel plenum
- Additional NOx capability Dynamics Mitigations

The development processes followed a similar path as the previous APM development. In the beginning the right test stand and manufacturing processes were not available, so a Conceptual design was procured to get some experience quickly. The learning from this Conceptual design set was built into the Preliminary design hardware to test on the right test stand at the right conditions. As the issues were understood, a number of candidate improvements were built and tested using the Preliminary design hardware. In the end the candidate features were down-selected and the updates worked into a detailed design that was put through its paces.

Production Ready Conceptual Design

The Conceptual Production Ready design work included new premixers and combustion cap. Detailed analysis was completed for items that were critical to completing initial lab testing. This analysis included tolerance stack ups, CFD, and structural analysis. Initial fired testing of the Conceptual Production Ready hardware was completed in a test. In that 16-hour fired test the system demonstrated good operability and emissions, matching or exceeding the projections for the prototype. Aft face temperatures were high enough in fired testing to require additional design work to lower the temperatures.

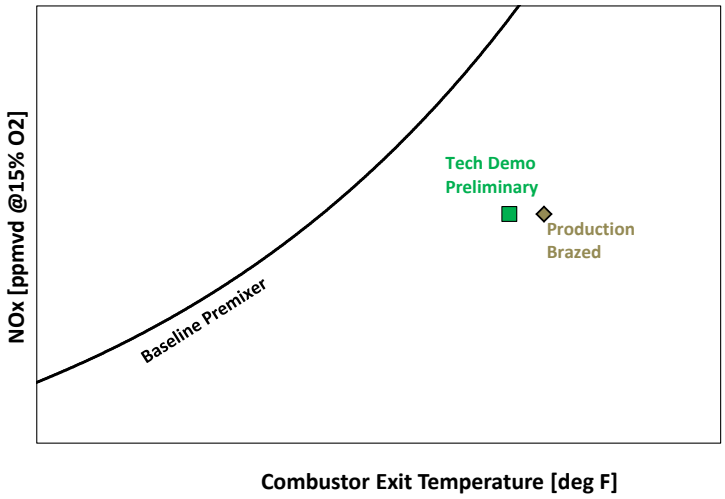

Figure 49: Conceptual Production-Ready APM

As a follow-on test, the Conceptual Production Ready APM was prepared for a fired rig test in the target test stand. A flow test of the complete head end was conducted to measure effective area as a function of pressure drop. This data served as a quality check in the fired test and provided a benchmark for comparing future design variations.

Two fired tests were completed. The head end emissions performance was as expected for testing in the advanced system with staged fuel injection. NOx emissions at base load conditions with APM were lower than with the baseline premixer head end, with all other system architecture identical.

Production Ready Preliminary Design

The Conceptual design moved the APM to a better mechanical position. The testing highlighted a number of areas in need of improvement. The Preliminary design phase was used to evaluate a number of potential fixes for the areas needing improvement. Key fuel nozzle geometric

parameters were adjusted to reduce combustion dynamics at several frequencies observed in fired testing. Physics-based numerical modeling was conducted and the mechanical design team identified the envelope of possible geometric changes. Additional design changes were implemented to reduce combustor head end pressure drop, which benefits the efficiency of the gas turbine engine. Several new designs were evaluated using CFD. The best geometry was implemented in the Preliminary design hardware.

Candidate 1: First tested was an alternate aft face design aimed at reducing temperatures without additional cooling air bypassing the pre-mixer. The fuel nozzles performed similarly in emissions to the conceptual design version. However, the tolerance to reactive fuels was significantly degraded. As intended, the new aft cap design accomplished a sizeable reduction in the hot face temperature throughout the test. In Figure 50, the temperature (normalized) indicated by a single thermocouple at the same location is plotted during testing of the original and the new (alternate) cap design at comparable conditions.

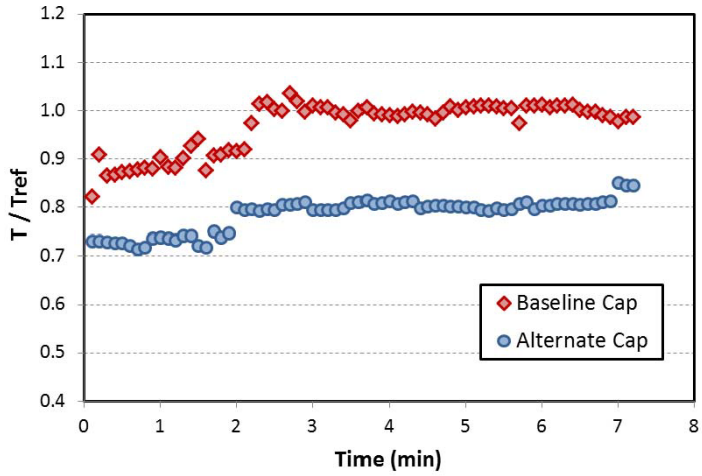

Figure 50: Normalized Hot Face Temperature

Temperature comparisons at multiple locations during a single test point at equivalent conditions in both tests are shown in Figure 51. Clearly the new cap design reduced aft face temperatures consistently over the surface area throughout the test. The challenge going forward then was to achieve the new cap design's thermal performance with little or no sacrifice in reactive fuel capability.

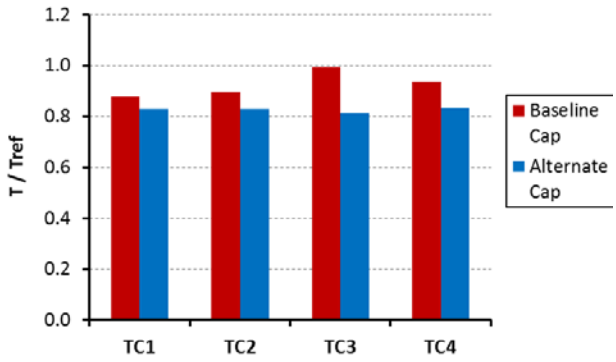

Figure 51: Normalized Hot Face Temperature Comparison

Candidate 2: Featured three candidate modifications. The goal was to retain the favorable temperatures observed in the prior attempt without sacrificing tolerance to reactive fuels. During the fired test, kHz dynamics were reduced over the full range of conditions explored. The updated air-side inlet flow conditioner reduced system pressure loss by 0.3%. Cap metal temperatures were lower than the previous iteration. Although the tolerance to reactive fuels was not explored in this test, the internal geometry of the premixer is the same as prior configurations that showed exceptional tolerance. There was a reduction in NOx capability relative to prior results. The team identified a number of items to be investigated through inspections and flow testing in order to find the cause.

Candidate 3: An alternate approach was tested which was simultaneously able to mitigate both high and low frequency dynamics tones previously observed. The testing was favorable from a dynamics standpoint, but still showed a deficit in NOx capability.

Candidate 4: A modification was tested, intended to optimize for the target combustor system. Candidate 4 included a number of the design changes from Candidate 2, and was expected to be incrementally better in dynamics. This configuration was unsuccessful at reducing any of the dynamics tones.

Detailed Design

The features of the detailed design were down-selected from the Preliminary design candidate modifications. The aft face geometry from Candidate 2 was chosen due to its low temperatures and expected restoration of the tolerance to reactive fuels. Candidate 3's dynamics mitigations were also selected. Further adjustments were made to address the loss of NOx performance.

Two fired tests were complete on the test stand. Combustion dynamics were below acceptable levels at all frequencies. Aft face temperatures were also within acceptable limits. Tolerance to reactive fuels was not tested, but the wetted surfaces are similar to previous configurations that demonstrated greater than 50% hydrogen capability.

System Emissions Performance

Figure 52 shows $NOx/T_{3.90}$ capability for the baseline combustor as well as thee system tests. The technologies developed under the current program improved $NOx/T_{3.90}$ capability over the baseline system.

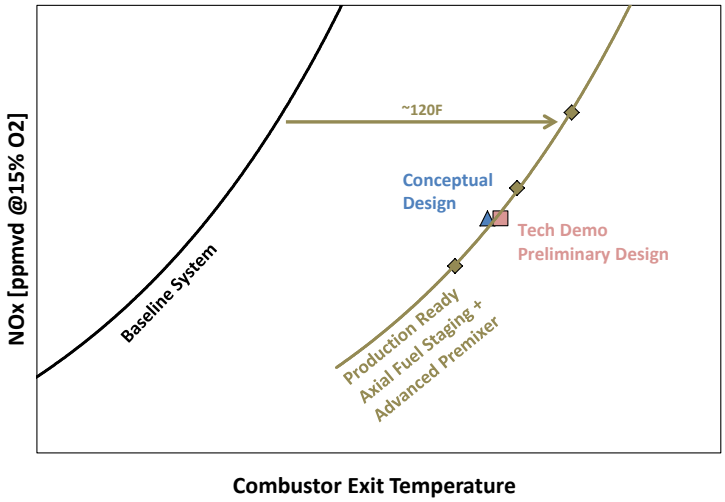

Figure 52: System NOx/$T_{3.90}$ Capability

Advanced Combustor Integration

Multiple integration concepts were evaluated using internal turbine and combustor design codes. CFD design of experiments exploring variations in key design features were utilized in establishing initial pre-test performance predictions. A multi-can cascade rig was constructed in the GTTL. Initial testing was completed using hardware that mimicked the baseline combustor and turbine. This test served to establish baseline performance and work out any problems associated with rig operation.

Testing at full flow conditions was completed for each of the integration concepts. Results were in line with pretest predictions, and detailed post-test data analysis was completed by the subject matter experts.

CONCLUSIONS

In Phase 1 of this program, the challenges of very low-NOx combustion of carbon-free syngas (primarily hydrogen fuel) were revealed. Phase 2 (Task 2.1) focused on overcoming the challenges and delivering a combustion system capable of robust operation on syngas and C-free syngas to meet the aggressive program targets. Early in Task 2.1, the micromixer was selected as the fuel-air premixer, the enabling component of the system. The micromixer employs small-scale jet-in-crossflow mixing in many tubes to balance low NOx emissions with reliable operation on high-hydrogen fuels. The micromixer is easily scalable. Early validation tests were conducted in small-scale single nozzle rig and later a single nozzle rig capable of full-scale nozzles. Later, multiple micromixer nozzles formed the foundation of the RLN1 and RLN7 combustion systems, tested in full can rigs in GE's Gas Turbine Technology Lab in Greenville, SC. The RLN1 achieved a milestone as the first-ever dry, premixed combustion system to operate with 100% hydrogen fuel.

The RLN high-hydrogen combustion systems proved to be very successful, with over 150 total fired hours in 30 rig tests at the “2012 H2 Turbine” full-load cycle condition with fuel containing over 90% hydrogen by volume of the reactants. While the RLN systems were generally optimized for base load operating on high-H2 fuel, successful operation was also achieved with traditional syngas containing CO and H2, and with backup fuels including natural gases (hydrocarbons), weak natural gases, and natural gas-hydrogen blends. Figure 53 highlights the impressive fuel flexibility of the micromixer technology. Fuels with successful operation in the program are plotted against reactivity (inverse of blowoff time) on the vertical axis and modified Wobbe index on the horizontal axis. Note that fuel nozzles may be sized differently to maintain appropriate pressure ratios with the widely differing fuels. This is standard practice for existing dry-low NOx natural gas systems, which do not have near the wide operating space as the micromixer.

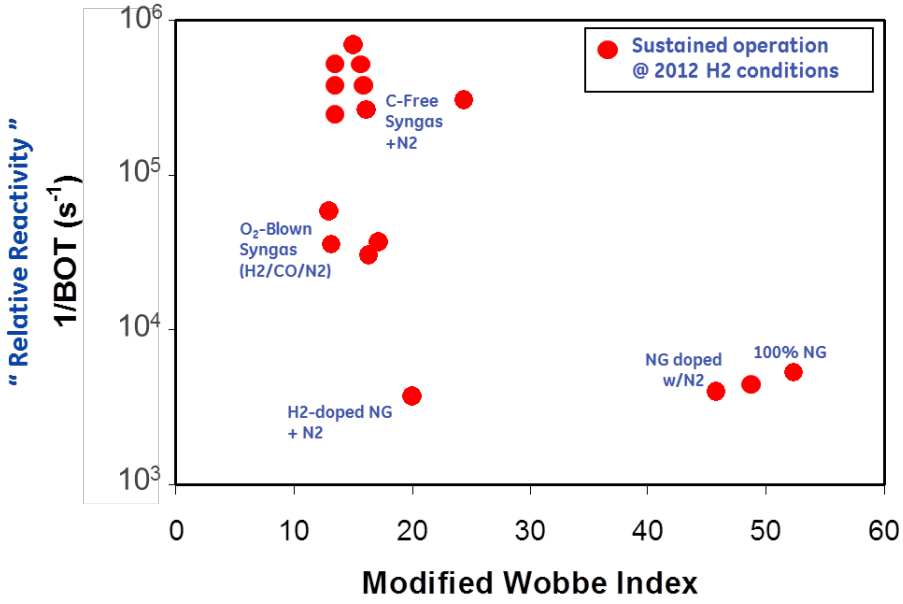

Figure 53: Fuels with successful operation in the full-can (RLN) combustion systems in the program plotted in reactivity and Wobbe index space.

Figure 54 shows the NOx history in full can rig testing through Phase 2 of the program. The bars show full-can NOx emissions at a 2012 H2 Turbine full-load exit temperature with vitiated air and H2-N2 fuel including a small amount of natural gas. From the first full-can hydrogen test to the final pre-production hardware demonstration test, continual improvement in emissions was made without compromising robust hydrogen operability.

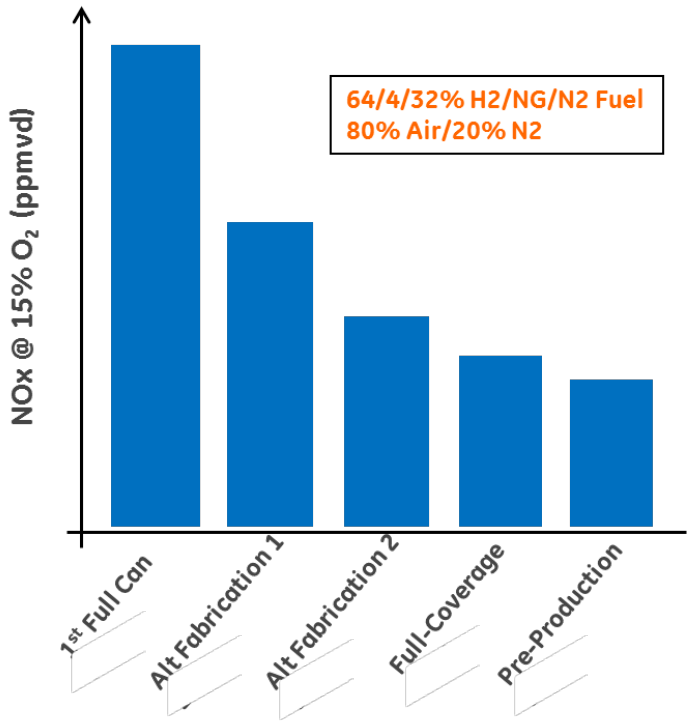

Figure 54: Measured NOx history from full-can tests with vitiated inlet air and high-H2 fuel throughout Phase 2 of the program shows continuous improvement without compromising hydrogen operability.

The outcome of Task 2.1 of the program was a dry low NOx combustion system capable of operating reliably on syngas, carbon-free syngas, and a wide range of additional fuels. The system cost was brought in line with current natural gas combustion system to support plant capital cost targets. The high-hydrogen combustion system was fully demonstrated to consistently achieve single-digit (ppm) NOx emissions while operating at aggressive H2 gas turbine cycle conditions to meet program goals for IGCC-CCS plant efficiency and output.

The program also achieved its stated objectives: to develop designs for an Advanced Combustor Architecture and Advanced Combustor Integration that enable firing temperature increases thereby improving efficiency while still delivering low NOx emissions, handle hydrogen and fuel flexibility, extend turndown, and maintain existing inspection intervals and current reliability levels. Turndown capability was extended. The system maintained the capability to run greater than 50% hydrogen in the fuel, and the tolerance to fuel MWI changes are three to five times the baseline system.

Advanced Premixer

The Advanced Premixer, APM, matured significantly under the ARRA program. Initial issues with pressure drop, flame stability, cost, and complexity were addressed. Additional design changes increased $NOx/T_{3.90}$ performance and operational flexibility. The APM demonstrated better $NOx/T_{3.90}$ capability and three to five times the MWI capability of the baseline premixer. Though the original hydrogen premixer's resistance to reactive fuels was sacrificed to some

degree, the capability remains greater than 50% hydrogen which far exceeds the baseline premixer.

COMBUSTION MATERIALS

This section summarizes the successful results of the development of (1) an improved TBC based on 8wt% yttria stabilized zirconia (8YSZ) with a dense-vertically-cracked (DVC) microstructure for better combustor component life, and (2) an advanced low k TBC for phase stability at higher temperature and lower thermal conductivity with no debit in life or other properties.

EXPERIMENTAL METHODS

Improved TBC

The improved TBC was achieved through improvements to the air plasma spray process to produce an improved microstructure. Other physical properties of the coating, such as tensile strength were also tested to ensure they were sufficient. The improved process involved several iterations of coating trials and results to ensure good coating characteristics, a repeatable process, and a process that is friendly to production by improving other coating properties such as powder deposition efficiency. The ultimate test of a TBC system is the furnace cycle test (FCT) which is performed at a series of elevated temperatures. TBC spallation life at a specific temperature is the product of the cycles-to-failure and the hold-time in hours.

Advanced Low k TBC

The advanced low k TBC was developed using a new material in order to achieve a coating with a lower thermal conductivity, phase stability to a higher temperature, and adequate life. Improvement of the air plasma spray process was completed, as in the above improved TBC system. As-sprayed and thermally aged samples were evaluated for phase stability and thermal conductivity was measured. As in the improved TBC, TBC spallation life was determined through FCT.

RESULTS AND DISCUSSION

Improved TBC

Results of FCT show that the improved TBC system has better TBC spallation life, i.e. >2X than that of the current system (Figure 55).

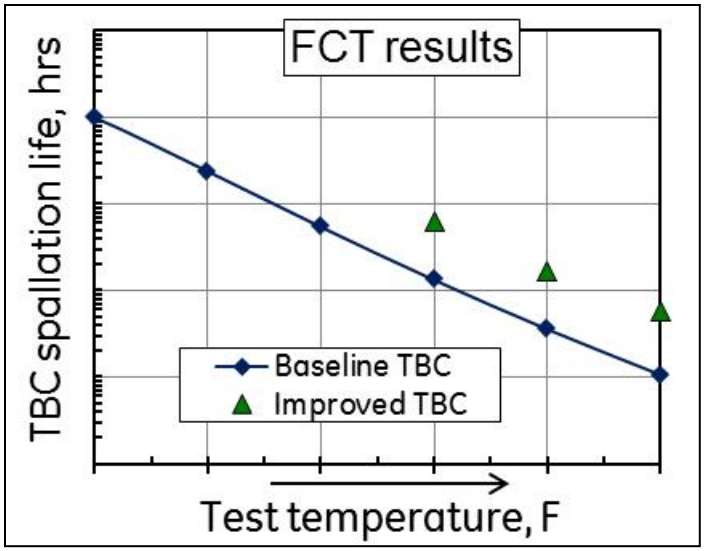

Figure 55: TBC Spallation Life of the Improved TBC vs. Baseline

The improved TBC system was also demonstrated on a transition piece and a combustion liner.

Advanced Low k TBC

One key quality of the advanced low k TBC system is its thermal conductivity. Reduced thermal conductivity is important in combustion components because the higher firing temperature requires more temperature gradient through the TBC. A standard TBC would have to be applied thicker. Thicker TBCs are especially challenging on combustion components due to the large size of the components and the necessity to coat the internal portion of the components. Thicker TBCs may also result in a rougher surface finish. Combustion components are not as easily polished as hot gas components. The low k TBC shows a significant reduction of thermal conductivity over the current TBC system (Figure 56).

Figure 56: Thermal Conductivity of the Advanced Low k TBC vs. Baseline

Phase stability is another coating quality that is important for new GE gas turbines. The current TBC with 8YSZ coating is phase-stable to an Aging Parameter (AP) of ~55K, but the operating conditions for the new gas turbines can reach AP values in excess of 60K. Phase stability of the advanced low k TBC, as measured by X-ray diffraction (XRD), has been shown up to AP of 63K and testing is on-going.

The effect of aging is evident in the cross-sectional scanning electron microscopy (SEM) micrographs (Figure 57). Figure 57a is the cross-sectional micrograph of an as-sprayed coating showing open porosity and fine cracks typical of plasma sprayed coatings. Figure 57b is the cross-sectional micrograph of a coating aged to 63K AP showing only close/round porosity as a result of long term aging and sintering.

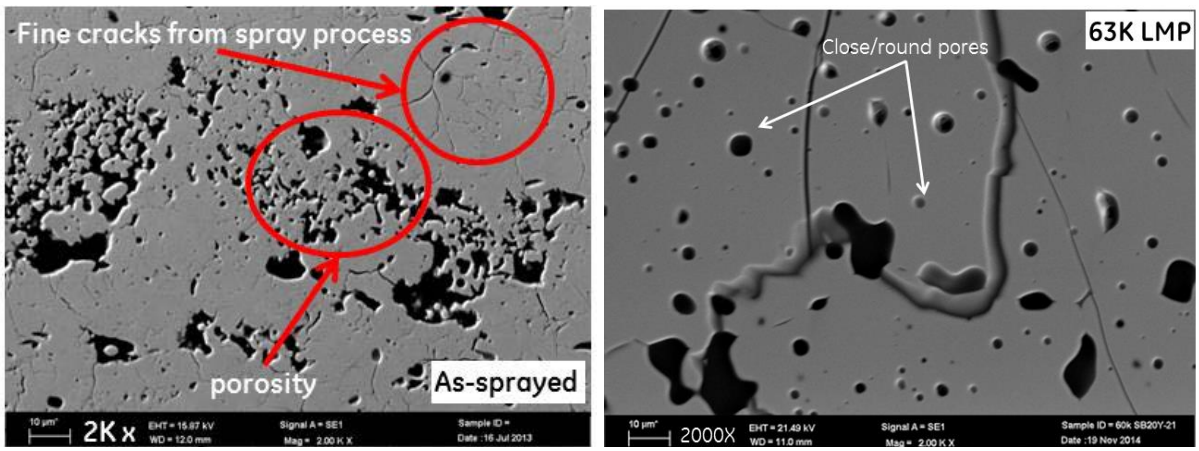

(a) (b)

Figure 57: SEM Micrographs of Advanced Low k TBC (a) As-sprayed & (b) Aged at 63K AP

The advanced low k TBC system was sprayed to ~1.5X thickness over current coatings and still able to achieve satisfactory tensile strength. This thicker coating gives additional design space for controlling TBC surface temperatures as well as substrate alloy temperatures. Results of FCT show that the advanced low K TBC system has better TBC spallation life, i.e. >2X than that of the current baseline TBC system (Figure 58).

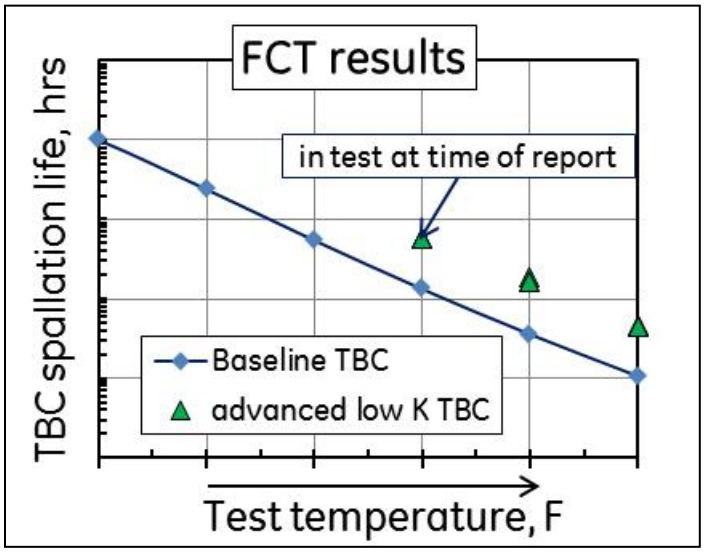

Figure 58: TBC Spallation Life of the Advanced Low k TBC vs. Baseline

The ability to transfer a coating from development coupons to an actual component and still achieve acceptable coating quality is an important part of enabling new technologies. In addition to successfully coating combustion liners, these parts were placed in an existing turbine as a field trial. In November 2014, two (2) liners coated with the thick improved TBC with 8YSZ

coating and two (2) coated with the new advanced low k TBC coating (Figure 59, Figure 60 and Figure 61) were installed in a customer unit. These parts underwent their first borescope inspection in April 2015. They had 3,644 fired hours with 3 starts. They had no signs of coating distress or spallation (Figure 62 and Figure 63).

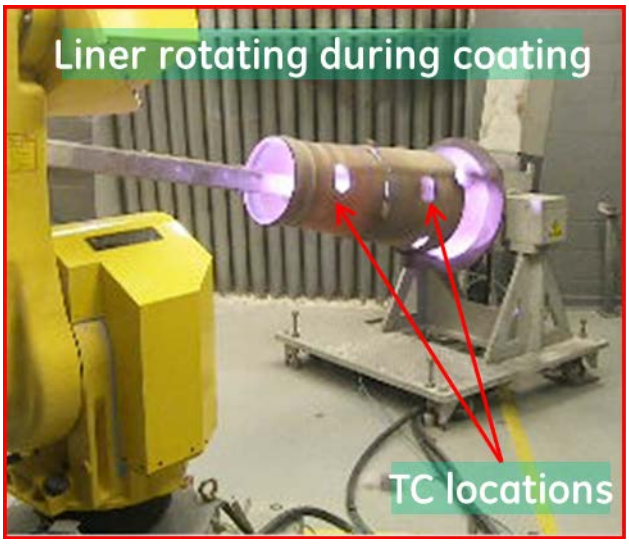

Figure 59: Photo of Application of the Advanced Low k TBC to a Combustion Liner for Installation in a Customer Unit

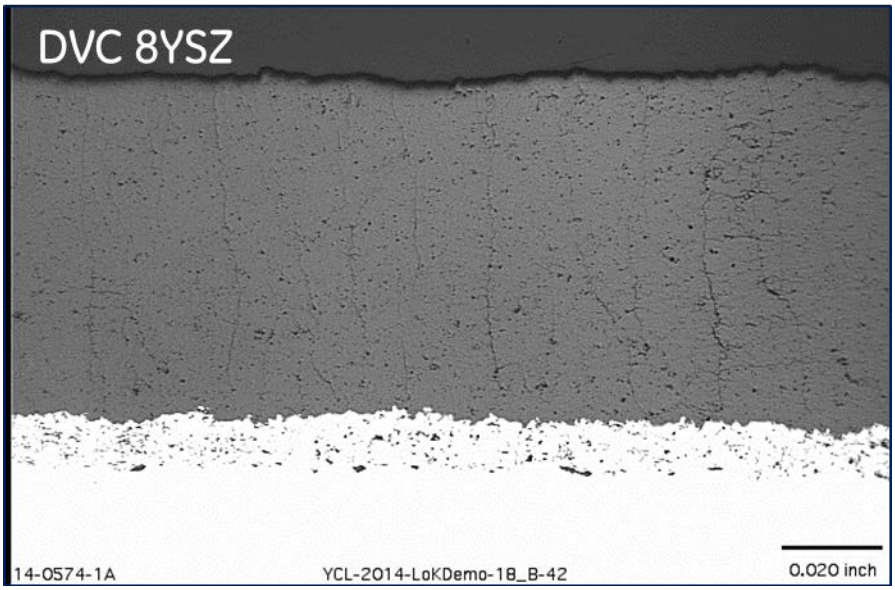

Figure 60: DVC Microstructure of the Improved TBC Applied to a Combustion Liner for Installation in a Customer Unit

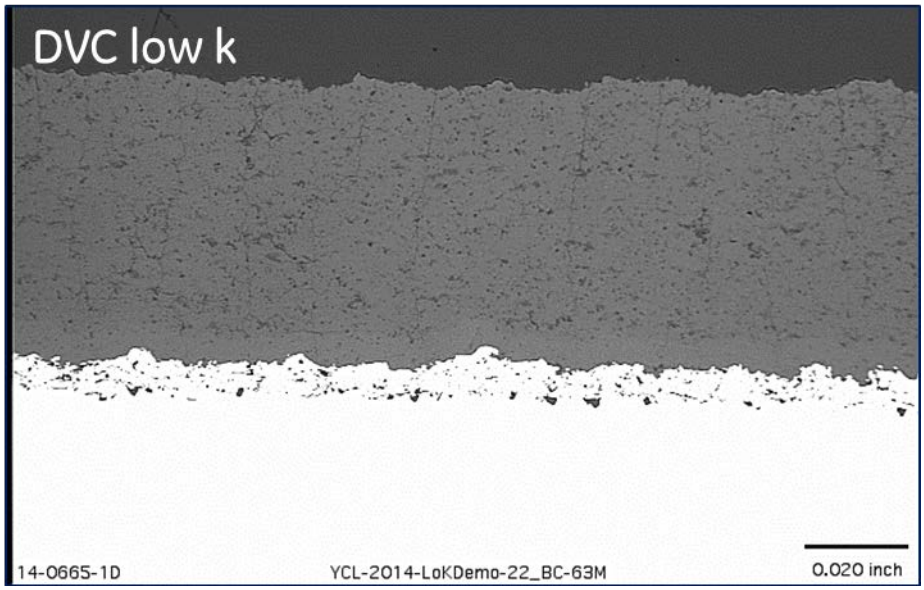

Figure 61: DVC Microstructure of the Advanced Low k TBC Applied to a Combustion Liner for Installation in a Customer Unit

Figure 62: Improved TBC on a Combustion Liner after 3,644 hours in a Customer Unit

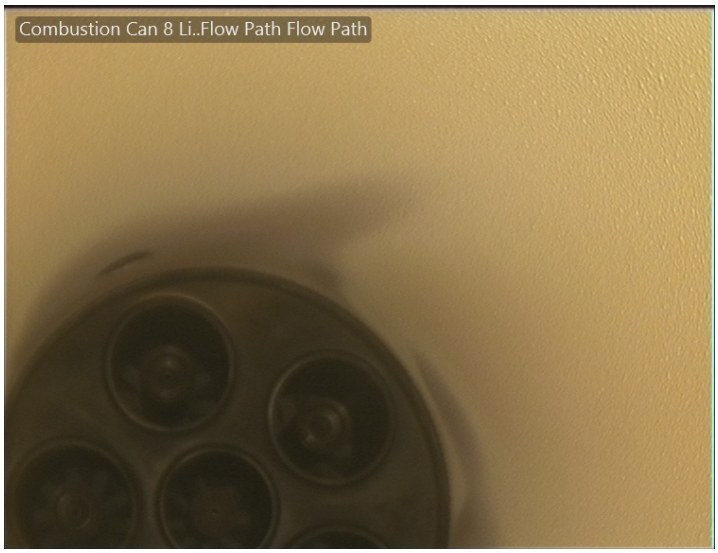

Figure 63: Advanced Low k TBC on Combustion Liner after 3,644 hours in a Customer Unit

CONCLUSIONS

The combustion coating program completed under Task 2.6.3 was very successful, resulting in a low k TBC that improves the efficiency of the gas turbine system through enabling higher operating temperature and allowing increased service intervals. It is being incorporated into the design for several new GE gas turbines.

SUPPORTING MATERIAL DEVELOPMENT

This section report summarizes the successful results of technical development in the areas of coatings and advanced alloys. For coatings there was success in the development of (1) new coatings capable of operating in a fuel flexible environment at higher firing temperatures and (2) an advanced low k TBC for phase stability at higher temperature and lower thermal conductivity with no debit in life or other properties. For alloys the report summarizes the results from (1) the development of a highly oxidation- and corrosion-resistant Re-free Ni-base superalloy, (2) Class 3 design curves for the application of alloy in gas turbine environments, (3) cast high-integrity nozzles of different sizes and structural complexities and (4) machining and welding trials required for downstream fabrications.

EXPERIMENTAL METHODS

Coatings and TBC

Metallic Coating Development
The goal of the metallic coating development subtask was to meet the environmental challenges arising in an IGCC/High Hydrogen turbine from the presence of corrosive deposits combined with high H_2O in the hot gas path (HGP).

The initial steps to identify the technology need were as follows:

1. Conduct baseline study on existing IGCC units
2. Devise laboratory tests that replicated the damage mode observed in the baseline units and screen state-of-the-art material systems.
3. Use the projected wet turbine operating environment of an IGCC/High Hydrogen turbine as input for additional screening test development to assess material capability in a broader operating condition range
4. Develop new metallic material options for capability enhancements over state-of-the-art

GE's approach was to focus on bond coat upgrades in lieu of base alloy solutions. Rigorous testing of various MCrAlY (metal-chrome-aluminum- yttrium) type bond coats was conducted.

Hot Gas Path Material and Coating Testing
Burner rig testing is commonly used to measure the oxidation of a metallic coating and substrate combination. This is done by testing at various times and temperatures in order to measure the thermally-grown oxides (TGO) and make estimations as to a coating-substrate system life. This program focused on several hot gas path (HGP) alloys and metallic coatings. Water was injected into the burner rig environment in order to achieve higher moisture content, as is typical for High Hydrogen gas turbines or other fuel flexible environments. Testing was done at 1700°F (927°C), 1800°F (982°C) and 2000°F (1093°C) for up to 10,000 hours.

Hot Gas Path Advanced Low k TBC
The advanced low k TBC was developed using a new material in order to achieve a coating with a lower thermal conductivity, phase stability to a higher temperature, and adequate life. Improvements to the air plasma spray process were completed. This was helpful in achieving an improved coating structure in this new family of coatings. As-sprayed and thermally aged samples were evaluated for phase stability and the thermal conductivity was measured. TBC spallation life was determined through furnace cycle test (FCT). It should be noted that the

advanced low k TBC discussed here is the same material discussed in Section 2.6.3. However, some notable differences for this discussion, as it relates to the HGP, are different alloys, some additional test requirements (such as erosion) and different components for which to develop a successful coating system.

Alloys

Single Crystal Alloy Development
Three advanced single crystal alloy compositions were down-selected for scale up trials. These trials included making small master heats of each of the advanced alloy compositions, and then making slab and bucket castings. After heat treatment, low cycle fatigue (LCF), creep, and tensile test specimens were machined from the slabs made for each of the down-selected alloy compositions. Trial bucket castings were also produced.

Equiaxed Alloy Development
General Electric has patented a highly corrosion resistant single crystal (SX) alloy (US Patent#: 6905559), which contains 1.6%wt Re. The alloy developed in the current program was based on this alloy with the following changes: (1) reducing Re to 0% for cost reduction; (2) changing alloy from SX to equiaxed (EQ) grain structure so that large complex components such as nozzles could be cast; (3) improving other properties to be better than the current nozzle alloy Rene' 108 so as to be applied in turbines with ever increasing firing temperatures.

The alloy development started with thermodynamics based modeling to select possible compositions based on (1) the dominant strengthening phase volume fraction; (2) <90°F freezing range (insurance for superior castability and weldablity); (3) >100°F heat treat window; and (4) dense surface oxide scale mainly consisting of oxides of chromium and aluminum. The 1st round of modeling yielded 18 compositions. Slabs of these compositions were acquired from a US foundry for screening tests which included corrosion, oxidation, and mechanical properties.

Two compositions stood out after evaluation of the overall performances of the first round alloys and the second round composition selection and improvements were subsequently conducted which combined the winning compositions and was targeted to solve the issues revealed. Collaborations with Ames Laboratory accelerated the improvement of final alloy composition. Sufficient amounts of slabs were acquired from the same foundry and used for systematic property test programs to construct Class 3 design curves. In the meantime, casting trials were successfully conducted for stage 1 nozzles of 3 GE advanced gas turbines and technologies/processes for the deployment of the alloy were also fully developed and tested.

The program was focused on developing a Re-free Ni-base super alloy for the next generation static hardware used in the hot gas path of advanced baseload gas turbines. The current alloy used for early stage nozzles and shrouds is Rene' 108, therefore project critical to quality characteristics (CTQs) were selected with reference to required service properties of Rene' 108, as shown in Table 3.

Table 3 - Project CTQs

CTQ's	Ranking	Rene' N5	Rene' 108	SX Rene' N2	New Alloy
Corrosion resistance	1	Low	Medium	High	2X Rene' 108
Oxidation resistance	1	High	Medium	High	2X Rene' 108
LCF	1	High	Medium	High	~Rene' 108
Creep	3	High	Medium	Medium	~Rene' 108
Castbility	4	Difficult	Satisfactory	Difficult	~Rene' 108
Phase Stability	3	Stable	Stable	Marginal	Stable
Cost	5	High	Low	Medium	~Rene' 108

RESULTS AND DISCUSSION

Coatings and TBC

Metallic Coating Development

Comparative tests were executed in controlled laboratory environments using air and air-steam mixtures at ambient pressure. Assessment of accumulated bond coat damage with and without corrosive deposits under isothermal and thermally cycling conditions indicated that degradation was typically accelerated when steam was present in the environment.

Corrosive-salt-assisted screening tests were conducted using Na_2SO_4 and a GE-developed 4-sulfate mixture, Figure 64 and Figure 65. The recipe of the 4-sulfate mixture is based on debris collected from field run hardware that represents the foreign matter typically entering the unit. Post-test evaluation indicated that the bond coat resistance to the 4-sulfate mixture was much greater than to Na_2SO_4.

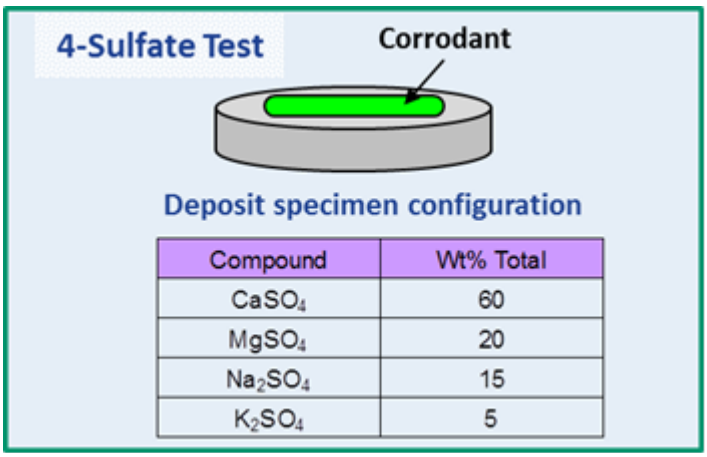

Compound	Wt% Total
$CaSO_4$	60
$MgSO_4$	20
Na_2SO_4	15
K_2SO_4	5

Figure 64: GE-developed 4-sulfate mix based on residue collected from field run hardware

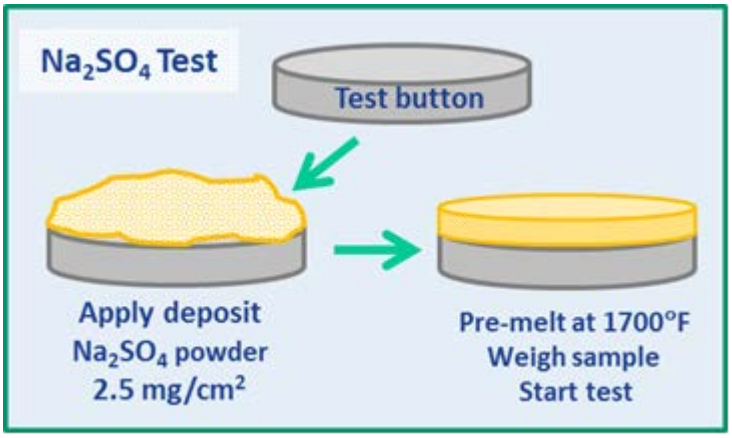

Figure 65: Schematic of Na_2SO_4-assisted corrosive salt screening tests run in 20% steam containing test rigs

These findings indicated that the risk of damage through field ingested debris in the IGCC/High Hydrogen unit was low. Comparing steam tests to air-only exposures it was found that the presence of steam was accelerating the degradation. However no indications were observed suggesting a change in the damage mechanism. With these findings, integrated TBC system testing was done without corrosive deposits for final coating down select.

The growth of the interdiffusion zone was measured on all samples once they had completed their planned hours of test. The results at the highest temperature tested are shown in Figure 66. It can be seen that “Coating C” has the slowest interdiffusion.

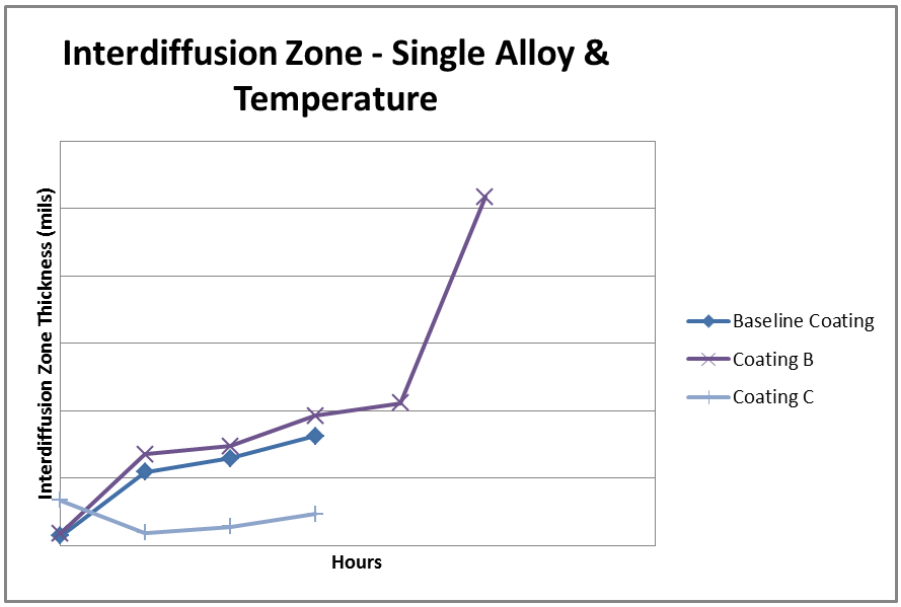

Figure 66: Interdiffusion Zone for 3 Coatings on HGP Alloy

For the burner rig testing, the % beta-phase remaining in the coating was also measured (Figure 67). Again, this data is shown for the highest temperature tested. Similar to Figure 66, "Coating C" had the highest amount of beta-phase after testing.

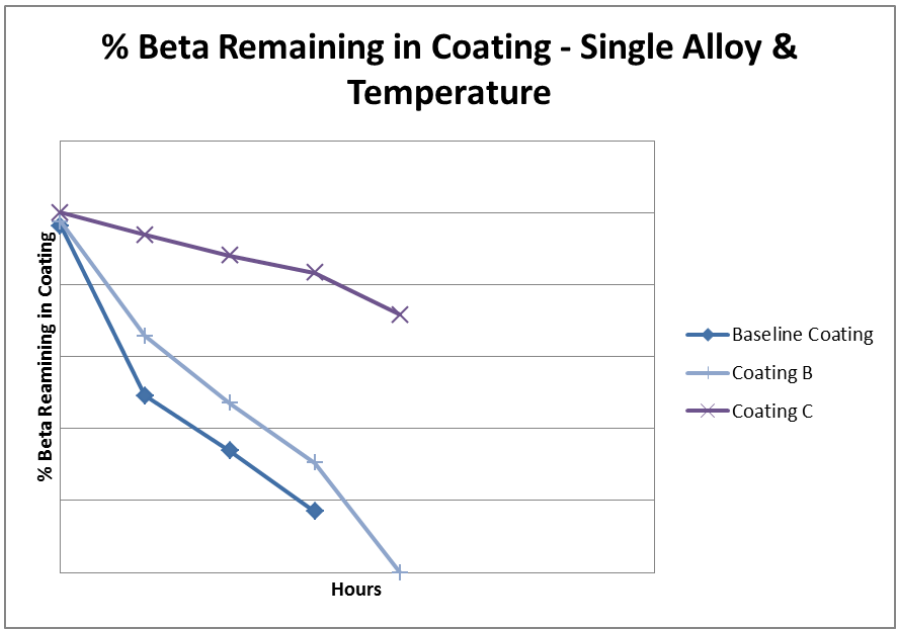

Figure 67: % Beta Phase Remaining in Coating for 3 Coatings on HGP Alloy

Hot Gas Path Material and Coating Testing

The growth of the interdiffusion zone was measured on all samples once they had completed their planned hours of test. The results at the highest temperature tested are shown in Figure 68. It can be seen that Coating C has the slowest interdiffusion regardless of the alloy, followed by the remaining coatings on Alloy 3, followed by the remaining coatings on Alloy 1. The Baseline Coating and Coating B have the largest and fastest growing interdiffusion zone on Alloy 2.

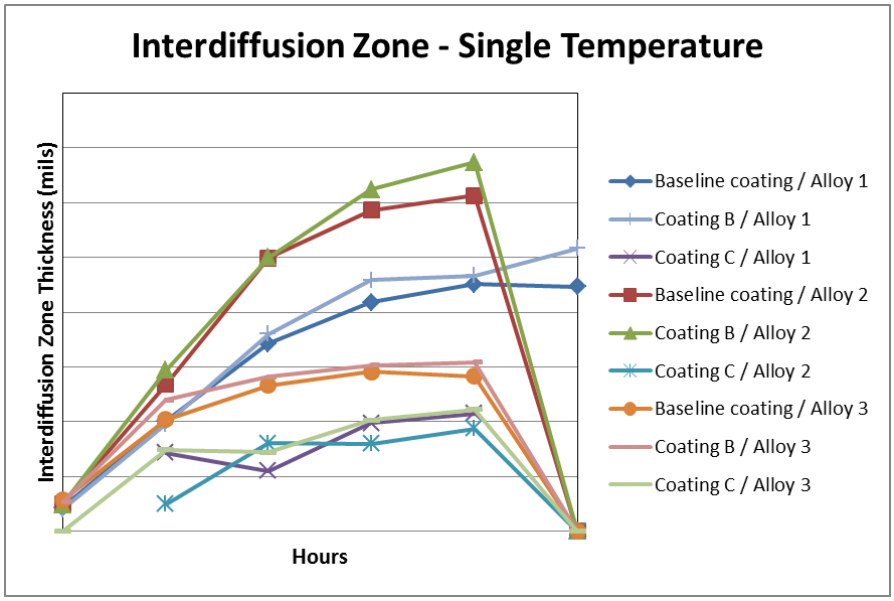

Figure 68: Interdiffusion Zone for 3 Coatings and 3 Gas Turbine Alloys

For the burner rig testing, the % beta-phase remaining in the coating was also measured (see Figure 69). Again, this data is shown for the highest temperature tested. Similar to Figure 68, Coating C had the highest amount of beta-phase after testing. It is not a surprise that the Baseline Coating and Coating B have similar data as these two coatings are very similar to each other.

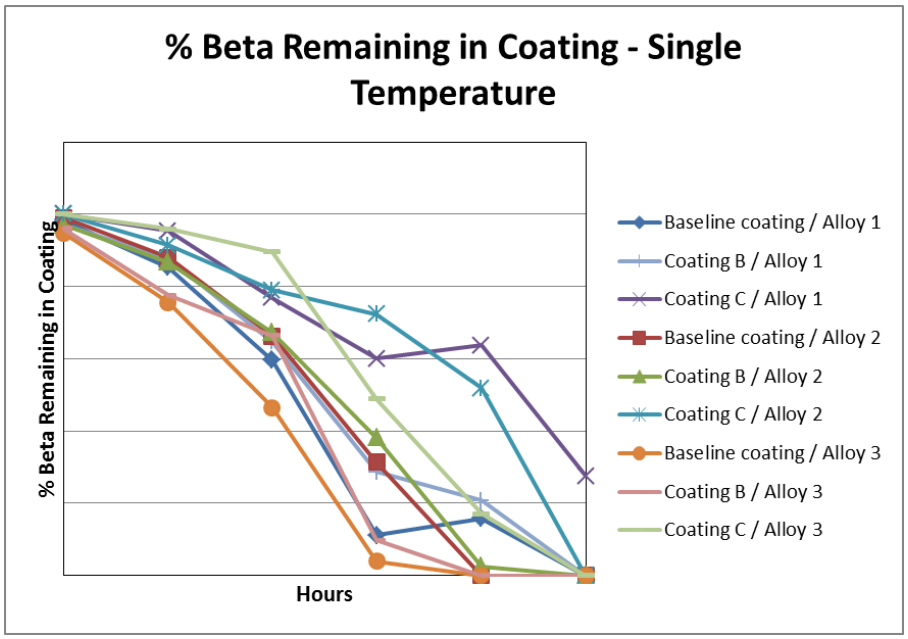

Figure 69: % Beta Phase Remaining in Coating for 3 Coatings and 3 Gas Turbine Alloys

Hot Gas Path Advanced Low k TBC

One key quality of the advanced low k TBC system is its thermal conductivity. Reduced thermal conductivity is important in HGP components because the higher firing temperature requires more cooling of the HGP components. If the TBC can keep the components cooler, less cooling air is needed, thereby increasing efficiency. The low k TBC shows a significant reduction of thermal conductivity over the current TBC system (see Figure 70).

Figure 70: Thermal Conductivity of the Advanced Low k TBC vs. Baseline

Phase stability is another coating quality that is important for GE new gas turbines. The current TBC with 8YSZ coating is phase-stable to an Aging Parameter (AP) of ~55K; but the operating conditions for the new gas turbines can reach AP values in excess of 60K. Phase stability of the advanced low k TBC, as measured by X-ray diffraction (XRD), has been shown to AP of 63K and testing is on-going.

The effect of aging can be evident in the cross-sectional scanning electron microscopy (SEM) micrographs (see Figure 71). Figure 71a shows the cross-sectional micrograph of an as-sprayed coating showing open porosity and fine cracks typical of plasma sprayed coatings. Figure 71b shows the cross-sectional micrograph of a coating aged to 63K AP showing only close/round porosity as a result of long term aging and sintering.

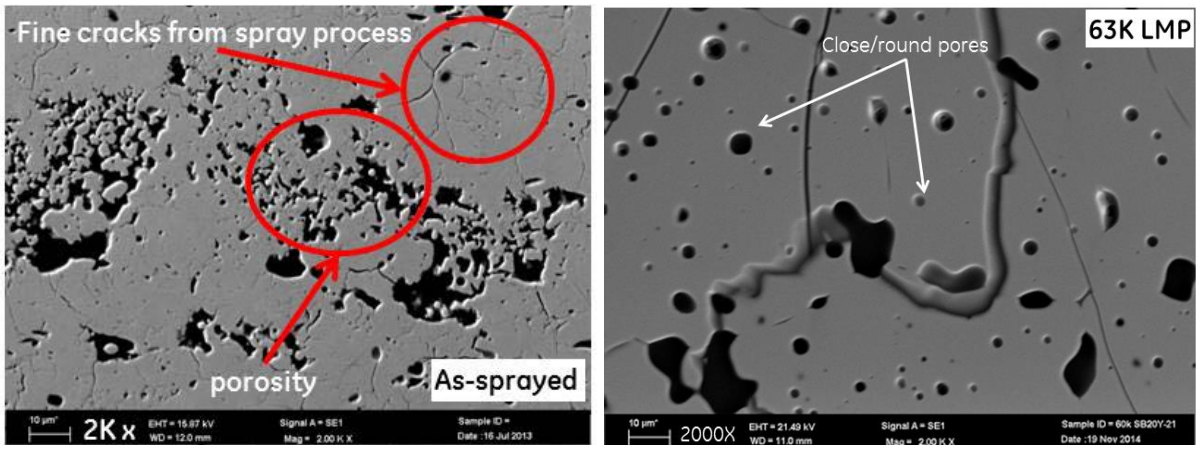

(a) (b)

Figure 71: SEM Micrographs of Advanced Low k TBC (a) As-sprayed and (b) Aged (at 63K AP)

The effect of aging can also be seen in the room temperature erosion performance of the coating (see Figure 72). The baseline 8YSZ sees a significant increase in erosion rate as it transforms, whereas the advanced low k TBC shows a slight improvement over time. It should be noted that the slightly higher erosion rate of the advanced low k TBC is not a concern because gas turbines are filtered and we have not observed any significant erosion damage in any gas turbines.

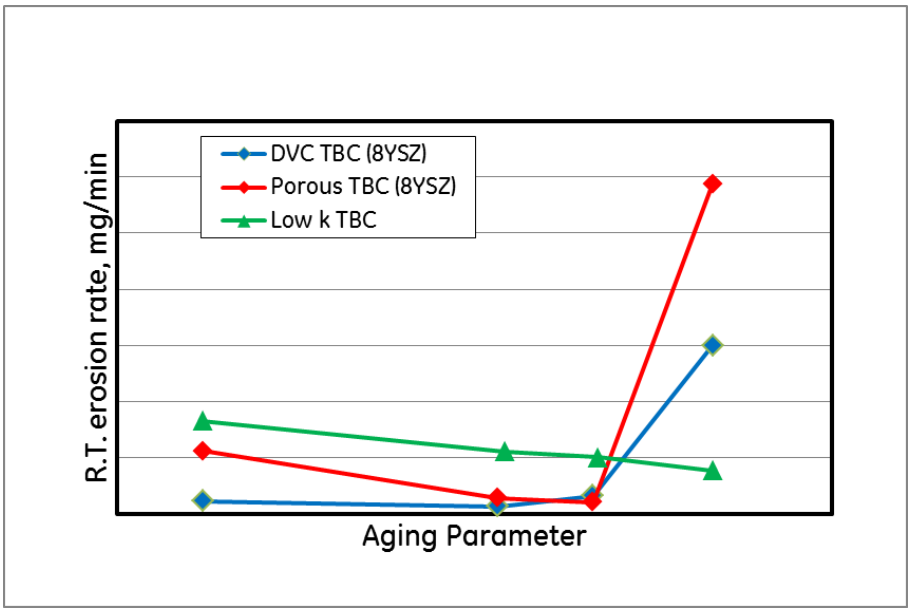

Figure 72: Room Temperature Erosion of the Advanced Low k TBC vs. Baseline

The advanced low k TBC system was sprayed to 1.5X thickness over current coatings and still able to achieve satisfactory tensile strength. This thicker coating gives additional design space for controlling TBC surface as well as substrate alloy temperatures. Results of FCT show that the advanced low k TBC system has equal TBC spallation life (see Figure 73). It should be noted that the improvement seen in 2.6.3 for Combustion was primarily due to a change from a porous to a DVC-microstructure.

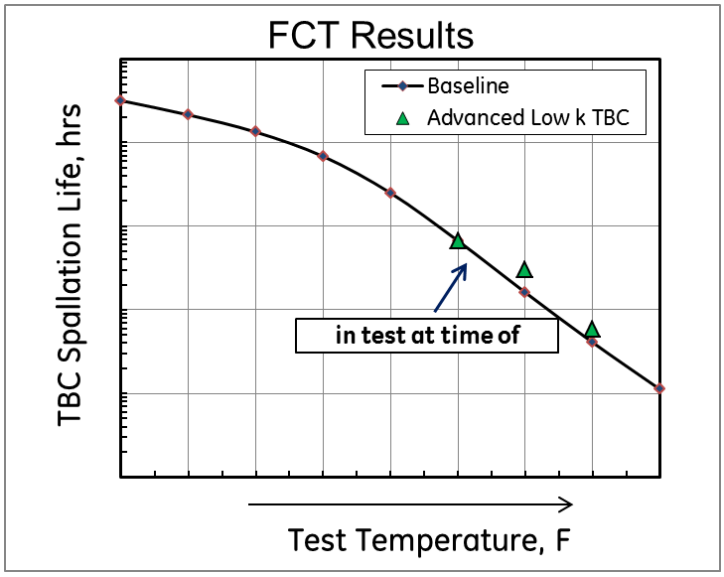

Figure 73: TBC Spallation Life of the Advanced Low k TBC vs. Baseline

The ability to transfer a coating from development coupons to an actual component and still achieve acceptable coating quality is an important part of enabling new technologies (see

Figure 74 and Figure 75). In addition to successfully coating buckets, these parts were accepted by a customer in an existing turbine as a field trial. In the case of HGP components, there are some post-coating processes that occur before parts can be shipped. One of these processes is the polishing of the coating. Due to some differences in the physical properties of the advanced low k TBC, some changes needed to be made in the polishing process, but it was successfully developed and applied to the buckets installed at a customer site. In November 2014, twelve (12) first stage buckets coated with the new advanced low k TBC coating were installed in a customer unit. These parts underwent their first borescope inspection in April 2015. They had 3,644 fired hours with 3 starts. They had no signs of coating distress or spallation.

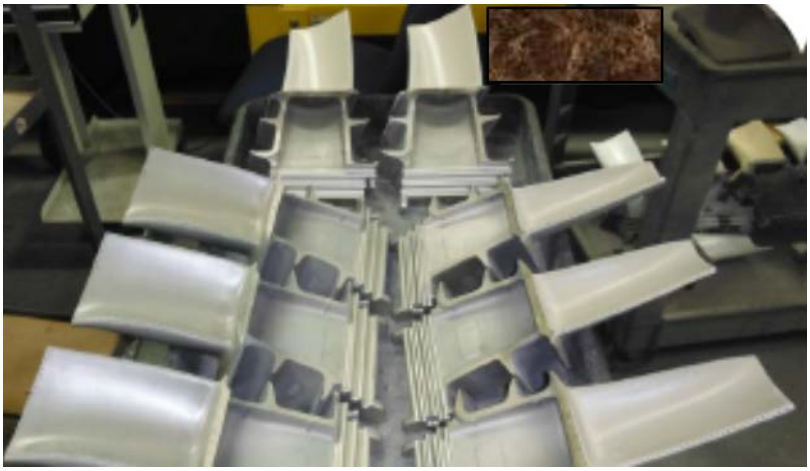

Figure 74: Photo of Buckets Coated with Advanced Low k TBC and Polished for Installation in a Customer Unit

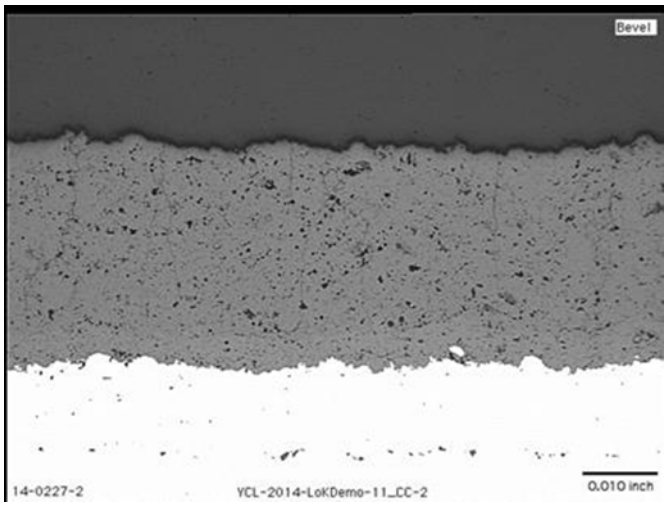

Figure 75: DVC Microstructure of the Advanced Low k TBC Applied to a Bucket for Installation in a Customer Unit

One other post-coating process that was developed under this program, but not needed for the customer installation, is nozzle hole drilling. Again, due to some differences in the coating properties, some modifications needed to be made to the standard process, but trials at our vendor were successful.

Alloys

Single Crystal Alloys
Results from the mechanical tests (low cycle fatigue, creep and tensile) indicated that one of the alloys had equivalent or better properties when compared to the baseline alloy. The results observed on the trial buckets are similar to the performance of the baseline alloy in production, with one exception. The experimental alloys, as a result of their chemical composition, exhibit defects due to a reaction product.

It became evident that achieving a significant improvement over the baseline alloy was going to require additional development. The decision was made to stop any further development on an advanced single crystal alloy composition.

Alloy Rene' N2M

Chemistry: The alloy was named as Rene' N2M and patent application has been filed.

GE's Phase Equilibria Tool, which automatically narrows down the composition range of each element and improves the overall chemistry selection based on the criteria input, was used in each round of the alloy development.

Heat Treatment: A thorough investigation was performed through microstructural examination of samples with different thermal processes and the focus was placed on solution temperature. Figure 76 is typical microstructure showing that the intergranular eutectic nodule was fully solutioned and the white particulates are carbide in eutectic. Table 4 show how the γ' solution percentage varies with the solution temperature.

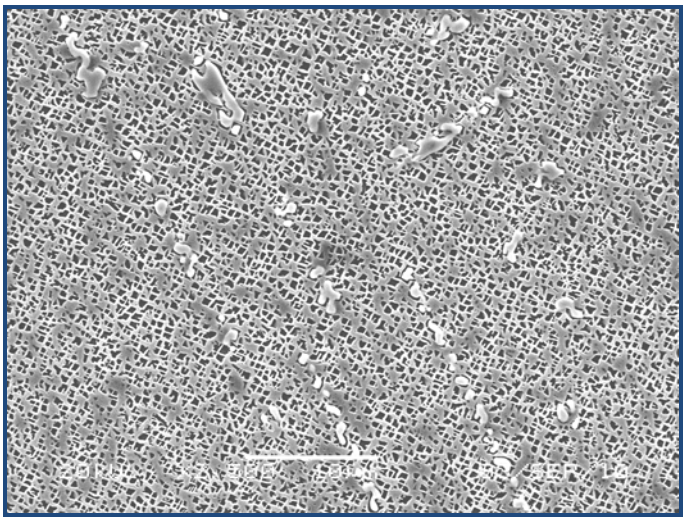

Figure 76: Microstructure Showing a Eutectic Nodule is Fully Solutioned

Table 4 - Effect of Solution Temperature on Percent γ' Solutioned

Solution Temperature, ^{o}F	Solutioned γ', %	Incipient Remelting
2200	~48.1	No
2225	~91.5	No
2250	>99.5	No
2275	100	No

Hot Corrosion: Hot corrosion was tested with GE Aviation's facility simulating the Type I hot corrosion environment. Figure 77(a) shows that the samples moved out of a furnace for corrosion screening tests and it shows that the screened alloys (X3, IX4) had much intact surfaces which cannot be matched by Rene' N500. Figure 77(b) gives the quantitative measurements from the cross-sections prepared metallographically, which shows that the surface damage of most screening alloys (blue bars) is less than 1/3 of that for Rene' N5 (dashed line near the top of Figure 77(b)).. In Figure 77(b), the red bar is for the direct comparison of Rene' N500 tested together with the screen alloys. The improved corrosion capability of Rene' N2M is due to the fact its surface scale are dominated with Cr- and Al-oxides; while Rene' N5, the scale mainly consists of Ni- and Al-oxides.

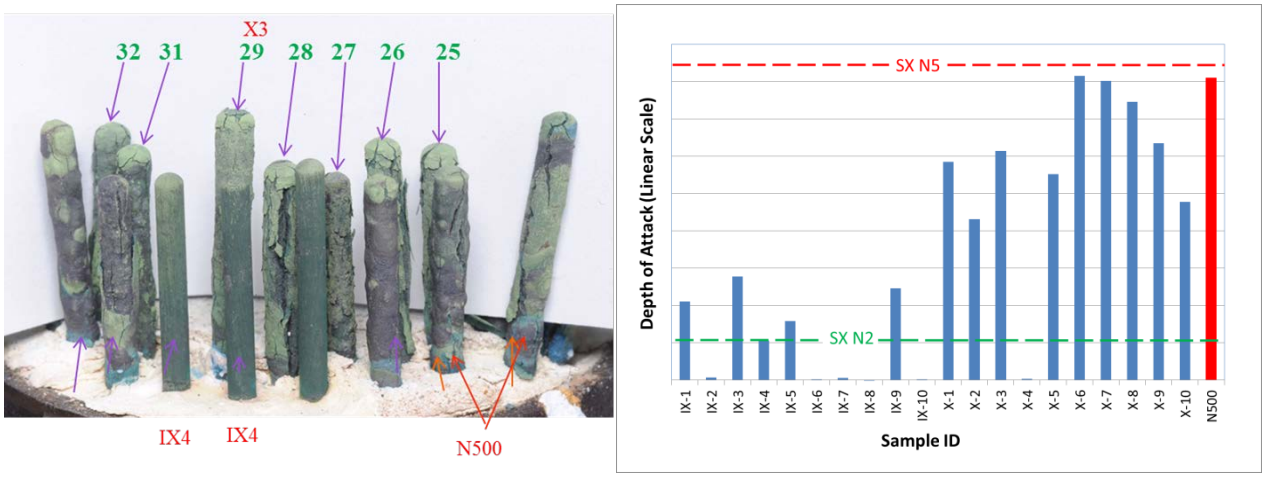

Figure 77: 600 Hours' Hot Corrosion Tests (1700oF/5ppm Sea Salt/0.4%S) of 1st Round of Rene' N2M (a) and Comparison with Rene' N500 and Rene' N5 (b)

Oxidation: Oxidation tests were performed with two different atmospheres: one burner rig simulating natural gas as fuel and the other simulating IGCC environment where some amount of water steam was intentionally injected into the flame. Both tests showed better oxidation capability of Rene' N2M. Figure 78 is the test results from simulating IGCC environment: surface damage due to oxidation and flakeoff of Rene' N2M is about 1/3 of that for Rene' 108.

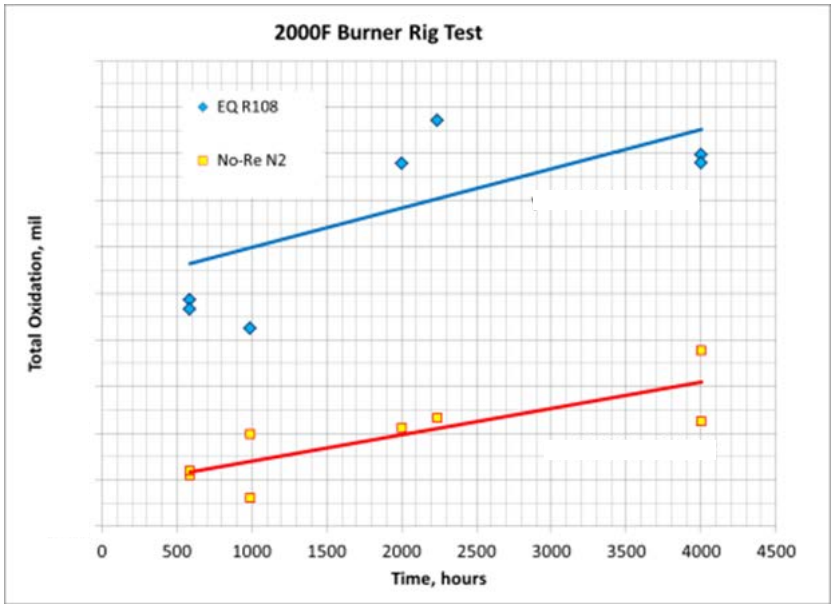

Figure 78: Comparison of Oxidation Damage of Surfaces of Rene' 108 and Rene' N2M

The significant improvement in the oxidation resistance of Rene's N2M arises from 2 fundamental changes in the structure of surface oxide scale. In comparison with Rene' 108,

Rene' N2M contains higher Al and Cr, but lower Hf: the former change makes the oxide scale dense and more adherent to the unaffected matrix; the latter reduces the grain boundary segregation and minimizes the oxide flakeoff due to preferential grain boundary oxidation. Figure 4 shows the difference of the oxide scales in Rene' 108 (Figure 79(a)) and Rene' N2M (Figure 79(b)).

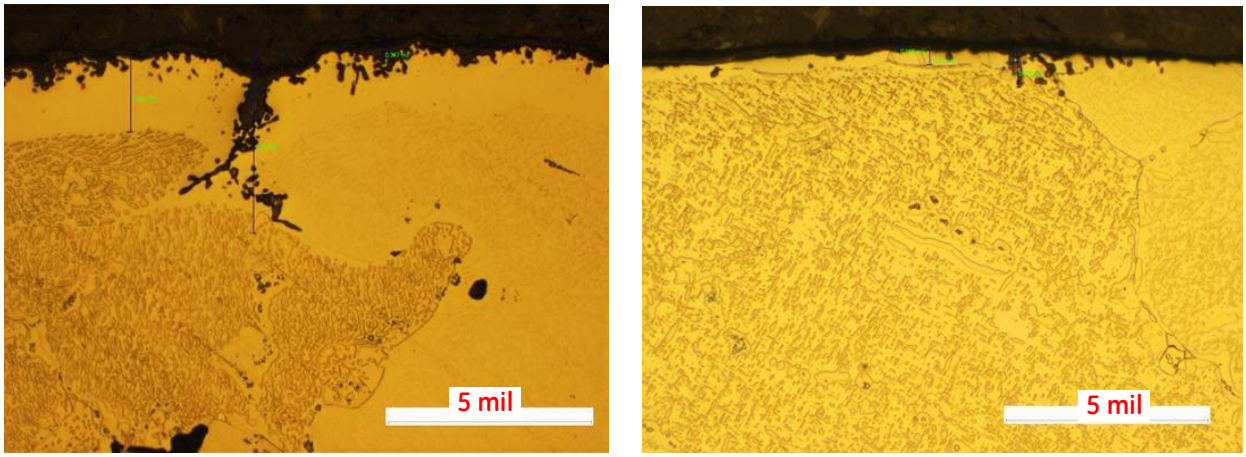

Figure 79: Comparison of Surface Oxidation and Depletion in Rene' 108 (a) and Rene' N2M (b) after 2339 Hours at 2000°F

Eight Class 3 design curves for oxidation property of Rene' N2M were published internally. The curves are based on the burner rig tests up to 8000 hours.

Mechanical and Physical Properties

Systematic tests of mechanical and physical properties required for design of components used in the hot gas path of a turbine were performed and 81 design curves, most of which are Class 3, were published internally.

A high level summary of mechanical properties is that Rene' N2M has about the same strength from room temperature up to 2000°F (1093°C) (Figure 80(a)) and incrementally better LCF than Rene' 108 (Figure 80(b)); but the creep capability could not match that of Rene' 108 (Figure 80(c)). Specific efforts have been made to improve the creep capability of Rene' N2M through increasing the amount of grain boundary strengthening phases, but it was found that there were limits for the carbide forming elements Figure 81 shows a microstructure where P-phase cuts through the γ/γ' matrix. It has also been found that increase in the carbide forming elements tends to form continuous hard brittle carbides along grain boundaries, which drastically reduces ductility of the alloy.

For design requirements for front stage nozzles and shrouds, especially first stage hardware, environment damage due to oxidation and corrosion and LCF (including thermal mechanical fatigue) are most critical, and creep rarely becomes a concern for mechanical design. From these considerations, the alloy development team stopped pursuit for further improvement in

creep capability of Rene' N2M. The creep debit in comparison with Rene' 108 is the only property that does not meet the project CTQs (Table 3).

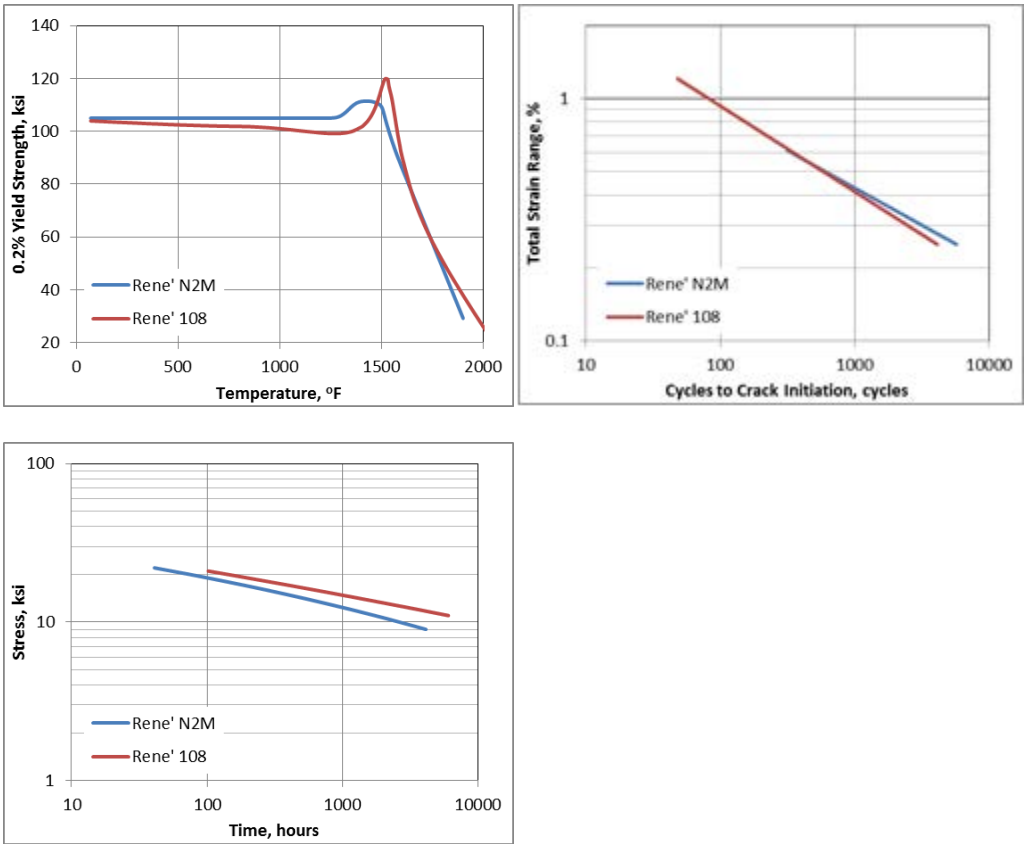

Figure 80: Comparison of Mechanical Properties of Rene' N2M with Rene' 108 (a) 0.2%YS; (b) 1800°F (982°C) LCF; (c) Time to Reach 0.5% Creep at 1800°F (982°)

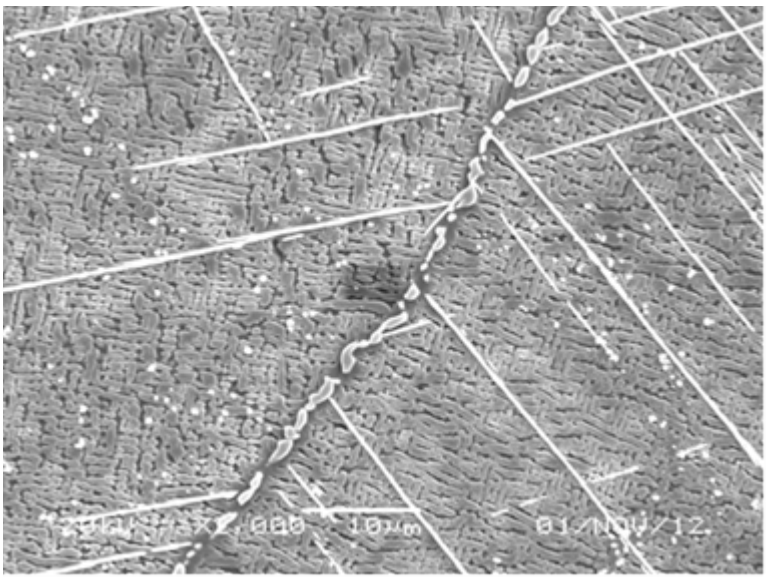

Figure 81: Occurrence of P-phase Needle with Cr and Mo beyond the Spec Limits

(2) Scale-up Alloy Making and Nozzle Casting Trials

With the success in slab castings for testing, a single master heat of up to 800lbs was prepared with conforming chemistry. With the scale-up of alloy making, stage 1 nozzle castings were tried: three trials successfully yielded 10 stage 1 nozzles with varying weight and structural complexity. Figure 82shows a stage 1 nozzle made of Rene' N2M.

The nozzles were cast using the same molds and casting process parameters that had been developed by a foundry for Rene' 108. All metallurgical evaluations (grain etch, metallurgical cutup and non-destructive inspections) show conformance to relevant specifications for these nozzles. There was no linear indication, which occasionally occurs in a nozzle made of Rene'108, requires laborious rework and is one of the major scrap factors.

Figure 82: (a) A stage 1 nozzle cast with Rene' N2M.

(3) Weldability and Machinability

Capability to do limited weld repair was systematically tested per GE's welding specifications. Figure 83 shows the result of comparing Rene' N2M with Rene' 108. For a cavity up to 0.50" in diameter, the maximum crack length in the weld affected zone of Rene' N2M is very comparable with that of Rene' 108, indicating that there is no significant difference in weldability between these two alloys.

Machining trials were completed through datum machining at a foundry and slash face milling at GE Greenville Plant. There was no noticeable difference in the tool wear and there was no cracking observed through NDT inspection on machined surfaces.

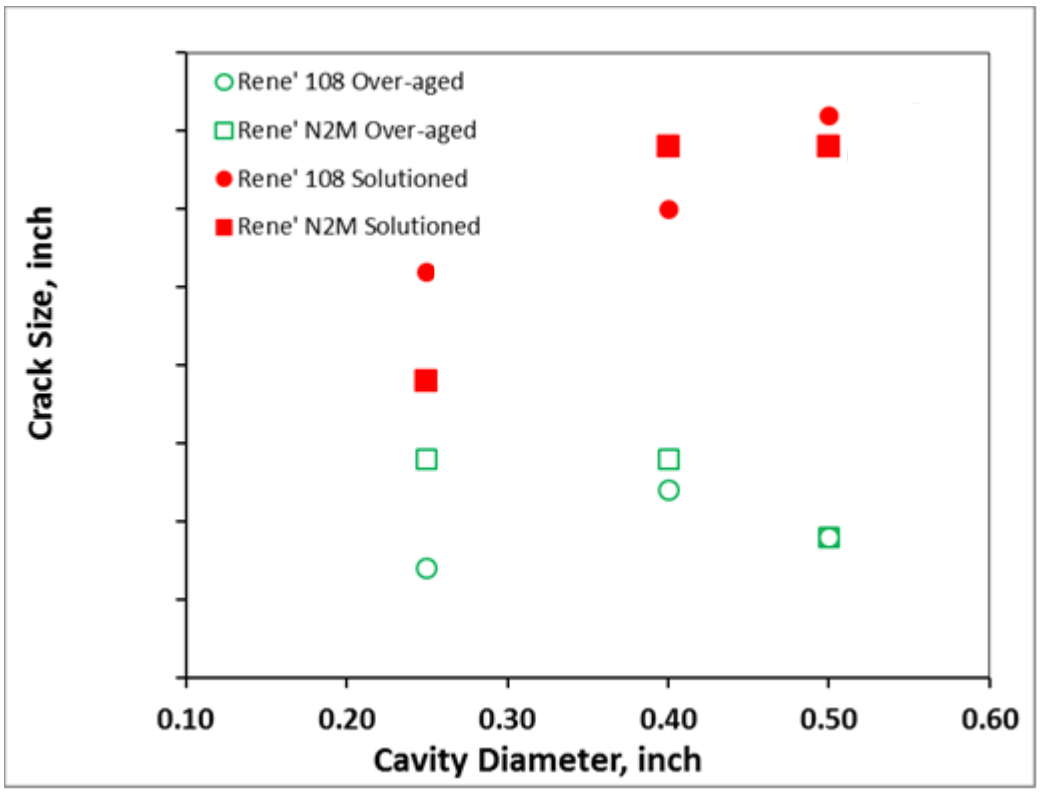

Figure 83: Longest Crack Size in HAF of Weld Tested in Rene' N2M and Rene' 108

CONCLUSIONS

Coatings and TBC

The metallic coating program completed under Task 2.3 was very successful, resulting in an advanced bond coat which has greater resistance to contaminants and allows for a higher bond coat temperature, thereby improving the efficiency of the gas turbine system through enabling higher operating temperature and allowing increased service intervals. The HGP coating program completed under Task 2.7 was also very successful. It provided insights into the oxidation behavior of new coatings and alloys. It also resulted in a low k TBC that improves the efficiency of the gas turbine system through enabling higher operating temperature and allowing increased service intervals. It has is being incorporated into the design of several new GE gas turbines.

Alloys

Under ARRA 2.7, a highly oxidation and corrosion resistant superalloy, Rene' N2M, was successfully developed, which enables stage 1 static hardware to reliably operate beyond the temperature limited by Rene' 108 alloy. Verifications of the scale-up of the alloy by making, complex nozzle castings and necessary downstream fabrication processes laid a solid foundation to deploy this material in upcoming products. In addition, without Re and with reduced Hf, the alloy is also cost effective.

DESIGN FOR HIGH TORQUE TRANSMISSION

This section of the report summarizes the results of the bi-axial testing performed in subtask 2.2.6 to address torque transmission limitations in gas turbine rotors. When evaluating high cycle fatigue (HCF), the industry has adopted the use of uniaxial testing to generate Goodman Diagrams (alternating stress vs mean stress plots). The mean stress and dynamic alternating stress are in the same direction in the gage section of the specimen (i.e. uniaxial). Design evaluation has relied on Von-Mises approaches to collapse 3D stress fields in actual parts to effective mean and effective alternating stresses which get evaluated against the uniaxial generated Goodman Diagram. This approach has worked successfully for designing and lifing of gas turbine rotors.

The limits of the above approach impose a limitation on the design of new gas turbines get larger and have higher levels of torque being transmitted through the rotor. The question arises, “Are the limits imposed by uniaxial Goodman Diagrams too conservative?” Specific locations on rotors (spacer arms for example), have high mean stress in the hoop direction and alternating stress in the axial direction. To achieve high torque transmission, more detailed understanding life verses the stress tensor is needed. A bi-axial test specimen (described in the next section) was designed to achieve high hoop mean stress as seen in a gas turbine (GT) rotor spacer arm. High internal pressure is supplied to this hollow specimen to induce the hoop stress. The bi-axial specimen is put into an MTS servo hydraulic machine to impose alternating axial stress which simulates the high cycle gravity sag loads.

In order to ground the testing, loading conditions were chosen to simulate the uniaxial testing. For these tests the bi-axial specimens failed as expected on the uniaxial generated Goodman curve. Test conditions were then prescribed on the bi-axial specimen where the mean stress was in the hoop direction and the alternating stress axial direction. The levels were chosen so that they exceeded the uni-axial Goodman Curve. Results showed that runout (>10,000,000 cycles) were achieved for hoop stresses that were 10% higher than the uniaxial Goodman Diagram. Hence, rotor sections with these high stress states have more life entitlement that originally calculated.

EXPERIMENTAL METHODS

Specimen Design:
Several design iterations on the custom bi-axial specimen were performed. The final design is shown in Figure 84.

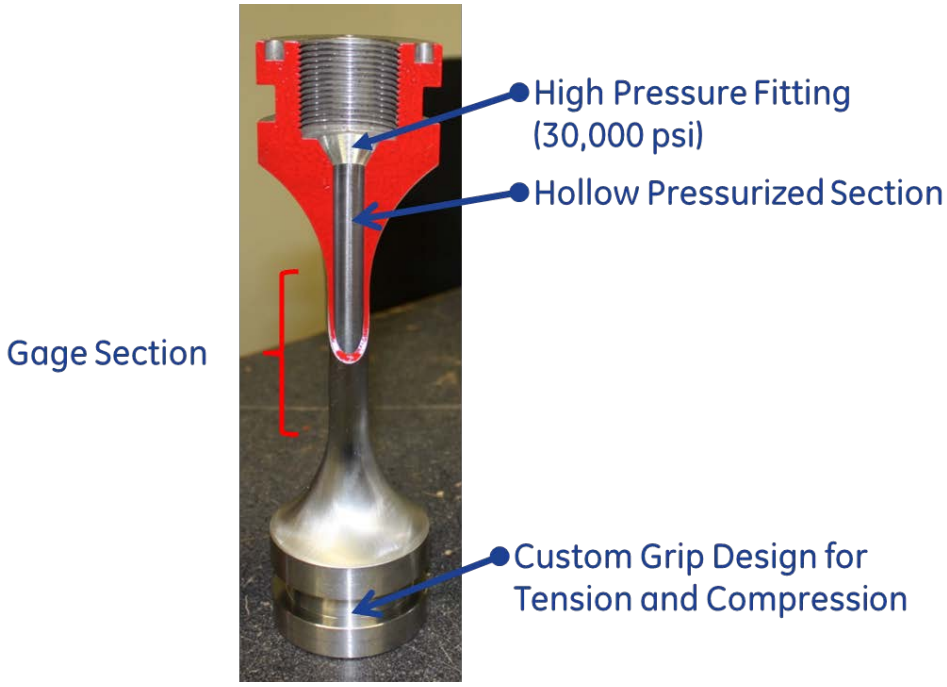

Figure 84: Bi-axial Test Specimen

The specimen has a hollow gage section so that it can be filled with high pressure fluid up to 32,000 psi pressure. The pressure generates a 3D state of stress at the inner diameter (ID) of the specimen and with 32,000 psi pressure the effective means stress is 123 ksi with a hoop component stress equal to 104 ksi. The pressure generates an unwanted axial mean stress. Hence custom grips were designed so that they can tightly grip and impose both tension and compression. The axial loads are adjusted to first zero out the unwanted axial mean stress from the pressure and then impose a dynamic axial force range that achieves the desired axial alternating stress.

The specimens were made out of a GE supplied compressor wheel (see Figure 85) made out of a NiCrMoV alloy. This was chosen because the missing section of the wheel was used to generate a GE-funded uniaxial Goodman Curve with conventional specimens. Hence, a direct comparison can be made from the same forging.

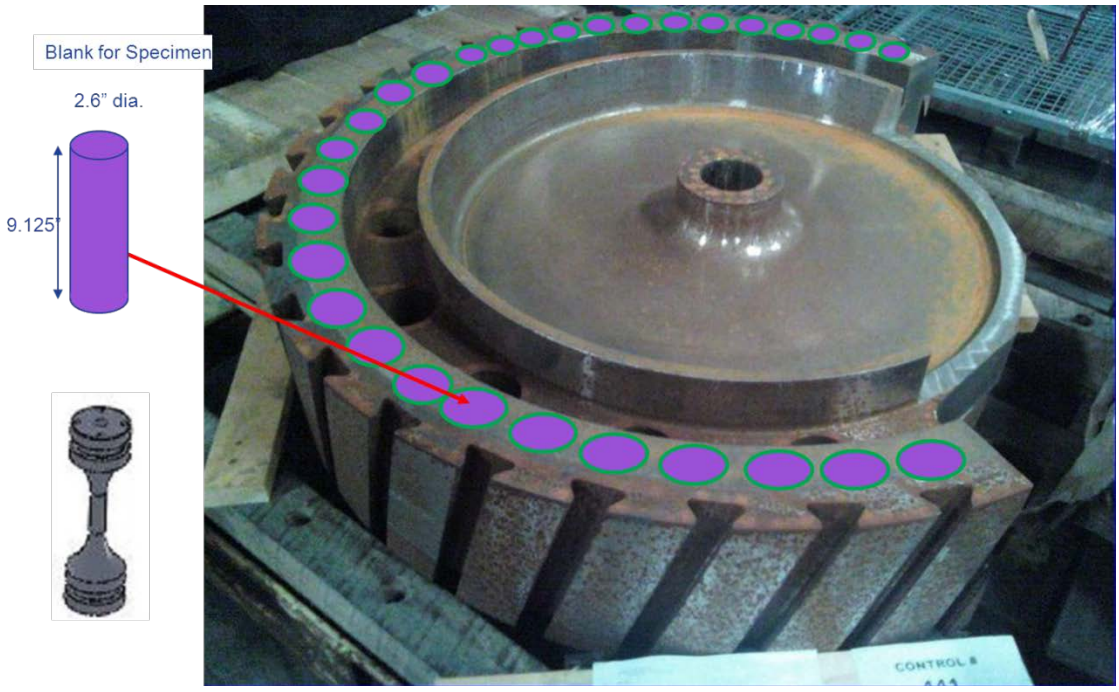

Figure 85: Bi-axial specimens extracted from NiCrMoV Wheel

The final specimen design is 9.00" tall and 2.50" in diameter on the grip ends. The gage section is 2.00" long with an outer diameter (OD) equal to 0.600" and an ID equal to 0.436". These final gage dimensions were chosen with the following key specifications in mind: manufacturing with a uniform wall thickness, ability to achieve stresses from the pressure and applied loads that hit targets beyond the uniaxial Goodman Curve, to interface with the GE-funded custom grips and to accommodate the high pressure filling and pressurization of the hydraulic fluid. Development was needed to produce a low stress ground surfaces on both on the OD and ID surfaces of the specimen gage section.

The design of the specimen involved significant development. Conventional specimens are low stress ground to remove residual stress from the specimen in order to remove this variable from the final results. The bi-axial specimen is larger than convention specimens and has the internal hole. Since the high internal pressure causes the internal surface to have a higher stress, special attention was placed on the machining of the ID. An Aviation-approved testing facility was chosen for the specimen manufacturing. They used a special light honing and internal polishing process to finish the ID of the specimens. Specimens were sent for residual stress measurement. Figure 86 shows the locations where residual stresses were evaluated. A hole was drilled to allow access to the ID of the gage section. Measurements of the OD and ID were made at opposite ends of the gage section, 90 degrees out of plane so that the presence of the hole did not interrupt the residual stresses on the surface. The values of residual stress vs depth listed obtained are consistent with GE's experience with other Aviation-approved test vendors.

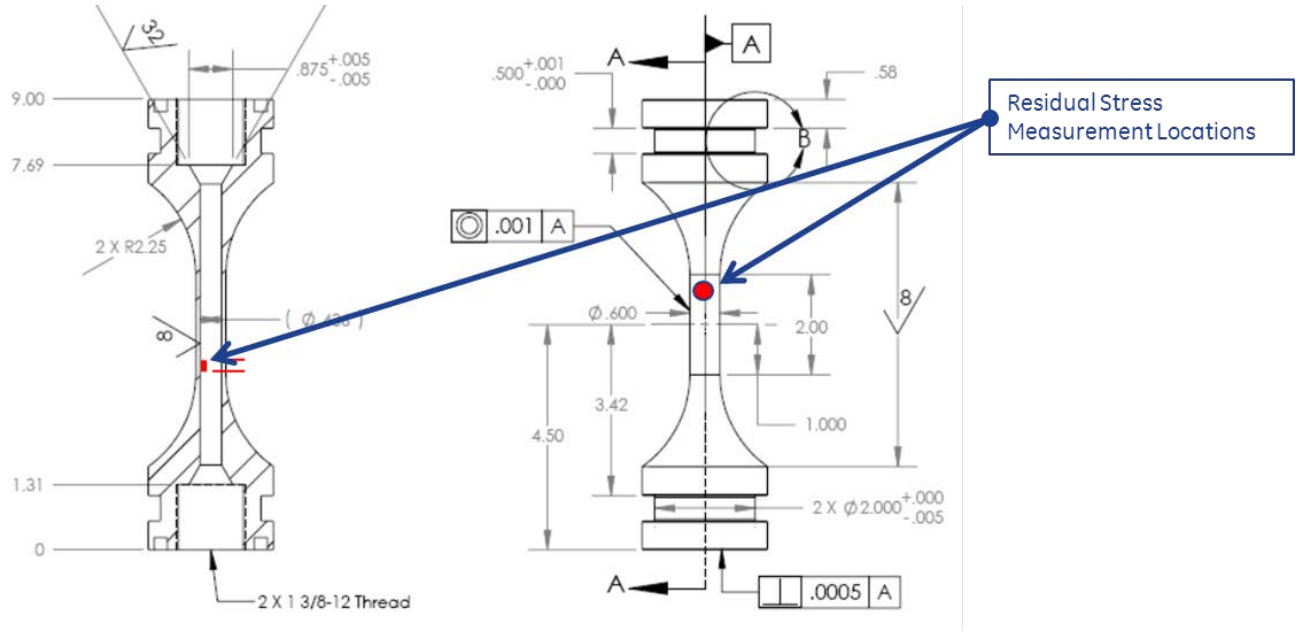

Figure 86: Bi-axial stress specimen showing the locations for residual stress evaluation

Testing at Elevated Temperature:

The initial goal of the testing was to be able to perform at elevated temperatures. The challenge was to find a fluid that could act as a hydraulic fluid and that has a high auto-ignition temperature in the event of leakage. The best fluid found was Krytox GPL107 (perfluoropolyether oil) from DuPont, which can be used up to 600°F (316°C). Testing of the fluid and specimen showed that at 30,000 psi the specimen had a volume change of 1% and the Krytox had a volume change of 100%. The specimens were designed to leak before burst. About 1 cubic inch of fluid was released upon specimen failure. The target was to have a desired pressure at temperature. Since the volume of the specimen only changed slightly, only pressure and temperature data needed to be generated for the specimen filled with Krytox. The question to be answered was "What is the required room temperature and pressure needed so that when heated to the desired temperature, the desired pressure is also achieved?" These results looked promising; however above 350°F (177°C) and 25,000 psi the specimens could not hold pressure. The root cause was that the high pressure fitting (cone section) could not hold pressure if the differential temperature between the specimen and fitting exceeded 65°F (18°C). This sensitivity required specimen design changes. Therefore, the program shifted to obtaining room temperature data only. Hydraulic fluid was used which was less viscous for easier filling at room temperature and there was no longer any flammability concerns.

Room Temperature Testing:

Figure 87 shows the biaxial specimen in the GE supplied custom grips. The grips split design allowed for ease of assembly, accommodated filling the specimen with hydraulic fluid and

pressurization. The safety head (green) utilizes a burst disk so that the specimen cannot be over pressured.

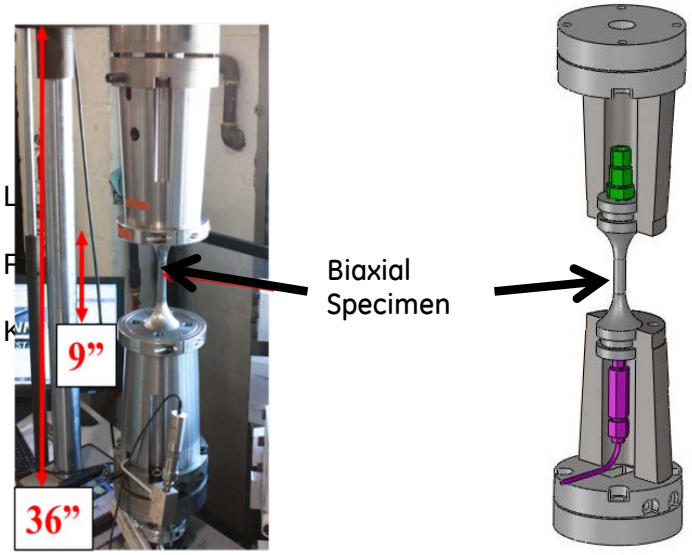

Figure 87: Biaxial test specimen in the MTS test rig

RESULTS AND DISCUSSION

Infinite life screening was assumed at 10,000,000 cycles and due to the cost of the specimens, screening for an endurance limit was done with the same specimen.
The NiCrMoV Goodman uniaxial generated curve is shown on Figure 88 (blue curve). The bi-axial generated data (red and black) is plotted on the curve and represents the stress at the ID of the specimen gage section. Note that the internal pressure causes radial and hoop stress gradients resulting in the ID having higher component and effective stresses that the OD surface. The red data are the test conditions when the R-ratios are chosen so that they equal the R-ratios of the uniaxial specimens that generated the Goodman curve. Note that the red data falls right on top of the Goodman curve as expected. The black circles represent the effective mean and alternating stresses in the biaxial specimen when the stress states simulate that of a rotor spacer. The three test plotted 6b, 8a and 9b did not fail. Test 6b and 8a ran to 10,000,000 cycles and test 9b ran to 9,000,000 cycles at which point the pressure in the specimen dropped below 95% of its original value because of facility issues. The black arrows indicate that the specimens did not fail and could have been run at higher stress levels before failure would be expected. Hence, when there is a constant mean hoop stress and a completely reversing alternating axial stress, the life is distinctly longer. Biaxial Test Log

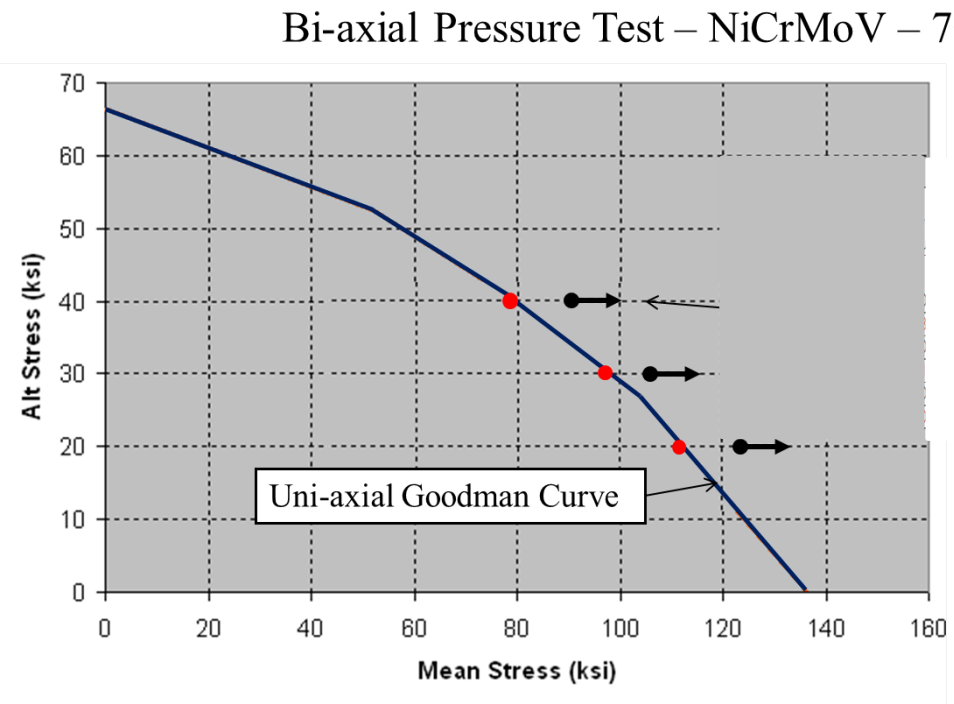

Figure 88: Bi-axial generated data (red and black) plotted on the uni-axial generated Goodman curve (blue). The bi-axial data plotted here is the ID surface of the specimen which has a higher stress than the OD surface. Note the runout of the R<-0.67 bi-axial specimens! These bi-axial stress conditions represent the R-ratios and lives of high stressed areas in rotor rim locations.

CONCLUSIONS

The bi-axial test program was successful at room temperature. Initial attempts to test at elevated temperatures were not successful but ideas for future testing look promising.

The material for the bi-axial testing was taken from the same forging as the uniaxial specimens that generated the Goodman curve making the comparison ideal. Bi-axial specimens when stressed the same as the uniaxial specimens failed as expected. Whereas, bi-axial specimens stressed to R-ratios close to that of rotor spacer stresses exhibited distinctly longer lives. This was a very important conclusion for large base loaded high torque gas turbines.

ACTIVE CLEARANCE CONTROL

This section of the report summarizes the systems work that has been performed to date under Subtask 2.2.7, Active Clearance Control Development, including model development, performance analysis, various sensitivity studies, and control system strategies.

Active Clearance Control (ACC) is the ability to change the radial gap between bucket tips and shrouds (clearance) on command. In this study, this is accomplished by changing the bulk temperature of the casings to which the shrouds are affixed. The clearance between the rotating bucket tip and static shroud allows combustion gases to bypass the buckets without extracting work. ACC allow a reduced clearance and resulting improved performance at steady state full speed full load (FSFL) conditions compared to the clearance needed to prevent bucket to shroud contact, or rubbing, during transient operation of the turbine (from a cold starting condition to FSFL, and from FSFL to shutdown).

This study evaluated geometric as well as cooling configurations to provide the desired clearance. The benefit of clearance reduction varies from stage to stage with the first stage being the most significant followed by the second stage. A parametric model (both geometric and thermal) was developed for the first stage to analyze temperatures, displacements, and stresses. From this model, Design of Experiment techniques were utilized to identify the required resources to meet clearance objectives along with the robustness and ramifications of meeting the objectives.

Geometric variations consisted of one or two circumferential ribs on the outer surface of an inner turbine shell with variable widths, heights, and axial locations. Additionally, material thicknesses throughout the structure were also variable. The cooling configurations considered were impingement on the base of the ribs and convection through internal tubes. Moreover, the heat transfer coefficients, cooling fluid temperatures, and location of cooling features were variable.

With sufficiently cold cooling air either of the geometric or cooling configurations can provide the desired clearance. However, other considerations such as stress and deformation, along with complexity, control system configuration and costs must also be considered in determining a specific solution.

The control strategy put in place for this system allows for maximum possible performance without risking turbine failure. The system is able to make use of both heating and cooling air to adjust the casing temperature to decrease the risk of component rubs during startup and shutdown and increase performance at steady state.
In summary the ACC concept development was successful and the ability to achieve performance targets was demonstrated.

TURBINE RIG FOR AERODYNAMICS TECHNOLOGY VALIDATION

This subtask benchmarked enabling aero technologies on cold flow turbine rigs for large industrial gas turbines to achieve gains in turbine efficiencies through advanced flowpath concepts.
Figure 89 and Figure 90 show a schematic and a photograph of the test rig installed in the test cell in preparation for testing. The test plan was divided into three elements: advanced diffuser characterization, turbine mapping, and performance sensitivities.

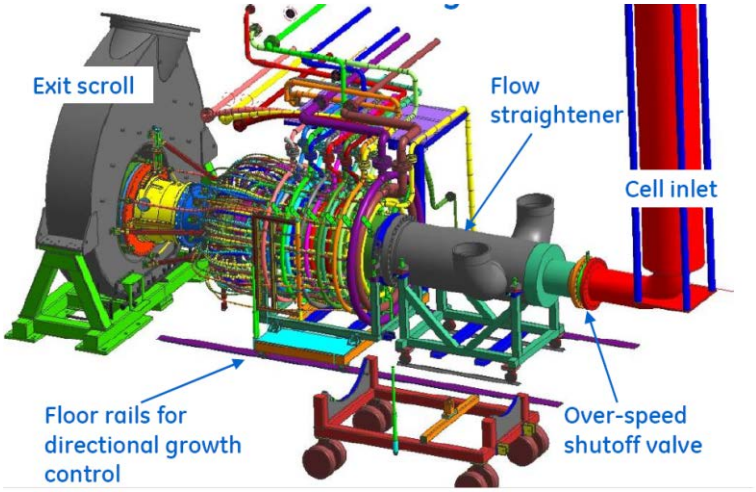

Figure 89: Turbine Aero Validation Rig

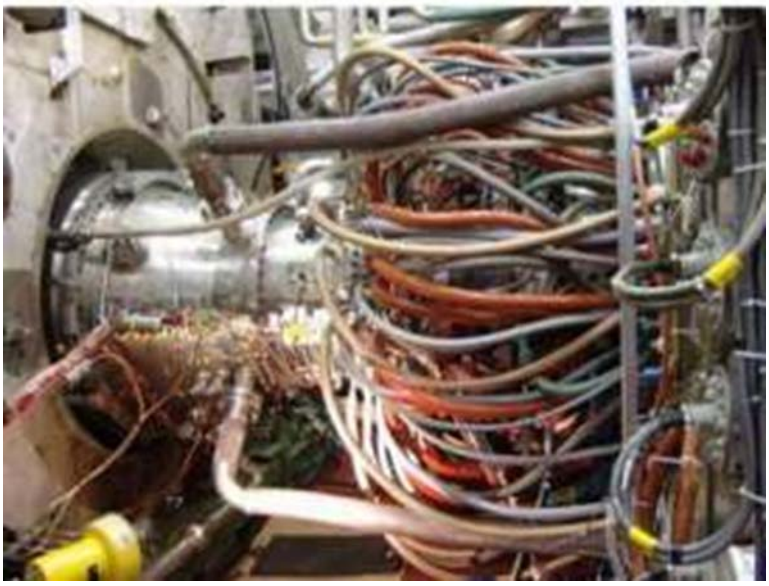

Figure 90: Turbine Aero Validation Rig - Photo

Prior starting the diffuser characterization, there was a rig mechanical shake-down with rotation where test data systems and instrumentations were checked. In addition, a vibration survey was conducted to clear the rig for test operation. The first element of the test plan addressed the characterization of an advanced diffuser. The diffuser was evaluated at several test conditions; extensive wall static pressures, as well as flowpath traverses, were used in the data collection. The turbine mapping was conducted over several pressure ratios and speed. The speed variation enabled a better understanding of the efficiency behavior at constant pressure ratio. Typical performance sensitivities like tip clearance, wheel-space purge flows and high exit Mach number were also conducted.

Evaluation of the results was completed and several post-test activities were completed, as summarized below:

- The data quality was assessed relative to (steady-state) design point repeatability and rig stability during flowpath traverses: the test data quality was good and comparable to previous tests held in the same facility.
- The secondary flow circuit data matching activity was completed. Details were added to the flow model to better match test data, and account for all leakages and purge flows entering the flowpath as part of a turbine performance audit.
- The results for the advanced diffuser technology suggested good correlation with pre-test prediction.
- There was good correlation between test rig turbine efficiency and pre-test predictions across the load range. Some test trends were identified and evaluated with further CFD assessment.

A post-test diagnostic flow check was conducted on the rig to validate leak assumptions of the initial secondary flow data match: specifically, the integrity of some of the internal manifolds

were checked. The results of the test invalidated some of the data match assumptions, and pointed towards additional troubleshooting efforts that were required to complete the system flow data match, increase system flow model fidelity, and verify individual delivery circuit flows.

Post-test CFD analysis was completed. The data match focused on design and off-design trends, relative to efficiency and profiles. Figure 91 shows the comparison of the data match vs. the predictions. It can be seen that the efficiency predictions were good in the region relevant to natural gas operation, however, were less accurate in IGCC relevant conditions.

The rig static structures were fully disassembled and visually inspected. Minor hardware damage was noted at the trailing edge of the component sharp corners in the cooling holes although the damage does not appear to have had an impact on testing.

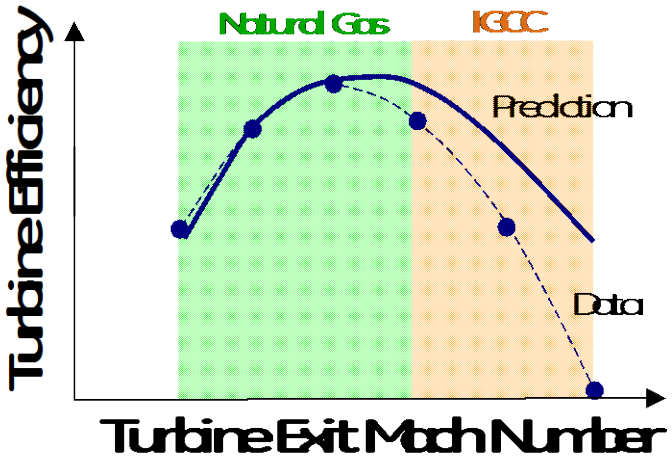

Figure 91: Efficiency Predictions vs. Test Data

MECHANICAL DEVELOPMENT FOR LARGE ANNULUS TURBINE

This section of the report focuses on the results of the final last stage bucket (LSB) that has evolved from multiple iterations. Tests in a wheel box (WB) facility were performed for five iterations in a step by step systematic approach to study tip shroud and damper wear couples.

EXPERIMENTAL METHODS

Bucket Testing

The wheelbox facility is in an underground bunker that spins a rotor containing buckets. Valves throttle airflow through the nozzles to control excitation force. The rotor is spun up to a desired speed and then strain gages and laser probes measure the vibratory stress in the buckets. The data are processed to determine the natural frequency, amplitude, and damping. A series of tests are run for each configuration with a range of excitation forces.

In order to develop a more thorough understanding of the behavior of a latter stage bucket configuration, a plan was developed to perform a series of wheelbox tests on a baseline bucket configuration as well as technology variants of this configuration. Figure 92 shows the wheelbox rig as it was setup during the first series of tests.

Figure 92: Original Wheelbox Test Rig

Baseline Bucket

The data obtained from these tests was utilized to improve design tools and processes used in the bucket development. The first test in this series was completed with a baseline configuration typical of current industry best practice. The air valves used to provide the bucket excitation forces were configured to minimize the number of manifold changes required in order to reduce turn-around times between test configurations. The baseline buckets were re-instrumented and installed in the wheelbox rotor. Prior to the resumption of testing, it was necessary to perform a high-speed balance of the assembled rotor in order to insure that all rotor responses were at an acceptable level over the entire testing range. The balancing was successfully completed with no loss of bucket instrumentation.

The next round of tests was setup identically to the first test series but with a change to the platform. The purpose of these tests was to separate the shroud's contribution to the overall bucket damping from that of the platform damper. This series of tests was performed to provide a better understanding of the effectiveness of the platform damper and to gain a thorough understanding of the various sources of frictional damping present in a typical latter stage bucket. Different valve configurations were used to excite the buckets in order to obtain responses for a range of drivers.

Testing of three different versions of higher annulus area (HAA) buckets was completed under the program using a similar test sequence to the earlier testing.

See Figure 93 for the most recent bucket spin test rig as installed in the STL facility.

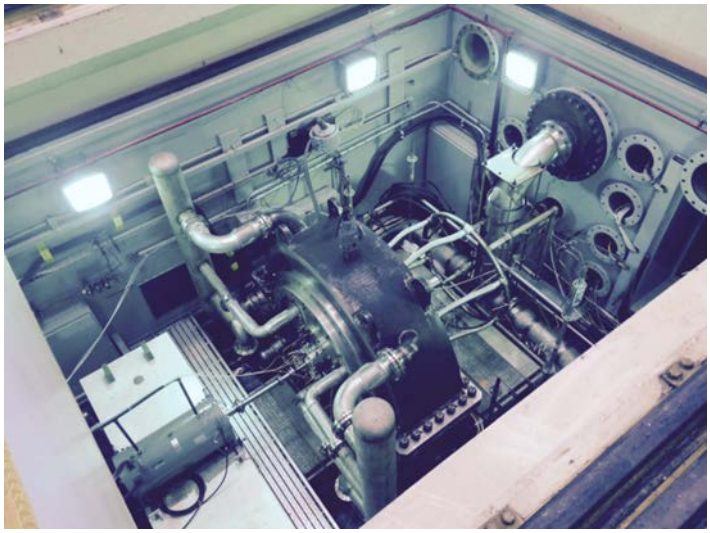

Figure 93: Rig Installed at Steam Turbine Lab in Schenectady NY

Finite Element Analysis

In addition to the manufacture of the buckets, work was performed to determine the feasibility of using explicit finite element analysis (FEA) in the aeromechanics analyses of large shrouded buckets. Simplified finite element models were analyzed to determine whether explicit FEA could be used to perform forced response and damping analyses of advanced bucket concepts. Figure 94 illustrates the match between predicted ANSYS frequencies for a simplified blade model and those produced by a frequency sweep of that model using explicit FEA.

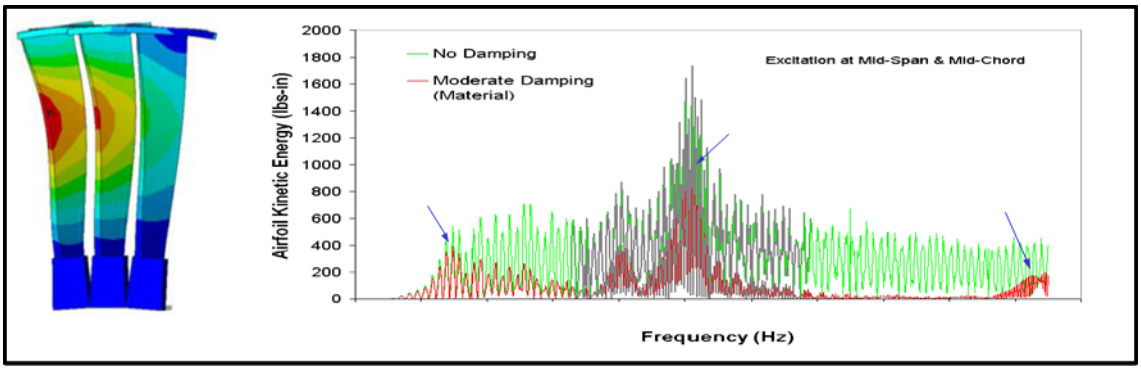

Figure 94: Comparison between predicted ANSYS frequencies and explicit FEA

Additionally, runs were performed with explicit FEA using simple block and spring models in order to create damping predictions that could be compared against hand calculations. Figure 95 shows the simplified geometry used for validation of explicit FEA damping predictions.

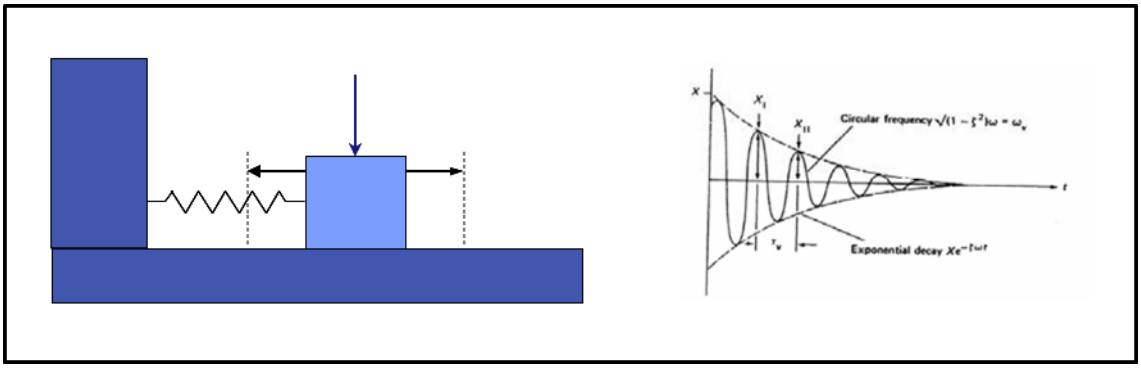

Figure 95: Geometry used for explicit FEA damping calculations

The explicit FEA analyses required considerable computation resources to complete runs in a timely fashion even for simplified models.

RESULTS AND DISCUSSION

Baseline

The measured vibratory responses matched reasonably well with the analytical pre-test predictions made using the modal analysis process developed with data from the baseline wheelbox testing and GE fleet engine data. However, some of the higher frequency modes were slightly below the predicted values. Upon investigation, the test data indicated that the buckets ran at a higher temperature than was expected due to increased windage heat up.

After the first test point, thermal paint was applied to some of the buckets in order to gain a better understanding of the wheelbox temperatures. Preliminary results from the thermal paint

indicated that the HAA buckets ran hotter. Once the higher temperatures were taken into account, the test data correlated well with the pre-test frequency predictions for all modes. This provided verification that the analytical processes being developed were doing an adequate job of capturing the physics of the problem.

New Configuration #1
Frequencies were found to match well with calculated values. Damping was better than expected for all modes of concern as compared to the baseline configuration.

New Configuration #2
Strain gage and light probe data responses showed similar vibratory response amplitude and damping trends.

In addition, a follow-on rainbow test of the second HAA concept was performed with an alternative platform damping concept. Results indicated changes in damping both minor/major due to design changes made on the bucket.

New Configuration #3
Results indicate good effectiveness of the variant damper design when compared to the baseline third iteration, as supported by a significant decrease in response amplitude for the vibratory modes of interest, as demonstrated in Figure 96. All indications show good agreement between analytical models and test data.

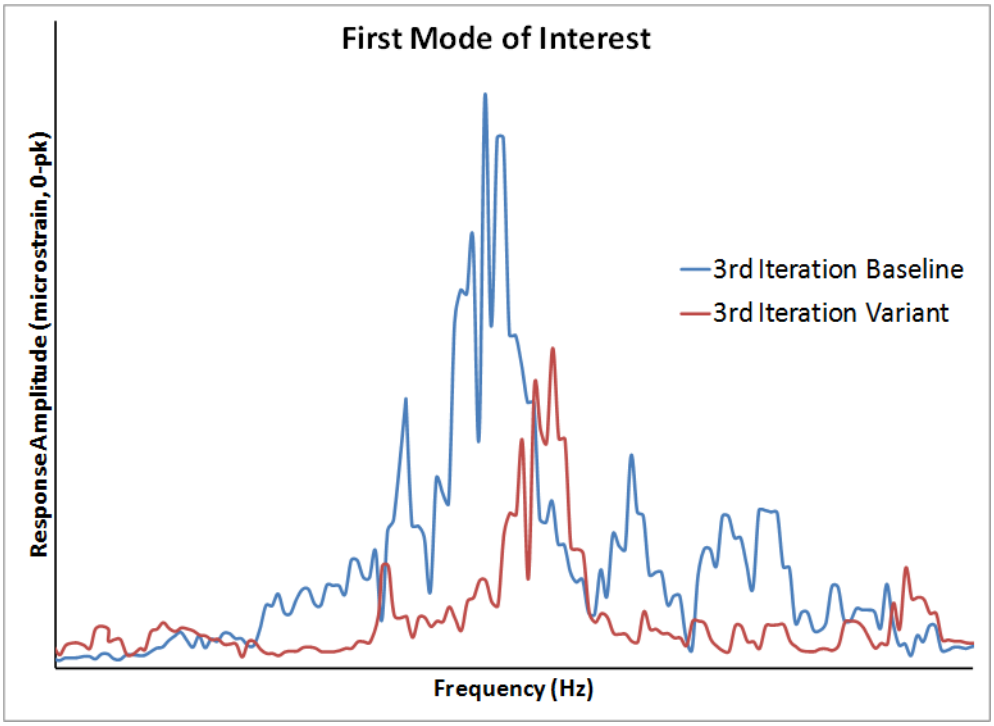

Figure 96: Response Amplitudes for Iteration 3 Baseline and Alternative Damper Configurations

CONCLUSIONS

Designs were developed and tested for a baseline large latter stage bucket as well as 3 new configurations leading up to a final configuration for a large latter stage bucket. Multiple bucket designs analyzed and tested. Hardface coatings were developed for certain component features. Damper configurations were down selected and installed for test to evaluate effectiveness. Tests provided key data used to validate bucket natural frequency and mechanical damping design tools / predictions. The analyses and results from all testing have fed directly in the best practices and design guidelines that GE uses to create larger latter stage buckets.

ADVANCED SENSORS

This portion of the program focused on the development of gas turbine sensing technologies capable of: (1) performing in the hot and harsh environment of the gas turbine hot gas path, and (2) enabling real time measurement of metal and gas temperatures, pressures, flow rates, and gas constituents in the combustor, and the turbine sections. The use of real-time data from advanced sensors and electronics in the control of gas turbines has the potential to enable improved performance, emissions, and operability. This task focused on the technology of utilizing and integrating a variety of advanced sensor technologies into gas turbine control and operation.

The team established gas turbine domain specific parameters of interest and measurement accuracy, repeatability and reliability criteria, and carried out an extensive survey of capability of sensors to meet these requirements. This was done by an extensive flow down of performance, and prognostics & health monitoring (PHM) application requirements to identify key sensing requirements. This was further broken down into sensor specific requirements with numerical targets and specification limits. The most significant sensing gaps exist in the turbine hot gas path, where existing sensor technology cannot survive in the harsh environment. Three distinct sensor technologies were selected for further evaluation, (1) Multi-color infrared (MCIR) Pyrometry, (2) Tunable Diode Laser Absorption Spectroscopy (TDLAS) and (3) Passive Wireless Sensors Technology (PWST). Laboratory and rig testing of these sensing concepts in as realistic an environment as possible was then carried out.

MCIR technology was developed to the point of being ready for long-term field testing (*It is noted that field testing of sensors was not in scope of this program*) – the team carried out a gamut of tests ranging from bench-top validation, to testing in validation rigs, to on gas turbine testing. TDLAS capability was demonstrated in high temperature, high pressure rig testing.

EXPERIMENTAL METHODS

An extensive flow down of gas turbine performance, and prognostics & health monitoring (PHM) application requirements was carried out with many domain experts. This established gas turbine domain specific parameters of interest and measurement accuracy, repeatability and reliability criteria. This was further broken down into sensor specific requirements with numerical targets and specification limits. A bottoms-up review of detailed technical options for selected parameters of interest was completed. An extensive survey of capability of sensors to meet these requirements was carried out. The focus was mainly on harsh environment capability. Hot gas path monitoring & detection (M&D) requirements and importance rankings are presented in Figure 97 and a Pareto of appropriate sensor technologies that could enable highly ranked M&D requirements are presented in Figure 98.

Hot Gas Path

Product Requirements

Customer Expectation	Importance	State Estimation - Tracking Filters	PIVT	Multi-color IR pyrometry	Embedded Wireless Sensors	Tunable Diode Lasers	Filtered Rayleigh Scattering	Fiber Optic Sensors	Surface Acoustic Wave	Single wavelength IR	Phosphors	Ultrasound, laser, coriolis flow meters	Capacitive	Acoustic Pyrometry	Visual, UV optical detectors, cameras	Coupled resonators	Integrated Sensing Structures	Laser Doppler Vibrometry	Ultrasound for pressure	Fabry-Perot Probes (e.g. Oxensys)		Total
[redacted]	5				l				l			l	h		m	l	m	l				100
[redacted]	5	l	l	h	h			m	h	h	h			l	l	m						275
[redacted]	5			m	h			l	m			l	l					m				105
[redacted]	5	h	h			m	h	h						m								210
[redacted]	5	h	h			h	h	l				m		m					m			230
[redacted]	5	h		h	h			l	m		m	l					m					190
[redacted]	5	h	h	h		h	h	l						m								245
[redacted]	4			h	h				l	h	m				l	l						132
[redacted]	4	l	m					h				l	h		m	m		m				128
[redacted]	4	m	l				l					m										32
[redacted]	4		l				l					h										44
[redacted]	4	h	l				l					l	l						l			56
[redacted]	4	m	h	m	l	m	h	l	l					l								124
[redacted]	4				m				l			l	l									24
[redacted]	3	l						l						l								9
[redacted]	3					h		l	l													33
[redacted]	3		h	m	m	h	h	h	m			l		l								141
[redacted]	3	h	h			l	m	l				l		l			l		l			81
[redacted]	3	l				h																30
[redacted]	3	l	l	h	h			m	h	h	h			m	m							168
[redacted]	3					h	l	l	l													36
[redacted]	3	l						l														6
[redacted]	3	l	m		l	l	m	l														30
[redacted]	3					l		m														12
[redacted]	2	l		h	m					h	m					l						52
[redacted]	2		m		l		l		l								l					14
[redacted]	2				m			l	l		l	l										14
[redacted]	2			h	m				l		m				h							50
Total		293	272	270	251	234	233	185	140	126	113	98	94	72	63	38	35	32	22	0		

Figure 97: Gas Turbine hot gas path monitoring and detection (M&D) needs and candidate sensor technologies. Potential sensor solutions are specified in different columns. The specific detection needs are arranged in the rows and are GE proprietary and have been blanked out.

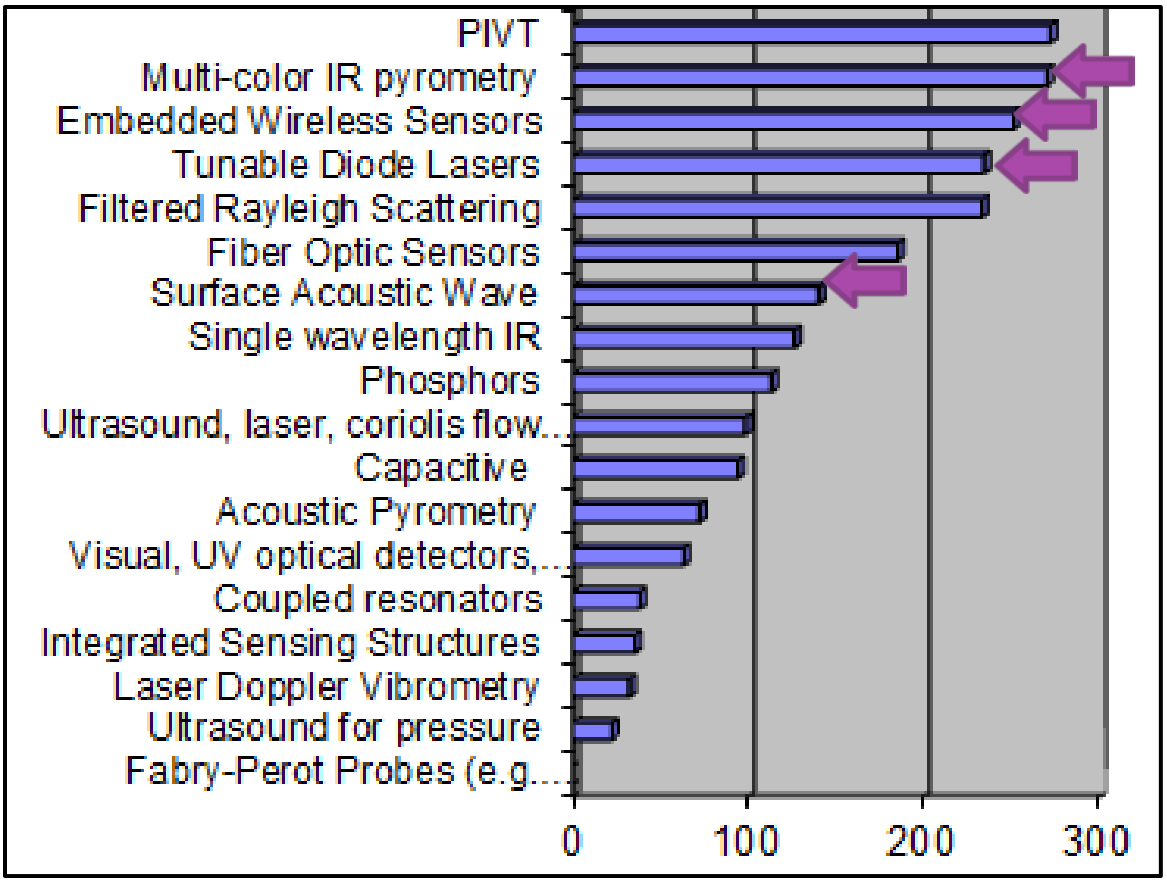

Figure 98: Pareto of candidate hot gas path sensing technologies. Arrows indicate technologies selected for this program.

The results of the Pareto, and other factors, led to consideration of three main gas turbine hot gas path applications and corresponding primary sensor technologies:
Gas and component temperature imaging and measurements in the hot gas path, using technologies, such as**:**

Multi-color infrared (MCIR) Pyrometry
Tunable diode laser absorption spectroscopy (TDLAS)

Distributed smart sensors that are fully passive (not requiring any external power) and utilize wireless communication, such as:

Surface Acoustic Wave (SAW) sensor technologies
Direct deposited radio frequency (DDRF) sensor technologies

The SAW and DDRF technologies were lumped together in one subtask called “Passive Wireless Sensors Technology” (PWST) due to operational similarities between these two technologies. Both are readily capable of temperature measurements and could be developed for strain and pressure measurements.

Turbine emissions and fuel properties measurement using faster, lower cost, distributed sensors, such as:

Raman spectroscopic methods for fuel gas analysis
Fiber Bragg Grating (FBG) sensors for gas composition measurement

FBG sensors for gas composition measurements were not considered for further development as technology was deemed too immature to be ready for evaluation under this program. For other factors, the Raman spectroscopy was not selected for further evaluation.
Thus, as a final down-select, three distinct sensor technologies were considered for evaluation under this program – MCIR, TDLAS and PWST. Tradeoff matrices (see Figure 99, Figure 100, and Figure 101 below) for each of these selected technologies were completed to identify best experimental approach in each case. These approaches were selected to specifically address challenges associated with the hot and harsh environment in the gas turbine hot gas path:

- Physical access to locations of interest
- Power and signal connectivity to sensors and readers
- Certification and safety requirements for sensors
- Algorithms to extract features of interest in the presence of background noise

Laboratory, and factory rig testing of these sensing concepts in as realistic an environment as possible was then carried out.

Title

Pass 1 | Marg 0.5 | Fail 0

				System					Reliability			Manuf	Design
				2-d Mapping	Response Time& Rep Rate	Simulataneousity & Instantaneousity	Stability & Repeatability	Accuracy	TRL	Fluid Dynamical Disturbance	Sensor Life	Cost & Complexity Index	Optical Access Level
			Importance	5	4	4	3	3	3	4	5	3	3
			USL	5	10	5	50	75		5		5	5
			LSL	3	0	3	0	0	4	3	10000	3	4
			Tolerance	1	2	1	25	25	1	1	1000	1	1
			Units	AU	s	AU	F	F	U	AU	hrs	AU	AU
	No.	Concepts	Score										
☐	10	MCP Imaging Module	2.90	5	3	5	50	70	2	2	10000	2	3
☐	1	Filter Wheel approach	2.85	5	2	2	50	70	4	2	10000	2	2
☐	8	Scanning LOS Multicolor Pyro	2.60	2	5	1	50	70	2	3	10000	2	4
☐	2	Multicolor Pixel camera	2.45	5	2	5	75	70	1	2	10000	0	2
☐	9	Multicamera and filters	2.45	5	3	5	30	70	3	3	5000	0	1
☐	5	visible camera	2.45	5	3	5	75	25	1	2	10000	1	2

Figure 99: MCIR – primary approach selected is an integrated optical splitter module. Filter wheel approach was not pursued because of space constraints in the IR camera enclosure used in conventional IR system.

Temp Sensor Candidates

Pass 1 | Marg 0.5 | Fail 0

			System					
			Response Time	Accuracy	Stability and Repeatability	Reliability	Cost	TRL
		Importance	5	4	3	2	6	1
		USL	1	50			80	
		LSL			3	3		6
		Tolerance			1	1		1
		Units	sec	°F	AU	AU	$k	AU
	No.	Concepts	Score					
☐	3	Fixed Wavelength 2f/1f (H2O lines)	3.50	0.5	50	3	3	50	7
☐	4	Scanning wavelength 2f/1f (H2O lines)	3.42	1	50	3	3	50	5
☐	5	Fixed Wavelength 2f/1f (CO2 lines)	3.33	1	50	3	3	50	4
☐	1	Fixed wavelength direct absorption (H2O lines)	3.25	0.1	50	2	3	50	9
☐	2	Scanning wavelength direct absorption (H2O lines)	3.25	1	50	2	3	50	8

Figure 100: TDLAS – primary approach selected was two line ratio metric measurements. This was deemed to be the best approach overall compared to other available options.

Title

Pass 1 | Marg 0.5 | Fail 0

			System			Reliability			Manufacturability			Design Margin		
			Operating Temperature Range	Sensor Encodability	Accuracy	CTE matching	Sensor Adhesion	TRL	Cost	Ease of Assembly - Sensor	Ease of Assembly - Antenna	Temp & Strain	Wireless Range	Airflow Turbulence
		Importance	5	4	3	4	3	2	5	1	1	5	4	3
		USL			10	5	5		1	2	2	1		5
		LSL	750	100	1	3	3	3	0.2	2	2	1	3	3
		Tolerance	100	1	1	0	0	1	0.1	0	0	0	1	1
		Units	C	#	%	Index	Index	Index	1/k$	Index	Index	Y/N	cm	Index
	No.	Concepts	Score											
☐	3	Deposited RF Antennas	2.42	1000	1	10	3	3	3	0.5	1	1	1	5	5
☐	1	SAW	2.38	1000	1000	10	2	2	3	0.2	2	2	1	10	3
☐	2	DW RF Coils	2.17	1500	1	15	5	3	3	1	1	1	1	3	5
☐	4	IR Camera	2.04	1500	100000	10	5	5	6	0.01	2	1	0	100	5
☐	5	Wired Deposited Sensor	2.04	1500	1	5	3	3	6	0.1	0	2	1	0	3

Figure 101: Two PWST options were evaluated – Direct Deposited Radio Frequency (DDRF) & bonded Surface Acoustic Wave (SAW) sensors. There are pros and cons of each and it was decided to explore both and pick winner after analysis of gas turbine implementation and test data.

RESULTS AND DISCUSSION

A detailed requirements flow down and bottoms-up review of selected parameters of interest was completed. Three primary technologies for this program were selected. As summarized, given significant challenges posed by the gas turbine environment and limited technological alternatives, the results were highly encouraging.

Summary of results and learnings:

1. MCIR Pyrometry program reached a full conclusion and passed all the critical to quality criteria. A clear improvement in accuracy of temperature measurements was demonstrated with a minimal increase in complexity of the measurement system and analysis algorithm. MCIR is being considered as an add-on option to the conventional single color Pyrometry product development.

2. TDLAS capability in high temperature, high pressure rig testing was demonstrated. Temperatures in excess of 3000°F (1650°C) and pressures up to 300 psig were reached without any damage or loss in performance of the TDLAS system.

3. The wireless sensors program ran into many complications that led to the conclusion that this technology is not ready for gas turbine applications and there are many aspects that need further development.

CONCLUSIONS

The major technical challenges to the introduction of any new sensors to gas turbines limited the pool of potentially applicable technologies. The most significant sensing gaps exist in the turbine hot gas path, where existing sensor technology cannot survive in the harsh environment.

Some of the most promising technologies in the hot gas path environment were identified and tested. Three distinct sensor technologies were selected for further evaluation, namely, (1) Multi-color infrared (MCIR) Pyrometry, (2) Tunable Diode Laser Absorption Spectroscopy (TDLAS) and (3) Passive Wireless Sensors Technology (PWST). Laboratory and rig testing of these sensing concepts in as realistic an environment as possible was carried out.

MCIR technology was developed to the point of being ready for long-term field testing (*It is noted that field testing of sensors was not in scope of this program*) – multiple tests ranging from bench-top validation, to testing in validation rigs, to on gas turbine testing were performed.

TDLAS capability in high temperature, high pressure rig test was demonstrated.

PWST is not ready for gas turbine application.

COOLING FLOW REDUCTION

GE Power & Water and GE Global Research have conducted extensive research and technology development to improve cooling features for hot gas path parts to reduce required cooling flows and enable higher temperature operation both to improve efficiency and turbine throughput while reducing costs per kilowatt.

Among the areas explored were:

1. Improving film cooling both by understanding the impact of different cooling hole features as well as developing new film cooling concepts.
2. Developing improved internal cooling features.
3. Improved understanding of the heat transfer coefficients (HTCs) of a variety of cooling features.
4. Improving manufacturing techniques to allow the creation of advanced cooling features.

Experimental Objectives

The cooling flow reduction subtask had numerous experimental objectives over the extent of the program. Some of these programs built off the previous learnings and rigs, while others were developed to explore entirely different areas of heat transfer technology. Each one of these areas and phases focused on a different technology readiness level, and therefore was demonstrated on a certain type of test rig. As the technology readiness level increased, the test rig and geometric complexity increased along with the required analysis and data quality. This progression will be discussed at high level and will focus on the important lessons learned.

Film Cooling

Film cooling is one of the most important aspects in the cooling strategy for hot gas path components. Film cooling is when cooling air is ejected onto the surface through holes or slots in the wall of the airfoil leaving a protective blanket of cool air to shield the part from the hot gasses. The performance of film cooling is defined by the parameter film cooling effectiveness in Equation 1, where T_{rec} is the hot gas recovery temperature, T_{cool} is the coolant temperature exiting the holes and T_{aw} is the mixed stream (coolant and hot gas) temperature at the wall in the absence of heat transfer to the wall.

$$\eta = \frac{(T_{Rec} - T_{aw})}{(T_{Rec} - T_{cool})} \qquad \text{Equation 1}$$

Film cooling performance is determined by numerous geometric and fluid parameters. The work done under this program focused on understanding some of these sensitivities and improving the geometry. Film cooling design, in general, is coupled with the internal cooling requirements and the total amount of cooling air allowed by the cycle to meet part life. If the film effectiveness can be improved, then either cooling flow can be removed or part life/margin can be increased. Because many of the different geometry and flow conditions lead to film performance that behaves differently in different regimes, there are no universal scaling rules and much of the geometric and flow specific behavior must be determine experimentally. This section will discuss experimental and computation studies in film cooling over the life of the

program and highlight some key lessons learned. It has used numerous test rigs of various complexity and highlights will be given below.

Advanced Film: Hole Shaping

In the first phase of the program, improvements to standard diffuser film hole shapes were investigated by advanced hole shaping concepts. Many of these concepts had shown promise in simple lab tests and were investigated here in a more "engine relevant" environment. The first test rig was a five passage annular sector cascade that was a 42.5% scaled rig of a product turbine which had the correct airfoil shape and the correct Mach number distribution. Airfoil film, endwall film, and the resulting aerodynamic losses (among many others) were studied on this rig over several years.

Advanced hole shaping geometries were studied. The scaled film hole and both suction side and pressure side row locations were cut into low conductivity Ultem 2300 airfoils. The test airfoils were tested over a range of coolant flow rates (blowing ratios, 'M') and the laterally averaged film effectiveness curves were determined using an IR camera and simple post-processing techniques. Several geometries tested showed better film effectiveness than the baseline diffuser geometry at a nominal blowing ratio of 1.5 and some of the geometries performed worse. However, the relative behavior with respect to the baseline changed with blowing ratio. For instance at a blowing ratio of M=0.9, Hole Shape 1, Hole Shape 2 are on par with the baseline shaped hole. At a blowing ratio of M=1.2: Hole Shape 1 shows 12% increase compared with the baseline shaped hole. At a blowing ratio of M=1.5: Hole Shape 1 shows 20% increase compared with baseline shaped hole. Other configurations showed significantly more promise at the higher blowing ratio.

In light of these results Hole Shape 1 was tested on the pressure side and, in general, showed a benefit relative to the baseline diffuser. Pressure side film cooling tests show up to a 25% increase in film effectiveness using Hole Shape 1 over the range of blowing ratios tested.

Additional hole variations were studied given the improvement relative to the baseline diffuser. Small permutations to the footprint (indicative of potential manufacturing variation) were made and results for the nominal blowing ratio of M=1.5 determined. In general, there is some sensitivity to the variations but these always resulted in improved film effectiveness relative to the baseline. This is true across all blowing ratios but certain configurations tended to show the most improvement at the higher blowing ratios.

The need to test at engine scale, and new single airfoil, resulted in the building of a 2D cascade. The airfoil was a full scale, pitch-line product stage 1 nozzle airfoil contour with contoured sidewalls to create the right Mach number distribution on the airfoil surface. These sidewalls were designed using CFD. Figure 102 shows a cross section of the test rig with the airfoil and window placement can also be seen. The airfoil was designed to slide through the endwall of the test rig.

The airfoils used for this test were modular to allow for different test articles and coupons at different regions on the airfoil. Three airfoils were used so that three different configurations could be tested on a given test day. The airfoils were made from Ultem 2300 as well as the test coupons. End covers and blanks for the various coupon locations seal the airfoils with the help of RTV. A section view of the airfoil is shown in Figure 103 with the 3 film test locations. This view reveals a single plenum, instrumentation locations and the coolant supply tube.

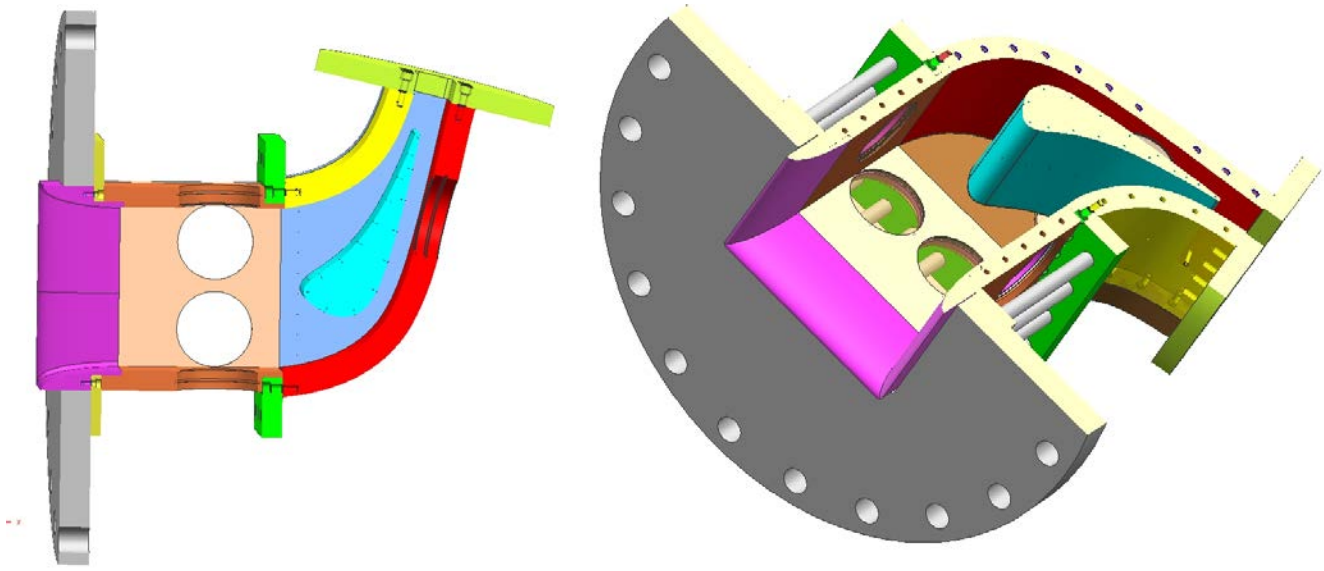

Figure 102: Test rig cross-section.

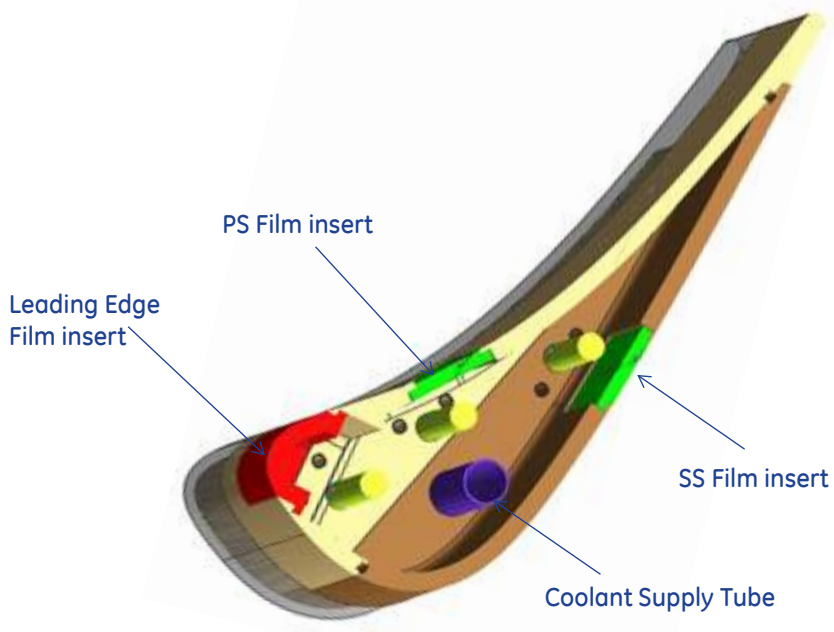

Figure 103: Cooled airfoil cross section.

The test plan for this investigation involved a comparison between the baseline diffuser, and two alternate configurations. For the pressure side tests, both alternate configurations are better than the baseline. This complete set of data, plus addition learnings indicated there was no advanced configuration shape that worked consistently across all test rigs and from pressure to suction side. Furthermore, these studies demonstrated that the underlying physics and scaling methodologies require more investigation.

Transpiration Cooling

Transpiration cooling is another technology that was investigated to increase the performance of film cooling over convention diffuser technology. Transpiration cooling, as was investigated here, used small discrete films holes to evenly distribute film over the surface of the airfoil. Other configurations were used, but the general idea targeted "transpiration" in the sense that a uniform temperature coolant gas that is injected through the wall with mass flux distribution (via local wall thickness or porosity) such that a constant temperature surface results. Two phases of transpiration cooling were investigated.

Transpiration cooling: Phase 1

The test rig to screen transpiration and transpiration-like film technologies was a single passage, 2D symmetric airfoil cascade. To achieve the desired Mach number distribution, the sidewalls required definition based on a desired flow rate, air temperature and airfoil profile. Thus, inviscid flowpath calculations were performed and the sidewall coordinates were adjusted so that the calculated Mach number distribution matched the desired Mach number distribution. Because of the symmetric nature of the test rig, two different sidewall contours were defined for the suction and pressure surfaces. Figure 104 shows a cross section of the test rig for both the suction and pressure surfaces. The airfoil as well as the window placement can also be seen.

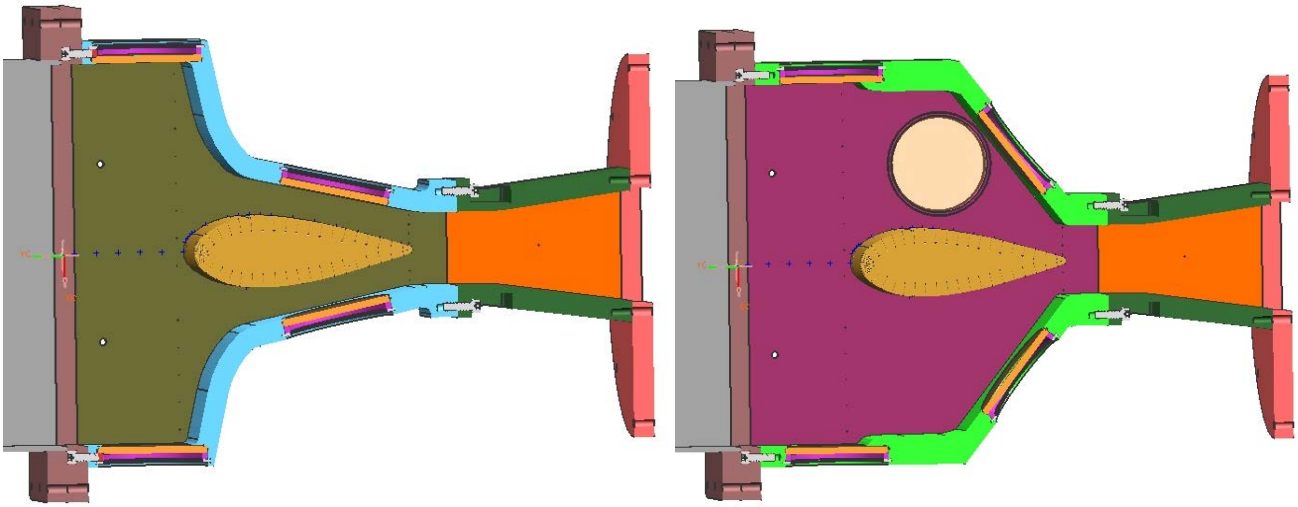

Figure 104: Suction and pressure surface test rig cross-sections

To baseline the new transpiration technologies, an airfoil with a row of diffuser shaped film holes was tested. The hole throat diameter was set at a nominal value and the holes were spaced in the span-wise direction. Different "Transpiration" configurations were tested. These multi-hole cooling arrays are made of small discrete film holes at a particular span-wise and axial spacing. The different transpiration configurations are altered by blocking different rows or hole patterns to reduce to the total flow area. This was done in several different ways (even for the same configuration) to assess the impact on cooling performance.

Transpiration cooling: Phase 2

Given the promise of transpiration configurations additional testing was desired. The test rig used to demonstrate the second phase of transpiration cooling technologies was the same single passage, 2D airfoil cascade used for chevron film testing described above. The airfoil was a full scale, pitch-line product stage 1 nozzle airfoil with contoured sidewalls to create the right Mach number distribution on the airfoil surface.

To baseline the new transpiration technologies, an airfoil with a row of diffuser shaped film holes was tested. This was the same baseline diffuser geometry used for comparisons with alternately shaped holes cooling technology. The film hole was angled to the local surface tangent. The hole had a nominal throat diameter and the holes were spaced in the span-wise direction.

It is important to note that this test rig and baseline film cooled airfoil were designed and used to support other GE Power & Water programs prior to the Transpiration effort. Given this fact, the baseline film cooled airfoil only had 1 film row location. Based on the decay of the measured film effectiveness, another row of film holes would likely be required given the amount of remaining surface area (to the trailing edge). Also note that the transpiration configurations were designed as a full coverage technology demonstration. This represented a situation in which the film geometries could not be compared 'back-to-back'. To overcome this situation, a second 'virtual' film row was added halfway between the first row and the trailing edge as seen in Figure 105. This location also coincidently corresponded to the location which the film had decayed from the first row and would need to be replenished.

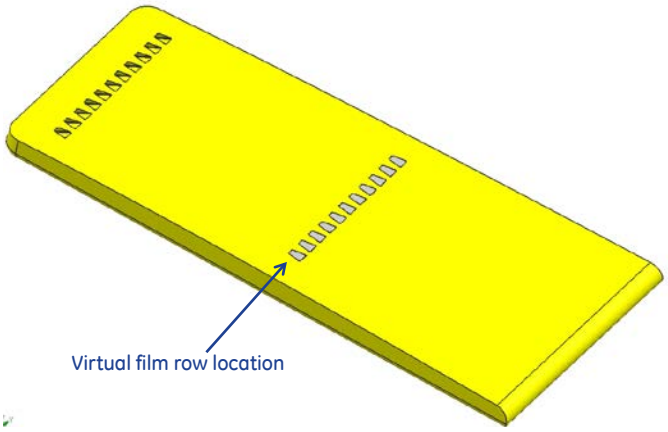

Figure 105: Baseline airfoil, 2 rows of diffuser shaped film holes

To create a single film effectiveness profile, the virtual film effectiveness from the second row has to be 'accumulated' with the first row, providing a film effectiveness profile all the way to the trailing edge.

Two different "Transpiration" or multi-hole cooling configurations were tested. As described, the intent was to explore two different design philosophies which covered the same surface area while constraining the total flow area (and flow rate) to that of two rows of diffuser shaped holes.

The first, designated as "Transpiration #1", followed the design philosophy of build, maintain and decay. The second transpiration configuration, Transpiration #2, took on a different design

philosophy. This configuration consisted of one continuous multi-hole array of constant spacing. These two transpiration configurations were manufactured into test inserts which could be interchanged to test the different configurations.

Transpiration cooling technology was also tested on the pressure surface in the 2D vane cascade to determine the performance and distribution in a different flow field environment. The results presented here are considered at two different cooling flow rates and in each case, the configurations had identical metered flow area and utilized the same total coolant flow. The results show that the transpiration technology appears to have more of an impact on the pressure side than it does on the suction side. This is also confirmed through and area-averaged analysis.

Computation LES Film Cooling Investigation
This numerical study sought to understand how metering hole diameter, L'/d, L/d, boundary layer thickness, Reynolds Number, and M_∞ affect film cooling performance. Additionally, this study validated the FLUENT LES code against experimental.

The operating conditions were chosen to match the laboratory setup as closely as possible so that the data could be validated against the experiment.

Numerical Method of Solution
For the operating conditions described in the previous section, the maximum Mach number was greater than 0.3 and the DR = 1.8, thus density variations due to velocity as well as temperature played a significant role in the solution and the flow had to be modeled as a compressible gas. The temperature variations of the specific heat and thermal conductivity were assumed negligible for the temperature range studied. In this study, large-eddy simulation (LES) was used to directly simulate the large scale motions of the flow. LES applied a spatial filter to the Navier-Stokes equations to decompose the velocity into a resolved and sub-grid scale (SGS) component. LES directly resolved the large scale turbulent fluctuations, which had the most influence on the solution. The SGS component represented small dissipative motions which have a more universal character and could be modeled easily with a simple eddy-viscosity model.

In film cooling there are multiple points of separation within the hole, a shear layer as the jet exits the hole, and complex vortex structures that form as the jet interacts with the freestream; historically RANS simulations have had difficulties accurately modeling these features, thus LES has shown to substantially improve cooling predictions.

The LES solutions in this study were obtained using ANSYS Fluent v14.5, using the wall-adapting local eddy-viscosity (WALE) SGS model. The pressure based coupled scheme was used with 2nd order pressure and bounded central differencing for density, momentum, and energy. The bounded 2nd order implicit transient formulation was used. The flow was initialized from a state-state solution at which point LES ran with an initial timestep calculated from $U_\infty \Delta t/d$ = 0.1 until a statistically steady state was reached. At this point the flow was time-averaged using a timestep calculated from $U_\infty \Delta t/d$ = 0.04. The computation grid, shown in Figure 106, was generated using ICEM CFD and consisted of 20 million hexa elements, with 8 million elements in the hole. The y^+ next to all walls was less than unity. The SGS eddy-viscosity ratio was less than 5 everywhere ensuring large scales are well resolved.

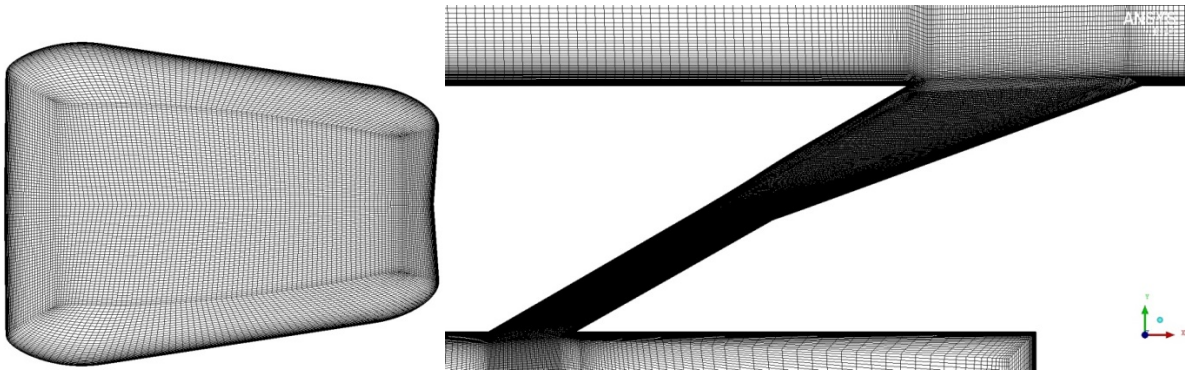

Figure 106: Computational Grid

Conclusions and Potential Future Work
A CFD study based on LES with the WALE SGS model was performed to evaluate the performance of a diffuser film-cooling hole with 2 different metering hole diameters injected axially to the HGP. To further evaluate the discrepancies in performance between the two holes a parametric study was introduced to isolate *L/d*, *Re*, and δ_{99}. A final set of calculations looked at the impact of the film-cooling performance when simulated with suction side conditions.

The study found that overall cooling is higher for the larger holes at all *BR*s and *L'/d* and that a long *L/d* is detrimental to film-cooling performance. It was shown that increasing *L'/d* shows a clear benefit for both hole diameters up to *L'/d* = 4.5. The impact of *Re* and δ_{99} is not completely clear, as the *L'/d* = 3.5 case showed higher *Re* and smaller δ_{99} is beneficial, while *L'/d* = 4.5 suggested the opposite to be true. Performance was seen to decrease on the suction side, with the largest impact in performance occurring for the smaller δ_{99}/d cases.

Internal Cooling
Internal cooling is critical to the overall cooling strategy of hot gas path components. Typical internal heat transfer technologies used in current designs include turbulated channels, impingement, and pin banks. This program investigated numerous other technologies for improving internal HTCs. As manufacturing capabilities increase, the use of improved internal heat transfer technologies such as highly porous materials, dense pin banks, and advanced impingement configurations become desirable. Thus, a simple test rig was designed and built to test improved internal heat transfer technologies.

The goal of the task was to reduce the amount of total coolant flow due to increased internal heat transfer. The different components and test sections were designed based on scaled engine geometry and flow conditions.

Figure 107 illustrates the experimental setup with the interchangeable insert in the middle. A total of ten test cases were examined for their heat transfer capabilities for a trailing edge or double wall type application in a gas turbine blade/nozzle. The test facility was composed of a plenum, developing flow section, aluminum test section, and an exhaust. The test section consisted of two parallel copper heaters. The test rig also had the flexibility to allow for impingement of air on the top surface of the test section in addition to the main cross flow.

The test cases consisted of a smooth channel to benchmark the test rig behavior, 2 geometries which represented the state of the art and 6 configurations which represented the new technology along with several different embodiments. Thermocouples were embedded along the top and bottom surfaces of the test insert. The details of the test section are shown in Figure 108.

As described, the characterization of the rig and measurement technique was completed using a smooth channel. Furthermore, the two configurations which represented the state of the art were tested and detailed analysis showed that the results were consistent with the predicted results. The 3 new technology test sections have been completed and the results showed superior HT capabilities at a cost of higher pressure drop. A detailed look at additional performance metrics (HTC and Pressure drop) suggests that at least one of the new configurations is an improvement over the current state of that art. Additional comparisons demonstrated key heat transfer physics when comparing results for test sections heated from one versus both sides.

Furthermore, the advanced impingement portion of the test matrix was also completed. These concepts also show great promise.

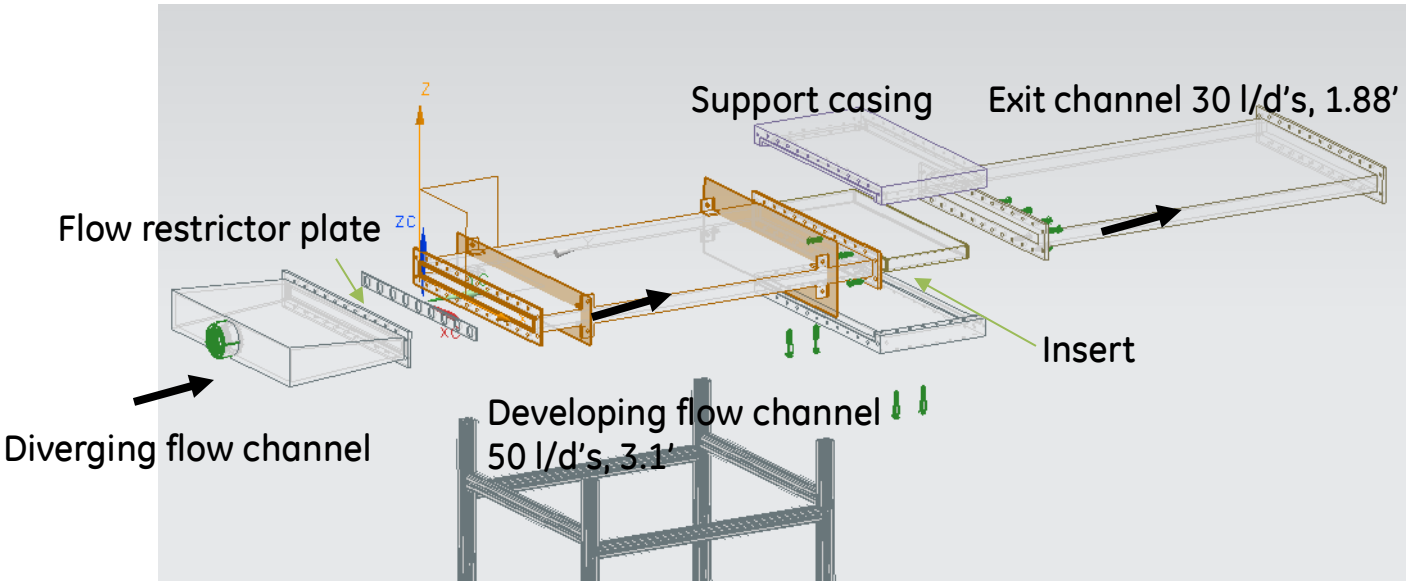

Figure 107: Exploded assembly view of internal heat transfer test rig.

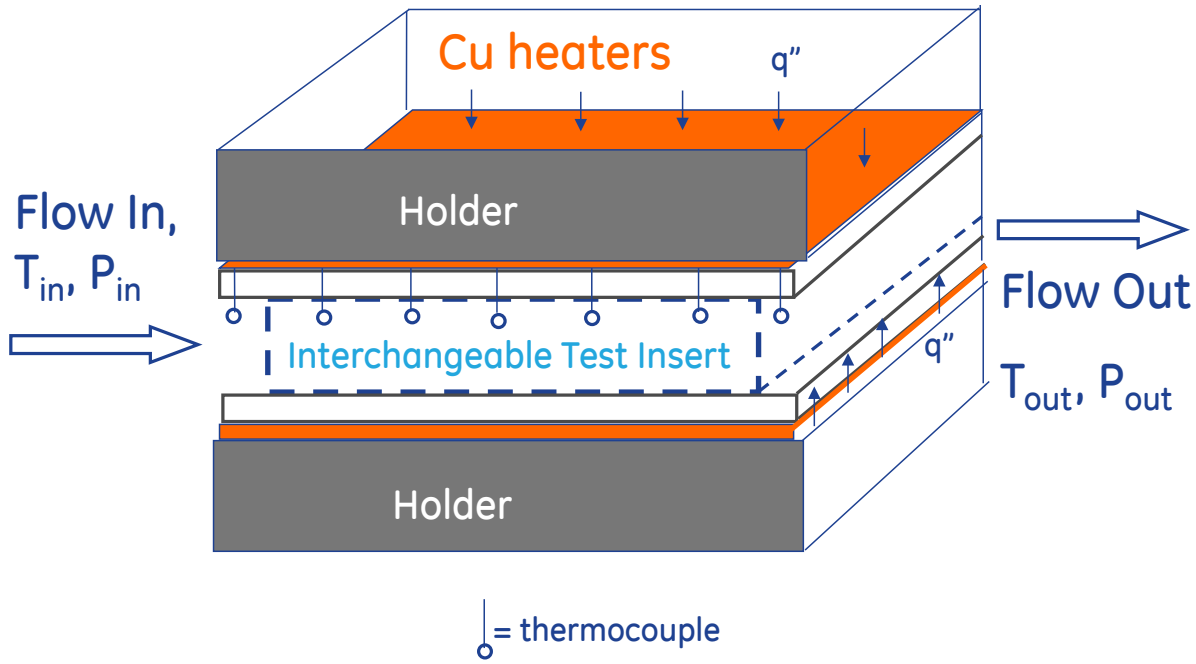

Figure 108: Details of internal heat transfer test section.

Rotating CFD

In addition to testing passage HTCs for different shapes, there was a need to understand the impact of rotation on passages, particularly as flow rates drop and Mach numbers go below the range of current correlations. Since rotating tests are difficult and expensive, high end CFD modeling was performed to look at these impacts.

To validate the methodology, models were run against the HOST rig (Figure 109) tests performed by NASA. A variety of meshes and turbulence models were attempted to determine the best match with data for both the stationary and rotating case with and without turbulators. Both CFX and Fluent codes were tested.

Runs were then done on GE specific hardware looking at the impact of heat transfer on different Mach and Rotation numbers on each passage through a rotating blade.

Figure 110 provided sample streamline views at the turn and through the passages respectively. Generally, what is observed at high rotation numbers for serpentine cooling passages is that the rotation of the walls drives a Coriolis affect strong enough to result in separation and recirculation. The Rotation number is analogous to the ratio of momentum imparted to the flow by the rotation of the walls to primary flow momentum driven by the pressure differential across the passage inlet and outlet.

In turbulated outflowing passages, the flow is concentrated against the pressure side and begins to recirculate back inward along the passage suction side at Rotation Numbers above 0.35. For non-turbulated passages, this effect is more extreme. Turbulators induce secondary flows which mix flow from the pressure and suction sides, resisting the development of a flowfield which has flow moving up one side and down the other.

In inflowing legs, Coriolis Effect acts opposite that of outflowing legs. Flow that moves from a greater radius to a lesser radius carries with it a greater mean tangential velocity than that of the walls at the lower radius. This causes flow to collect against the suction side. Inflowing legs, however, typically do not experience separation from the pressure side unless the rotation number exceeds 0.7 or more. This has been attributed to Buoyancy effects acting against the Coriolis affect for inflowing passages.

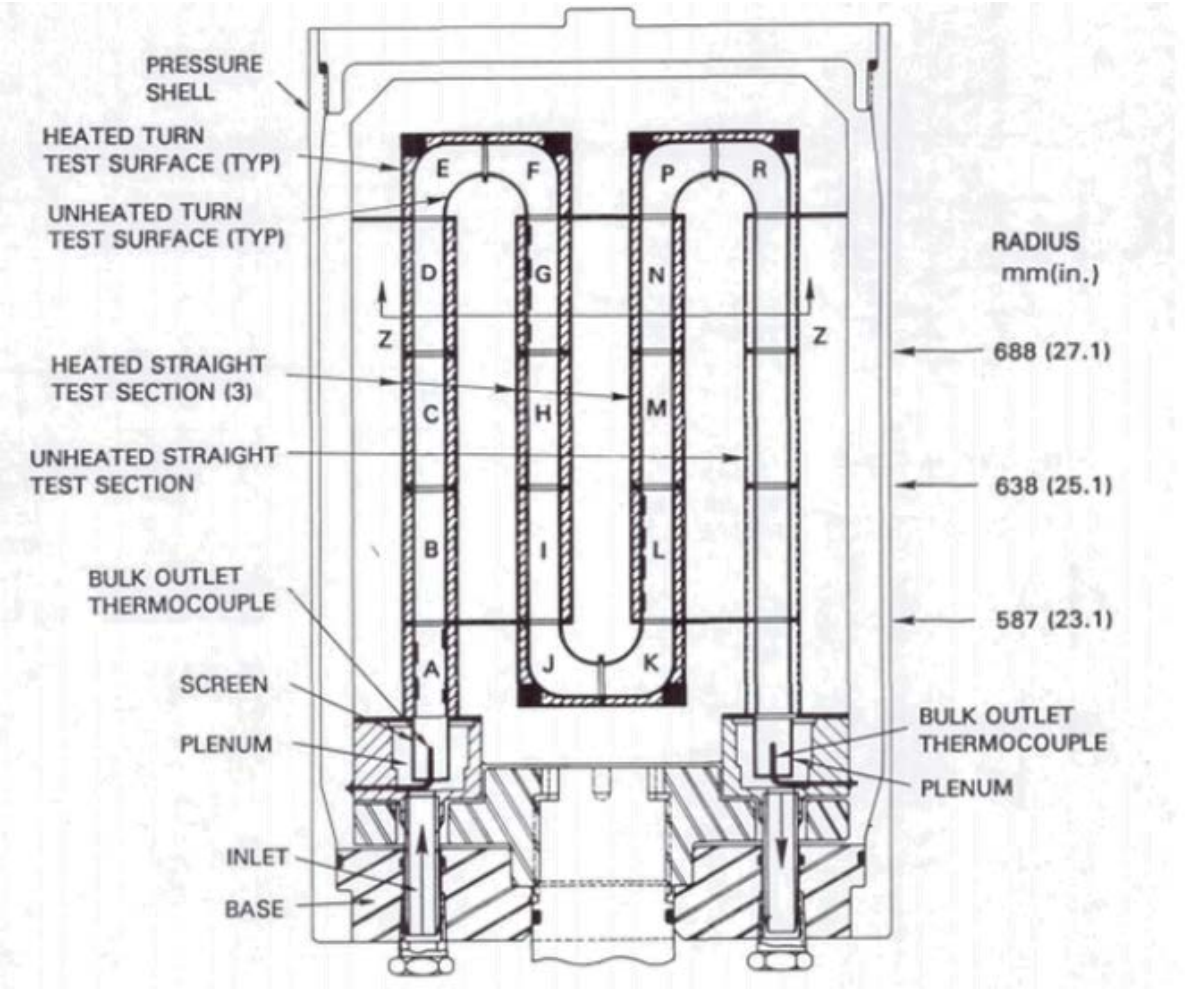

Figure 109: Host Test Rig

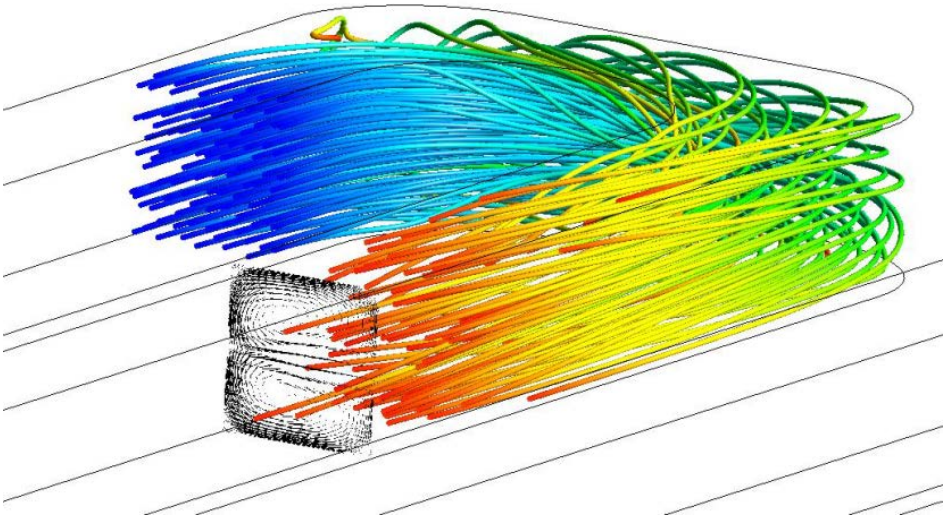

Figure 110: Sample Streamlines thru turn of rotating airfoil

Seal Slot HTC Testing

Seal slot HTC rig

Cooling flows can be reduced if better usage can be made of leakages to also provide cooling, Figure 111. However, leakage is unpredictable and the small gaps make HTCs hard to estimate. Therefore to utilize the cooling benefit, better estimates of the HTCs are required. A heat transfer rig was built to directly test the impact of the heat transfer coefficient of very small gaps from a seal, Figure 112. However, the variations in leakage proved too great to allow for an accurate measurement of HTCs.

To solve the problem, a new rig was designed and built to specifically focus on measuring the heat transfer coefficient for very small leak gaps of controlled size, Figure 113 and Figure 114. This rig uses a small controlled gap with a heater on one side under a copper block which represents the hot side pressurized load surface. The opposing side is a highly insulative, high temperature plastic representing the seal. Air is forced through the gap over a range of pressure ratios. Thermocouples measure the load face surface temperature. Knowing the power input, the air temperature change through the gap, and the flow rate, an average HTC can be measured. By varying both the gap and the surface roughness, estimates of HTCs for a range of seal configurations can be determined.

Initial testing was completed under this program for different gaps and surface roughness. Issues with leakage were found yet the initial results were promising. As expected the rougher surfaces showed augmentation over the duct and the smaller duct height showed relatively greater HTC by a consistent multiplier vs. predicted.

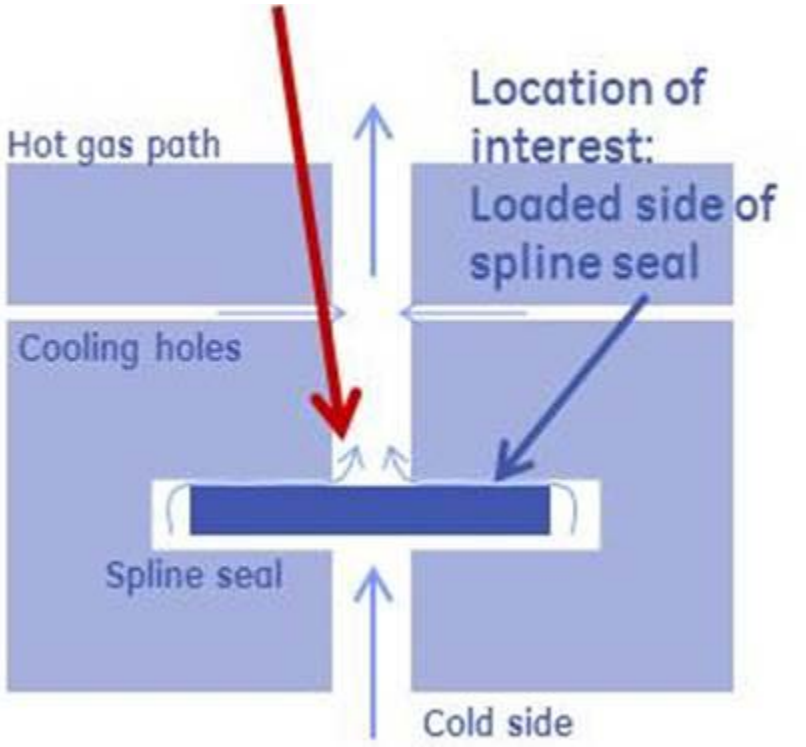

Figure 111: Seal Slot Leakage

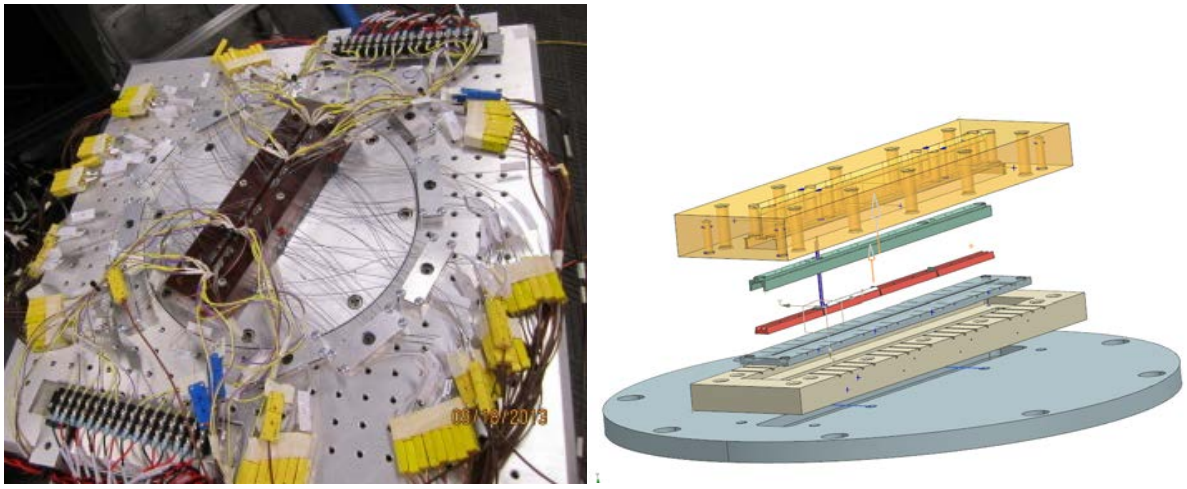

Figure 112: Original Seal Slot Test Rig

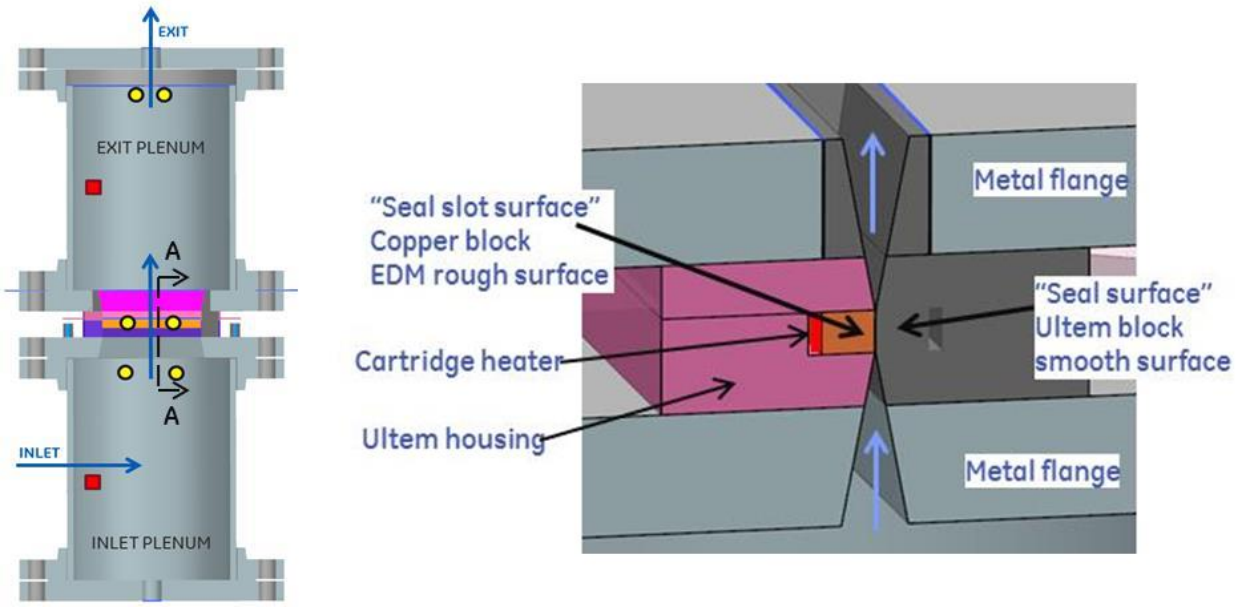

Figure 113: New Seal Slot HTC Rig

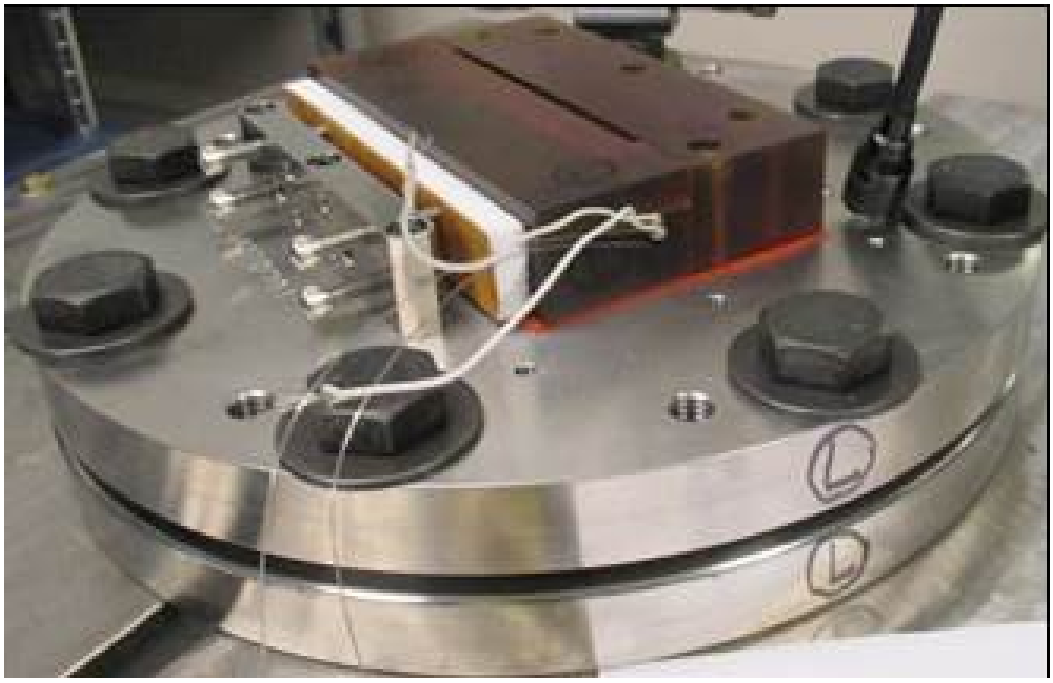

Figure 114: New Seal Slot Rig as built

Tipshelf cooling

Another important technology area covered under this program was to look at improved cooling in the blade tip region. Blade tips in general are one of the more difficult regions to cool due to hot gas flow on all three sides and specific design/manufacturing constraints. Furthermore, the

effective tip-gap not only affects heat transfer but also the aero performance of the turbine. To improve both the heat transfer and aero performance a “squealer” tip basic concept is used. The improved tip cooling configurations tested were based on the basic squealer tip design.

The test rig used for the tip cooling technology was the RACDOV (Rapid Airfoil Concept Design Optimization and Validation) cascade. It is a 6 passage 9FB S1B annular sector flowpath at 55% scale and is shown in Figure 115. The center blade is interchangeable and different test airfoils are made for each configuration. For the purposes of this particular study, the blades were rapid prototyped using DMLM (Direct Metal Laser Melting) and the leading edge and tip geometry/holes were machined to the required dimensions.

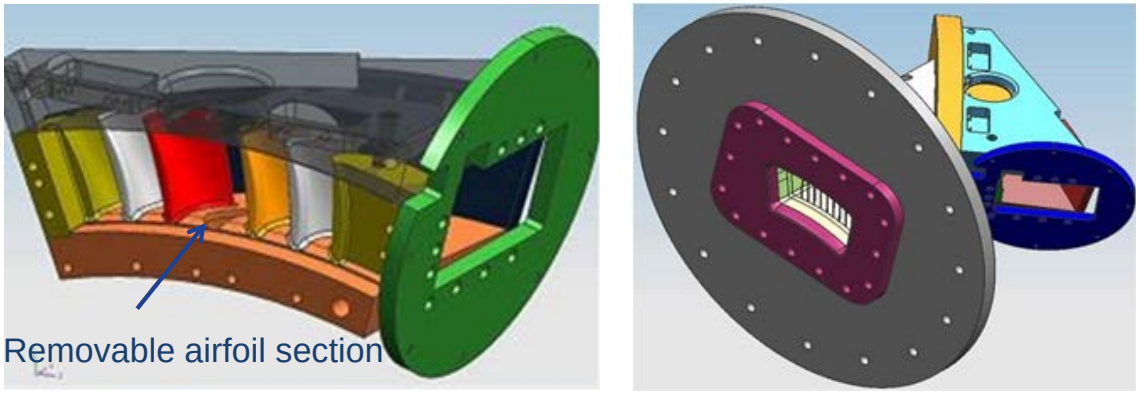

Figure 115: RACDOV cascade

A baseline configuration and 4 advanced configurations made up of combinations of holes and tip shelves were tested. In general, the results indicate that the different features can be located in different regions of the airfoil to provide additional benefit if manufacturing limitations and costs can be kept low.

Combined Demo

The overall objective of the DOE cooling flow reduction program was to take some of the best and most promising individual technologies and implement them into a fully cooled conducting airfoil to demonstrate the cooling flow reduction potential versus a baseline design. Given the design concepts, only a conducting airfoil test could really validate the cooling effectiveness of this technology due to the combined internal cooling and film effects. A current state of the art rig was used to determine these technologies when employed in a fully cooled airfoil model.

Four different combinations were tested at varying flow rates to determine which, if any, technologies showed promise. One of the four technologies was named the overall winner with design point cooling flow rates 75% of that of the other configurations.

Conclusions

GE Power & Water and GE Global Research conducted extensive research and technology development to improve cooling features for hot gas path parts to reduce required cooling flows and enable higher temperature operation both to improve efficiency and turbine throughput while reducing costs per kilowatt.

Among the programs accomplishments were:

1. Developed design quality film curves over a range of conditions and hole shape parameters.
2. Identified potential improved film concepts
3. Development of heat transfer coefficients for a number of critical design configurations that will allow both reduced design uncertainty and improved design.
4. Successfully tested the best internal and external features in a combined demonstration test that proved the potential to reduce cooling flows by more than thirty percent over the baseline.

Due to the success of these developments, multiple new technologies will be utilized in gas turbine product.

SEALING FLOW REDUCTIONS

INTRODUCTION

Subtask 2.2.4 – Leakage Flow Reduction Development – was focused on improving seal performances across the gas turbine. The initial four key areas of focus were: 1) the transition piece to first stage nozzle (TP-S1N); 2) the turbine interstage; 3) the turbine wheelspaces; 4) and the high pressure packing or compressor discharge. Baseline operating conditions were generally modeled on turbine GE gas turbine. Over time other significant opportunities for secondary flow control and improved leakage performance were identified, and the original four locations were expanded. Specifically, turbine wheelspace sealing was extended to blade tip sealing with improvements to the honeycomb, and TP-S1N static seals were extended to the hot gas path.

For each sealing technology development effort the following process was followed.

- Operating conditions including pressures and temperatures, shaft speeds (where appropriate) and geometric transients were determined.
- Options for improved sealing performance were identified and developed via analytical simulations and lab testing
- A preferred approach was selected and developed to the point where the technology was ready for consideration for an engine design.
- For some of these technologies, further work was done with GE funding to implement them into engine designs and put them into service.

EXPERIMENTAL METHODS

Transition piece to first stage nozzle sealing

Some large gas turbines have can-annular combustion systems that require an interface between discrete round combustion vessels and the annular stage 1 nozzle ring. The transition piece (TP) is that interface in GE turbines. The sealing between the discharge of the TP and the entrance to the first stage nozzle is particularly challenging because the TP covers several nozzles and on some turbines this number is not an integer. Transient motions between TP and nozzle can be large depending on how the combustion system is anchored in the compressor casing, and include radial and axial motions as well as curvature mismatches.

Leakage flow from this location is considered non-chargeable, as this flow goes through the turbine and produces useful work. This flow does however detract from flow going through the combustor, resulting in higher flame temperatures for a given firing temperature and, thus, higher emissions. Excessive leakage thus adversely affects emissions performance, and variation in the leakage affects the predictability and reliability of engine emissions.

There are three styles of seal systems for the combustor to turbine interface in common usage in GE products. The approach used in this program was to select an instance of each style and develop approaches to improve the sealing performance by a minimum of 20% and the style that resulted in the best performance after improvement would be the approach proposed to the new turbine design.

A flow test rig, named the TP Rig, was fabricated to evaluate seal performance. The rig simulates the sealing features of one transition piece with portions of the two neighboring TPs, and three first stage nozzles. The nozzle pieces rest on three screws and can thus be positioned with a wide range of gaps between them and the TP. The vessel is rated to 50 psig, thus allowing pressure drops across the seals that represent engine conditions. All testing is at room temperature. The rig is shown in Figure 116.

Relative deflections were calculated for a particular turbine, and these were applied to all three seal styles.

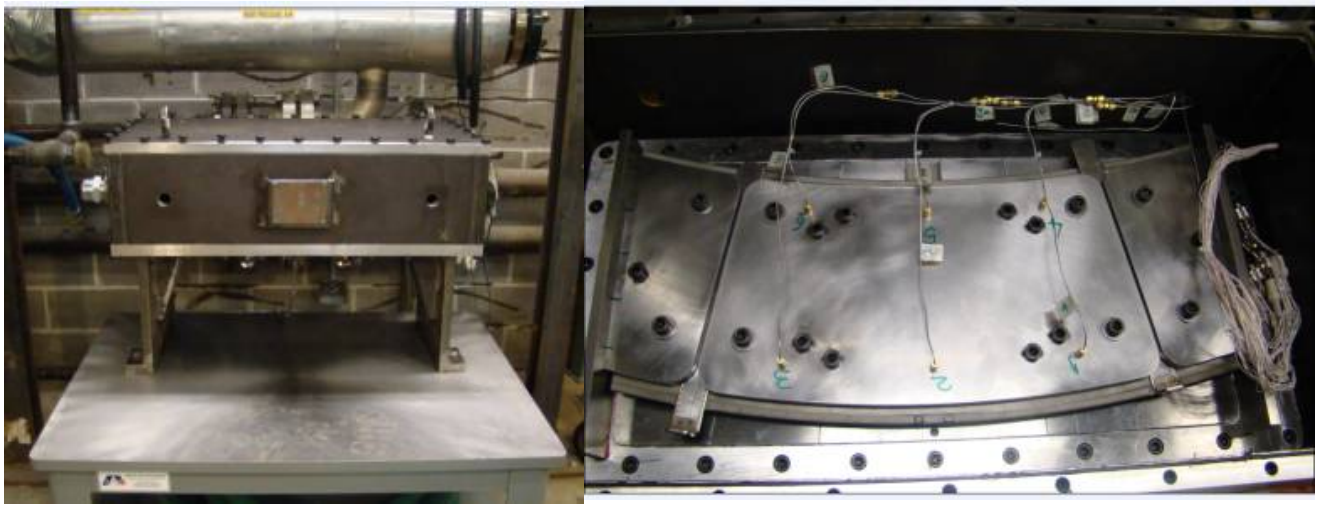

Figure 116 TP Rig: internal view shows the transition piece frame with the neighboring frame segments; 1st stage nozzle frames are under the TP frames.

Following the commissioning of the TP Rig tests were run on each style of seal. The plan was to select the best performer for further improvement. By sealing off each passage separately, opportunities were identified for performance improvement, each of which was then validated with further testing. The results and the improvements are shown in the Results and Discussion section.

Turbine interstage sealing

The turbine interstage location is very challenging to seal because of the magnitude of the radial transients on engine start-up. The clearance between the inner surface of the nozzle structure and the rotor is large when the engine is cold. This clearance closes on start-up to pinch and then reopens partially. In the event of a hot restart, the start-up pinch (which occurs at full speed and pressure) is considerably more severe than on a cold start. A sealing technology that could tolerate the transient without incurring damage during the pinch could provide an ideal solution.

The design of the turbine interstage seal underwent considerable evolution during the course of the program. As issues were uncovered with the various aspects of the seal design through test or simulation, changes and redesigns were implemented. An overview of the experimental and analytical work follow in this section, and the results are described in the Results and Discussion section.

Simulations were conducted with finite element and computational fluid dynamics (CFD) tools as well as MATLAB-based solvers. Experimental work leveraged several test rigs in GE's Seals Lab; these are shown in Figure 117 along with their capabilities. A cross section of the Large Scale Low Pressure with the seal location is shown in Figure 118. Tests were run throughout the development program to characterize the behavior of the various features of the seal as well as to evaluate sealing performance. .

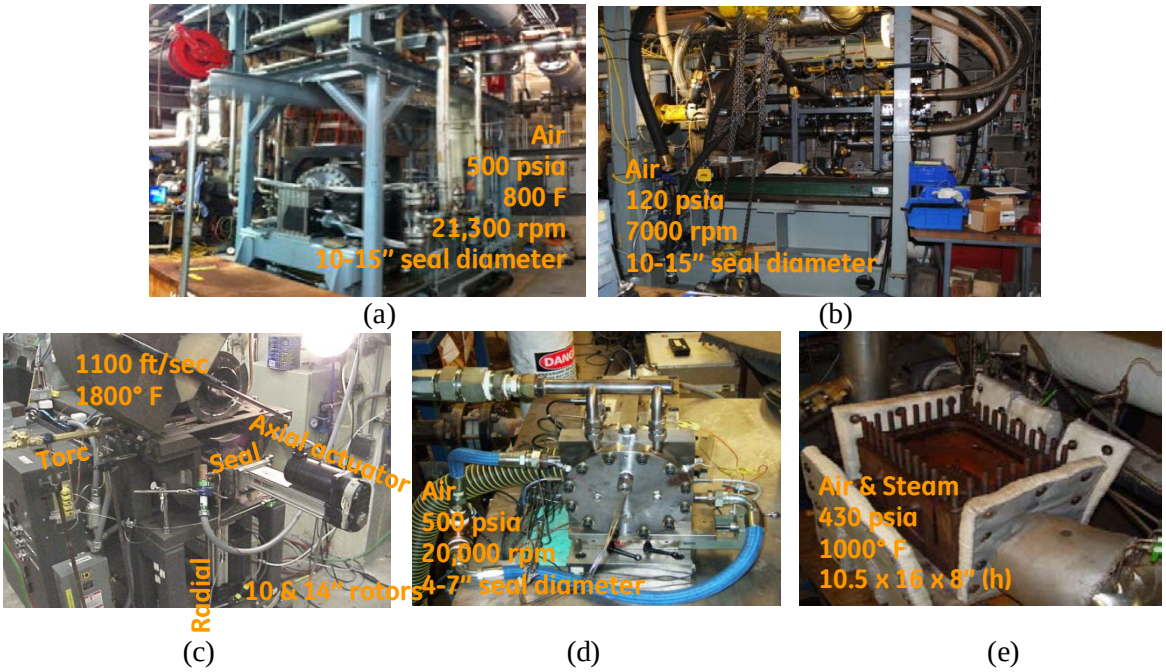

(a) (b) (c) (d) (e)

Figure 117 GE Seals Lab test rigs: (a) Large Scale High Pressure Rotating Rig; (b) Large Scale Low Pressure Rotating Rig; (c) Rub Rig; (d) Cold 5" Rig; (e) Shoebox Rig.

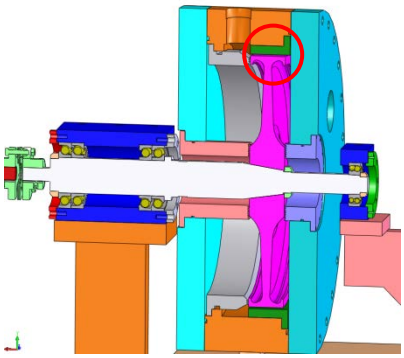

Figure 118 The seal location in the Large Scale Low Pressure Rotating Rig.

A static test fixture was designed and fabricated for the Shoebox Rig to quantify inter-segment leakage. The fixture consists of three seal segments, the rotor interfaces of which are extensively instrumented with pressure and proximity probes.

This seal design proved vulnerable to vibrations. Vibrations could be managed with the addition of wire mesh dampers, as discussed in the Results and Discussion section. However this solution is not considered adequately robust for operation in a power generation turbine with long maintenance intervals. A new fifth generation interstage seal design was completed.

A set of small scale interstage seal segments were fabricated and tested in the Cold 5" Rig. Static and rotating tests were conducted to characterize leakage performance and windage heating.

High pressure packing

The high pressure packing (HPP) seals the most valuable air in the gas turbine, so its sealing performance has a significant impact on overall engine performance. A challenge beyond sealing performance new and clean is the degradation of the seal over time.

Trade studies were completed to quantify the impact of the opening load point selection on part load performance and baseload performance, and how opening load varies across the ambient temperature range. Hardware was fabricated in the form of a 12" long seal section and tested in the Shoebox Rig.

Tests conducted at full pressure demonstrated predicted and repeatable performance. The effects of friction coefficients, initial clearance, and rate of change of pressure drop on opening and closing performance were quantified. High speed data was collected to capture the inertial effects of the seal opening and closing, to validate the single spring design and to characterize the behavior of the seal. A fixture shown in Figure 119 was developed to characterize the spring stiffness over the range of motion.

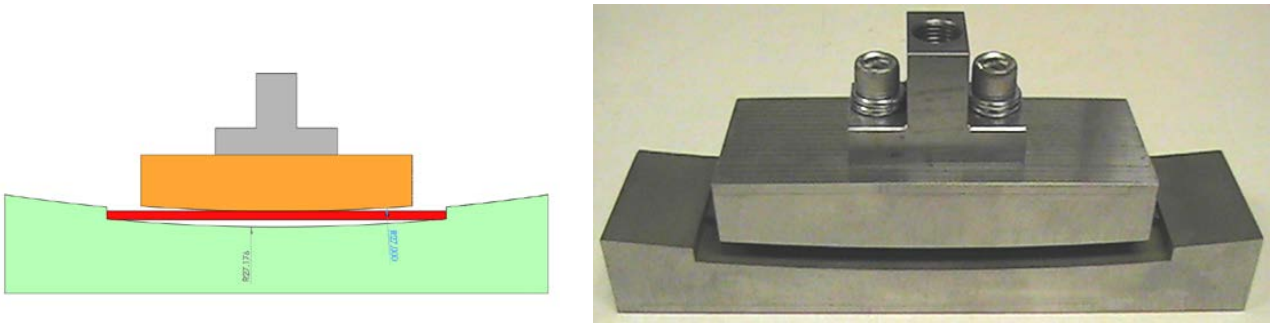

Figure 119 The spring stiffness measurement fixture for the HPP seal.

To achieve the desired closure and retraction behavior (fast, abrupt motion at a desired pressure differential), various design modifications were successfully implemented.

Analysis of the seal transients was conducted to identify closure and retraction points for the target engine. Validation testing requirements consisted of testing the opening and closing characteristics of the seal in a full ring. To that end a full scale test rig was designed and built. The rig was designed to be flexible enough to accommodate a single segment or multiple segments. The rig can run at full pressure and flow at room temperature. The rig is shown in Figure 120.

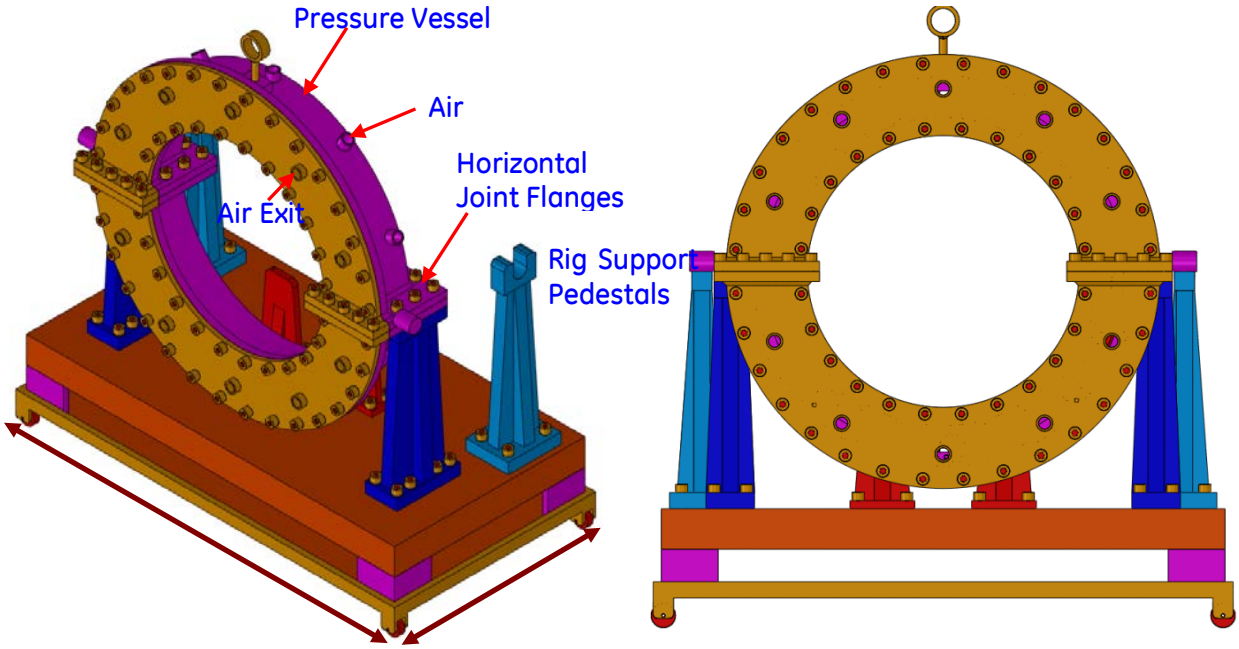

Figure 120 The Full Scale HPP Seal Rig.

Turbine wheelspace

The turbine wheelspaces have angel wing seals that act as discouragers for the purge flow that limits the ingestion of hot primary flow. As it is considered highly undesirable for these to rub and because radial transients in the hot gas path are large, they are generally assembled with large clearances. In this effort abradables were developed for the stator part of the seal. The impact of the selected geometry was studied in an attempt to provide flow restriction beyond the physical clearance reduction that might be achieved. The objective is to reduce the physical clearance between rotor and stator through the use of an abradable without increasing the probability of a hard metal-to-metal rub.

The impact on flow of the stator geometry was studied via simplified CFD models. No attempt was made to capture all the complexity of wheelspace flows; rather these models served to provide relative rankings. The magnitude of radial displacement transients relative to typical spray coat thicknesses have made it clear that honeycomb provides the ideal combination of flow restriction and thickness capability. The flow restriction was quantified via CFD various configurations. The geometries considered are shown in Figure 121.

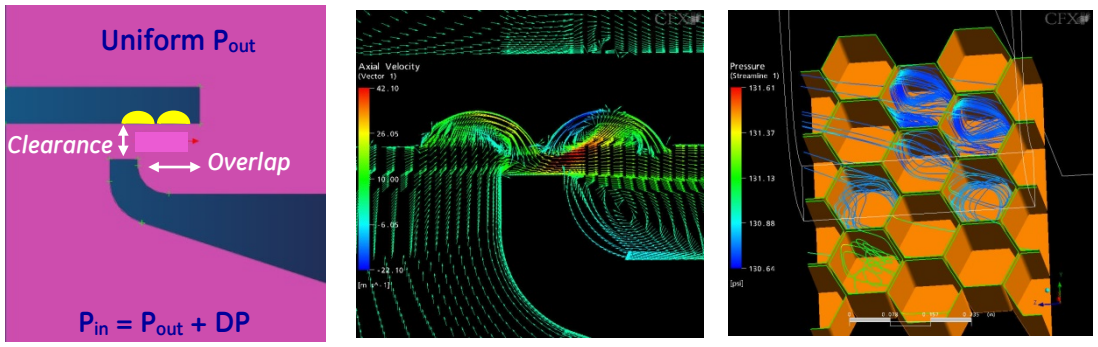

Figure 121 Angel wing configurations used for CFD studies of optimal stator surface geometries.

Tests with the specimen shown in Figure 122 were conducted on the Rub Rig shown in Figure 123 to characterize rub events and quantify the damage to the rotating blade. Low speed and high speed rub tests were conducted on honeycomb samples against a knife representative of currently operating equipment. A rub test matrix was developed to quantify the improvements in abradability, focusing on both full speed and full temperature conditions, as these are when the most aggressive rubs are expected, and also on low speed rubs, as these can be the most damaging rubs.

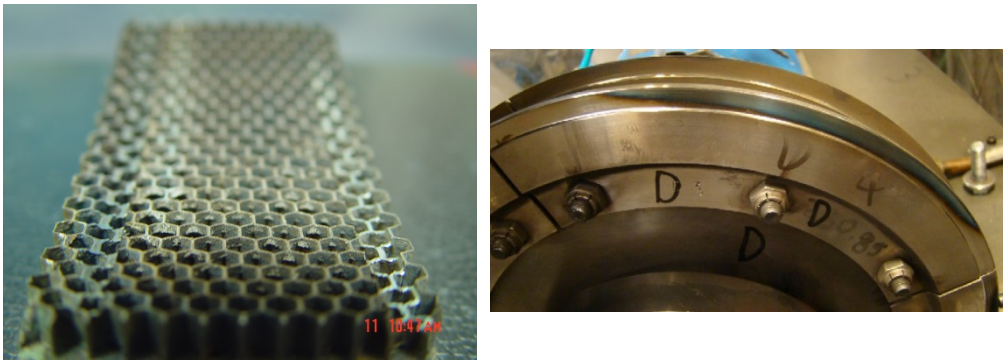

Figure 122 Typical honeycomb rub test specimen.

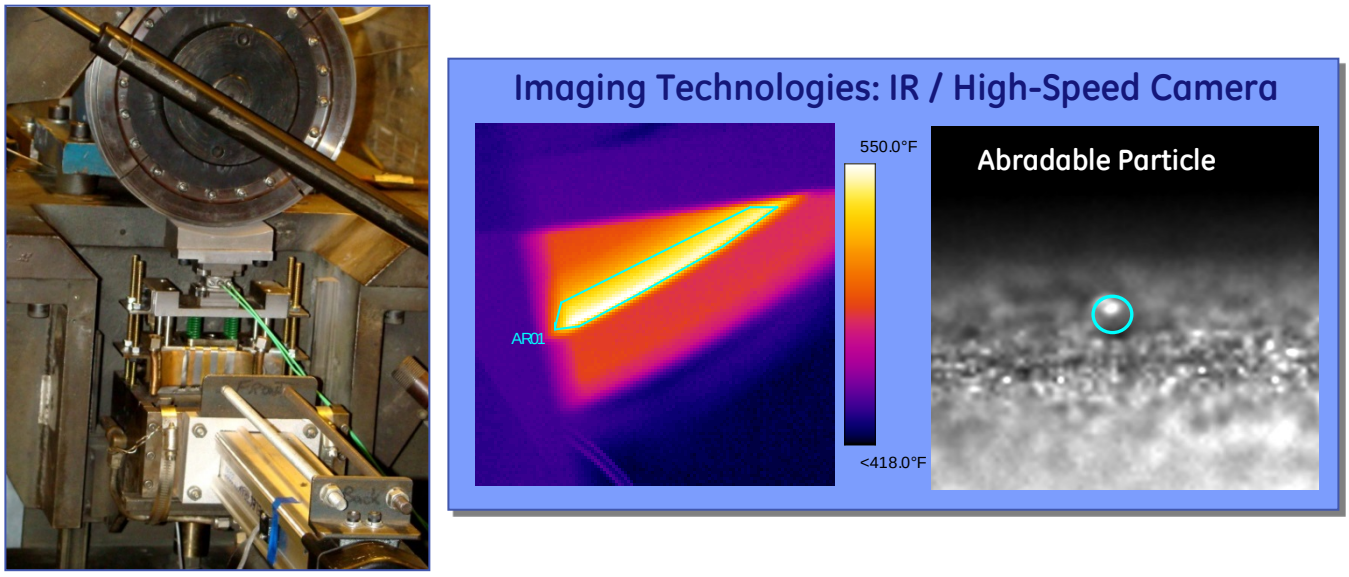

Figure 123 The Rub Rig and an example of thermal imaging data collected to characterize rub temperatures, with blade tip temperatures and abradable particle sizes shown in the right hand graphic.

The impact of reduced angel wing clearances, which is the primary benefit of the honeycomb at the angel wing seal, was quantified in the Hybrid Wheelspace Rig as part of Subtask 2.2.5.

Advanced static seals

Given the segmented construction of large gas turbine hot gas path sections, the performance of seals between shrouds and nozzles is critical to the overall performance of the engine. GE has long experience with cloth seals which are superalloy shims covered in wire mesh cloth. Design concepts were developed for advanced static seals that further limit the leakage flow through the use of smoother sealing surfaces. Figure 124 shows a traditional cloth seal and a first prototype of new designs.

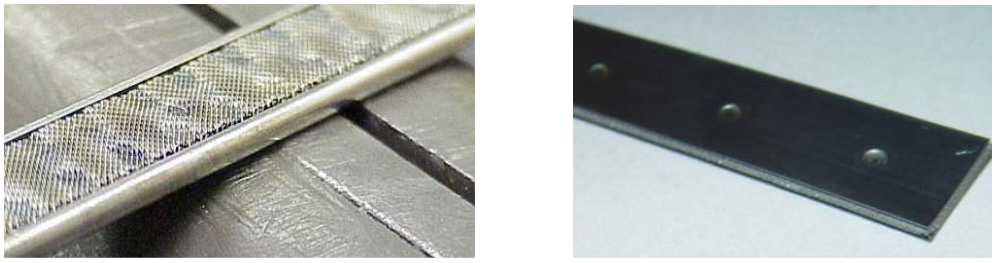

(a) *(b)*

Figure 124 (a) A traditional cloth static seal and (b) new shim-cloth-shim design concept.

A set of tests including torsional and bending stiffness characterization were conducted on the new seals to evaluate their compliance. The seals are shown in Figure 125.

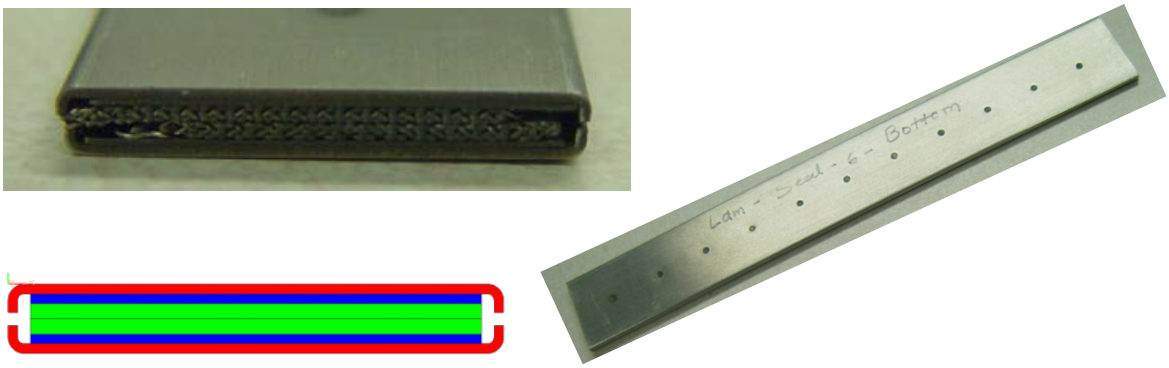

Figure 125 Optimized advanced static cloth seal with shims welded onto metal cloth.

Many shroud and nozzle seal locations consist of pairs of slots approaching each other at an angle with two straight seals installed. In an attempt to reduce the leakage between the seals, “L” shaped seals were designed and fabricated. These seals are intended for small radial and skew offset locations, so that the vertical and horizontal seals do not need to be independent. By having a single seal instead of two seals, the end gap leakage can be reduced significantly. Prototypes are shown in Figure 126 and the set-up used to evaluate them is shown in Figure 127.

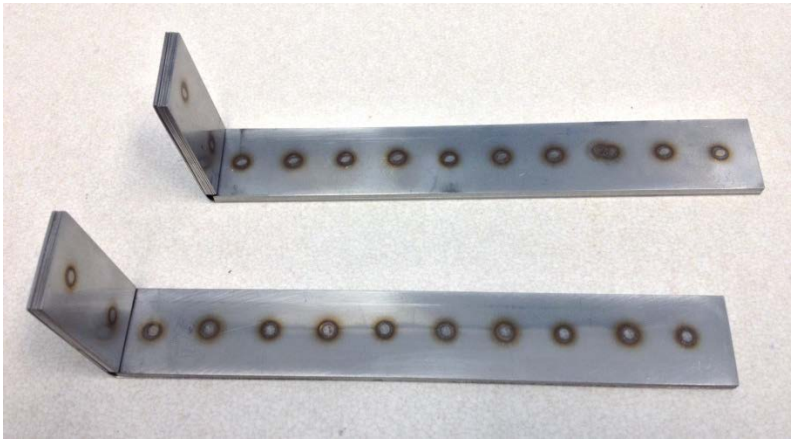

Figure 126 Prototype “L” shaped advanced static seals.

Figure 127 "L" shaped static seal rig set-up.

Circumferential seals

Cooling air is generally used to purge cavities in the static hardware in an effort to isolate the support structure of the hot gas path stator components from hot gas path temperatures. If a seal near the gas path interface could effectively limit ingestion into the cavities, then purge air could be reduced. Prototype advanced static seals that seal circumferentially from nozzle to shroud were developed. Other versions were fabricated to increase flexibility. Testing under aligned and misaligned conditions was carried out in a static flow rig shown in Figure 128. The rig is the same one used for TP-S1N seals shown in Figure 116 but with the internal components replaced with three blocks to represent shrouds and three blocks to represent nozzles. The shrouds can be moved independently relative to each other and to the nozzles.

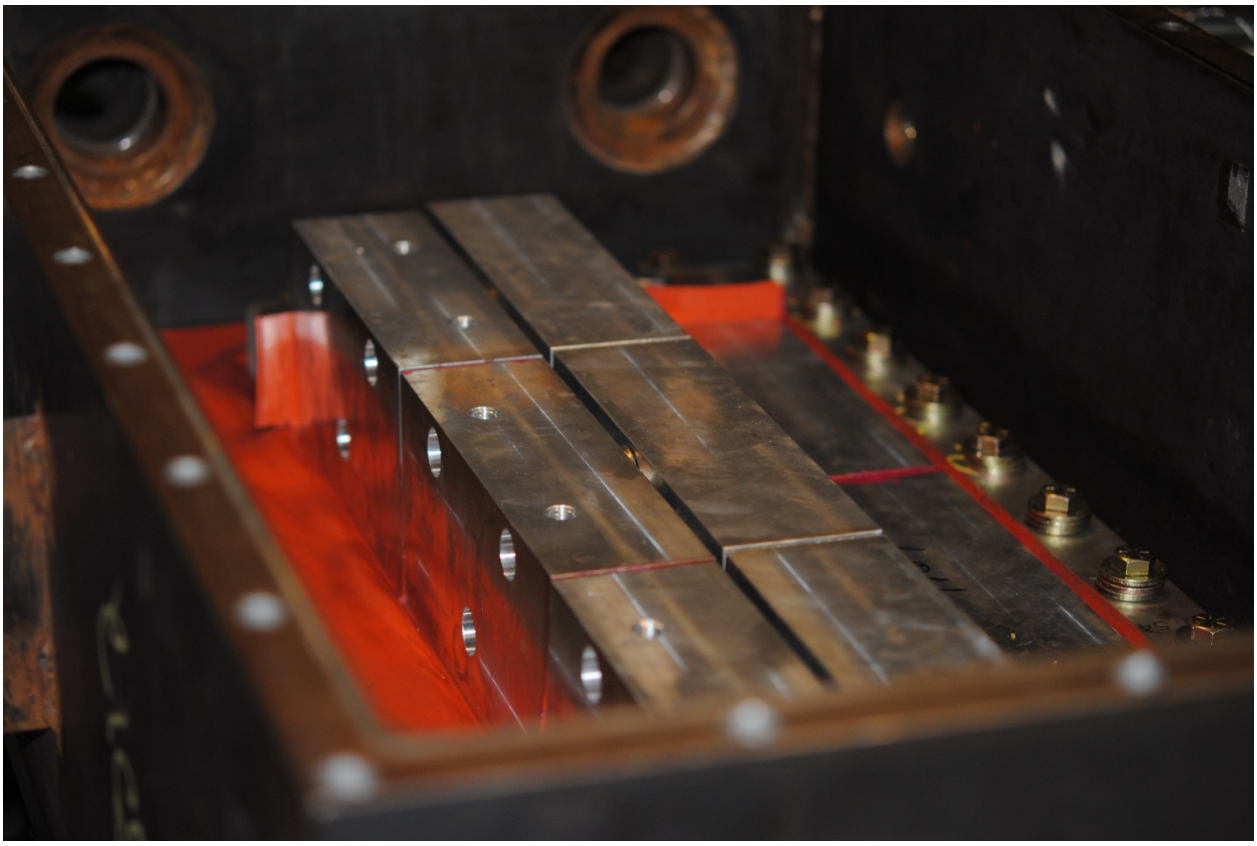

Figure 128 The rig used to evaluate the circumferential seal with three pairs of shrouds and nozzle blocks.

Very high temperature sealing

In order to meet performance demands of higher temperature sealing environments, new composite structured seal cross sections were developed and fabricated to replace the spline/shim advanced static seals. These new structures were made that could be subjected to a variety of thermal loading scenarios.

Blade tip sealing

A phenomenon observed in turbines in service is severe blade wear and metal transfer to honeycomb in the turbine section attributed to low speed rubs. In order to introduce the angel wing and shroud honeycomb seals with tighter clearances, a low speed rub test matrix was completed. A range of blade temperatures, honeycomb temperatures and incursion rates were studied to duplicate in the lab the damage observed in the field.

RESULTS AND DISCUSSION

Transition piece to first stage nozzle sealing

Tests were run on the baseline configuration with various combinations of gaps between the TPs and first stage nozzles. The total flow is not very sensitive to variations in relative position. Following the completion of the baseline flow tests, further tests were run on the hardware to identify the contribution of each flow path by selectively blocking off individual pathways. The corner leakage flows are significant contributors to the total flow.

Following the completion of the baseline tests, the two alternate seal styles were tested, and flow characterization of all three completed. In addition, tests of the baseline seal were run including a form of damage commonly seen in operation. A comparison of all the variations showing the breakdown by leakage path is shown in Figure 129.

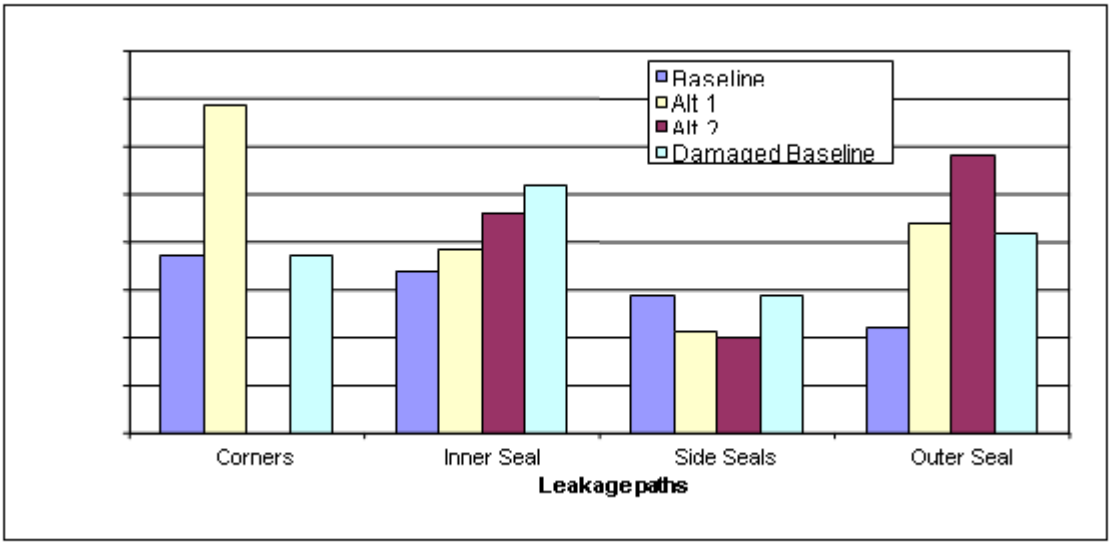

Figure 129 Flow through all TP-S1N leakage paths for all seals evaluated.

Following the performance characterization of the three styles of Transition Piece to First Stage Nozzle seals, the decision was made to down-select to two rather than a single design, eliminating the Alternative 2 style seal and keeping both the Alternative 1 and baseline styles and design improvements were identified for both seal styles. Jugular tests to quantify the improvements were conducted for the two seals. Based on the results the more promising modifications were implemented on new seals.

The optimized designs for both styles of seals were fabricated and tested. The measured performance improvement for both styles met or exceeded the target leakage performance improvement.

Turbine interstage sealing

Good results were obtained on the Cold 5” rig in terms of leakage performance and compliance for the first two design iterations. Typical test results from one of the seal designs are shown Figure 130.

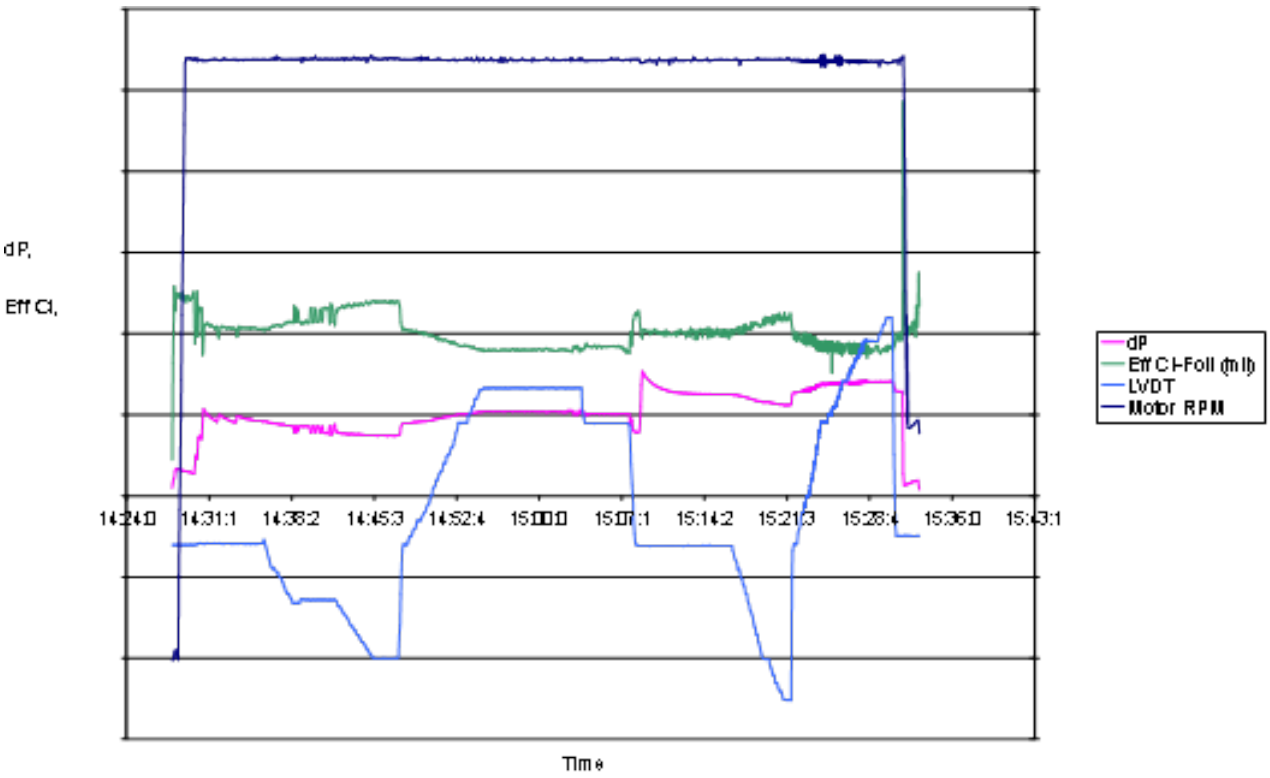

Figure 130 Leakage test results from o**ne of the two interstage seal configurations under evaluation.**

The intent of the Large Scale Low Pressure Rotating Rig tests was to retire risks associated with scaling. Initial results were in line with those from the Cold 5" Rig tests though somewhat lower; this is attributed to the shorter arc segments and thus the reduced impact of curvature mismatches between seal segment and rotor. The test series includes mapping performance across a range of pressures and rotor speeds, and determining the radial pinch capability of the seal across a range of pressures. This was accomplished with pressure sweeps as the vessel was moved laterally. Effective clearance through the tests remained approximately constant through the range. Typical results are shown in Figure 131.
:

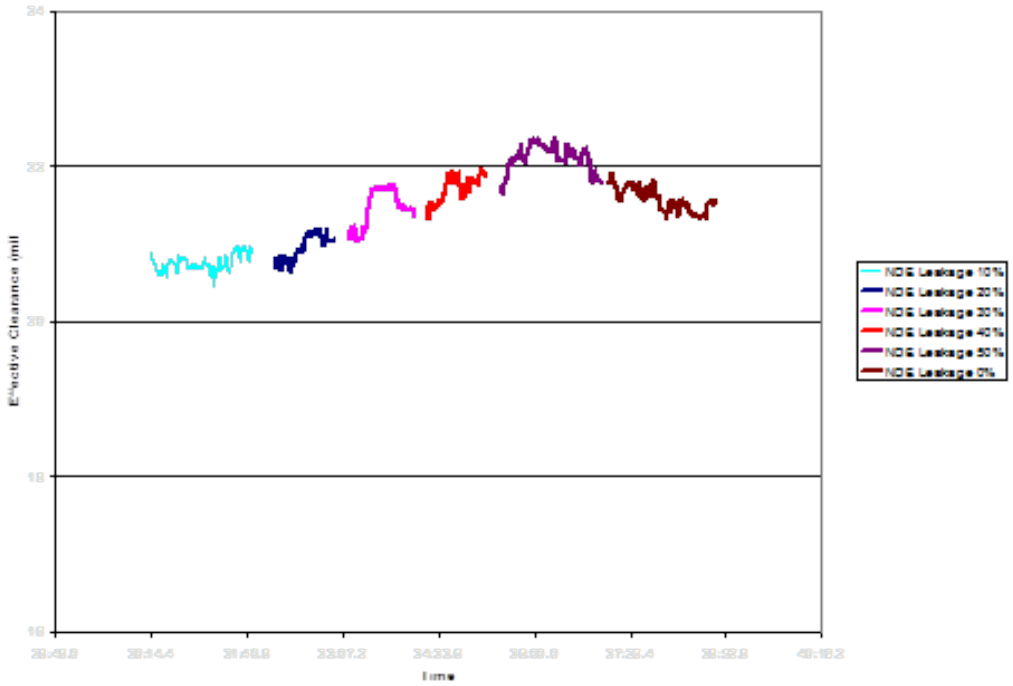

Figure 131 Typical interstage seal test results with lateral housing motion.

Static and rotating performance testing of the first seal design with separate springs and secondary seals demonstrated leakages close to target flow rates; results are shown in Figure 132. The ability to manage rotor transients was demonstrated via the rotating tests. During static testing vibrations of the segments were observed under certain flow conditions and a vibration mitigation solution was implemented. Once the ability to manage rotor transients had been validated, design improvements were developed to manage the full-scale rotor transients.

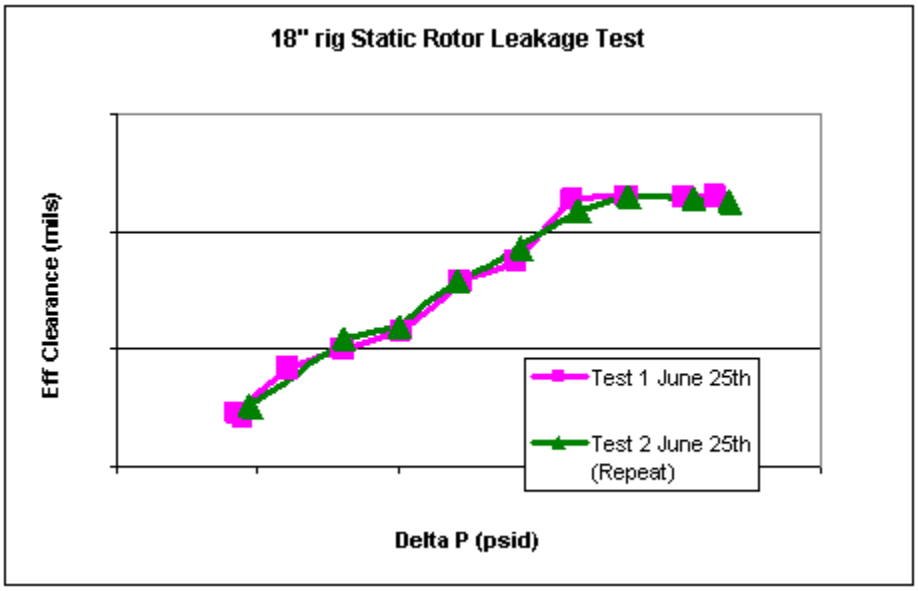

Figure 132 Interstage seal effective clearance versus pressure drop.

As the design evolution progressed to the fifth generation design a set of small scale seal segments were fabricated and tested in the Cold 5" rig. Initial non-rotating results showed that an effective clearance in line with the performance target can be achieved, as shown in Figure 133. Rotating tests resulted in good leakage performance and radial pinch results that matched predicted behavior. The same models predict a pinch capability at full scale and engine operating conditions that meet requirements. The incursion tests were conducted with a single seal segment; radial incursions were conducted with increasing radial closure until the seal rubbed the rotor. The rubbed seal was then retested to determine whether any performance degradation occurred as a consequence. The incursion capability of rubbed seal was identical to the unrubbed condition.

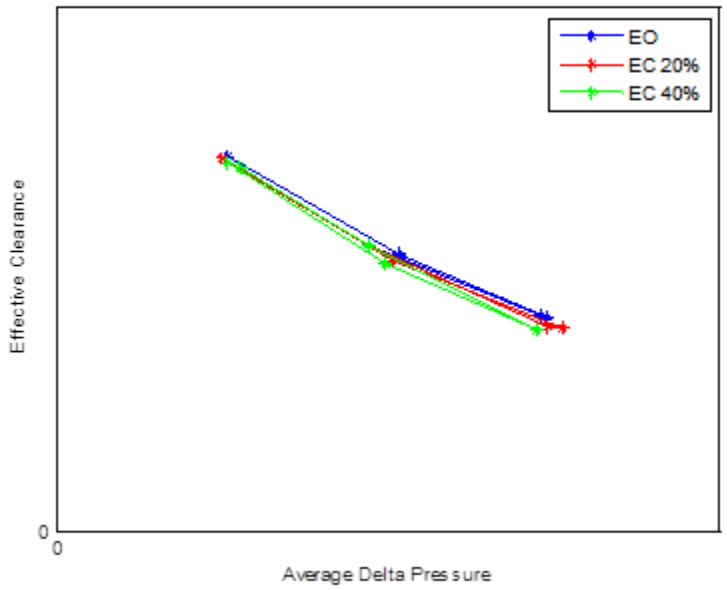

Figure 133 Non-rotating leakage flow results for the Cold 5" Rig seal. The various lines are for cases with the exhaust valve open or partially closed.

The sixth generation seal was developed as it was determined that the previous design was made vulnerable to rubs due to deformation of the seal. The analytical prediction for the new design was calculated and test results were used to set the conditions for the rotating tests in the Large Scale High Pressure Rotating Rig.

The seal demonstrated successful operation in the Large Scale High Pressure Rotating Rig across a range of operating conditions at high temperature, demonstrating the performance of the seal at near-engine conditions as well as good correlation between predictive models and test data. The test data provided valuable insight into the operating envelope limits for seal operation. Operating conditions during the test are shown in Figure 134. The effective clearance was in the same range as that measured in the static tests.

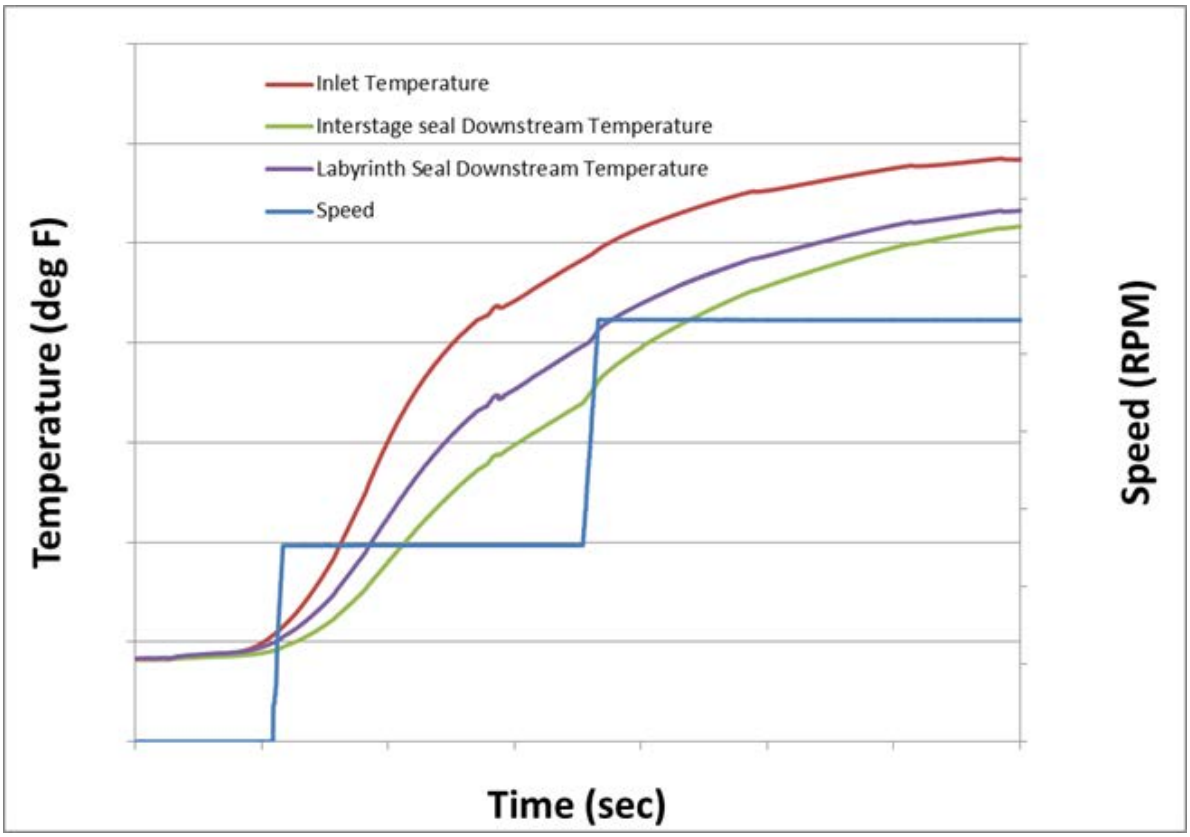

Figure 134 Operating conditions along with leakage observed during interstage seal rotating test.

As a result of these rotating, high temperature tests, considerable work went into the turbine interstage seal design to understand and address thermal management issues identified. Operating limits have been identified for the seal.

High pressure packing

Tests were run to determine the opening and closing behavior of the HPP seal in the tests of 12" (0.3m) sections. As the pressure differential exceeds target closure pressure, the seal sharply moves towards the rotor settling down in a low-clearance position. The seal retracts sharply away from the rotor as the pressure differential reduces below the threshold pressure. The closure and retraction DP can be tuned by changing the stiffness of the spring.

Closing performance was shown to be driven primarily by initial clearance and rate of change in pressure drop, whereas opening performance was shown to be driven by spring stiffness.

The impact on opening and closing pressures of variation in friction both static and dynamic between the seal and the holder was quantified analytically as shown in Figure 135. While this variation had little impact on seal closure, increased friction resulted in the seal retracting at a lower pressure and engine load point. This could result in increased brush seal wear. Trends

of closing pressure versus friction coefficient are shown in Figure 136. A new interface design was developed to reduce the impact of variation in friction coefficients. Friction force testing was carried out on the rig shown in Figure 137.

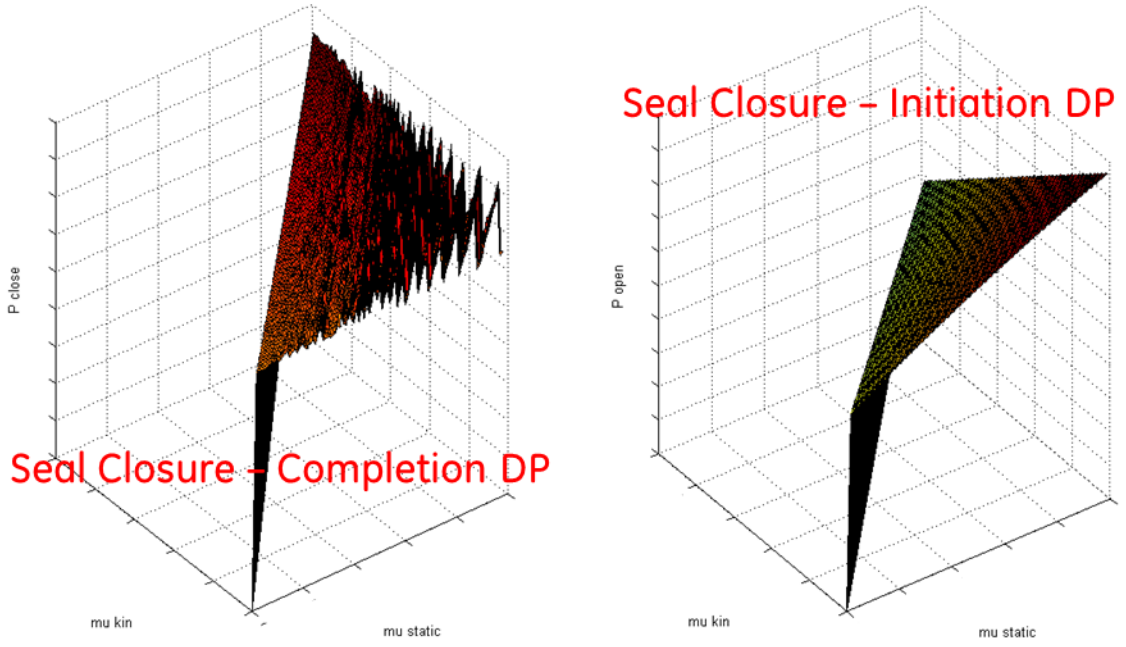

Figure 135 Impact of coefficient of static and dynamic friction on opening and closing pressure drops across the HPP seal.

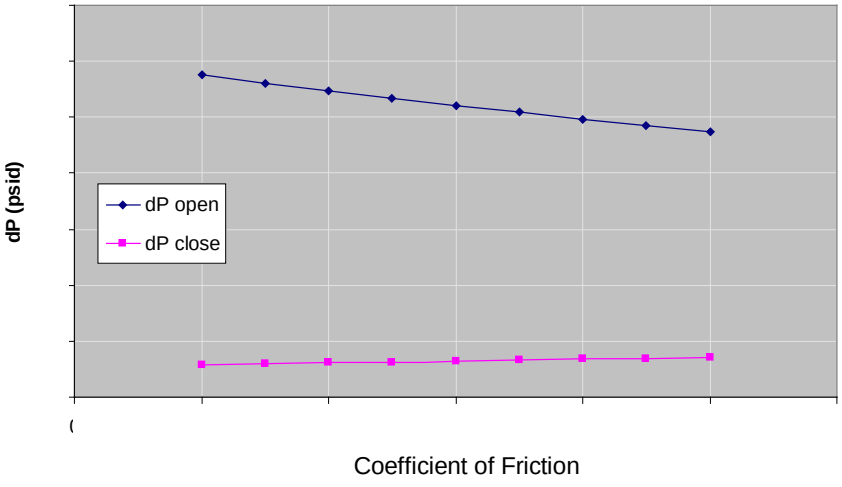

Figure 136 Impact of coefficient of friction on opening and closing pressure drops across the HPP seal.

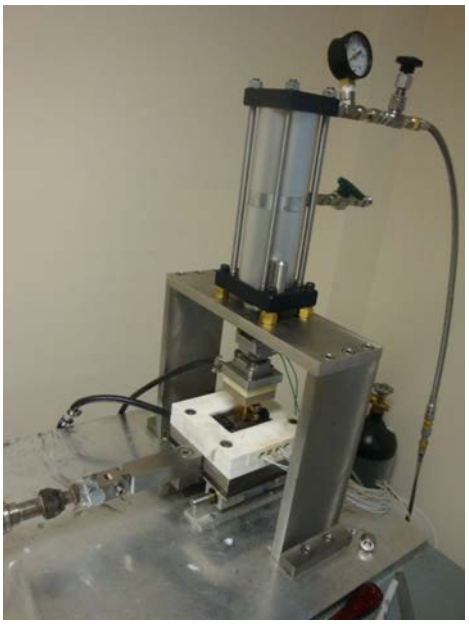

Figure 137 Friction force rig.

Using the fixture shown in Figure 119 the spring stiffness was characterized over the range of motion. The spring was demonstrated to be linear independent of loading rate. Results are shown in Figure 138.

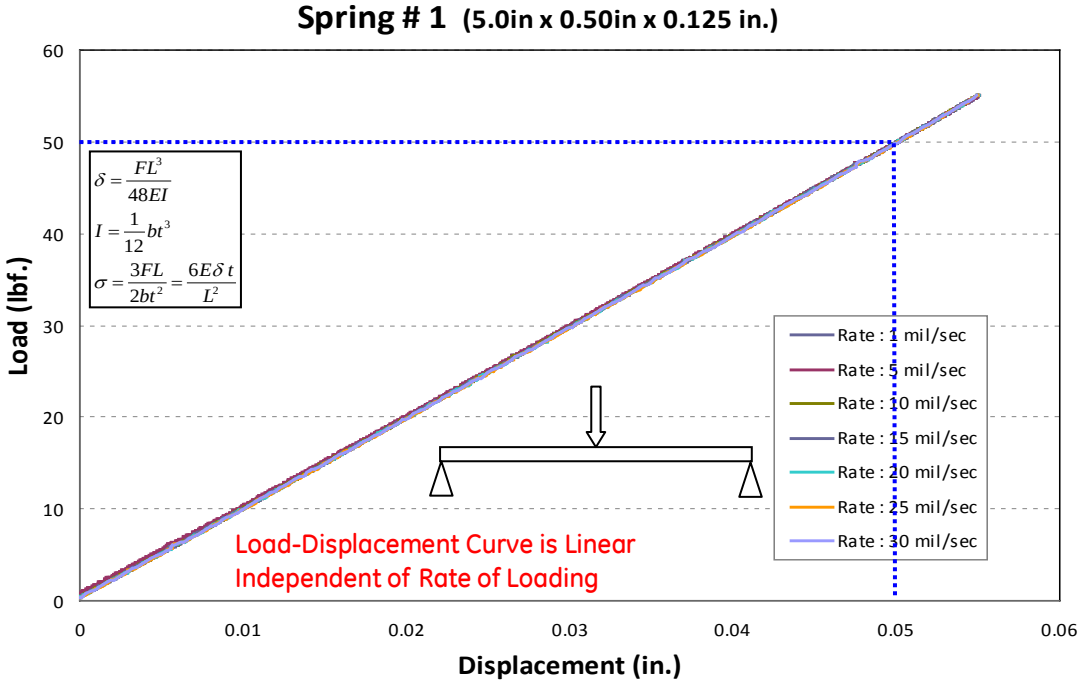

Figure 138 The spring stiffness measurement results.

Turbine wheelspace

Rub tests were conducted on the Rub Rig to characterize the abradability of honeycomb under different test conditions. The samples satisfied blade wear ratio requirement.

Advanced static seals

Static seals leakage performance was quantified in the Shoebox Rig. Sealing performance of the advanced static seal shown in Figure 125 are shown in Figure 139 and compared to two different traditional cloth seals as well as to a simple shim and an advanced static seal. The advanced static seal's performance under various levels of offset and skew are shown in Figure 140. This design shows leakage reductions to less than 50% of baseline, and excellent tolerance for radial and skew offsets.

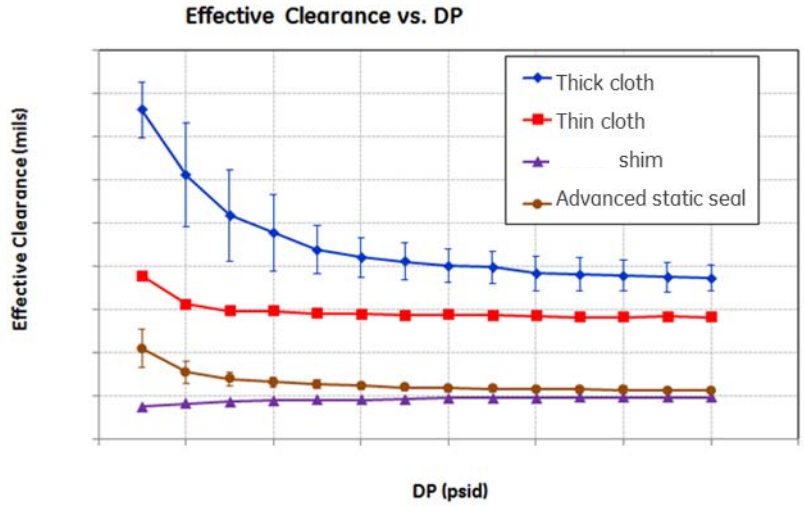

Figure 139 Effective clearance versus pressure drop for new static seal design, compared to the traditional cloth seals and to a simple shim.

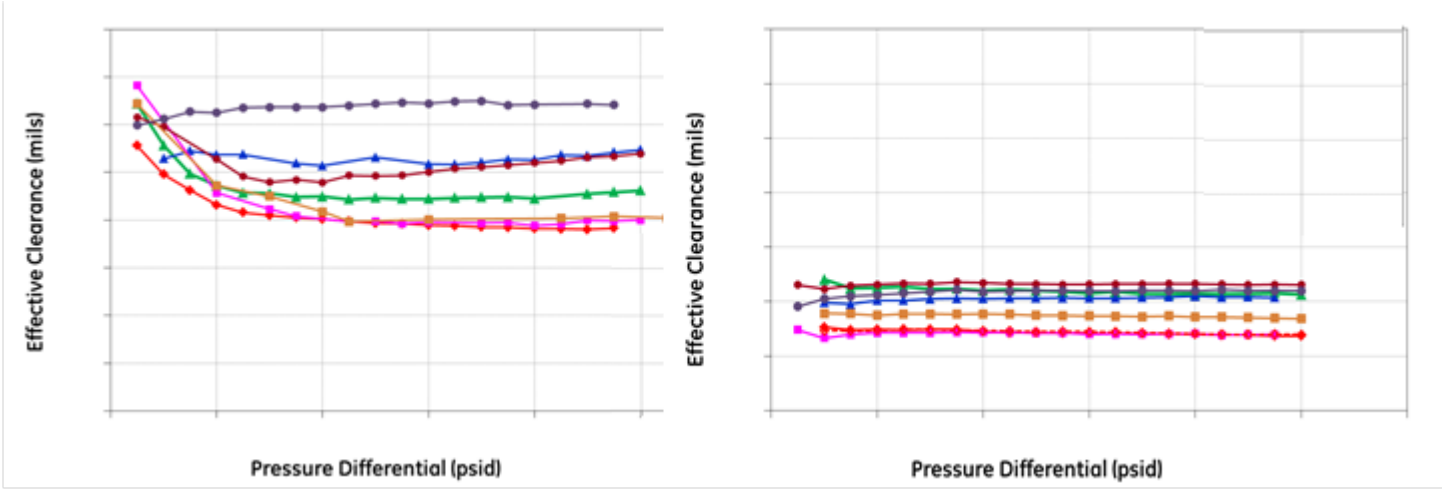

(a) Baseline cloth seal *(b) Advanced static cloth seal*

Figure 140 Effective clearance results for (a) baseline and (b) advanced static seals. Data includes the nominal configuration as well as skewed and offset slot configurations.

Leakage results of "L" seals with nominal slot geometries show significant performance improvement relative to the best advanced static seals, as can be seen in Figure 141. Seals tests were conducted with aligned and offset seals, and results compared to those of pairs of separate seals. Results show leakage performance to be better for the separate seals as can be seen in Figure 142. This indicates the importance of exact seal position and alignment.

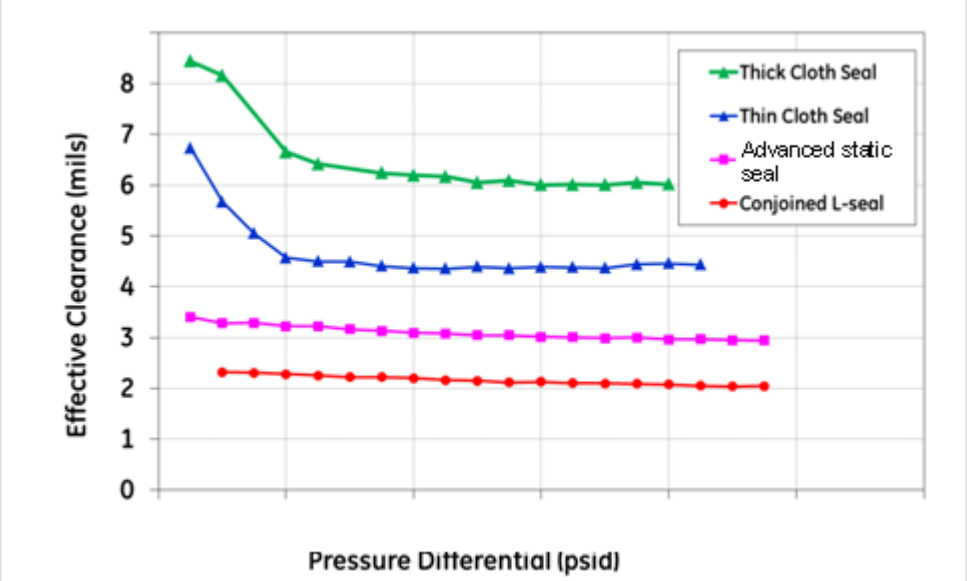

Figure 141 "L" shaped advanced static seal test results, compared with pairs of advanced static seals and traditional cloth seals.

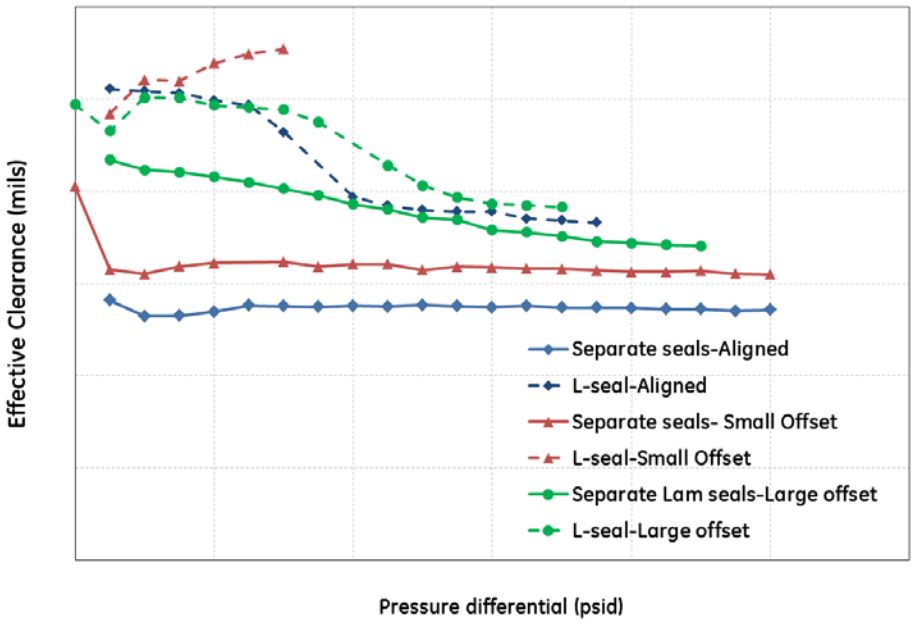

Figure 142 Comparison of leakage performance for separate advanced static seals and L-seal in various misalignment conditions.

Circumferential seals

Test results for the circumferential advanced static seal indicate leakage levels similar to those through nozzle-to-nozzle or shroud-to-shroud seals. The most promising design was approved for use on a production engine.

Very high temperature sealing
In order to meet performance demands of higher temperature sealing environments, new composite structured seal cross sections were developed and fabricated to replace the conventional spline/shim advanced static seals. These new structures were made in the form of buttons that could be subjected to a variety of thermal loading scenarios.

Examples of the new composite structured test buttons are shown in Figure 143. These were subjected to a variety of tests to explore their endurance to high temperature, thermal shocks from rapid heating and cooling, and exposure to combustion gases. From results such as these the most promising combinations have been selected and the associated fabrication processes will be refined.

Figure 143 Examples of composite structure seal sample used for fabrication and robustness trials.

Blade tip sealing
In tests intended to simulate the damage observed in the field from low speed rubs, teeth similar to those on bucket covers were rubbed against a baseline and an improved honeycomb. The improved honeycomb showed a great reduction in rub damage.

CONCLUSIONS

A number of sealing and secondary flow technologies were developed over the course of the program in order to meet the program's performance goals for an IGCC turbine or an IGCC with CCS turbine. Several of these reached the level of maturation that enabled deployment. These have been selected and approved for implementation in specific GE engines. Some are working their way through new engine test schedules, others have been implemented in the fleet on a retrofit basis. The conclusions for each technology are summarized as follows:

1 Three styles of TP-S1N seals were evaluated and two were selected for redesign to improve performance. Taking into account detailed simulations of engine transients and

associated relative motions, leakage was reduced significantly. Aspects of these design improvements have been incorporated into new engine designs.

2 Several generations of seals were developed for the turbine interstage location with its large clearances and severe interferences. Each improvement addressed issues identified in the test program. The final seal was successfully demonstrated at operating conditions at approximately of the target engine. .

3 A successful HPP seal was developed through simulation and testing of a single segment and of multiple segments up to a full 360 degree ring.

4 To minimize the clearance of angel wing seals in the turbine wheelspaces and thus limit hot gas ingestion, various abradable materials and stator geometries were evaluated. A material and geometry system was selected and validated via lab testing.

5 A new advanced static seal was developed to further reduce leakage flows between hot gas path stator components relative to cloth seals. Leakage rates were reduced significantly with excellent tolerance to misalignment between components. These seals are being deployed broadly both on a retrofit and on a new engine basis.

6 Building on the advanced static seal development, “L” shape seals were developed to address leakages between neighboring static seals. This showed a performance advantage in some operating situations.

7 Near gas path static circumferential seals were developed to isolate the stator component support structure from the gas path temperatures. The seals have been incorporated into new engine designs.

8 In anticipation of increasing seal slot temperatures, high temperature spline seal material systems were developed.

9 The improved honeycomb developed for the wheelspace angel wings was successfully modified for blade tip sealing and has been implemented into turbines on a retrofit basis.

TURBINE ROTOR PURGE FLOW REDUCTION

The program's goal for higher efficiency required higher firing temperatures, pressure ratios, and flow capacity. In addition, reductions in turbine cooling flow were required. This task focused on reduced cooling flows in the area of turbine wheelspace cavities.

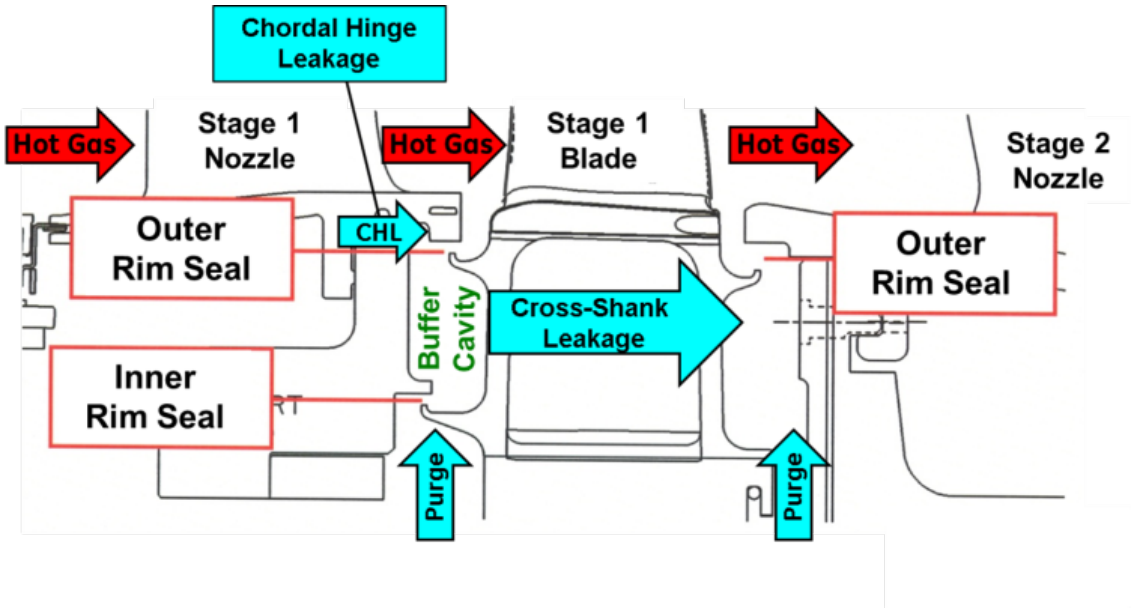

Figure 144: Forward and aft wheelspace cavities found in a typical power generation gas turbine

Turbine wheelspace cavities are the regions resulting from the gap left between the rotating and stationary hardware. Figure 144 illustrates the typical geometry surrounding the wheelspace cavities in a turbine section. As shown, mechanical seals are between the supporting structures of the stationary and rotating hardware, which are generally known as rim seals. Some rim seal designs have a single set of overlapping metal lips, also referred to angel wings, while others (example shown above) employ two sets of seals, one of which resides close to the hot gas path and another which resides further inboard. The two rim seals form a region known as the buffer cavity, which serves as a buffer zone that separates the inner wheelspace cavity and the trench cavity. The trench cavity is the small trench formed from the stationary and rotating hardware that resides in the hot gas path. There are many different designs of rim seals in terms of geometric features. The one illustrated here has small upturns at the end of the rim seal extensions on the rotor side. Other designs change the orientation or location of the upturn or do not have upturns at all. Also illustrated in Figure 144 are purge flows in the forward and aft cavities that are channeled from the compressor and delivered to the inner wheelspace. A leakage path from the interface between the inner support ring and the first stage nozzle row is also shown. This interface leakage, known as the Chordal Hinge Leakage (CHL), plays an important role in the total amount of flow purging out of the outer rim seal. Another critical leakage that occurs is across the blade-rotor attachment through the gaps in-between the blade shanks and is designated as the shank leakage.

The rim sealing mechanism is critical for preventing hot gas from ingesting past the seal(s) and migrating radially inward into the inner wheelspace, which can lead to various mechanical

failures due to increased temperatures. The effectiveness of such a sealing mechanism not only relies on the amount of purge air supplied, but also on the design of the rim seal geometry. As extracted compressor air is used to cool the wheelspace cavity components at the expense of reduced engine performance, designing better wheelspace rim seals is critical to achieving further performance improvements.

Objectives and goals

The program subtask's high level objective was to define an optimal rim seal geometry that met the targeted performance of 50% reduction in turbine rotor purge flows. To achieve this, the program set out to achieve the following goals:

1) Develop a method to characterize purge performance in an engine-representative environment.
2) Develop and validate computational and/or mathematical models with the capability of predicting the relative performance trends between different rim seal geometries investigated.
3) Develop physical understanding of the ingestion problem to intelligently prevent ingestion.
4) Develop a transfer function to take performance data back to full engine conditions.

Strategy/Approach

To achieve all the subtask's goals, it was first necessary to develop two parallel efforts, one focused on the development and operation of an adequate rotating turbine rig, and another focused on the development of sophisticated wheelspace cavity computational models with improved predictive capability. Both of these efforts were equally important to the development of optimal rim seal geometry and were dependent on each other throughout the life of the program. The data obtained from the experimental test vehicle was used to validate and improve the computational model. The validated computational models iterated on additional geometric features and provided recommendations for optimal geometries to later test in the experimental test facility. The computational effort also served to bridge the data captured in the experimental test conditions to the engine conditions.

Experimental Testing Approach

Making any form of measurements in a controlled manner on an actual gas turbine is both expensive and challenging. A scaled test facility offers a lot of options when conditions can be scaled down while still matching critical flow parameters. Several wheelspace cavity research test vehicles exist and have existed in the research community for the past few decades. However, very few are able to match all of the key parameters and conditions that affect the on-going physics. The ability to mimic more of the complex conditions and the capability to make useful and sophisticated measurements has increased tremendously over the years.

At the beginning of the program, it was determined that a unique, scaled-down turbine rig with both rotation and relatively high temperatures and pressures, was required to properly mimic the physics of interest. Additional requirements that went into the design of this new state-of-the-art wheelspace rig test facility included a combination of traditional and more sophisticated instrumentation that would allow for measuring performance as well as other conditions and

properties that would help build the physical understanding of the problem. Below is a description of the design and built testing facility and its capabilities.

1 ½-Stage Turbine Testing Vehicle – Rotating Rim Seal Rig (RRSR)

Figure 145: View of the Rotating Rim Seal Rig Test Facility

A new state-of-the art 1 ½ -stage turbine rig was designed and built to study the drivers of wheelspace ingestion on relevant gas turbine geometries in an engine-representative environment. The rig is shown in Figure 145and has been coined the Rotating Rim Seal Rig (RRSR). The RRSR was used to test multiple industrial gas turbine style rim seal designs and accumulated close to two and half years of operational experience.

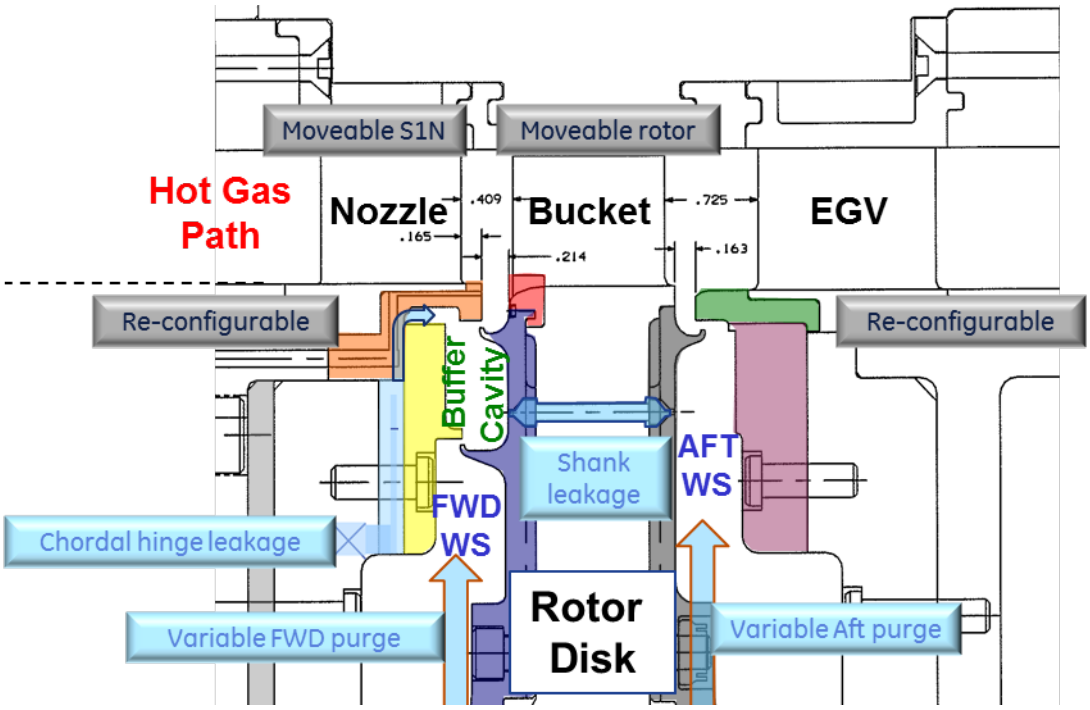

Figure 146: Cross-section of Rotating Rim Seal Rig Test Facility, with highlight of tunable flows in 1 ½ stage turbine

The RRSR is a 1 ½ stage turbine comprised of a first stage vane row, a rotor blisk with interchangeable rim seal geometry and an exit guide vane (EGV). Figure 146 illustrates the RRSR cross-section, highlighting the hot gas path and the forward and aft wheelspace cavities. As shown in the figure, the rig is capable of independently varying the forward purge, chordal hinge leakage, aft purge and the leakage across the shank. The shank leakage is reproduced by insert-able screws with desired open internal diameter that are screwed into the rotor blisk. In the first phases of the test program, the cross-shank leakage holes were plugged and sealed for sake of isolating the effects of other parameters. Most of the testing was concentrated on the forward wheelspace cavity, although some testing was carried out on the aft wheelspace cavity.

Figure 147 illustrates a top view of the vane, blade and exit guide vane rows. As shown, two rows of static pressure taps are located behind the stage 1 vane row and a third row is situated on the radial surface of the trench cavity on the vane (stator) side. These static pressure tap rows serve to characterize the pressure signature behind the vane row at operating conditions. Not shown in the figure, but very important to the rig operation, are total pressure and temperature rakes that reside upstream of the vane row as well as downstream of the exit guide vane row. The total temperature rake located upstream of the stage 1 vane row is used to set the operating temperature. The upstream pressure and downstream total pressure rakes are used to set the overall turbine pressure ratio. The upstream total pressure and static pressure downstream of the vane row are used to calculate a pressure ratio across the vane and thus set the exit Mach number and exit Reynolds Number, defined by Equations 1 and 2, respectively. Equation 3 shows the definition of the rotational Reynolds number, which is defined by the outer rim seal radius and rotational speed. The rig is designed to operate at a nozzle exit Reynolds

number of up to 1.0x10^7, at a rotational Reynolds number of around 6.0x10^6 and at a transonic Mach number at the nozzle throat.

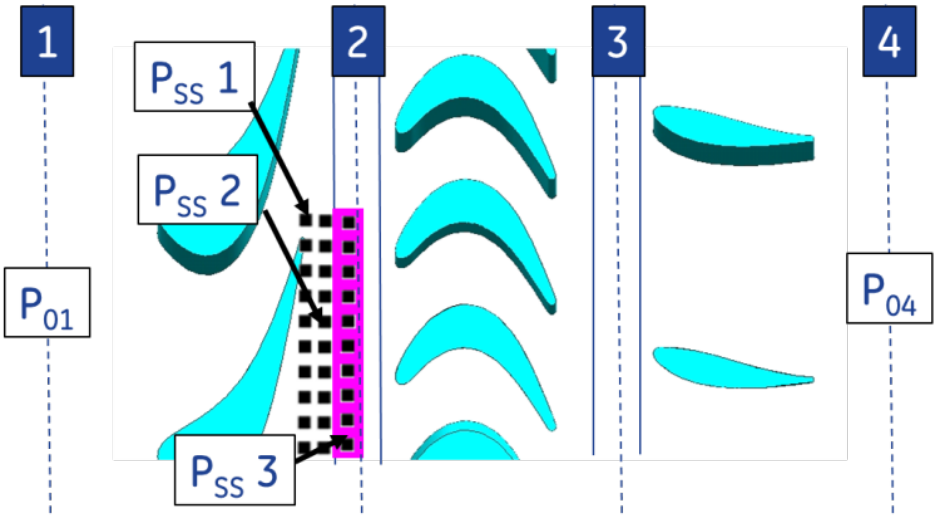

Figure 147: Aerodynamic view of 1 ½ stage turbine with highlighted static pressure tap row

$$\mathrm{Ma} = \frac{V_{Ax}}{SS}\mathrm{Ma} = \frac{V_{Ax}}{SS} \qquad \text{Eqn. 1}$$

$$\mathrm{Re}_{CAx} = \frac{\rho \cdot V_{Ex} \cdot C_{Ax}}{\mu} \qquad \text{Eqn. 2}$$

$$\mathrm{Re}_{\phi} = \frac{\rho \cdot \omega \cdot b^2}{\mu} \qquad \text{Eqn. 3}$$

A global view of the test facility with key auxiliary components is shown in Figure 148. The RRSR is a continuous flow test facility that typically operates over a 9-hour test window. High flow and pressure capacity compressors in-line with preheaters provide a continuous flow supply at a set temperature to the inlet of the rig. A control valve is used to attain the desired mass flow rate in the hot gas path. At a set flow rate, the speed of the turbine rotor is set by controlling the horsepower of the water brake, which is linked to the rotor through a drive shaft. In addition to measuring the rotor speed on the water brake sensor, a key phaser probe with better accuracy is used to set the desired rotor speed. The rotational Reynolds number is calculated using equation 3, above, which depends on the rotor speed and radius of the outer rim seal from the turbine centerline.

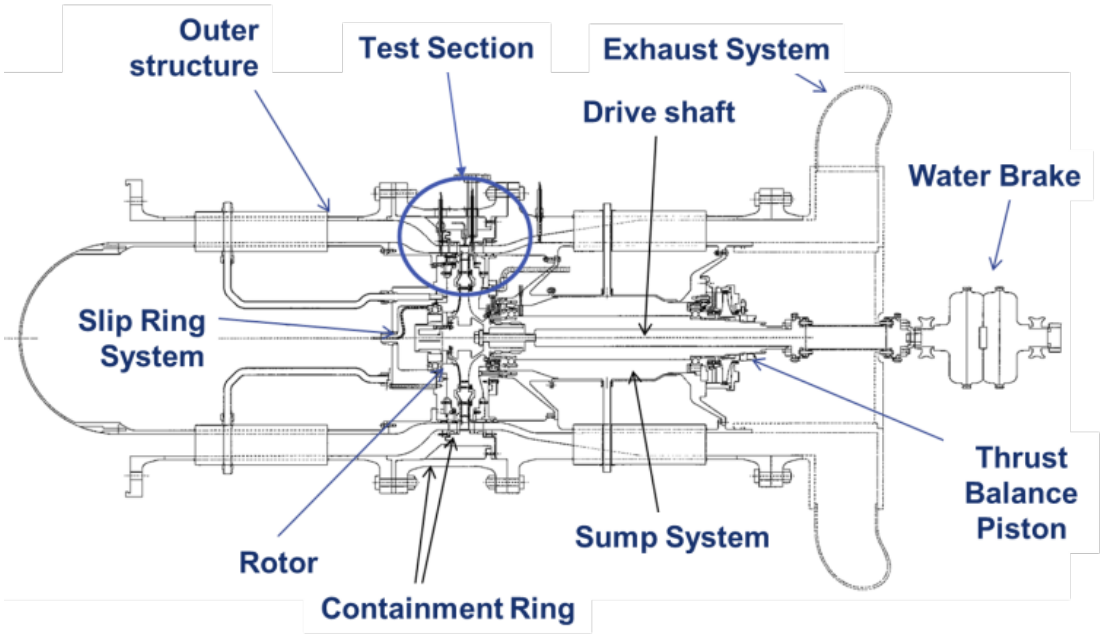

Figure 148: Global view of RRSR Test Facility with main auxiliary components

Table 5 – List of key Auxiliary Components.

No.	Auxiliary Components
1	Control Valves
2	Lube System
3	Water Brake
4	Air & CO2 Chillers
5	CO2 Vaporizer
6	Balance Piston
7	Extraction Blower
8	Emergency Stop Controls
9	Slip Ring Cooling System
10	Control Room & Work Stations

Table 5 lists the key auxiliary components of the test facility. It should be noted that the test section includes a containment ring in the event of a failure of the drive shaft and subsequent burst of the rotor blisk. It is also important to note that a slip ring system is used to transmit data captured on the rotor blisk from the rotating reference frame to the stationary reference frame and thus for recording by the data acquisition system. Lastly, two Gas Analyzers (Siemens ULTRAMAT 23) are used to measure the concentration of CO2/air mixture in the wheelspace cavity.

Figure 149 shows a view of the outer structure opened to expose the rotor blisk and stator hardware of the forward cavity. The two gas analyzer systems, shown in the background of the figure, are used in parallel to cut the measurement time in half at a given steady-state point.

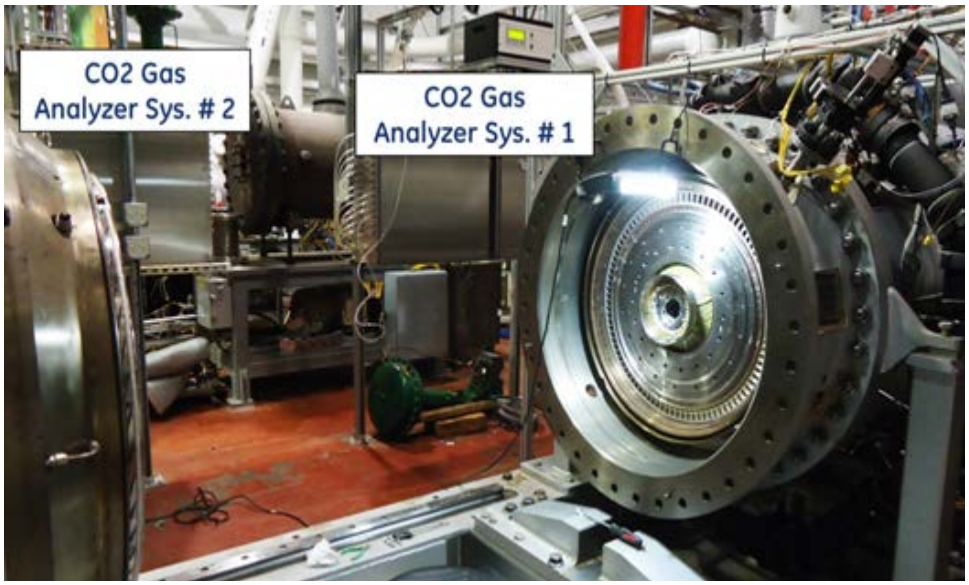

Figure 149: Exposed Rotor Blisk shows the rig's ability to exchange rim seal geometries on the rotor. The two CO2 Gas Analyzer systems used for CO2 sampling are shown in the background

The nominal conditions that are for matched aerodynamic conditions for a heavy duty gas turbine in the experimental rig. The total temperature rakes located at the inlet of the turbine are used to set the desired inlet total temperature of 400ºF (204°C) for each test. The total pressure rakes located upstream and downstream of the turbine section are used to set the total pressure ratio to 3.00. This is done by adjusting the inlet control valve to supply a hot gas path flow rate. The speed of the loaded rotor blisk is adjusted to a value of 7600RPM via the water brake. Throughout most of the testing, the flow rate of the forward wheelspace purge is the one modulated through a range of interest around a nominal setting. The chordal hinge leakage flow is generally held at a constant level. When the test is focused on the forward cavity, the aft cavity purge flows are held constant as well. At a minimum, three main purge flow levels were tested to characterize the sealing performance for each rim seal geometry investigated.

Rig Instrumentation

The RRSR is heavily instrumented in the wheelspace cavity regions as well as in the hot gas path. The various types of instrumentation found in this rig are listed in Table 6 and are discussed in the following section.

Table 6 – List of RRSR Instrumentation

No.	Instrumentation
1	Air & Metal Thermocouples
2	Total Temperature Rakes
3	Static Pressure Taps
4	Total Pressure Rakes
5	5-hole Probe
6	Dynamic & Static Kulite
7	Vibration sensors
8	Speed Sensors
9	CO2 Gas Analyzer Systems (2)
10	Flow Anemometer
11	Sonic Choke Meters
12	Slip Ring
13	Clearance Probes

As previously mentioned, total pressure and temperature rakes are located upstream and downstream of the turbine section. The total pressure rake, as shown in Figure 150, is comprised of five equally-spaced radial taps that span the height of the upstream passage and are oriented normal to the inlet flow. The total pressure rake located downstream of the exit guide vane (EGV) is of similar design and orientation. The EGV serves to remove the swirl from the flow as it exits the turbine section. The total temperature rakes are of similar design and are spaced similar to the total pressure rakes using K-type thermocouples in place of the pressure taps. All pressure signals are connected via rated pressure hoses to pressure scanner system with multiple range pressure cards. A five-hole probe is also installed aft of the rotor and can be traversed across the full span of the blade height. The five-hole probe is used to measure time-averaged total and static pressures and is also connected to the low frequency pressure scanner used for all pressure measurement instrumentation.

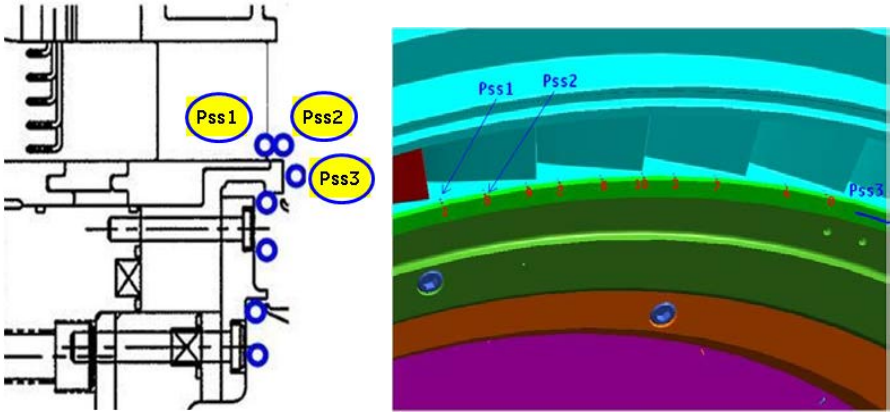

Figure 150: Three axial locations for measuring static pressure cross a single vane passage circumferentially

Sealing effectiveness can be evaluated in two ways, one based on air temperature measurements and another based on CO2 concentration measured through the provided sniffer ports. The air temperature-based sealing effectiveness is defined by equation 4, where the hot gas temperature, $T_{HGP,}$ is measured by air thermocouples located at the stage 1 nozzle trailing edge, the purge flow temperature, T_{Purge}, is measured by air thermocouples located at the ejection of the purge supply holes at the inner wheelspace, and the local air temperature, $T_{Local,}$ is measured by discrete local air thermocouples.

$$\eta_T = \frac{T_{Local} - T_{HGP}}{T_{Purge} - T_{HGP}} \qquad \text{Eqn. 4}$$

Defining sealing effectiveness from air temperatures is challenging as the local air temperature is affected by heat transfer to the metal surroundings, by windage heat generation, and the like. For this reason, the measurement of sealing effectiveness by a CO2-based sampling method is considered more reliable. The buffer cavity measurements are the critical data for determining ingestion, as a reduced CO2 concentration in this region signifies ingestion past the outer rim seal.

Figure 151 illustrates the bank of calibrated choked flow meters used to separately measure the CO2 and air streams delivered to the forward purge, aft purge, and chordal hinge leakage flows. A specific flow is tuned via flow from several CO2 and air flow meters, and each one is set to the desired composition on a mole fraction basis.

Figure 151: Bank of calibrated choke meters used to independently measure the flow rates of air and CO2, and the Air Chiller used for reducing secondary flow temperature

In inferring ingestion from CO2 concentration, the wheelspace purge and chordal hinge flows are supplied with 30% CO2 mixture by independent flow meters. The CO2 concentration measurements are normalized to a sealing effectiveness value defined by equation 5, where $CO2_{HGP}$ is the CO2 concentration of the hot gas path (which is essentially zero for an all-air

mixture), $CO2_{Purge}$ is the average CO2 concentration measured at the two innermost CO2 ports, and $CO2_{Local}$ is the CO2 concentration level measured locally at an individual CO2 sniffer. The sealing effectiveness parameter η_{CO2} equals 0 for a 100% ingestion scenario and 1 for a 100% purge scenario.

$$\eta_{CO2} = \frac{CO2_{Local} - CO2_{HGP}}{CO2_{Purge} - CO2_{HGP}} \qquad \text{Eqn. 5}$$

The CO2 gas analyzer systems comprise of a channel switching device operated by Programmable Logic Controllers (PLCs) and the actual gas analyzers. The gas analyzers come with a vendor rated uncertainty of 0.5% on the %CO2 scale. The bias uncertainty of the gas analyzers is further reduced by calibrating the analyzers before every test with the same known composition of a research quality gas bottle. Other research quality gas compositions are used to perform additional checks on each analyzer. Figure 152 illustrates the types of results from the calibration as carried out regularly on both gas analyzers over the entire operating range with the use of research quality CO2/air mixture bottles of known compositions.

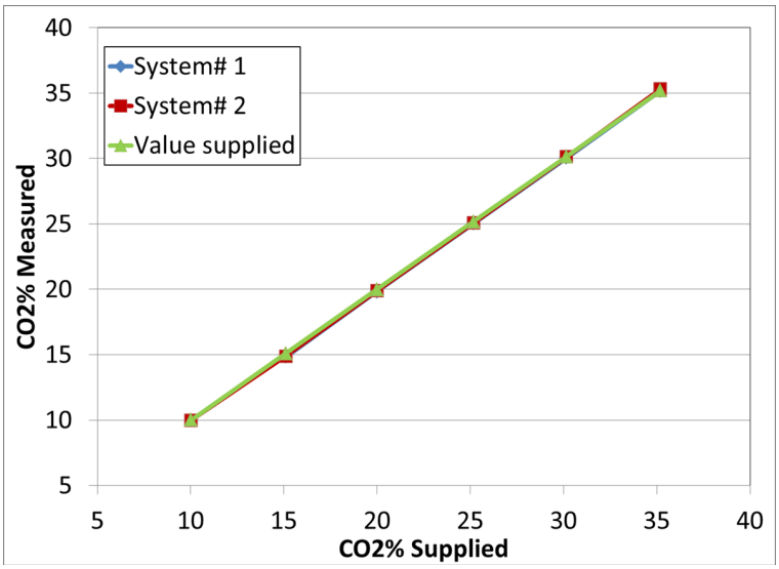

Figure 152: Calibration of the analyzer systems over the operating range

Geometries

A number of geometries were studied in this program within the scope of program. The DOE "Optimal Geometry" was defined with the learnings from rig test data for different geometries, together with CFD verification. This configuration was built and tested in the rig, and the data showed sufficient improvement in terms of purge flow savings.

Experimental Data

A significant amount of shakeout testing was conducted on the multiple components and instrumentation of the RRSR in order to arrive at a high level of quality control and measurement of the parameters of interest. The following section presents key measurements

taken over a typical 12-hour test. The continuous data signatures presented are intended to: 1) show the capability of the RRSR to reach relevant engine-matched conditions over its operating range; 2) demonstrate that thermal steady-state conditions are reached before collection of critical effectiveness data is recorded; and 3) show the qualitative aspect of the instrumentation being used to measure multiple parameters of interest.

Aerodynamic Operational Data

Figure 153 shows the 1Hz signature data for critical operating flow parameters held on the RRSR throughout the entirety of a typical test running for 12 hours. From the figure, it is observed that at the beginning of the test both the hot gas path flow and the rotor speed are brought up to operating condition gradually over a period of 2.5 hrs. The mass flow rate is adjusted to set the design Total Pressure Ratio across the 11/2 stages to 3.00. The measurement window is defined by the stability of the operating conditions; specifically, the hot gas path flow, rotor speed, inlet temperature, and total pressure ratio across the 11/2 stage turbine are monitored for steady-state operation. A typical test will have an 8.5 to 9 hour measurement window over which the purge flows are modulated to the desired values. Again, the RRSR operates with a continuous hot gas path flow through the entire measurement window and it can be seen from Figure 153 that the variations for all 3 parameters plotted behave with low or reasonable variation levels.

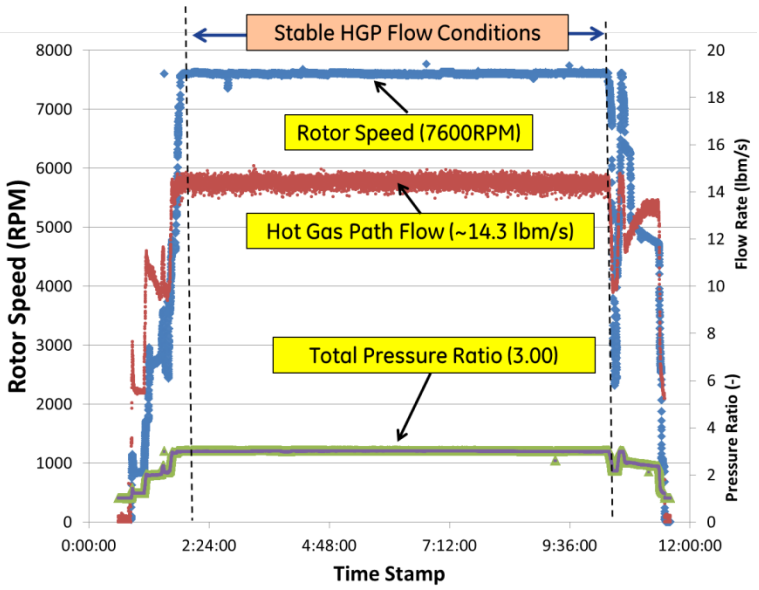

Figure 153: Time signatures of hot gas path operating conditions over a 12-hour test

Sealing Effectiveness Data

The sealing effectiveness η_T based on CO2 measurement, as defined in equation 5, in the buffer cavity was determined for two different clearances and for a range of purge flows. A number of the different configurations tested showed improved sealing effectiveness vs. the baseline.

Computational Fluid Dynamics Modeling Approach

One of the main objectives of the rig testing was to collect test data on varied sealing geometries and use them to validate the CFD tool in terms of how good they can predict the sealing efficiency and sensitivity of the results on geometry variations.

To achieve this goal, detailed CFD modeling guidelines were developed based on attempts to data match rig results. This is called the “reduced-order” approach, which has quick modeling turnaround time (<3 weeks) and were demonstrated to have the capability to predict the trend of geometry variations. Additional efforts were also made to further improve the predictability of the tool on delta basis. A 360-deg full wheel CFD model was also set up and run on two different geometries, to understand the effects of sector size and identify any low frequency physics that might have been missed from the sector model.

The “reduce-order” approach was validated in terms of trench prediction, and thus applied to sealing geometry design optimization. The final geometry tested by the rig, aka “Optimal Geometry”, showed improvement which met the goal of this program.

2 Vane/4 Blade Sector Model

The “reduce-order” approach was defined as following:

1) Mesh which relies on wall functions for the near wall treatment
2) k-ε turbulence model with scalable wall functions
3) Steady state run with frozen rotor General Grid Interface (GGI) as domain interface for ~1000 iterations;
4) Unsteady run with stator-rotor GGI domain interface, restarted from frozen rotor steady state results;
5) Minimum 3~4 full revolutions unsteady run time for stabilized cyclic pattern at monitoring points;
6) 1/2 ~ 1 revolution run time for time-averaged results.

The computation domain used in this approach included two nozzle guide vanes (vanes) and four blades, i.e. 2-I/4-B as shown in Figure 154 (a), with periodic boundary conditions applied at the two sector faces. A study on pre-test rig CFD modeling with different sector sizes, including 1-I/2-B, 2-I/4-B, 4-I/8-B, and 12-I/24-B, indicated that 2-I/4-B was the minimal sector size to capture ingestion at similar levels with other bigger sector sizes while the smallest 1-I/2-B sector significantly under-predicted the ingestion level.

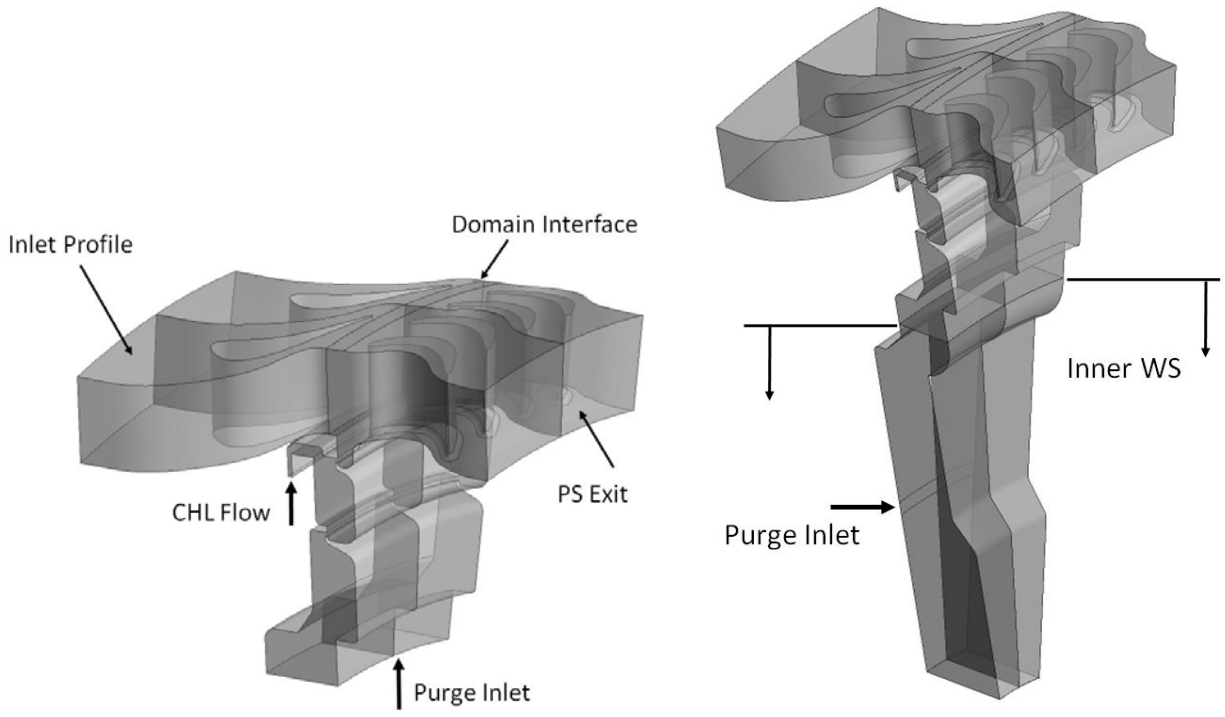

(a) Sector domain (b) Sector domain w/ inner WS

Figure 154: 2 Vane/4 Blade Sector CFD model details.

The comparison for the baseline configuration is shown in Figure 155, where CFD results were obtained from models with and without inner WS included in the modeling domain. The CFD results were time-averaged over the last one revolution after cyclic patterns were established with the unsteady runs. Data from all CO_2 ports in the buffer cavity were averaged in the comparison. CFD results were also obtained by averaging data over three lines on the same stator side at three radial locations where CO_2 ports were located.

The CFD prediction showed very good agreement for the baseline configuration with or without the inner WS included in the model domain. Including the inner WS led to a steeper reduction in purge efficiency from high to mid purge flow, and then flatten out for lower purge levels, but did not show significant prediction improvement overall compared to modeling results without the inner WS included.

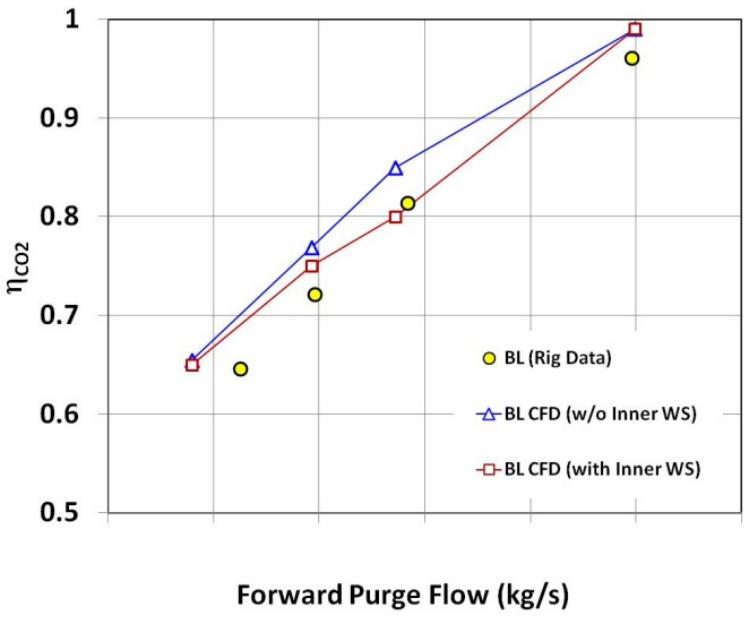

Figure 155: CO_2 comparison for BL configuration: with and w/o inner WS in modeled CFD domain

360-degree Full Wheel Model

Recent literature has shown that the size of the sector played a role in terms of limiting the ingestion flow physics to occur, thus under-estimate the ingestion flow significantly. It has been suggested that the right approach to capture the real physics was to run a full wheel 360-deg model, which showed some success on matching the rig test data at The University of Arizona.

As a part of this program, a 360-deg full-wheel CFD model was set up and run at two different purge flow levels on a supercomputer, as shown in Figure 156. This was created by duplicating the sector w/inner-wheelspace CFD domain for a full circle. Purge inlet, as discrete holes in the real rig, was modeled as a smeared slot at the stator-side of a lower wheelspace location. Other than this simplification, all other details in the rig were captured by this full wheel CFD model.

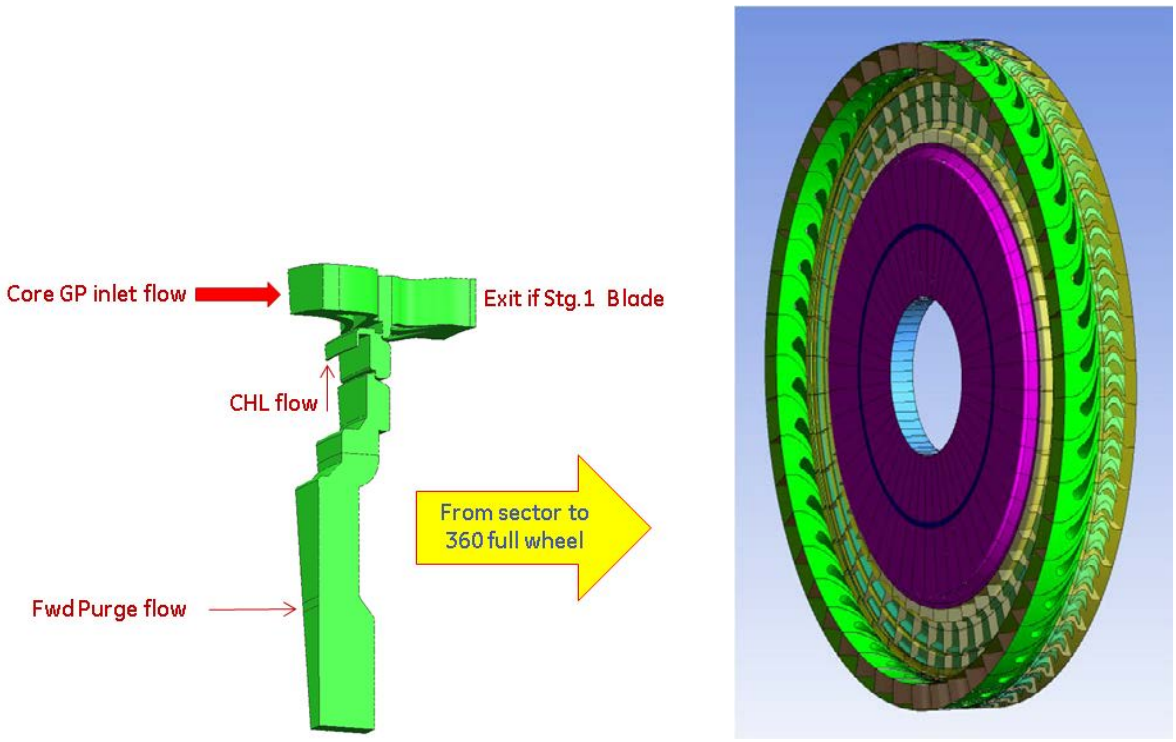

Figure 156: Full Wheel 48 Vane/96 Blade CFD model details.

Conclusions

Tests were conducted on different configurations to evaluate the geometry sensitivity on purge efficiency. The optimal geometry was developed with the help of both CFD and rig test data, and the test results indicated the goal of a 50% reduction in purge flow saving was achieved with the results shown in Figure 157.

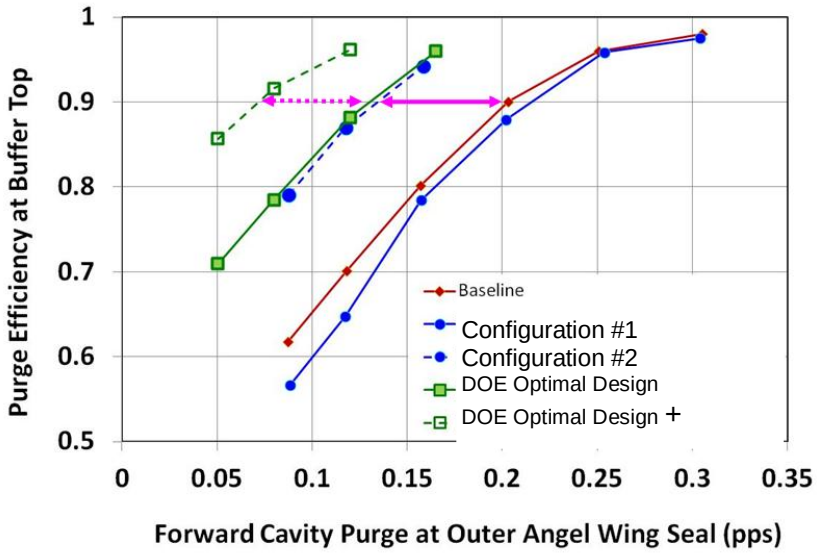

Figure 157: CO2 data for baseline, extended platform, and optimal geometry

Learnings from both the rig test data and CFD are being utilized in the design of new gas turbine products.

ADVANCED HOT GAS PATH TURBINE TECHNOLOGY

This subtask developed the architecture of the next generation for stage 1 hot gas path turbine components. New design architectures were investigated that enable reductions in the cooling flow requirements in order to achieve improved performance and reduced emissions. The program focused on architecture, cooling concepts, and casting development for new technologies.

Concepts were evaluated for both the stage 1 nozzle and the stage 1 bucket. Advanced cooling design and architecture concepts for the components were analyzed and a preferred approach selected for each. Casting trials of the preferred architectures were performed to assess the manufacturability of the concepts. Iterations between GE and the casting suppliers on the architecture features of the part were conducted to refine and improve the design.

Subtask 2.9 investigated architectures of the next generation of a stage 1 hot gas path turbine components. During this subtask, it was demonstrated that these architectures met program cooling flow reduction targets with no impact to part life, while having a positive cost/benefit ratio. The designs investigated in this program enabled a step change in stage 1 component design approaches and architectures. It is concluded that the stage 1 bucket and nozzle and small feature casting techniques developed in this project are economical and will be used to improve future gas turbine product offerings.

EXPERIMENTAL METHODS

A Heat Transfer Rig was built and tests were performed to measure heat transfer coefficients (HTCs) along passages of different aspect ratios and wall cross sectional shapes associated with an advanced design for the stage 1 buckets and nozzles of an advanced gas turbine. Baseline results showed a good match to theoretical average HTC estimates for a duct over a range of Reynold's numbers. Tests of non-rectangular cross sections showed that heat transfer effectiveness was similar or superior to rectangular ducts. The results of these experiments are presented in the *Results and Discussion* section of this report.

RESULTS AND DISCUSSION

Task 2.9 (ARRA) – Advanced Hot Gas Path Turbine Technology - Next Generation Stage 1 Turbine Architecture

This subtask developed architecture concepts of the next generation of a stage-1 hot gas path turbine airfoil. A new architecture design enabled reductions in the cooling flow requirements, and enabled achievement of improved performance and reduced emissions. The program focused on architecture, cooling concepts, and casting development for new technologies. In this task, concepts were evaluated for the stage-1 bucket (Element #1) and the stage-1 nozzle (Element #2).

Element#1 Stage-1 Bucket (S1B)

Advanced cooling design and architecture concepts for the selected airfoil were analyzed and a preferred approach selected. Casting trials of the preferred architecture were executed to assess the manufacturability of the concept. Iterations between GE and the casting supplier on the architecture features of the part were conducted to refine and improve the design.

At the onset of this project the advanced cooling design S1B design was approached from an optimum heat transfer design followed by a mechanical evaluation. The mechanical and heat transfer analyses were iterated (Figure 158) to arrive to the best design while not compromising the mechanical requirements. An example of mechanical analysis results can be seen in Figure 159.

Once a heat transfer concept was determined, the team evaluated the stress and low cycle fatigue life of the proposed non-traditional design. Geometric improvements were identified for low life areas and the model was updated for a subsequent iteration of analysis.

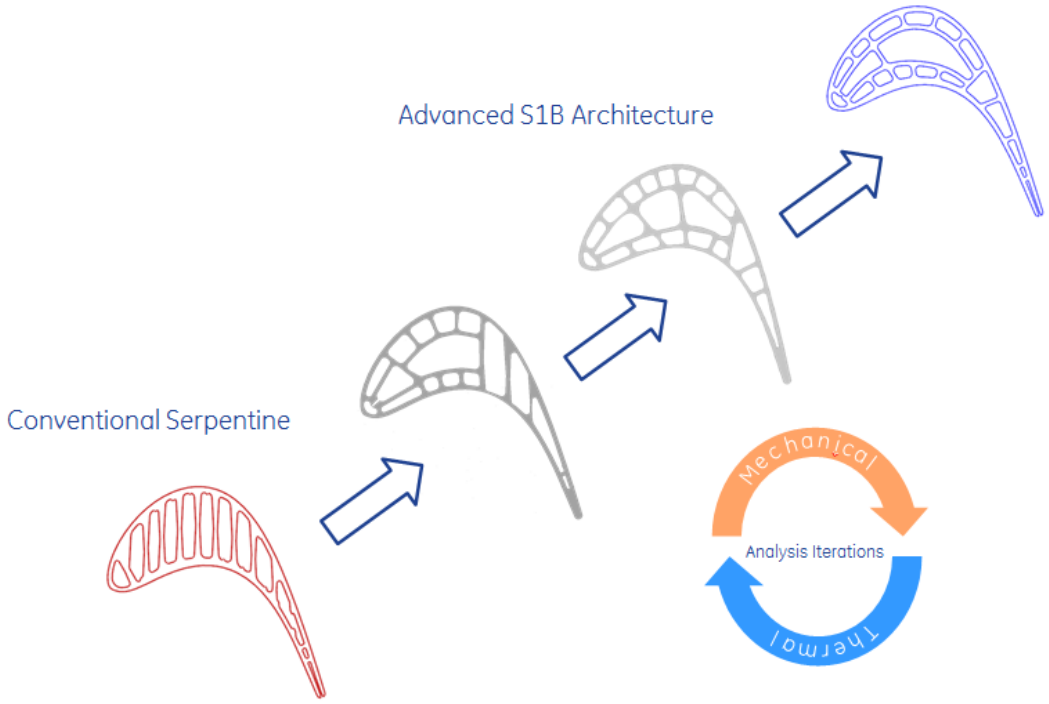

Figure 158: Design - Analysis Iterative Approach

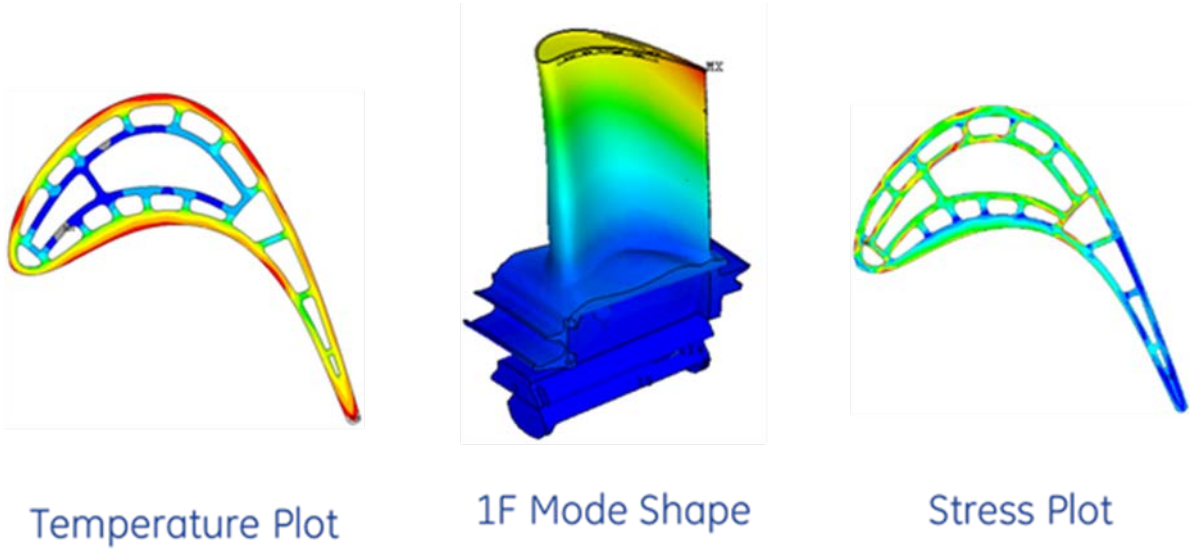

Figure 159: Example of Mechanical Analysis Results

Casting Trials

Casting demonstrations were performed at a casting vendor using an existing S1B production-part external geometry. The casting trials approach (example in Figure 160) was to use production process sheets as much as possible to reduce the amount of development-engineer touch time and evaluate the new design on equal footing with conventional casting procedures.

The castings were put through an analysis procedure including:

- Destructive evaluations:
  - Pressure side internal radial dimensions check; utilizing mechanical measurements.
  - Radial slices (3 airfoil and 2 shanks) to check pitch and chord; employing white light measurements.
- Chamber line cut, internal FPI and grain etch.

This analysis was performed extensively with favorable results.

During the casting trial development, the team encountered typical new technology trial-and-error occurrences. At the end of each casting trail, failures were noted and changes to design and processes were made prior to the next casting. In all, a total of 54 castings were produced.

At the end of the casting trials it was determined that this new advanced S1B design demonstrated favorable casting capability and yield.

Conclusions

During the S1B portion of the Next Generation Stage-one Architecture task, it was demonstrated that the cooling flow reduction met the program targets with no impact to part life. The part cost target is dependent on part yield. Cost targets were made keeping in mind the flow benefit that the technology brings into the equation. By approaching the product cost goal on dollars per output and fuel consumption derivative, it is concluded that this technology is economical and can be used to improve future gas turbine product offerings.

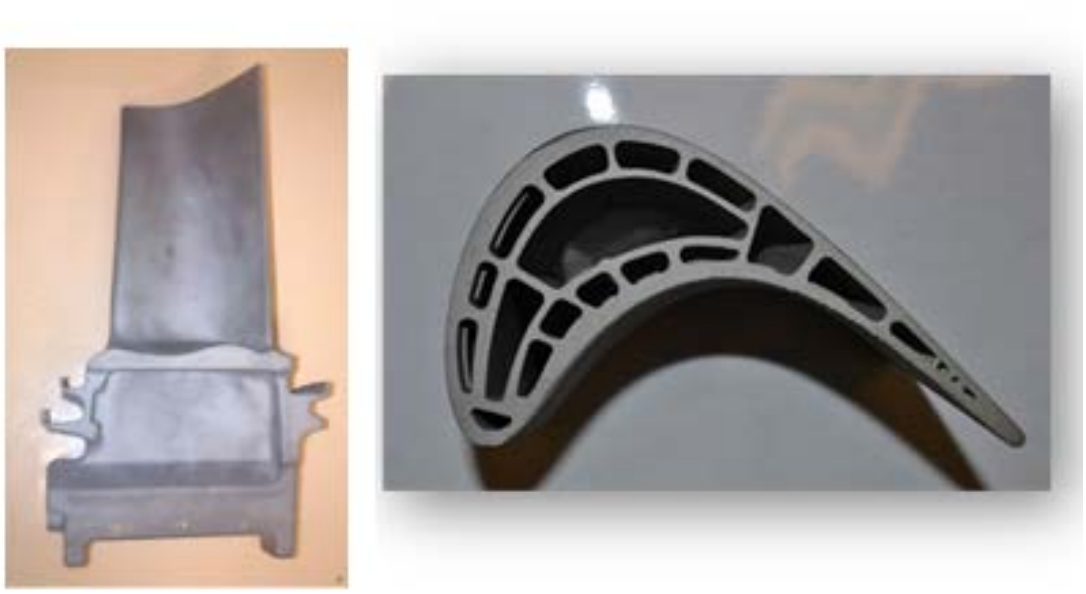

Figure 160: Casting Trails

Serpentine Passage Heat Transfer Rig

A Heat Transfer Rig (Figure 161) was built and tests were performed to measure heat transfer coefficients (HTCs) along passages of different aspect ratios and wall cross sectional shapes associated with an advanced design. One wall has a series of foil heaters along the length that allows controlled heating of the wall while measuring power inputs. Embedded just beneath the hot wall is a grid of thermocouples so hot wall temperature can be measured along the flow length at the centerline and nearer the wall edges to determine the impact of secondary flow characteristics from where the hot wall meets the intermediate walls.

To measure HTCs, air is forced thru the duct at a known rate (Reynold's number). By measuring heater power, local wall temperature, and inlet and outlet air temperatures, both local heat transfer coefficients and average heat transfer coefficients can be calculated. HTCs are measured over a range of Reynold's number. The cold wall location (Figure 162) can then be moved and the test repeated to obtain the impact of varying aspect ratio. The cold wall can also be replaced to test the impact of a different cross sectional shape.

Baseline results showed a good match to theoretical average HTC estimates for a duct over a range of Reynold's numbers. The test rig was also able to capture the predicted variation of HTC along the length of a duct.

Tests of non-rectangular cross sections showed that heat transfer effectiveness was similar or superior to rectangular ducts. Varying aspect ratios indicated that certain aspect ratios could negatively impact heat transfer. Centerline heat transfer was typically lower than heat transfer closer to the edges, indicating possible secondary flow effects. However, heater variance resulting in higher centerline power could have accounted for some of these effects. Future testing with turbulators will attempt to see if this effect can be replicated.

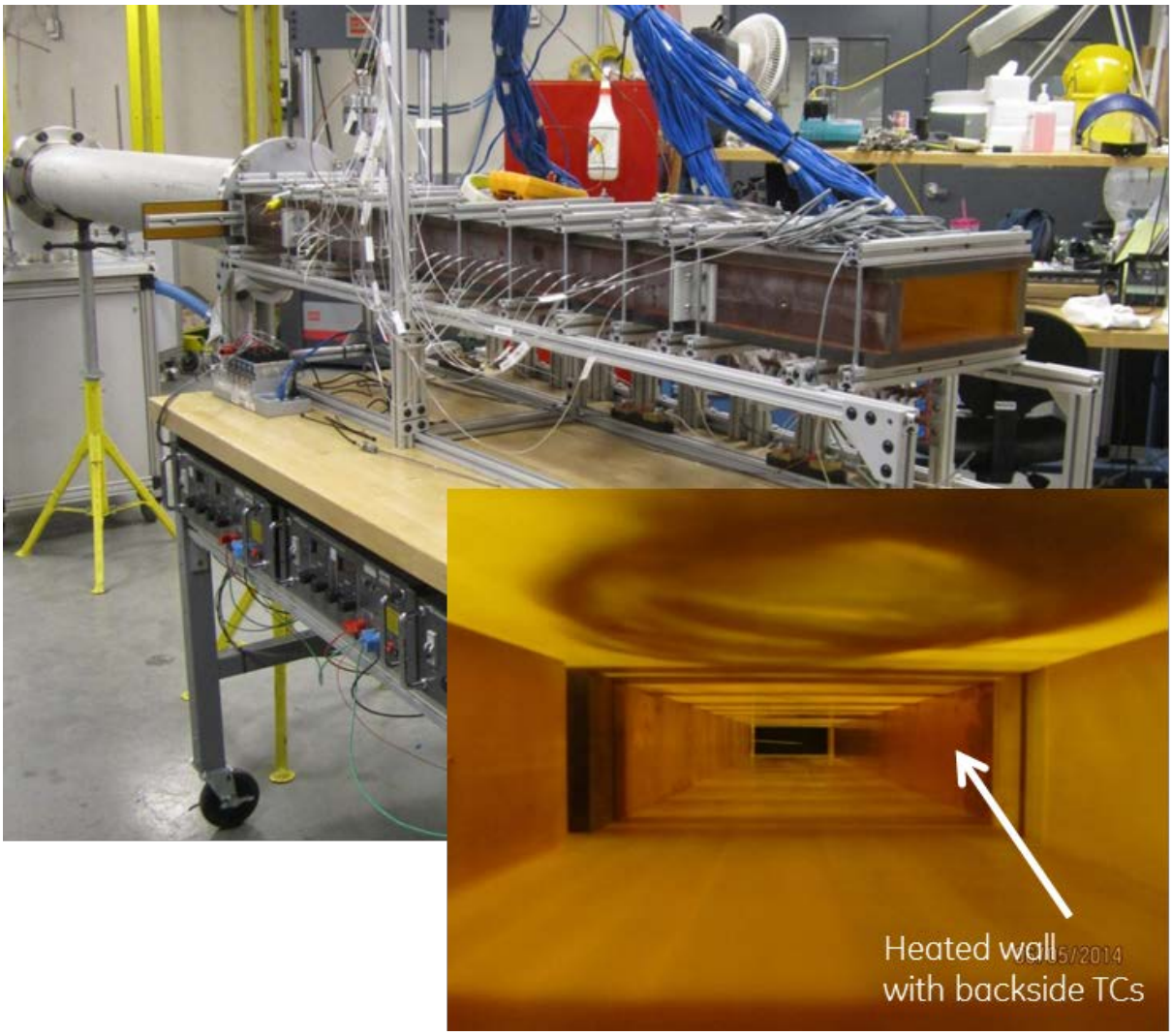

Figure 161: Heat Transfer Rig

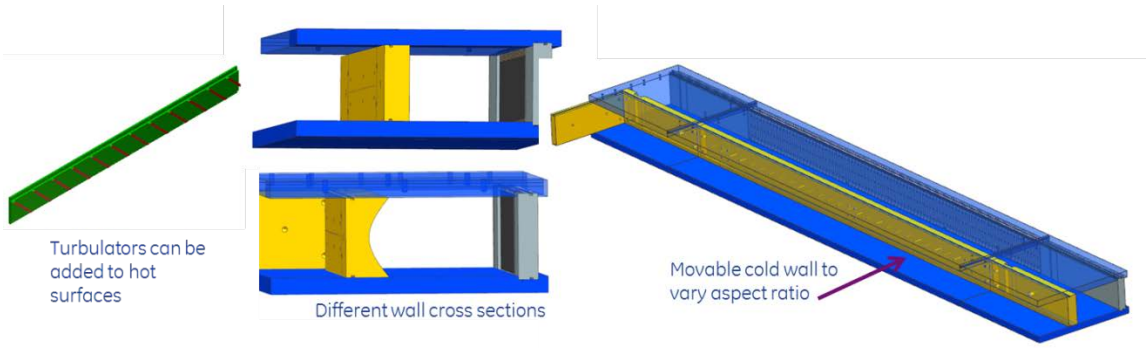

Figure 162: Heat Transfer Rig details

Element#2 Stage-1 Nozzle

The nozzle development focused on determining the S1N architecture required for higher turbine inlet temperatures, lower cooling flows, and increased turbine efficiency. Over sixty (60) concepts for improved first stage nozzle cooling were identified and assessed for performance benefit, cost, and risk. A broad range of ideas were generated, including materials improvements that allow for higher operating temperatures, new geometries that increase cooling effectiveness, and alternative cooling concepts. A survey of these technologies showed that some of the concepts, such as those employing complex internal cooling geometries or incremental material improvements, would not have sufficient benefit to warrant further study under this program. Others were eliminated due to high levels of risk and estimated cost. For the remaining concepts, more detailed product cost estimates, performance benefits, and technology risks were evaluated in order to determine a net value for each technology. Based on these net value ratings, the top architectures were identified for further evaluation. These top concepts include one advanced material option, one new cooling technology, and one alternate cooling concept.

Manufacturing feasibility and durability testing was conducted on two methods of manufacturing the cooling features. These methods were also analyzed against baseline to assess heat transfer improvement and mechanical life. Cooling benefits and life analyses results showed improvement against conventional cooling feature geometry.

Vendor machining trials were executed to demonstrate vendor capability with special process machining of advanced features in a contour surface as well as trials for machining exit features through thermal barrier coatings (TBC). Additionally, casting trials were completed to investigate alternate manufacturing options (casting trials are detailed in section below).

Heat Transfer Analysis

Detailed Heat Transfer analyses were performed on the S1N inner and outer endwalls where cooling was added at the trailing edge section of both. The design uses roughly the same cooling flow as the baseline part. However, analysis shows that the cooled sections will be notably cooler and have a more uniform temperature profile than the base part.

A parametric study was performed around different cooling geometries. Results showed that the geometry had a minor impact on performance

Durability Testing

A material was developed to support the cooled concept. Material physical properties, low cycle fatigue (LCF), furnace cyclic, ballistic, and JETS tests were completed and data analyzed (Figure 163). Thermal mechanical fatigue test results were very favorable, revealing no thermal barrier coating spallation.

Additionally, six tests totaling 90 hours of operation at over 2500°F (1371°C) were completed in a combustion test stand on the cooled nozzle bars. These bars showed no evidence of distress. Figure 164 shows images of the nozzle bars post-test.

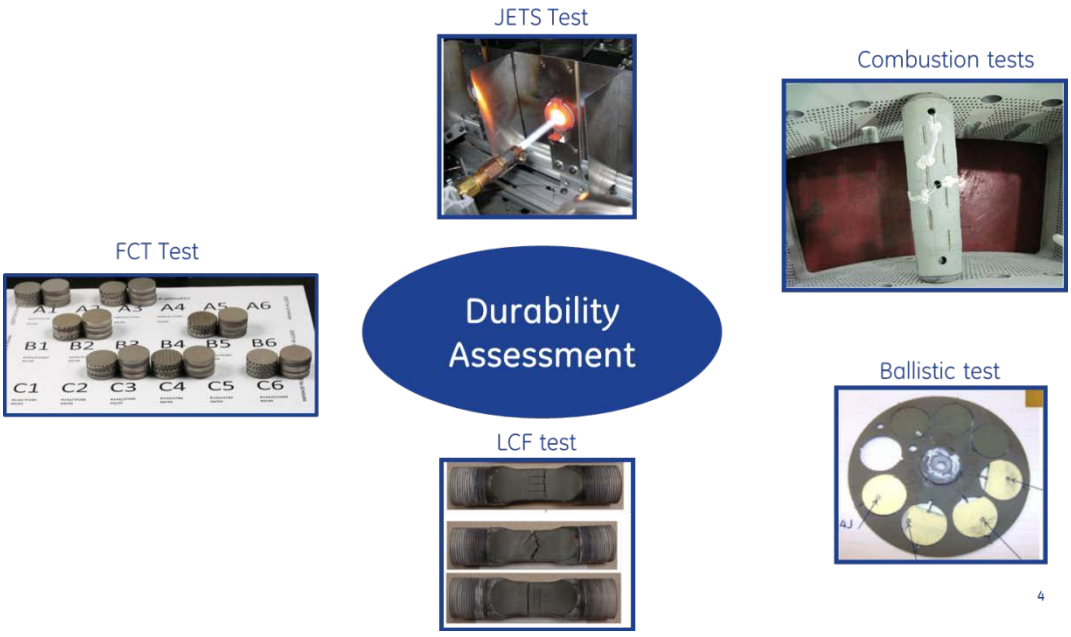

Figure 163: Durability Tests

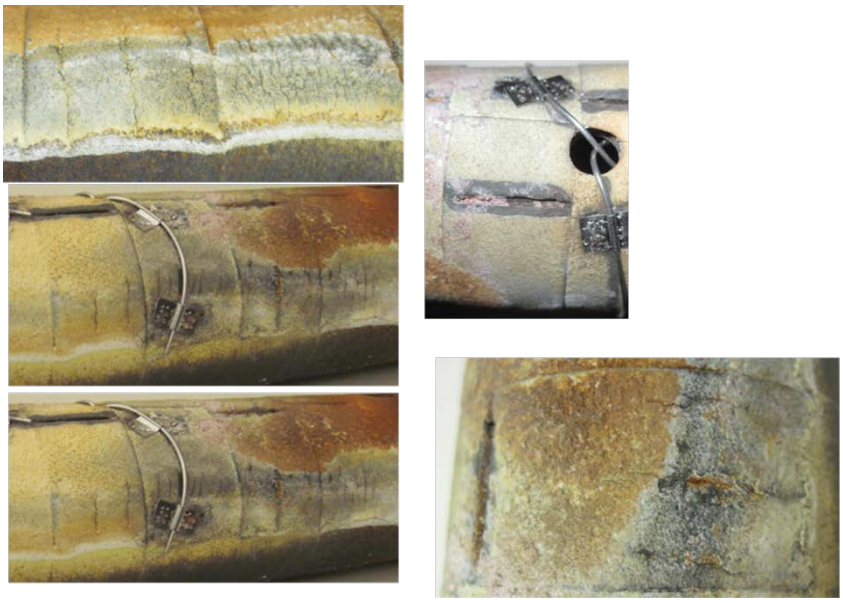

Figure 164: Nozzle bar post tests

Field Demonstration

Three nozzles were modified with the developed cooling technology on the inner and outer side walls to be included in a prototype field test at a customer site. The field test itself was outside the scope of the program.

Conclusion

Out of the sixty concepts originally evaluated for the nozzle development a final architecture was developed and evaluated. Heat transfer analyses, mechanical fatigue and feature tests showed favorable results with respect to performance benefit without any debit to life and cost.

Element #2 Stage-1 Nozzle Small Feature Casting Trials

The objective of this activity was to determine the casting limitations of small features (pins and channels) in wax. Typically, small features, such as enhancement bumps, are made from ceramic core in the investment casting process.

These casting trials were broken down into two phases at two different vendors, each with unique casting parameters. Figure 165 shows the slabs of pin arrays and channel geometries, varying in diameter, height and length.

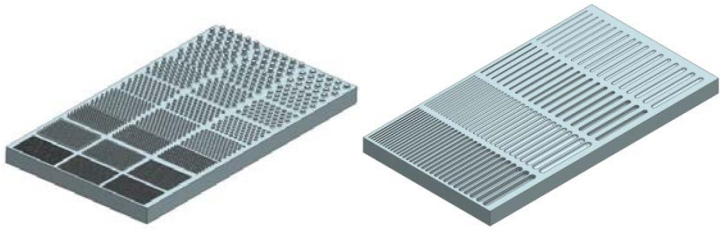

Figure 165: Small Feature Slabs

Casting Trial Results

In Phase-1, the casting parameters were (purposely) not optimized in order to get a baseline to current casting parameters and results. Figure 166 highlights some of the pins and channel geometries that had defects. It was concluded that the shallower channels produced the best results, whereas the deeper channels tended to exhibit a greater frequency of defects. Larger pin diameters proved to be successful, however, as the pin diameters decreased the rate of defects increased.

In Phase-2, the parameters were optimized for the small features. There were better casting results compared to Phase-1, which was expected since the parameters were developed specifically for these small features. The formation of crisp edges on the large pins were still proven difficult, as well as complete filling of tall, small pins. Figure 166 shows the defects that were observed in Phase-2. Only one pin array has visual defects, and a smaller portion of channels had fill issues in the corners.

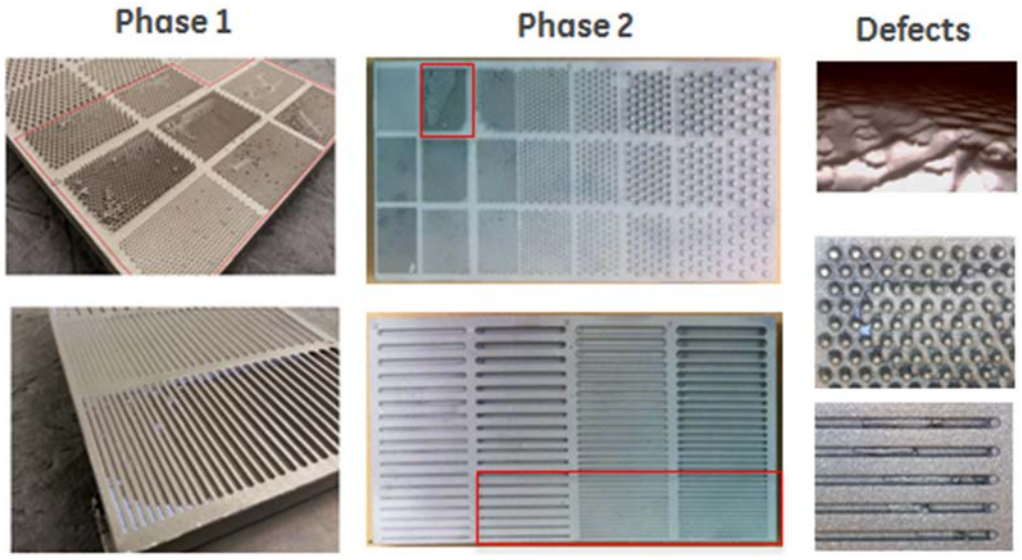

Figure 166: Castings of Small Feature Slabs

Phase-2 had much better results than Phase-1. Ultimately, this S1N architecture task bounded the limits of as-cast pin and channel geometry and spacing, and this technology can be leveraged in future gas turbine engine component designs.

CONCLUSIONS

Subtask 2.9 investigated architectures of the next generation of a stage 1 hot gas path turbine components. During this subtask, it was demonstrated that these architectures met program cooling flow reduction targets with no impact to part life, while having a positive cost/benefit ratio. The designs investigated in this program enabled a step change in stage 1 component design approaches and architectures. It is concluded that the stage 1 bucket and nozzle and small feature casting techniques developed in this project are economical and can be used to improve future industrial gas turbine product offerings.

CMC & EBC DEVELOPMENT

The objective of this program was to develop fuel flexible (coal derived hydrogen or syngas) gas turbine technologies for IGCC and IGCC with CCS applications that meet DOE program goals. The path to obtaining the overall program goals included CMC and EBC Development. Specific tasks included continued monitoring of a full set of stage 1 CMC shrouds within a GE 7FA gas turbine that completed over 21,740 hours of continuous operation. Observations were made that included both CMC and EBC degradation as a function of field operational hours. The majority of CMC activities were focused around developing a new CMC component. This application required two phases of design as well as sub-scale and full-scale testing. Over the course of more than three years, a total of 31 full-scale CMC components were fabricated. A significant amount of additional testing was conducted to understand the wearing mechanisms from the contact between a CMC and metallic interface. In total over 500 hours of full-scale testing was completed resulting in a CMC component with a TRL of 4.

Engine Durability Test 2, CMC Stage 1 Shrouds

A three plus year field test of Ceramic Matrix Composites (CMC) stage 1 shrouds was completed. Previous CMC field experience included an engine durability test with a rainbow of Stage 1 CMC Shrouds which amassed more than 5,000 fired hours and 14 cycles. In 2006 a Solar CSGT was retrofitted with a CMC combustion liner and ran for 12,822 hours and 46 cycles. During this field test, the gas turbine was monitored with bi-yearly borescope inspections and reports providing detailed field data on performance and degradation. Overall the CMC Shrouds amassed a new record of 21,740 hours and 126 starts before being removed during a scheduled hot gas path inspection.

The shroud architecture that was used for the first engine durability test was modified in some aspects for recent test to assure a longer lasting architecture. The design of the CMC shroud remained the same except for some changes to the Environmental Barrier Coatings (EBC) coatings. Figure 1 details a representative circumferential cross-section of the first engine durability hardware. The CMC shroud is a U-channel shape forming the flow path to reduce the over tip leakages associated with hot running gaps between the bucket tip and inner shroud. There is a metallic block on the backside of the CMC shroud that is used to radially position the shroud relative to the intended flow path. This metallic block is loaded using a spring that is located in the outer shroud block and cooled by compressor air. The shroud is generally uncooled except for some unmetered leakages around the spring and loading block.

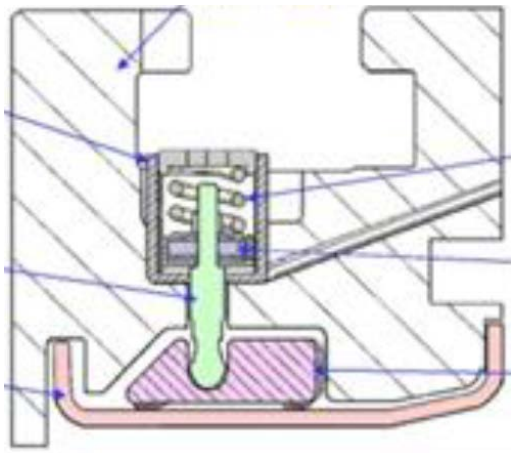

Figure 167: General Schematic of CMC Shroud Architecture

The objectives of the engine durability test two were to understand the long term impacts on the CMC substrate and the EBC coatings. Previous field experience did not have a significant enough amount of time at typical operating conditions to provide the necessary information. The recent field trial involved the installation of a full set of CMC stage 1 shrouds in a 7FA unit, as shown in Figure 2.

Figure 168: Engine Durability Test 2, Stage 1 CMC Shrouds

Each of the outer shroud blocks contained three inner CMC shrouds as shown in Figure 3. These CMC shrouds were coated with EBC to protect them against moisture at elevated temperature. Without EBC, volatilization of the silicon carbide composite would result and, with enough time, the CMC shroud would disintegrate.

Figure 169: Stage 1 CMC Shrouds

To understand the long term impacts on the EBC coatings, several EBC coating architectures were employed other than the traditional baseline EBC architecture shown in Figure 3. The goal was to assess the durability of different coating architectures in a real engine environment and then relate that information back to laboratory tests. About 70 percent of the shrouds had the baseline EBC coating or some variant of that architecture.

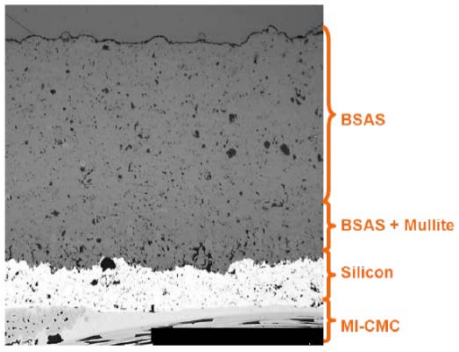

Figure 170: Baseline EBC System

Over the course of the three years and 21,740 hours of engine operation, a total of 10 borescope inspections of the shrouds were completed. In general the shroud conditions were assessed every 1000-3000 hours. During those inspections several shrouds were tracked in particular due to some known and intended defects in the CMC substrate and EBC coatings before installation. The results provide valuable data for use in future applications of CMC components in gas turbines.

The completion of the CMC field trial marked an important milestone in the development and deployment of CMC components.

Sub-Scale Component Design and Fabrication

A sub-scale CMC component was developed.
The mold and ply shapes were designed and manufactured and the component was laid on the mold. It enabled an understanding of the ability of the CMC plies to conform to the desired shape. A mold was designed which implemented all the learned lessons.

Testing of Sub-Scale Components

Complete components were instrumented and tested.

A number of discoveries were made during the testing that enhanced the understanding of key attributes needed for a successful design.

Phase 1 Design and Fabrication of CMC Component

A full-scale CMC component was designed.

The system architecture was adapted for the full-scale CMC component design and the initial sizing of critical features was completed with the aid of GE internal tools. Many of the normal features associated metallic components were altered to allow for manufacturing of the composite laminate structure. These very changes proved critical to the overall design and manufacturing success of the Phase 1 design.

The Phase 1 composite CMC component fabrication began with tool design and fabrication in early 2012. See Figure 171 for a representative CMC laminate cross section.

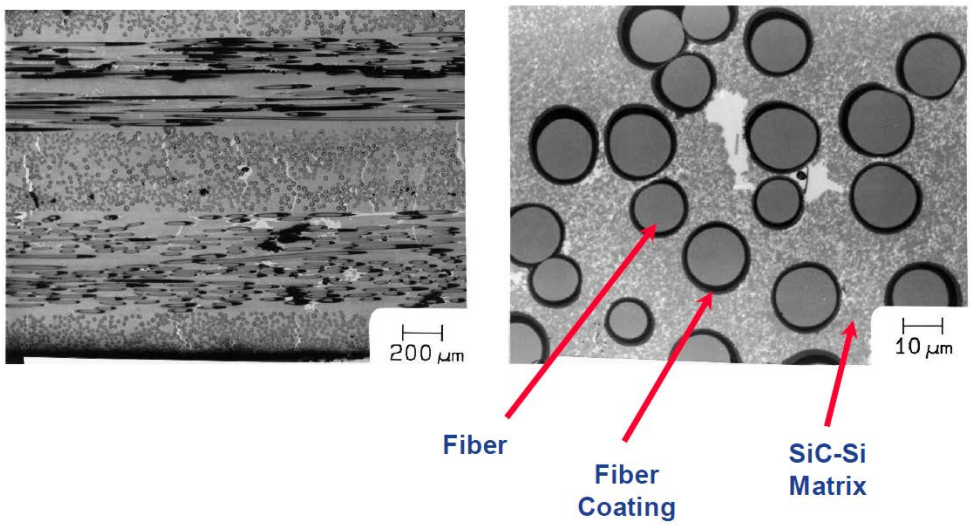

Figure 171: Typical SiC CMC Laminate Cross Section

Prior to creating the composite laminate, care was taken to minimize the material usage for each build. The plys were all cut from unidirectional fiber pre-preg tape. The nesting of the ply shapes was optimized resulting in roughly 60 percent tape usage efficiency. This material loss can be attributed to the shape and spacing of each ply in the nesting. After the ply shapes were cut and sorted, the fabrication of the CMC component could begin.
The process of curing CMC SiC-based articles can vary but the most typical methods of finalizing a pre-preg laminate CMC component is to either use continuous vapor deposition or melt infiltration of silicon to consolidate the remaining carbon into silicon carbide at high temperatures exceeding the melting point of silicon. See Figures 6 and 7 for general schematics of the pre-preg layup and melt infiltration processes.

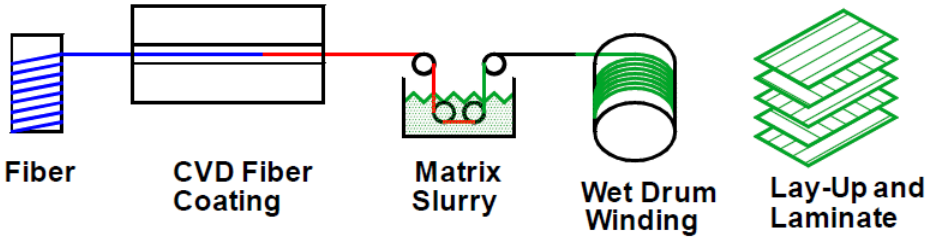

Figure 172: Pre-preg Layup Process

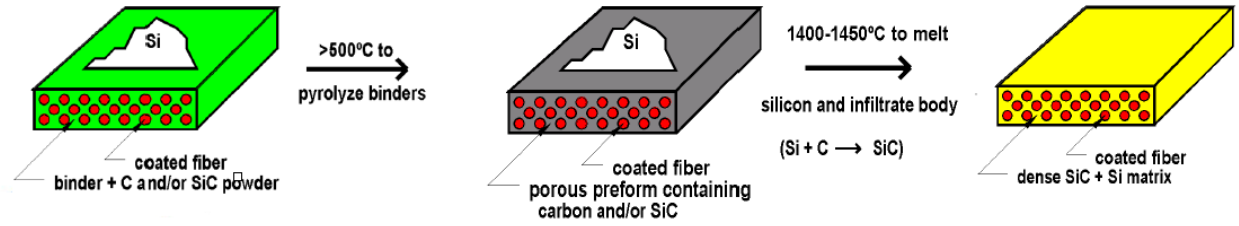

Figure 173: Melt Infiltration Process

The process called melt infiltration, MI, was used. Un-like the continuous vapor deposition, CVD, process, MI generally results in greater mechanical properties and thereby lends itself well to more applications. The MI process consists of three steps; autoclave, burn-out and melt infiltration. During autoclave, the pre-preg CMC plys are compacted in an oven under pressure to help in the consolidation, or de-bulking, of the laminate. The pressure is used to draw out some intermediate chemicals used during the layup of the CMC component and close any voids in between the ply stacks. The off-gassing of these chemicals is known to be important to the overall yield of each CMC article and care is taken when designing the tool in order to aid in the depletion of these chemicals.

The final processing of the CMC components was completed using silicon melt infiltration. This is where the residual unreacted carbon fuses with the liquid silicon to form SiC. It was found that with larger components the level of porosity or residual unreacted carbon left over after MI was generally greater than has been previously seen on smaller components. This kicked off a CMC design of experiments that led to a greater understanding of how the current three-step processing of SiC MI composites affect the porosity and therefore yield of full-scale CMC components.

Several post processing elements were needed prior to testing the full scale CMC components. The first was machining of the SiC article to the final net. Typical machining of a metallic component requires hard dense ceramics as cutting tools. Since the CMC component is innately a hard ceramic, diamond tooling was required to machine the components. Overall the machining of the CMC components used traditional grinding methods to remove the excess material.

The fabrication of 19 full scale Phase 1 CMC components was completed.

Testing of Phase 1 Components

This testing made improvements upon a series of smaller scale CMC component testing that was conducted earlier. The learning from those tests helped to select the system architecture and to further the art of CMC material systems.

Testing on the Phase 1 components provided the first source of full-scale relevant data for the CMC components. The fabrication of these components was not without difficulties. Several features within each of the components were considered to be compromised and non-ideal for rigorous testing. After some characterization, they were determined to be fit for test in an effort to advance the art and understanding related to the design and manufacturing implications. In total, 9 components were tested.
The first test objective was to resolve any modeling uncertainties that were inherit in the testing system and setup of the CMC component itself. Two system configurations were used to determine their effect on the CMC components.

Testing was undertaken to understand the vibratory response of the CMC components with regard to physical geometry differences and stiffness variations. Geometric and internal variation plays an important role with regard to composite structures. Unlike traditional metallics, composite properties are orthotropic in nature and their mechanical properties can be tailored in all directions. From a design standpoint, this can provide flexible alternatives to a traditional metallic because strength or toughness can be altered in a direction that is most susceptible to fracture. The processing of composites can also alter the properties of the material because they undergo several thermal processing cycles. Ceramic matrix composites undergo very high temperature processes that can cause residual stresses and affect the material capability. The net shape of these components can also vary based on the uncured ply thickness, causing dimensional variation. This net shape variation was expected to have an effect on the test results.

Several parts had infant mortality failures near peak loading. A root cause analysis (RCA) concluded that portions of the laminate were orientated in the opposite direction as design intended. Additionally it was found that excessive machining of material combined with the movement of plies during part densification in two critical areas had also led to decreased mechanical capability and strength. The remaining 6 components were found to have been manufactured and processed as intended and were successfully tested.

Fatigue data was captured to further understand how a CMC material system initiates a crack and then propagates through the laminate construct during cyclic loading. Three components underwent fatigue testing at various cycle magnitudes to provide lifing.

Secondary incites of the testing included the EBC coating effect, allowing the designers to understand the response differences due to the coating mass and the processes involved in coating CMC's.

In all over 400 hours of testing was completed on 6 components, with a minimum of at least 34 to 134 hours on each test component. Over 397 data points were taken of the two configurations tested.

Phase 2 Design and Fabrication of CMC Component

In an effort to reduce the risk and increase the durability of the CMC components a second iteration called the Phase 2 design was performed which took learning from the previous Phase 1 design and other related testing.

For example, an attachment location on the CMC component critical to the mechanical system was redesigned. This area employed a thickness change through the use of ply drops. In the Phase 1 design, these ply drops were large laminate stacks. The new method called for smaller laminate stacks that were of alternating lengths, and or staggered, to inhibit cracks. A bi-product of this change led to increased and repeatable compaction in this attachment location not seen on the phase 1 design component.

The new design allowed for simple ply shape geometries which helped to increase the ply cutting yield of the unidirectional tape to over 65 percent. New tooling aids and simplified composite ply shapes ultimately led to a 2x reduction in overall layup time.

The processing of this larger Phase 2 design CMC article started off with the optimized methods that were used on the six Phase 1 design components that were subjected to testing. It was known that thickness of the CMC components would likely dictate changes in the traditional curing processes. The first Phase 2 design component underwent the same processing as with the Phase 1 design. Non-destructive CT inspection techniques were used to show the high level of porosity within regions of the article that had been noted on early Phase 1 design components. Over the next two full-scale processing iterations, modifications were made to the uncured processing that eventually led to a near perfect Phase 2 CMC component.

Testing of Phase 2 Components

Testing performed on six of the Phase 2 design components. Overall these six CMC components were structurally superior to the previous Phase 1 design. A new coating method was assessed that would be utilized in the CMC to metallic attachment interface to decrease wear concerns.

Testing was successful. Previously the EBC coatings applied to the Phase 1 design did not hold up well in testing. An issue of contamination from the test facility was resolved and the EBC held up well.
In all, over 28 hours of testing was completed on 6 components resulting in over 1,500 data points on a number of various locations.

CONCLUSIONS

Numerous observations and conclusions were drawn from the work completed over the duration of this program. Many of those conclusions related to the fabrication of CMC components for gas turbine applications. During the fabrication of the Phase 1 full-scale components, it was noticed that several processing changes needed to be made and developed in order to produce

acceptable component yields for these larger parts. Additionally as the CMC component grew geometrically to become a more robust component, Phase 2 offered its own difficulties of producing acceptable parts that would be required for production.

As for long term CMC testing in fielded gas turbine engines, the 7FA stage 1 shrouds which amassed over 21,740 hours of continued operation provided an extensive set of EBC and CMC exposure data.

SYSTEMS STUDY

IGCC Plant with Carbon Capture Application

The primary objective of this program was to evaluate gas turbine technology improvements in an Integrated Gasification Combined Cycle (IGCC) plant with 90% carbon capture and sequestration (CCS). Improvements in plant performance, emissions, and cost form the basis for DOE program goals. A systems level approach was used to achieve the DOE program goals. Fuel Flexible (coal derived hydrogen or syngas) Gas Turbine Power Island System Requirements were based on the DOE IGCC Performance Goals for 2015 which outlines a coal-based power system with:

- Plant Efficiency increase of 2 to 3% for 2010 and 3 to 5% for year 2015.
- NO_x Reduction to less than 3 ppm @ 15% O2 with coal derived hydrogen or syngas by 2015.
- Contribute to IGCC capital cost reduction

As a means to approach these goals, eight key performance parameters were identified to quantify turbine performance improvement:

1. IGCC Plant Net Efficiency
2. IGCC Plant Specific Output
3. IGCC Plant NOx emissions
4. Combined Cycle Efficiency
5. Combined Cycle Specific Output
6. Turbine Simple Cycle Efficiency
7. Turbine Specific Output
8. Turbine Exhaust NOx emissions

A Baseline IGCC System was chosen by: (1) Determining the appropriate gasifier and F-Class Baseline Plant configuration, (2) Evaluating the overall heat and mass balances for the Baseline IGCC Plant, and (3) Developing an Integrated IGCC Simulation Analysis Model for the Baseline IGCC Plant configuration.
This Baseline System was chosen on the basis of a design which was representative of GE Frame 7FA current technology with sufficient public information to perform a detailed performance comparison with the results for that configuration by the Integrated IGCC Simulation Analysis Model. This Reference plant design is the Tampa Electric Polk IGCC case with:

- ISO ambient conditions
- Kentucky No. 9 Coal
- GE Energy slurry fed oxygen blown gasifier
- High pressure cryogenic Air Separation Unit
- HP steam heat recovery similar to Tampa Polk IGCC study
- COS hydrolysis, wet particulate removal
- Syngas saturation, heating and low temperature heat recovery
- Amine based Acid gas cleanup and sulfur recovery
- 7FA gas turbine with 2250^{o}F (1232°C) firing temperature
- Gas Turbine N_2 injection
- 3 pressure HRSG

- Reheat 1415 psig/1000°F (538°C)/1000°F (538°C)/ 1.5 in. steam turbine Cooling pond, transformer and plant auxiliaries included

Table 7 provides an overview of the system level goals for each of the relevant machines for this program including the baseline plant, the 2010 IGCC plant, the baseline FutureGen plant, the 2012 FutureGen plant, and the 2015 IGCC/H2 plant. The trend was towards increasing firing temperature and compressor pressure ratio to attain the efficiency and emissions goals of this program.

Table 7 - Overview of Target System Goals

					DOE Goals	
	GT	Fuel	Comb	Tfire	Efficiency	NOx Emissions
Base Tampa IGCC	7FA	Syngas	Diffusion	2250	Base, Syngas	<15 ppm
2010 IGCC	7FB	Syngas	Hybrid	2500	+ 2-3 % pts	<3 ppm**
Base FutureGen	7FA	Hydrogen *	Diffusion	2250	Base, Hydrogen *	<3 ppm**
2012 FutureGen	7FB	Hydrogen *	Advanced	2500	+ 2-3 % pts	<3 ppm**
2015 IGCC/FutureGen	7FB+	Hydrogen *	Advanced	2650	+ 3-5 % pts	<3ppm**
* 65% H2/35% N2 Fuel Gas Mixture, 90% CO2 Capture ** Include SCR If not achieved by Advanced Combustor						

Detailed performance models were developed for syngas and high hydrogen fuels with 90% carbon capture capability. A number of analyses were performed to determine conditions for optimum performance and cost. Influence coefficients were developed to identify key contributors to performance gains and to isolate operating regions wherein program goals could be attained. A summary of the most relevant findings are noted below.

The table below (Table 8) summarizes overall plant performance with the eight key performance parameters for the baseline and 2015 plant with coal derived hydrogen and syngas fuels. The 2015 plant includes technologies funded by the program in areas of combustion emissions, turbine cooling, and materials. Advances in materials enabled firing temperature to be increased by 400 degrees Fahrenheit.

Table 8 - Overall Plant Performance

		FA Base CCS Hydrogen	2015 GT CCS Hydrogen	Delta	FA Base Syngas	2015 GT Syngas	Delta
Plant Net Efficiency, HHV	%	28.0%	36.3%	8.3%	35.9%	43.9%	8.0%
Plant Specific Net Output	kW/pps	251	329	31%	315	380	21%
Plant Emissions	ppm	2	2	-	15	2	-
Combined Cycle Efficiency, HHV	%	64.3%	71.8%	7.5%	66.1%	72.7%	6.6%
Combined Cycle Specific Output	kW/pps	357	407	14%	391	432	10%
Turbine Simple Cycle Efficiency	%	40.0%	45.1%	5.1%	40.6%	44.2%	3.6%
Turbine Specific Output	kW/pps	221	256	15%	240	263	10%
Turbine Exhaust Emissions	ppm	<5	<4	-	15	<4	-
Installed Cost Reduction	$/kW	Base	-	>20%	Base	-	>20%
COE Reduction	c/kWH	Base	-	>20%	Base	-	>20%

The 8% improvement in plant efficiency far exceeds the 5% goal and highlights the capability of the technology introduced in this program.

The table below (Table 9) provides a performance scorecard for the intermediate, as requested by DOE, 2010 and 2012 cycles.

Table 9 – Performance Scorecard for 2010 and 2012 Offerings

		FA Base CCS Hydrogen	2012 GT CCS Hydrogen	Delta	FA Base Syngas	2010 GT Syngas	Delta
Plant Net Efficiency, HHV	%	28.0%	32.2%	4.2%	35.9%	40.0%	4.1%
Plant Specific Net Output	kW/pps	251	312	24%	315	364	16%
Plant Emissions	ppm	2	2	-	15	2	-
Combined Cycle Efficiency, HHV	%	64.3%	68.3%	5%	66.1%	68.3%	2.2%
Combined Cycle Specific Output	kW/pps	357	409	15%	391	422	8%
Turbine Simple Cycle Efficiency	%	40.0%	42.1%	2.1%	40.6%	40.7%	0.1%
Turbine Specific Output	kW/pps	221	252	14%	240	252	5%
Turbine Exhaust Emissions	ppm	<5	<5	-	15	<5	-
Installed Cost Reduction	$/kW	Base	-	-	Base	-	-
COE Reduction	c/kWH	Base	-	-	Base	-	-

The 4% improvement in plant efficiency far exceeds the 2-3% goal and highlights the capability of the technology introduced in this program.

Industrial Gas Turbine Applications

For the ARRA portion of the project the overall objectives of the Systems and Performance Evaluation were (1) to evaluate Industrial Gas Turbine Technology improvements at plant level with carbon capture and sequestration, (2) improve industry wide plant efficiency by 5% and reduce carbon dioxide and nitrous oxide emissions to 2 ppm and (3) contribute to significant economic benefits.

These objectives were achieved using detailed performance and cost models calibrated to two unique plant configurations with defined boundary conditions typical for steel mill and refinery applications.

Plant Configurations

Two plant configurations were considered at base load steady state conditions, (1) IGCC Steel Mill and (2) IGCC Refinery. These represent common applications for IGCC technology. This technology includes five basic technology steps (1) air separation unit to supply pure oxygen,

(2) a gasification plant where syngas is produced, (3) syngas cooling, (4) gas clean up, and (5) a combined cycle power plant. Steel mill and refinery internal processes were not modeled in this analysis. Representative process streams exported to and imported from each application were assumed. The steel mill imports oxygen, nitrogen, and steam and exports a blast furnace gas (BFG) of known composition and temperature. The BFG is mixed with syngas exiting the gasifier and the mixture is sent to the syngas scrubber to remove impurities. The refinery imports hydrogen and steam, and exports a process gas which is sufficiently clean to be injected directly into the gas turbine. The bottoming cycle for each configuration is designed to supply steam at the conditions required for each application. To best quantify plant performance, Combined Heat and Power (CHP) was used. This term is often used to describe fossil-fired power plants that generate multiple product streams, usually thermal energy and electricity.

Co-firing was also considered in the analysis. This scenario arises when the power demand and process needs are to be met while the chemical process plant is out of service. The gas turbine is fueled with natural gas along with process gas from either the steel mill or refinery and the process needs are met from an external source.

IGCC Steel Mill

The plant consisted of a standard Integrated Gasification Combined Cycle (IGCC) plant operating at ISO (59°F (15°C), 14.7 psia, 60% RH) ambient conditions with Illinois #6 bituminous coal feedstock in a GE high pressure coal slurry quench oxygen blown gasifier. Syngas exits the gasifier at 1014.7 psia and 2420°F (1327°C). Compressed air from the compressor discharge of the gas turbine coupled with supplementary air from an auxiliary compressor are sent to a cryogenic air separation unit (ASU) which supplies 95% oxygen (mole-basis) to the gasifier. Syngas exiting the gasifier is cooled then cleaned of particulate matter (PM), mercury (Hg), and sulfur compounds before injection into the gas turbine. Syngas cooling occurs in a radiant syngas cooler (RSC) and the heat removed in the process is used to produce high pressure steam for expansion in the steam turbine. The power block in the reference plant configuration, consisted of a 1998 vintage 6FA gas turbine (GT), steam turbine (ST), air cooled electrical generator, and a two pressure non-reheat bottoming cycle in a 2x1 configuration. A water-gas-shift reactor converts carbon monoxide (CO) to carbon dioxide (CO_2), and a Selexol-based Acid Gas Removal (AGR) unit separates the hydrogen sulfide and CO_2. The nominal 90 percent CO_2 reduction is accomplished by adding sour-gas-shift (SGS) reactors to convert CO to CO_2 and using a two-stage Selexol process with a second stage CO_2 removal efficiency of up to 95%. Carbon dioxide is compressed and sequestration occurs at 2200 psia. Hydrogen sulfide to the GT is limited to 20 ppm.

Compressed blast furnace gas (BFG) from the steel mill is mixed with syngas from the gasifier. Pollutants in the BFG necessitate cleaning of the BFG prior to injection in the gas turbine. The flow of BFG from the Steel Mill was calculated based on BFG-to-GT fuel heat consumption ratio of 0.20. Composition of the blast furnace gas is given in Table 10.

A process flow diagram gives a graphical depiction of the system, Figure 174.

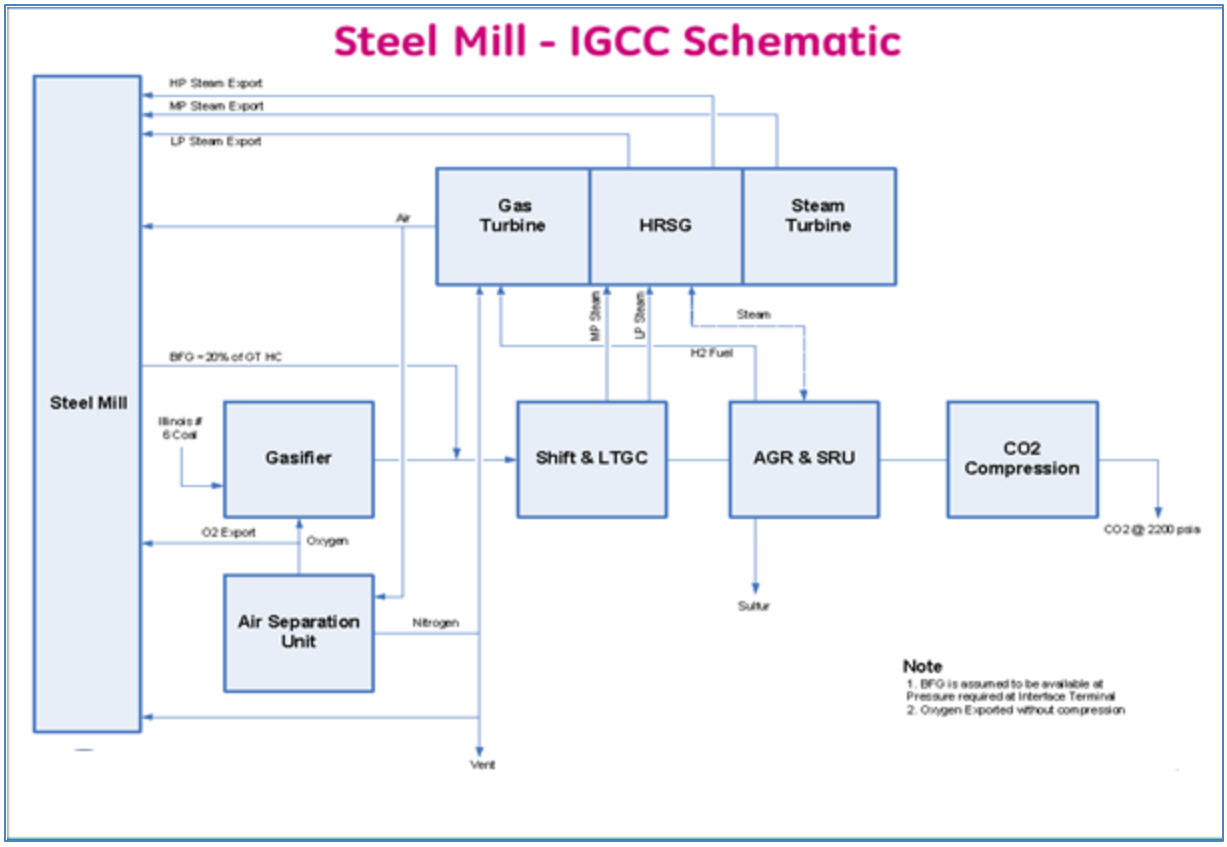

Figure 174: Process flow diagram for steel mill

Table 10 - Blast Furnace Gas Composition

Blast Furnace Gas		
Temperature	F	110
Pressure	psia	30
LHV	Btu/lb	1,064
HHV	Btu/lb	1,080
Molar Composition		
Carbon	%	2.4000%
Nitrogen	%	56.4000%
Methane	%	0.1000%
H2O	%	3.4000%
CO	%	23.3000%
CO2	%	14.4000%

IGCC Refinery

The plant consisted of a standard Integrated Gasification Combined Cycle (IGCC) plant operating at 80°F (27°C), 14.7 psia, 57.5% RH ambient conditions with medium sulfur petroleum coke (petcoke) feedstock in a GE high pressure coal slurry quench oxygen blown gasifier. Syngas exits the gasifier at 1014.7 psia and 2450°F (1343°C). Compressed air from the compressor discharge of the gas turbine coupled with supplementary air from an auxiliary compressor are sent to a cryogenic air separation unit (ASU) which supplies 95% oxygen (mole-basis) to the gasifier. Syngas exiting the gasifier is cooled then cleaned of particulate matter (PM), mercury (Hg), and sulfur compounds before injection into the gas turbine. Syngas cooling occurs in a radiant syngas cooler (RSC) and the heat removed in the process is used to produce high pressure steam for expansion in the steam turbine. The power block in the reference plant configuration, consists of a 1998 vintage 6FA gas turbine (GT), steam turbine (ST), electrical generator and a two pressure non-reheat bottoming cycle in a 2x1 configuration. A water-gas-shift reactor converts carbon monoxide (CO) to carbon dioxide (CO_2), and a Selexol-based Acid Gas Removal (AGR) unit separates the hydrogen sulfide and CO_2. The nominal 90 percent CO_2 reduction is accomplished by adding sour-gas-shift (SGS) reactors to convert CO to CO_2 and using a two-stage Selexol process with a second stage CO_2 removal efficiency of up to 95%. Carbon dioxide is compressed and sequestration occurs at 2200 psia. Hydrogen sulfide to the GT is limited to 20 ppm.

A process flow diagram gives a graphical depiction of the system, Figure 175.

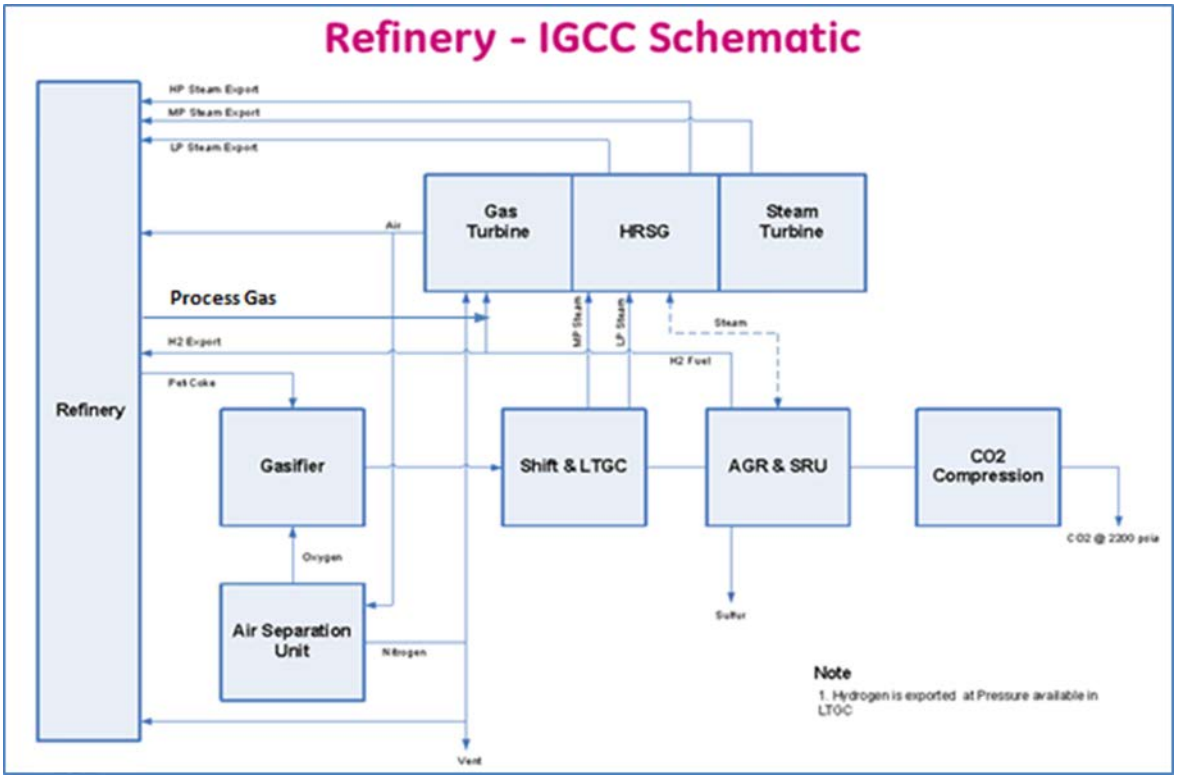

Figure 175: Process flow diagram for refinery

Process gas from the refinery at 130°F (54°C) is mixed with syngas from the AGR prior to injection in the GT. The mass flow is controlled to 10% GT heat consumption. The constituents of the process gas are shown in Table 11, below.

Table 11 - Refinery Gas Composition

Refinery Off Gas		
Temperature	F	130
Pressure	psia	900
LHV	Btu/lb	19,893
HHV	Btu/lb	21,760
Molar Composition		
Hydrogen	%	23.0%
Nitrogen	%	4.0%
Methane	%	34.0%
H2O	%	0.3%
CO	%	0.7%
Ethane	%	16.0%
Propane	%	3.0%
Ethylene	%	11.0%
Propene	%	6.0%
1-Butene	%	2.0%

Baseline Configuration

The power block consisted of two 6FA gas turbines fired at base load exhausting to a 2PrNRH bottoming cycle. The IGCC plant, uses petroleum coke (petcoke) in a wet feed GE high pressure quench gasifier, a wet syngas treatment and purification unit, a conventional high pressure air separation unit (ASU) and a 6FA gas turbine co-fired with refinery gas as fuel in a combined cycle configuration providing air extraction to ASU and export steam to the refinery. Gas turbine performance was evaluated at 80°F (27°C), 14.7 psia, 57.5% RH ambient conditions. When run at base load with methane fuel, this gas turbine produces approximately 66 MW with a simple cycle efficiency of 33%. This cycle model was configured for syngas operation and includes an oversized stage one turbine nozzle for compatibility with the higher mass flows common in such applications. Combustor area is varied to produce an overall pressure drop of 5%.

Air from compressor discharge is sent to the ASU and diluent nitrogen is returned to the combustor. The magnitude of each stream is optimized to satisfy ASU requirement, power augmentation needs, and NOx emissions constraints.

Strategy/Approach

A system level plant study was performed to determine the factors which impacted overall performance, cost and emissions. A Design of Experiments approach was utilized to generate system level data for processing. Regression analysis was performed across the gas turbine and plant level design spaces. Optimization techniques were applied to the regressed transfer

functions, along with validation runs to ensure accurate results. Post-processing analysis was used to identify the key factors which enabled program goals to be met.

The gas turbine model for the study uses the PREDATER framework to explore the gas turbine design space. PREDATER (Preliminary Robust Engineering and Design Analysis Tool to Estimate Return) is a gas turbine combined cycle conceptual design model, assembled as an Integrated Design Environment (IDE) tool. IDE tools allow various independent code modules to be combined into a functional collection, by automating the input/output of each code module and handling all necessary data transfers. PREDATER allows for thorough evaluation of a conceptual design space.

The transfer functions developed by executing the gas turbine model were then integrated with the plant model to arrive at overall IGCC plant performance. This composite model was then used to quantify status performance against program goals. The graphic below, Figure 176, illustrates some of the output from the design process and enables identification of key contributors to performance metrics. Independent parameters are shown on the horizontal axis and dependent parameters are shown on the vertical axis.

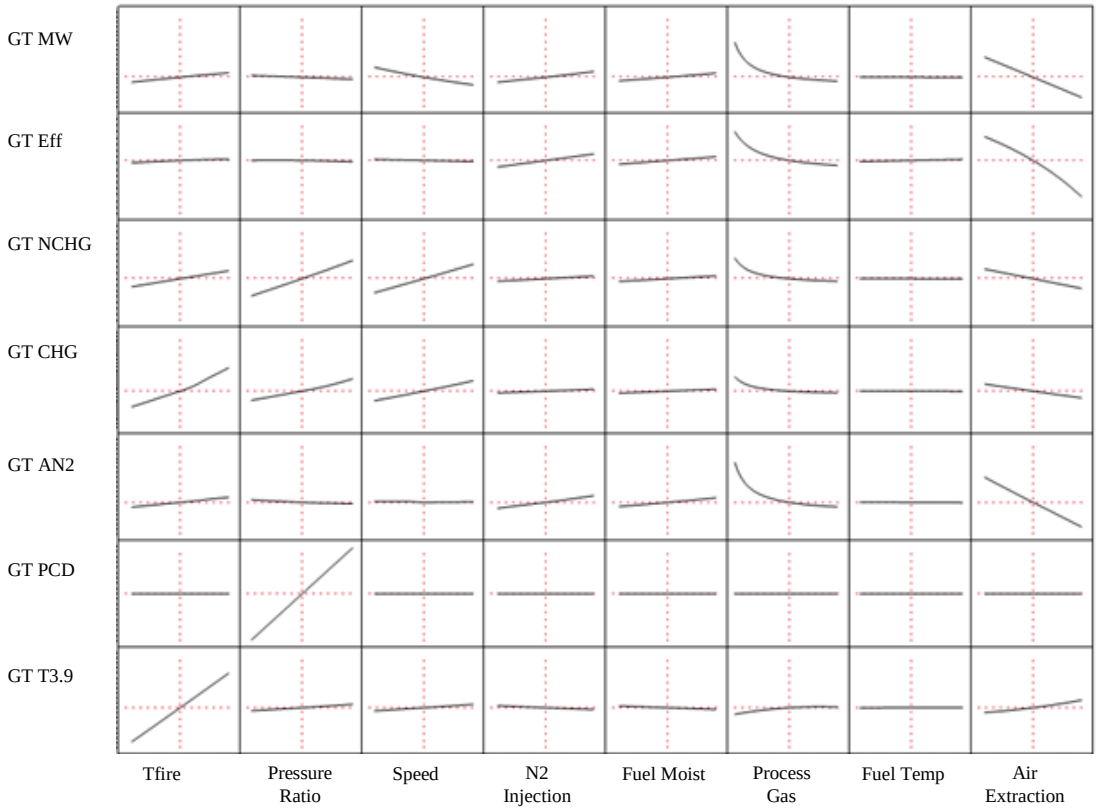

Figure 176: Example of Predater output

An optimized flow path was determined for each scenario. The graphic below, Figure 177, illustrates the variation in turbine flow path geometry observed within some of the cases considered.

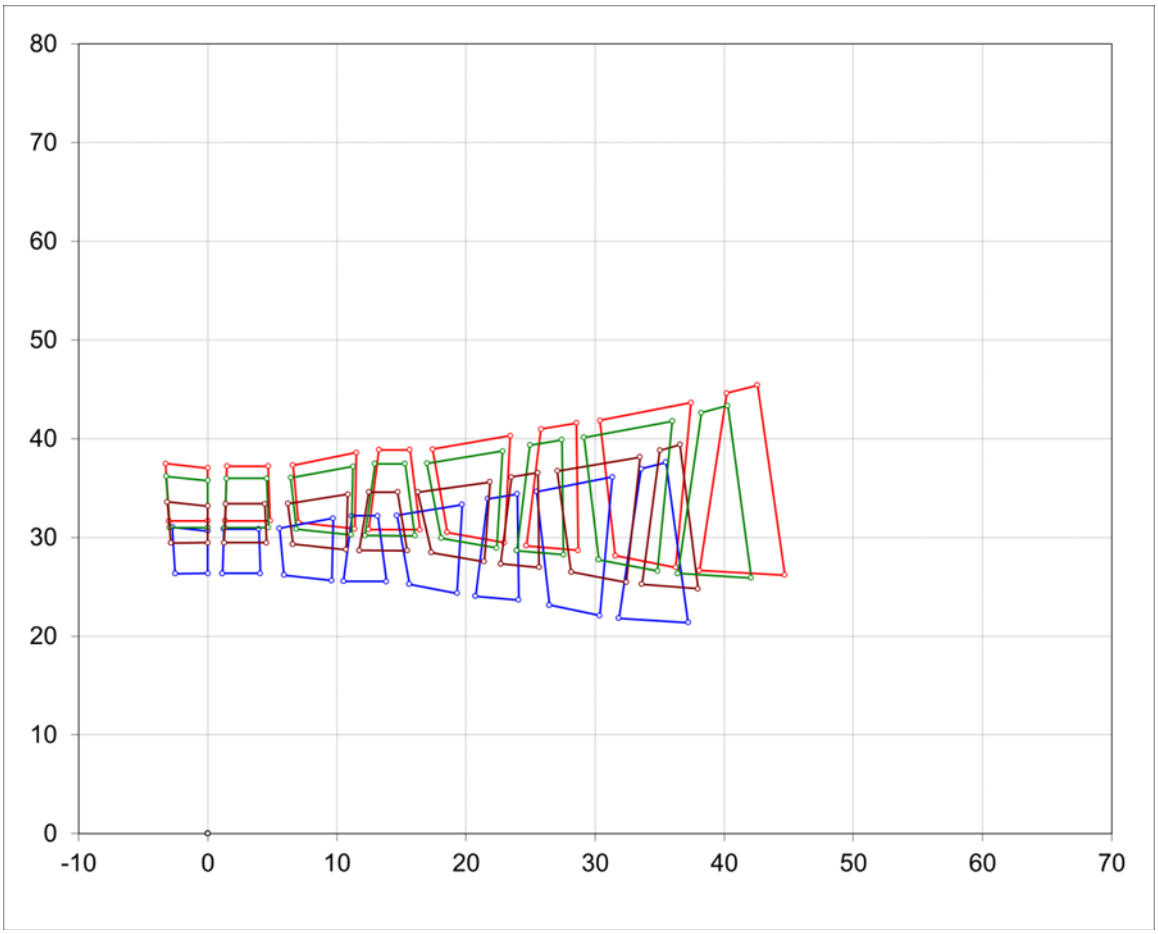

Figure 177: Optimized flowpaths for each scenario

The next decision was to determine if the 5% efficiency goal could be met if a single turbine flow path was used in each scenario.

The chart below gives CHP efficiency increase above the baseline configuration for each scenario, i.e., IGCC Refinery, IGCC Steel Mill, Co-fired-Refinery, and Co-fired Steel Mill. The blue bars denote use of a single gas turbine flow path optimized for the IGCC Steel Mill and the red bars denote use of a natural gas optimized flow path.

A 5% improvement in CHP efficiency was demonstrated for each of the eight scenarios.

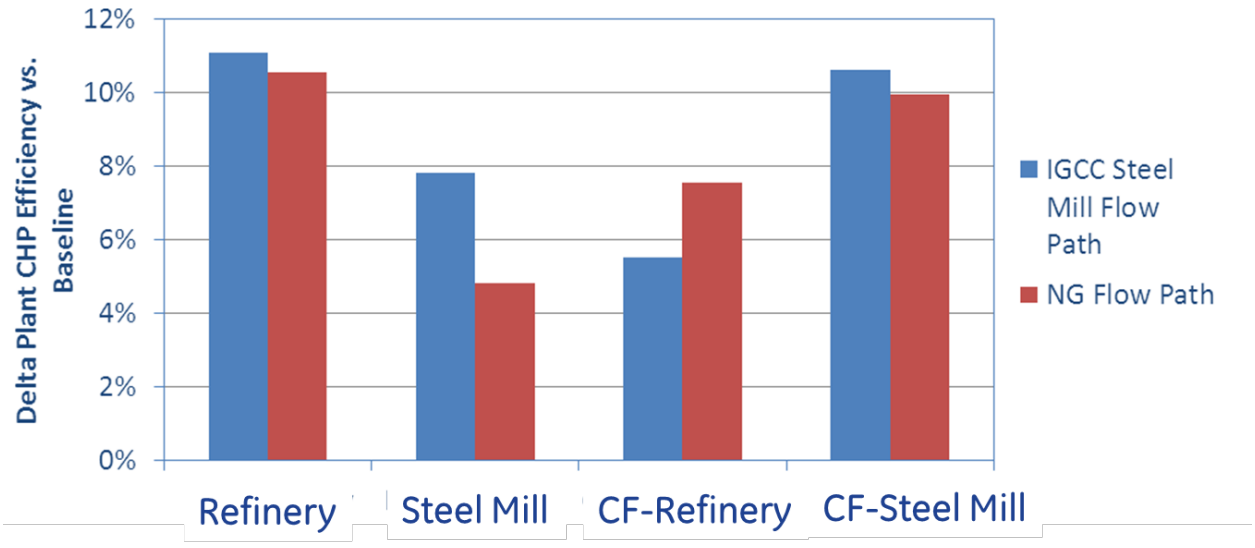

Figure 178: Efficiency increases per scenario

OVERALL PROGRAM CONCLUSIONS

The objective of this program was to develop the technologies required for a fuel flexible (coal derived hydrogen or syngas) gas turbine for IGCC that met DOE turbine performance goals. The overall DOE Advanced Power System goal was to conduct the research and development (R&D) necessary to produce coal-based IGCC power systems with high efficiency, near-zero emissions, and competitive capital cost. To meet this goal, the DOE Fossil Energy Turbine Program had as an interim objective of 2 to 3 percentage points improvement in combined cycle (CC) efficiency and a final goal of 3 to 5 percentage points improvement in CC efficiency above the state of the art for CC turbines in IGCC applications at the time the program started. The efficiency goals were for NOx emissions of less than 2 ppm NOx (@15 % O2). As a result of the technologies developed under this program, the DOE goals were exceeded with a projected 8 point efficiency improvement. In addition, a new combustion technology was conceived of and developed to overcome the challenges of burning hydrogen and achieving the DOE's NOx goal.

The ARRA-funded portion of the project was focused on gas turbine technology advances that are aimed at offsetting CCS penalties and improving emissions performance in preparation for CCS in industrial applications. GE Power & Water has extensive experience in supplying gas turbines for use in industrial applications such as refineries, petrochemical, iron and steel mills. Systems based on advanced gas turbines offer efficient energy conversion solutions that meet the challenge of fuel diversity, while maintaining superior environmental performance. The DOE's goal for more than five percentage point improvement in efficiency was met with cycle analyses performed for representative IGCC Steel Mill and IGCC Refinery applications.
This project built upon existing gas turbine technology and product developments, and developed and validated the necessary turbine related technologies and sub-systems needed to meet the DOE turbine program goals. The scope of the program did not cover the design and validation of a full-scale prototype machines with the technology advances from this program incorporated.

Key elements of the whole project are summarized below:

Combustion: Simply stated, the combustion goal for the program was "reliable, ultra-low NOx combustion of high hydrogen fuels for advanced gas turbine cycles".

The outcome of Task 2.1 of the program was a dry low NOx combustion system capable of operating reliably on syngas, carbon-free syngas, and a wide range of additional fuels. The system cost was brought in line with current natural gas combustion system to support plant capital cost targets. The high-hydrogen combustion system was fully demonstrated to consistently achieve single-digit (ppm) NOx emissions while operating at aggressive H2 gas turbine cycle conditions to meet program goals for IGCC-CCS plant efficiency and output.

Task 2.6 achieved its stated objectives for this area: to develop designs for an Advanced Combustor Architecture and Advanced Combustor Integration that enable firing temperature increases thereby improving efficiency while still delivering low NOx emissions, handling hydrogen and fuel flexibility, extend turndown, and maintaining existing inspection intervals and current reliability levels. $NOx/T_{3.90}$ capability was improved, turndown capability was extended, and the system maintained the capability to run greater than 50% hydrogen in the fuel, and the tolerance to fuel MWI changes were three to five times the baseline system.

Materials: The materials task was intended to develop alloys that are specifically tailored to withstand elevated temperatures in the hot gas path in the high moisture, and potentially highly corrosive environments of hydrogen fueled industrial applications with CCS. This will enable industrial gas turbine applications with CCS improved efficiency through higher firing temperature while preserving traditional hot gas path component durability.

The HGP coating program completed under ARRA 2.7 was very successful. It gave insights into the oxidation behavior of new coatings and alloys. It also resulted in a low k TBC that improves the efficiency of the gas turbine system through enabling higher operating temperature and allowing increased service intervals. It is being incorporated into the design for several new GE gas turbines.
Under ARRA 2.7, a highly oxidation and corrosion resistant superalloy, Rene' N2M, was successfully developed, which enables stage 1 static hardware to reliably operate beyond the temperature limited by Rene' 108 alloy. Verifications of the scale-up of the alloy by making, complex nozzle castings and necessary downstream fabrication processes laid a solid foundation to deploy this material in upcoming products. In addition, without Re and with reduced Hf, the alloy is cost effective.

Sensors: The sensors task focused on the technology of utilizing and integrating a variety of advanced sensor technologies into gas turbine control and operation. This would enable the gas turbine to operate with reduced margin due to real-time knowledge of actual parameters that are affecting component conditions and operation.
The most significant sensing gaps exist in the turbine hot gas path, where existing sensor technology cannot survive in the harsh environment.
Three distinct sensor technologies were selected and tested in laboratory and rig conditions for further evaluation under this program, namely, (1) Multi-color infrared (MCIR) Pyrometry, (2) Tunable Diode Laser Absorption Spectroscopy (TDLAS) and (3) Passive Wireless Sensors Technology (PWST).

Next Generation Stage 1 Architecture: This task developed technology that enables turbine cooling flow reductions and henceforth improved efficiency.

Subtask 2.9 investigated architectures of the next generation of a stage 1 hot gas path turbine components. During this subtask, it was demonstrated that these architectures met program cooling flow reduction targets with no impact to part life, while having a positive cost/benefit ratio.

Cooling/Sealing/Purge Flow Reductions: Under this task extensive research and technology development was conducted to improve cooling, sealing, and purge flow features for hot gas path parts. This reduced required flows and enabled higher temperature operation to improve efficiency and turbine throughput while enabling low NOx operation.

Multiple technologies developed in this area are now being introduced into GE's new and existing gas turbines.

CMC: The CMC task was focused on key elements of CMC development for use in gas turbine hot gas path components. The CMC material characteristics have the potential to enable uncooled components in selected turbine stages, thereby increasing efficiency.
Numerous observations and conclusions were drawn from the work completed over the duration of this program. Many of those conclusions related to the fabrication of increasingly complex CMC components for gas turbine applications. During the fabrication of the Phase 1 full-scale components, it was noticed that several processing changes needed to be made and developed in order to produce acceptable component yields for these larger parts. Phase 2 offered its own difficulties of producing acceptable parts that would be required for mass production.

Long term CMC testing in fielded gas turbine engines was performed with the 7FA stage 1 shrouds amassing over 21,740 hours of operation provided an extensive set of EBC and CMC exposure data.

In summary, the DOE goals were met with this program. While the commercial landscape has not resulted in a demand for IGCC gas turbines, many of the technologies that were developed over the course of the program are benefiting the US by being applied to new higher efficiency natural gas fueled gas turbines. At the time of the writing of this report 17 of the technologies developed under this program and scheduled for utilization in GE's advanced gas turbine products.